Combustion of Synthetic Fuels

Combustion of Synthetic Fuels

William Bartok, EDITOR
Exxon Research and
Engineering Company

Based on a symposium sponsored
by the ACS Division
of Petroleum Chemistry
at the 183rd Meeting
of the American Chemical Society,
Las Vegas, Nevada,
March 28–April 2, 1982

ACS SYMPOSIUM SERIES **217**

ACS Symposium Series

M. Joan Comstock, *Series Editor*

FOREWORD

The ACS SYMPOSIUM SERIES was founded in 1974 to provide
a medium for publishing symposia quickly in book form. The
format of the Series parallels that of the continuing ADVANCES
IN CHEMISTRY SERIES except that in order to save time the
papers are not typeset but are reproduced as they are sub-
mitted by the authors in camera-ready form. Papers are re-
viewed under the supervision of the Editors with the assistance
of the Series Advisory Board and are selected to maintain the
integrity of the symposia; however, verbatim reproductions of
previously published papers are not accepted. Both reviews
and reports of research are acceptable since symposia may
embrace both types of presentation.

PREFACE

W<small>ITH THE INEXORABLE DEPLETION</small> of premium fossil fuels, oil and gas, it appears that synthetic fuels derived from coal, shale, and tar sands will become part of the overall energy supply in the United States. Synthetic fuels comprise an array of different products including coal derived liquids and gases, shale oil, and methanol. In comparison to conventional fuels, the principal changes that will be introduced by the advent of synthetic fuels affect their production, refining, and end utilization. These are interrelated issues because the end utilization imposes product-quality requirements to which synthetic fuel properties should conform; conversely, it may be possible in certain instances to modify the design of combustion hardware to accommodate properties peculiar to synthetic fuels. This alternative would be particularly attractive from the standpoint of energy efficiency, thus decreasing the need for costly hydrogenative refining steps.

In the utilization of synthetic fuels, the key issues are impact on performance, equipment integrity, and emission characteristics of combustion hardware. Emissions of oxides of nitrogen and soot are the most actively researched emission problems for continuous combustion systems, which range from burners to gas turbine combustors.

This volume provides an overview of current fundamental and applied combustion research studies that address the use of synthetic fuels. The main emphasis in these studies is on the combustion of liquid fuels, ranging from research on spray atomization to pilot-scale testing of the combustion of synthetic fuels.

I wish to thank the contributing authors for their efforts and to acknowledge the help received from Jack Fisher in the early stages of organizing the ACS symposium.

WILLIAM BARTOK
Exxon Research and Engineering Company
Linden, NJ 07036

December 1982

Research Issues and Technology—An Overview

A. A. BONI and R. B. EDELMAN
Science Applications, Inc., La Jolla, CA 92038

D. BIENSTOCK
U.S. Department of Energy, Pittsburgh Energy Technology Center, Pittsburgh, PA 15236

J. FISCHER
Argonne National Laboratory, Argonne, IL 60439

The need to conserve energy and to control pollu-
tant emissions while at the same time introducing a
new generation of fuels derived from coal, oil
shale and tar sands is introducing severe re-
quirements on the design and retrofit of combustion
equipment. The different chemical and physical
properties of these synthetic fuels leads to
substantial differences in their combustion
characteristics and emissions. In particular there
is the potential for increased soot formation,
higher NO_x emissions, increased and modified
radiation and heat-load distribution, and increased
contamination and fouling of combustion and heat
transfer surfaces when compared to more conven-
tional fuels. Staged combustion techniques to
simultaneously control NO_x and soot production are
being developed. However, various burner, boiler
and furnace configurations are involved in
practical applications and they each have different
aerodynamic flow patterns and turbulence character-
istics. These flow field characteristics couple
with the fuel physical and chemical properties in
controlling the efficiency, emissions and fuel
flexibility characteristics of practical systems.
The U. S. Department of Energy, Advanced Research &
Technology Development Program in Direct Utiliza-
tion, AR&TD (DU), is providing the scientific and
technical information for improved, expanded, and
accelerated utilization of synthetic fuels in the
generic utility and industrial market sectors. In
the present paper, we review the current under-
standing of synfuel combustion, and present an
overview of the AR&TD (DU) program.

With the reduction in the availability of conventional hydro-carbons for fuels in the transportation, utility, and industrial sectors, there is a need to include fuels produced from low hydrogen-to-carbon ratio sources, such as coal, oil shale, and tar sands. Various processes are being developed to produce coal-derived liquids, solids and gases, oil from shale, and heavy oils from tar sands. It has been established that the cost and energy intensive requirements to refine these syncrudes to a hydrogen-carbon ratio and boiling range more typical of conventional fuels is very large (1). Therefore, there is a large economic driving force for the design, development, and implementation of combustion equipment capable of burning synthetic fuels of widely vary-ing properties in a thermally efficient and environmentally ac-ceptable manner.

Concurrently, the need to conserve energy and to control pollutant emissions is also forcing improvements in combustion ef-ficiency and reductions in pollutant emissions of existing energy-conversion devices using present-day fuels including heavy and residual oils. The requirements on the design of combustion equipment to meet these objectives will be severe and will demand substantial improvements in our ability to understand the combus-tion process and its controlling parameters. Many recent studies have considered the combustion of synthetic fuels, c.f. Black, et al. (2), Bowman and Birkeland (3), England, et al. (4), and Muzio, et al. (5). The problem is that current combustor tech-nology has evolved slowly, is based upon empirical methods, and contains little consideration for fuel flexibility. The situa-tion is particularly acute now because of the present uncertain-ties in fuel supplies and the corresponding uncertainties in design for fuel flexibility. Because of these uncertainties, equipment manufacturers and industrial users are currently re-luctant to make the necessary investments required for either retrofitting or manufacturing new equipment designed specifically for synthetic liquid fuels.

There is a near term need for existing equipment to utilize synthetic fuels and low grade residual fuels that have many of the same combustion problems. Also, there is a longer term need to develop new and advanced equipment to meet the role these fuels may play in the future. Because of the preponderance of existing combustion equipment in place it is necessary to modify current burner devices and systems for synthetic fuels use. Until recently, petroleum-based fuels have been both plentiful and cheap, and design practice has not had to consider the impact of fuel type. Improvements that have evolved have been of mechanical design rather than aerothermochemical. This is no longer sufficient and a better understanding of the effect of synthetic versus conventional fuel properties on combustion pro-cess control is required. Through the understanding of the per-formance of existing hardware and of the effect of fuel types (conventional and synthetic), design criteria for modifying cur-

rent systems can be established. Moreover, this understanding of
the effect of fuel type on the combustion process forms the basis
for new concept development and will contribute to the upgrading
of design procedures through a reduction in the level of empiri-
cism underlying current design methodologies.

Technical Issues Related to Combustion of Synfuels

The physical and chemical properties of synthetic crudes are
different from those of petroleum. Increased NO_x and soot pro-
duction are the principal problems of the combustion of synthetic
fuels, and control concepts for these two problems are in con-
flict. Fuel-rich combustion decreases NO_x but augments soot pro-
duction, while fuel-lean combustion decreases (and can eliminate)
soot production but augments NO_x emissions. Moreover, control
procedures can affect combustion efficiency and heat-transfer
distribution to the chamber surfaces. Table I, taken from Grumer
(6), illustrates some specific relevant properties of synthetic
liquid fuels and petroleum-based fuels. The principal differ-
ences between these fuels as related to their combustion behavior
are summarized in Table II.

In the following discussion, we consider these property dif-
ferences and illustrate their effect on the combustion process
and combustor peformance by use of data available in the litera-
ture.

The higher aromatic content and the lower hydrogen-to-carbon
ratio are chemical properties which combine to promote the
increased formation of soot and other related combustion
problems. Figure 1, taken from Naegeli (7), illustrates the
correlation of increased smoke emission with reduction in H/C
ratio for measurements on a T63 gas turbine combustor operating
on aromatic-doped petroleum fuels. Similar results have been re-
ported by Pillsbury, et al. (8, 9). The increased soot formation
is responsible for the increased luminosity and corresponding en-
hanced thermal radiation from synfuel flames, c.f. Figure 2,
again taken from Naegeli (7). These results and those reported
by Pillsbury, et al. (8, 9) indicate the success in using the H/C
ratio of the fuel to correlate the sooting tendency and the en-
hanced thermal radiation which occur for low H/C ratio fuels.
The sharp increase of exhaust smoke when the H/C is reduced below
2 is significant, because synfuels made from coal may approach a
H/C ratio of 1.2 whereas petroleum fuels have a H/C ratio of
about 2.

From a heat-transfer point of view, the high soot concen-
trations resulting from the combustion of synthetic fuels will
tend to cause both higher radiation heating and more severe
fouling of heat-transfer surfaces. Depending on the soot con-
centration and temperature of the combustion gases, as much as 95
percent of the total heat transfer in a furnace or a gas turbine
combustor may take place due to radiation; Sarofim (10). The

TABLE I PHYSICAL AND CHEMICAL PROPERTIES OF COAL LIQUIDS*

	SRC LT. ORG. LIQ.	SRC WASH SOLV.	SRC REC. SOLV.	H-COAL LIGHT	H-COAL MEDIUM	EXXON EDS FUEL	No. 2 FUEL PETROLEUM
SPECIFIC GRAVITY	0.811	0.943	1.031	0.875	0.9426	0.960	0.855
GROSS HEAT OF COMB., BTU/LB	19,000	17,050	17,229	18,800	18,331	18,343	19,500
KINEMATIC VISCOSITY, CS							
@ 104°F	1.03 @ 50°F	1.75	6.04	1.14	2.56	2.67	2.61
@ 212°F	–	0.77	1.45	0.61	0.99	1.11	1.09
CONRADSON CARBON RESIDUE, WT %	<0.01	0.07	4.95	0.03	0.08	0.03	<0.01
BOILING POINT RANGE, °F	125–394	302–458	411–730	208–467	367–586	311–686	358–672
AROMATICITY	28.0	61.0	76.0	32.0	43.0	53.0	15.0
CARBON, WT %	83.63	84.48	89.10	87.09	88.37	89.59	86.68
HYDROGEN, WT %	12.2	9.2	7.7	11.3	10.0	10.0	13.0
NITROGEN, WT %	0.29	0.35	0.69	0.16	0.33	0.08	0.006
SULFUR, WT %	0.57	0.26	0.30	0.14	0.09	0.03	0.2
OXYGEN, WT %	3.3	5.7	2.2	1.3	1.2	0.3	<0.1
ASH, WT %	<0.01	<0.01	<0.01	<0.01	<0.01	0.0	<0.01

*Grumer, Reference 6.

Table II

SUMMARY OF SYNFUEL CHARACTERISTICS RELATIVE TO CONVENTIONAL FUELS

o   High Aromatic Content
o   Lower Hydrogen Content
o   High Fuel Nitrogen Content
o   Lower Volatility
o   Higher Ash Content
o   Higher Trace Element Content
o   Lower Thermal Stability
o   More Corrosive in Nature
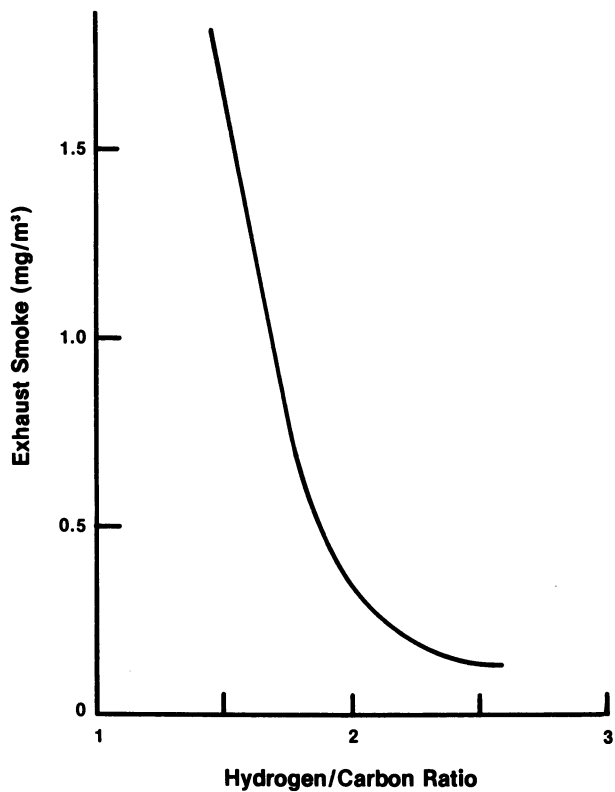o   Lower Heat of Combustion

Figure 1. Effect of hydrogen to carbon ratio on exhaust smoke.
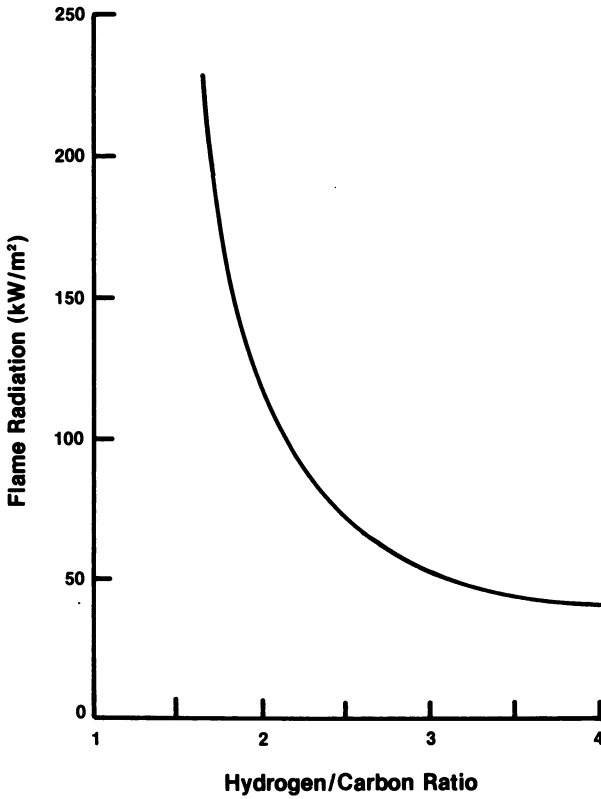(Reproduced with permission from Ref. 7. Copyright 1978, ASME.)

Figure 2. Effect of hydrogen to carbon ratio on flame radia-
tion. (Reproduced with permission from Ref. 7. Copyright
1978, ASME.)

importance of increased soot concentrations in the hot gases to
wall heat flux is very well illustrated in Figure 3, taken from
Toor (11), and developed from the data given by Gosman, et al.
(12).

o   Radiative heat flux is the major mode of heat transfer for
     the typical combustor conditions described in the caption
     over a wide range of carbon concentrations.

o   Both radiative heat flux and the total heat flux are at
     their maximum value corresponding to a particular optical
     thickness. Higher soot concentrations, resulting in in-
     creased optical thickness, may lead to lower wall heat
     fluxes.

     The first point is obvious, because soot is an efficient
emitter and radiation emissions are dependent on the fourth power
of temperature, whereas, convective heat transfer is dependent on
the first power of temperature. For non-uniform temperatures,
such as encountered in practical combustion systems, the lower-
temperature, soot-laden gases near the walls of the furnaces may
actually decrease the amount of radiation arriving at the walls
thus decreasing the wall heat flux.
     The major contributors to radiation are soot, carbon diox-
ide, water vapor, inorganic particulates and other intermediate
products whose concentrations depend upon the particular fuel.
The presence of solid particles such as ash and carbonaceous
material affects the radiation heat transport as they are
continuous emitters, absorbers, and scatterers of radiation.
Carbonaceous particles tend to be large relative to the wave-
length of radiation and have surfaces with high absorptivity.
     Toor and Boni (13) gave results of an investigation in which
they assessed the effect of flow conditions and surface reflect-
ivity on the wall heat flux for a model combustion chamber. They
employed two approximate radiation heat-transfer procedures.
These were the Mayer-Goody molecular band model used in conjunc-
tion with a modified Curtis-Godson scaling approximation to ac-
count for inhomogeneous gases along a line of sight, and a second
technique involving a simpler band model, the just-overlapping
line model, and an exact integration of the radiation transport
equation. Three absorbing emitting species, H_2O, CO_2 and soot
were considered. Figure 4 presents a typical result of the
calculations made by Toor and Boni (13) who also reported on the
effect of temperature profiles, concentration profiles, and soot
on radiation quantities in a model combustor. Of particular note
is the strong contribution shown for the presence of soot.
     The formation of soot in a combustion system has been shown
to correlate well, at least to first order, as a function of the
H/C ratio of the particular fuel. However, for a specific fuel
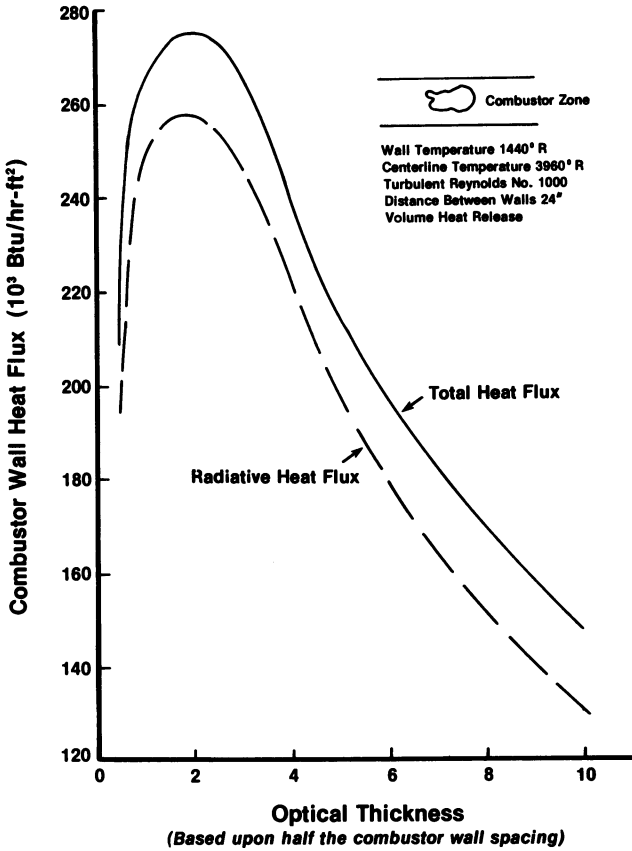the actual amount of soot formed is a function of the combustion

Figure 3. Radiative, convective, and total heat flux to the combustor wall. (Reproduced with permission from Ref. 11. Copyright 1979, Science Applications, Inc.)
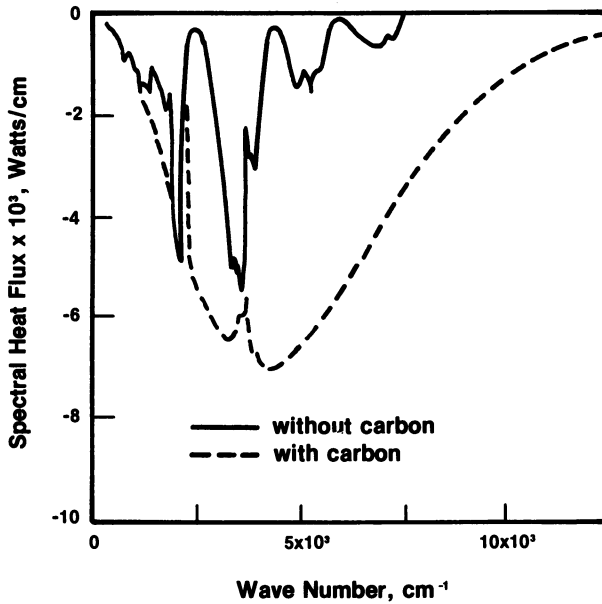
Figure 4. Effect of carbon on the wall heat flux with diffuse walls. Results of coupled radiation–aerodynamic model calculations by Toor and Boni (1974).

system with particular emphasis on the droplet distribution, evaporation, fuel/air mixing, etc. For vaporized fuel and air mixed to stoichiometric proportions, a non-luminous flame results upon burning. However, reduction of the amount of air to below the stoichiometric ratio (fuel-rich combustion), results in the formation of carbon particles at some oxygen/carbon ratio. Subsequent decrease of the oxygen/carbon ratio results in the presence of unoxidized carbon in the combustion products. This result was illustrated very nicely by the early work of Wright (14), c.f. Figure 5. In Figure 5, results are shown for two different combustion systems operating with toluene/air. The upper curve illustrates the results obtained in a flat-flame system while the lower curve demonstrates the behavior of a backmixed, well-stirred reactor. Thus, we also observe that fuel/air mixing is an important determinant of sooting behavior. The intense back-mixing system permits a wider range of soot-free combustion than does a flat flame, where diffusion controls the mixing of products and reactants.

Since carbon is not expected to be formed under equilibrium conditions at the temperatures characteristic of combustion and at an oxygen/carbon ratio in the range of 1.3-2.0, it is apparent that the formation of carbon is a kinetic process. Its presence will therefore depend on the time available for formation and oxidation relative to the flow time available. Wright, (15) for example, interpreted the backmixing observations as an indication that the polymerization process to form soot is a higher order process than the fuel oxidation process. In any event, the essential point to be made here is that the combustion of low H/C ratio fuels, without flame luminosity or soot is made possible by proper preparation of the mixture, including intense mixing in the combustion zone. This point has been made by Longwell (1) who also presented data on the equivalence ratio for incipient carbon formation for fuels with H/C ratio which varied from 2.33 (hexane), 1.14 (toluene), and 0.91 (methyl naphthalene). Table III, taken from Longwell (1) illustrates these points.

Table III

STOICHIOMETRY FOR CARBON FORMATION

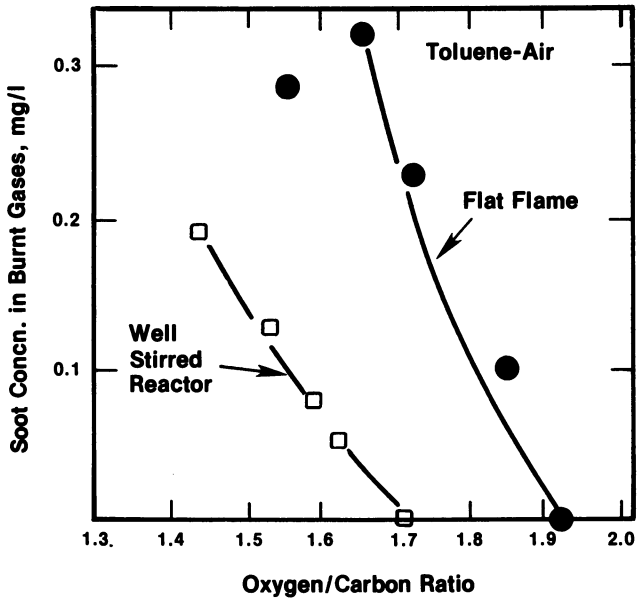| Fuel	H/C	O/C=1	Equivalence Ratio for Incipient Carbon Formation	
			Flat Flame	Well-Stirred Reactor
Hexane, C_6H_{14}	2.33	3.17	1.45	–
Toluene, C_7H_8	1.14	2.57	1.34	1.50
Methyl Naphthalene, $C_{11}H_{10}$	0.91	2.45	1.03	1.51

Figure 5. Soot production in laminar and backmixed system for a toluene-air flame. From Wright (1968).

The organically bound nitrogen found in syncrudes, Table I, accounts for the increased NO_x emissions in synthetic fuel flames. This source of NO_x is in addition to the thermal NO_x formed at the elevated temperatures which promote N_2-O_2 reactions. However, the organically bound nitrogen can be the dominant source of NO_x, as shown in Figure 6, which has been taken from the furnace data of Grumer (6). An additional source of relevant data on residual oil flames (0.05-0.79 wt. percent nitrogen) has been reported by Pershing, et al. (16), and reproduced in Figure 7. They reported that fuel-NO_x formation increased approximately linearly with increased nitrogen content over the range that they studied. It can be seen from Figure 6 that this trend is expected to continue for the nitrogen content of typical synfuels. Figure 7 also illustrates that the percentage conversion of bound nitrogen to NO_x decreases with increasing nitrogen content. Of lesser concern for synthetic fuels is the SO_x problem because of the lower sulfur content compared with that of petroleum crudes. However, doping studies have shown that fuel-bound sulfur can enhance fuel-bound NO_x formation (6).

The fuel physical properties of importance to the combustion process are the viscosity, surface tension, and volatility. The viscosity and surface tension are known to affect the droplet size distribution produced by a given fuel injection system, Figure 8. For example, with the increased values of these properties, we would expect larger fuel droplets from synfuels atomized from the same atomizer used for conventional fuels. Coupled with lower volatility, synfuel droplets are expected to take longer to evaporate than petroleum liquids, Figure 9. For a longer droplet lifetime, there will be a longer time for the fuel to coke. In combination, the droplet size distribution and droplet lifetime affect the large-scale fuel/air distribution and consequently affect the heat-release distribution, emissions and efficiency. In addition, the presence of droplets creates small-scale fuel/air inhomogeneities that can persist depending upon the liquid volatility. These inhomogeneities also affect heat-release distribution, emissions, and efficiency. However, Pershing, et al. (16) found that with a rapid-mix burner operating under fuel-lean conditions, hydrocarbon and nitrogen volatility was not a first-order parameter for NO_x production, fuel NO_x was insensitive to droplet size, but thermal NO_x increased with decreased mean droplet size.

Table IV summarizes the expected impact of the synfuel physical and chemical properties on the combustion process. In general, the properties of alternative and synthetic liquid fuels vary considerably as the fuel types range from unrefined to hydrogenated liquid fuels from coal, shale, and tar sands. Synthetic fuels of various levels of refinement will be used by the industrial, commercial, and utility sectors to produce thermal enegy for direct process heat, mechanical energy, steam, hot water, and the production of electricity. Consequently,
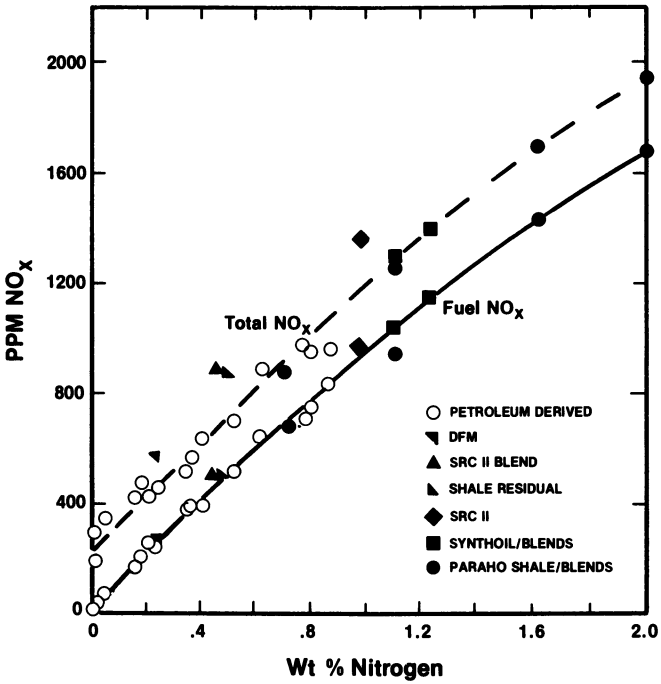
Figure 6. Effect of fuel nitrogen content on total and fuel NO_x. From Grumer (1979).
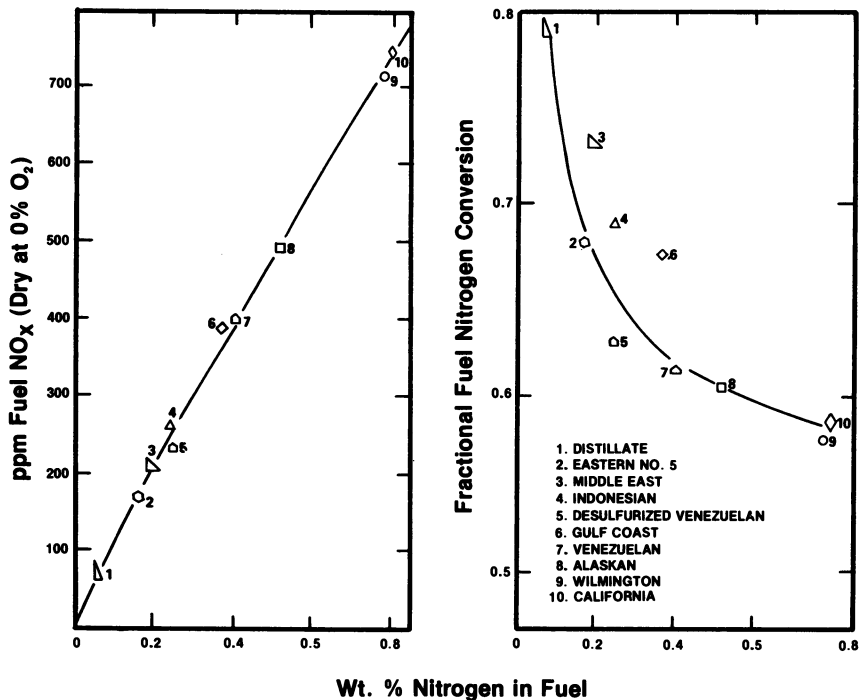
Figure 7. Importance of fuel nitrogen content. All data taken in AR/O$_2$/CO$_2$, tunnel furnace, ultrasonic nozzle, 5% excess O$_2$. (Reproduced with permission from Ref. 16. Copyright 1979, The Combustion Institute.)

LIQUID	DENSITY (g/cc)	VISCOSITY (poise)	SURFACE TENSION (dynes/cm)
Ethylene glycol	1.12	0.199	48
Water	1.00	0.010	73
85% methanol/ 15% glycerin	0.88	0.014	23
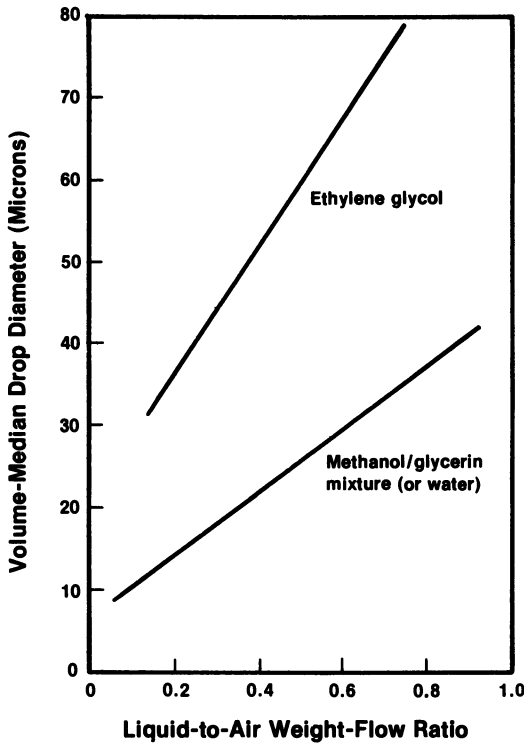
Figure 8. Effect of density, viscosity, and surface tension on droplet size.
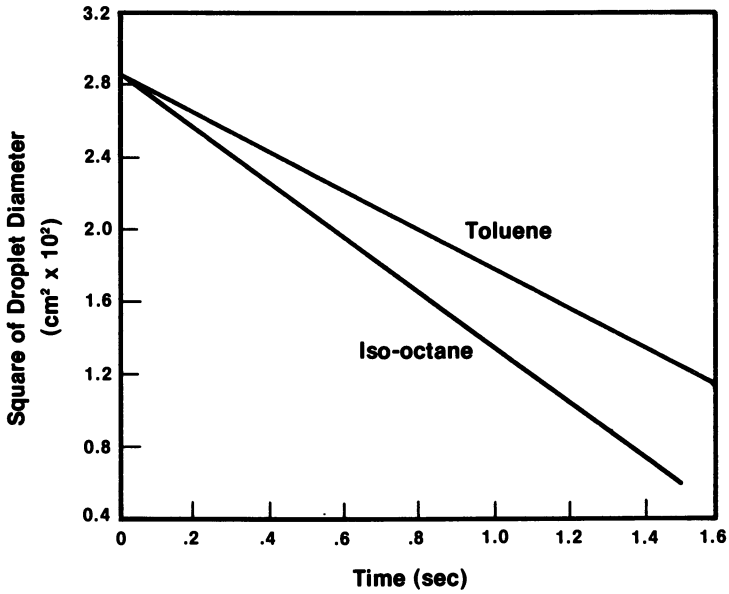
Figure 9. Effect of volatility on evaporation time for fuel droplet burning in oxygen–nitrogen atmosphere.

Table IV

SUMMARY OF SYNFUEL COMBUSTION IMPACTS

PROPERTY	EFFECT	IMPACT
o Lower H/C Ratio o Higher Aromaticity	o Increased Soot Formation	o Modified Radiation and Heat-Load Distribution o Longer Ignition Delay o Pollutant Emissions
o Higher Fuel Bound Nitrogen and Sulfur	o Increased NO_x and SO_x Formation	o Pollutant Emissions o NO_x Control Possibly Requires Staged Combustion
o Higher Ash and Trace Metal Content	o Inorganic Particulate Formation	o Modified Radiation and Heat Load o Deposition/Surface Damage
o Viscosity o Lower Volatility	o Spray Characteristics	o Heat Release Distribution; Ignition Delay o Emissions

various boiler and furnace equipment configurations are involved
in the fuel-utilization problem. The burner and burner/furnace
or boiler combination involve various aerodynamic flow patterns
and turbulence characteristics. these flow field characteristics
couple with the fuel physical and chemical properties in control-
ling the efficiency, emissions, and fuel flexibility character-
istics of practical systems. Understanding these phenomena and
their coupling would provide the link between the combustion
process and the system parameters which can be controlled by the
designer.

Overview of the Advanced Research and Technology Development Program (AR&TD)

As seen in the last section, there are many issues related
to the clean and efficient utilization of synfuels in modern com-
bustion equipment. A body of data, models, and experience
relevant to combustion processes already exists. Advanced
information is being generated continuously, yet gaps exist and
new information is required. The technical complexity of combus-
tion and the rapidity with which synfuels will be utilized re-
quires that the highest technology available be employed in
upgrading combustor design. The multitude of individual proces-
ses that constitute the overall combustion process must be or-
ganized and focused, providing the furnace and boiler manu-
facturers with the technology base required for the timely im-
plementation of synthetic fuels. Because of the complexity of
the combustion process, neither data nor modeling alone can
elucidate the controlling parameters that affect combustion
system performance. Both data and models are needed to sort out
the coupling of the many simultaneous processes that comprise the
combustion process. The integration of balanced data acquisition
and modeling activities is required to accomplish this delinea-
tion and understanding of the individual processes.

The goal of the U. S. Department of Energy AR&TD Program in
Direct Utilization (DU) is to provide scientific and technical
information which is applicable to several end-use concepts for
fossil-fuel utilization. Programs in this area, when coupled
with other ongoing research and development activities will pro-
vide a generic technology base for improved, expanded, and ac-
celerated utilization of synthetic fuels in the utility and
industrial market sectors. As indicated previously, the prin-
cipal combustion related problems associated with the utilization
of synthetic fuels are the evolution of nitrogen species and soot
formation. In addition, as a high priority has been placed on
coal-derived liquids, programmatic emphasis is on spray combus-
tion. The AR&TD (DU) program considers all aspects of the
physics and chemistry of the combustion process and is comprised
of the following study categories:

- Injection/Physical Processes
- Preignition
- Combustion
- Pollutant Formation
- Fouling
- Computational
- Advanced Concepts

The AR&TD (DU) program is an integrated analytical and ex-
perimental program which will establish comprehensive technical
data bases and develop the necessary understanding whereby ad-
vanced combustion systems, which utilize synthetic fuels, can be
designed to operate in an efficient and environmentally accept-
able manner.
    This program will create a hierarchy of data bases to
represent the critical combustion phenomena which have been
observed to control combustor operation. These elements will be
developed into a base of information which may be used to design
and evaluate the thermal efficiency and pollutant output of
burners in combination with furnaces and boilers. Existing
experimental data and new data to fill existing gaps will be
factored into models so that a more complete understanding of
combustor operation will result.
    A quantitative understanding of certain primary combustion
phenomena, e.g., liquid fuel-droplet vaporization and burning,
gas phase chemical reaction kinetics, radiation heat transfer
from combustion products, and mixing of reactants and combustion
products, is required to develop a rational approach for the ef-
fective utilization of synfuels in industrial boiler/furnace
systems. Those processes are defined by the interaction of a
number of mechanisms which are conveniently described in terms of
physical and chemical related processes. The physical processes
are:

1. Liquid fuel injection and atomization
2. Spray penetration and spreading
3. Droplet breakup
4. Droplet evaporation
5. Heat transfer by radiation and convection
6. Aerodynamic flow patterns
7. Turbulent mixing

and the chemical related processes include:

1. Pyrolysis
2. Bound nitrogen conversion
3. Droplet combustion
4. Gas phase oxidation
5. Particulate formation
6. Particulate oxidation
7. PAH formation and oxidation

Although the physical and chemical processes are grouped separately, they are mutually coupled in the combustion process. Due to the complexity of these processes and the lack of complete fundamental information describing them, the design practice has been to resort to rule-of-thumb methods developed from experience and qualitative analysis. The more critical current need for improved utilization, efficiency, and environmental control has led to the requirement for the development of more rational design criteria based upon a mechanistic rather than an empirical basis. Substantial information can be obtained from relatively small laboratory-scale experiments which isolate particular phenomena of interest. These experiments are only of limited practical value since their results cannot be scaled-up to represent the complex coupling between phenomena in industrial furnaces and utility boilers. Development of mathematical models is an essential part of the technology base required to define and explain the many interactions involved in combustion processes and which will lead to scaling and design tools. To relate performance and efficiency to geometry, fuel type, and mode of operation requires that small-scale laboratory experiments as well as larger-scale testing be used to verify the combustion and combustor models. Figure 10 depicts the phenomena which comprise the combustion processes, their interactions, and the manner in which they influence combustor behavior. As one proceeds down this list of phenomena, the interactions become increasingly complex and important. The models and/or data bases which represent the phenomena and which will be the output of the program are indicated on the right-hand side of the figure.

The current composition of the AR&TD program and its focus is summarized in Table 5. Here we indicate the various contractors and the study areas emphasized in the various projects. It can be seen that the principal focus of the program is on the major areas of concern related to synfuel combustion, viz NO_x emissions and soot formation. The program is balanced with both analytical and experimental studies, with the principal experimental activities taking place in bench-scale apparatus. Several of the studies will also include measurements performed in environments relative to industrial combustor and commercial-scale burners.

It is not possible in the present paper to describe the content and results of these programs because of space limitations. However, results from these projects will be presented later in this Symposium by representatives of their respective organizations.

Summary and Conclusions

The clean and efficient utilization of synthetic liquid fuels requires a detailed understanding of the chemical, physical, and combustion characteristics of these fuels as they burn in utility and industrial combustion equipment. We have
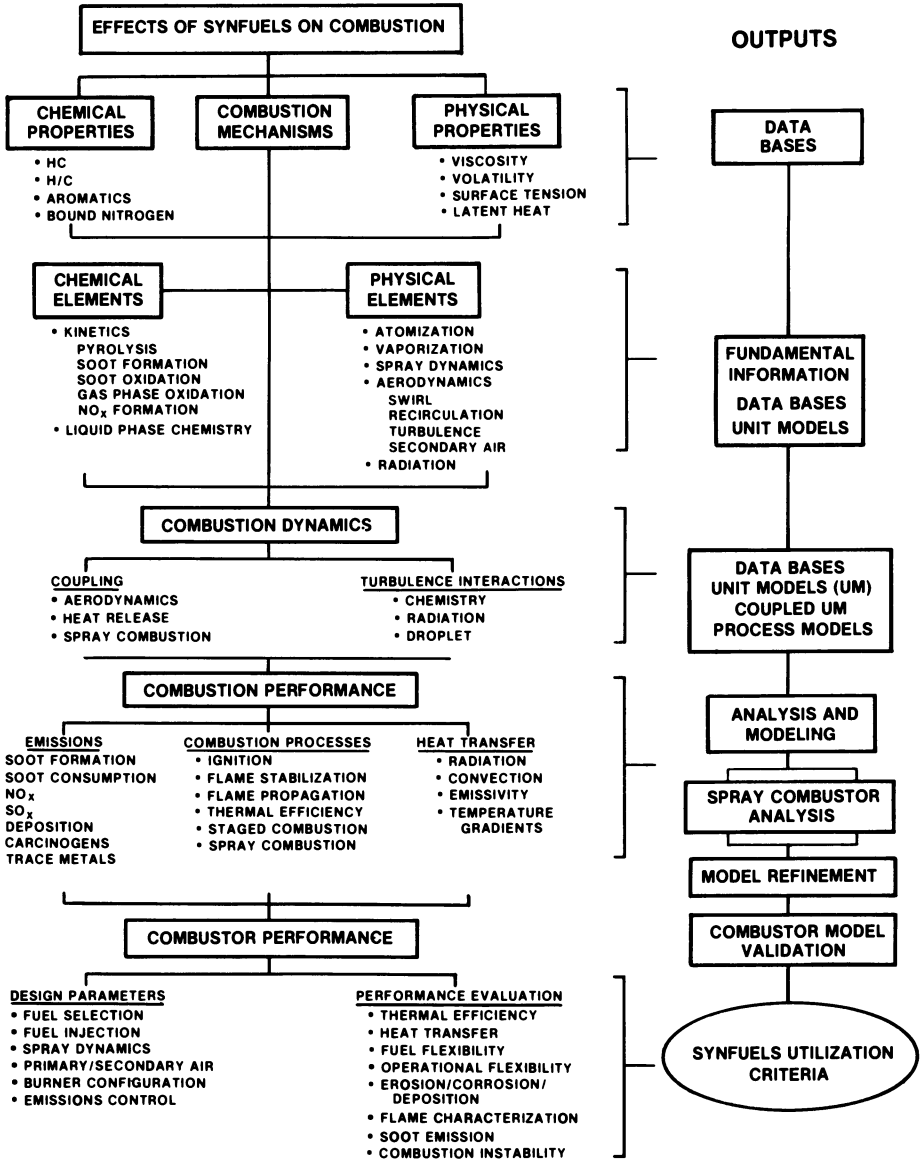
Figure 10. Effect of synfuels on combustion.

TABLE V
AR&TD STUDY AREA – CONTRACTOR MATRIX

Contractors (columns):

- **C1** — SPECTRON DEVELOPMENT LABORATORIES — Synfuel Spray Combustion Characteristics
- **C2** — CARNEGIE-MELLON UNIVERSITY — Characterization of Chemical Composition of Multicomponent Liquid Fuel Droplets During Combustion
- **C3** — BATTELLE COLUMBUS LABORATORIES — Aromaticity and Staged Combustion
- **C4** — UNITED TECHNOLOGIES RESEARCH CENTER — Soot Formation Characteristics in Alternate Liquid Fuels
- **C5** — PRINCETON UNIVERSITY — Chemical Kinetic Mechanisms of Combustion
- **C6** — UNITED TECHNOLOGIES RESEARCH CENTER — Combustion of Spray Droplet Arrays
- **C7** — PHYSICAL SCIENCES, INC. — Pollutant Formation
- **C8** — ENERGY & ENVIRONMENTAL RESEARCH CORP. — Soot Formation in Fuel Droplets
- **C9** — AEROCHEM — Soot Formation in Synfuels
- **C10** — GULF R&D — Component Effect on Soot Formation and NO_x Production
- **C11** — MASSACHUSETTS INSTITUTE OF TECHNOLOGY — Coal Liquid NO_x Control
- **C12** — EXXON RESEARCH & ENGINEERING COMPANY (SCIENCE APPLICATIONS, INC., Subcont.) — Characterization of Continuous Combustion Systems
- **C13** — SCIENCE APPLICATIONS, INC. — Fundamental Combustion, Design and Performance

STUDY AREA	C1	C2	C3	C4	C5	C6	C7	C8	C9	C10	C11	C12	C13
CHEMICAL PROPERTIES OF FUELS		E, A	E, A	E		E							X
PHYSICAL PROPERTIES OF FUELS		E, A	E, A	E									X
CHEMICAL REACTIONS – LIQUID PHASE			E, A		E, A	E							A
SPRAY DYNAMICS	E												E, A
EMISSIONS (NO_x, SO_x)			E, A		E, A		E, A	E, A	E	E, A	E, A		E, A
PARTICULATES (Other Than Soot)												E, A	E, A
SOOT		A	E, A	E		E	E, A	E, A	E	E	E, A	E, A	E, A
DROPLET STUDIES	E							E, A					A
AERODYNAMICS										E, A	E, A		E, A
HEAT TRANSFER											E, A		E, A
BENCH-SCALE SPRAY COMBUSTION	E		E, A			E	E, A	E, A			E, A		E, A
SUBSCALE INDUSTRIAL COMBUSTORS													E, A
COMMERCIAL BURNERS													

X – Consolidation and Assessment
A – Analytical Study (Not Necessarily Modeling But Could Be Data Reduction Only)
E – Experimental Study

seen that the performance of combustion equipment with synthetic fuels is considerably different than with conventional fuels and that the design and/or retrofit of equipment to burn these fuels will require extrapolation beyond the current data base with tools that do not currently exist or have not been validated. Results to date have indicated that the ability to burn these fuels with minimal soot and NO_x emissions will require the development of staged-combustion systems. It has been shown that the sooting limits for aromatic fuels occur at mixture conditions at which hydrocarbons are first observed in the combustion products, and that the minimization of fuel nitrogen conversion requires operating at the higher fuel-air ratio prior to the breakthrough point (17, 18). The results have been obtained under rather idealized conditions, i.e., either in a jet-stirred combustor or in a staged-combustion facility designed to control the flow and mixing characteristics.

Nevertheless, these results are consistent with a number of other recent studies performed in a variety of burner/furnace systems (19-22). Staged combustion of heavy oils with a nitrogen content ranging from 0.3% to 0.7% by weight for operation at 1MW ($\sim$3 x 10^6 Btu/hr) resulted in a minimum of NO_x emissions for a fuel-air equivalence ratio of 0.6-0.7 shown in Figure 11, taken from Payne, et al. (19). The minimum NO_x emission level depended on burner type (Figure 11) and the percent nitrogen in the fuel. This latter result for staged combustion is shown in Figure 12 taken from the work of England, et al (22). Extension of these results available to date to utility boiler scale and conditions is not straightforward except as general guidelines, in that fuel injection, droplet-air mixing, droplet vaporization, etc. will inevitably result in mixture inhomogenieties on a microscale within practical equipment.

The current AR&TD program is providing the understanding of synthetic fuels combustion necessary to accelerate the utilization of synthetic fuels in full-scale equipment. Through these programs and the data produced therein, an extensive data base and modeling capability will be established and validated for combustion of synfuels under conditions applicable to practical combustor operation. From this integrated information, the AR&TD program will yield effective utilization criteria for full-scale applications.
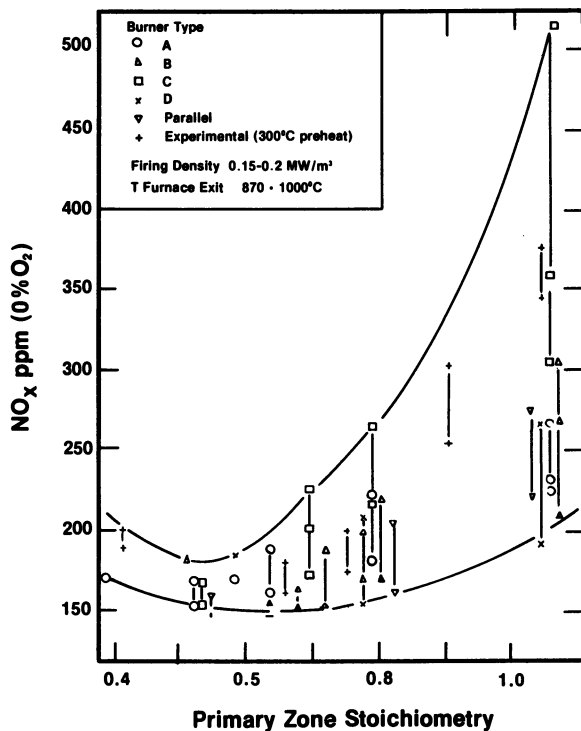
Figure 11. Burner optimization for low NO_x-emission with staged combustion. (Reproduced with permission from Ref. 19. Copyright 1980.)
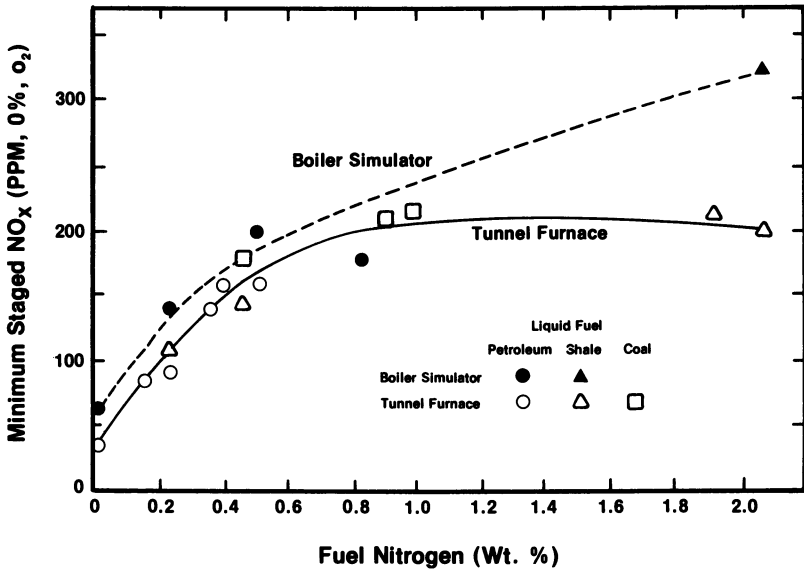
Figure 12.   Minimum NO_x achievable under staged conditions.
(Reproduced with permission from Ref. 22.   Copyright 1979.)

Literature Cited

1. Longwell, J. P., "Synthetic Fuels and Combustion," Sixteenth International Symposium on Combustion, The Combustion Institute, Pittsburgh, PA, 1976; pp. 1-15.
2. Black, C.H., "Review and Analysis of Spray Combustion as Related to Alternative Fuels," Argonne National Laboratory, ANL-79-77; 1979.
3. Bowman, C.T., and Birkeland, J., Alternate Hydrocarbon Fuels: Combustion and Chemical Kinetics, Progress in Astronautics and Aeronautics, Vol. 62, published by American Institute of Aeronautics and Astronautics, New York, 1978.
4. England, G. C., Heap, M. P., Pershing, D.W., Nihart, R. K., and Martin, G.B., "Mechanisms of NO$_x$ Formation and Control: Alternative and Petroleum-Derived Liquid Fuels," 18th Symposium on Combustion, The Combustion Institute, 1981.
5. Muzio, L. J. and Arand, J. K., "Combustion and Emission Characteristics of Coal-Derived Liquid Fuels," EPRI Report AP-1878, 1981.
6. Grumer, J., Cohn, A., and Stein, T. R., "Combustion of Coal Derived Liquid Fuels," Paper Presented to Symposium On New Fuels and Advances in Combustion Technologies sponsored by Institute of Gas Technology, 1979.
7. Naegeli, D. W., and Moses, C. A., "Fuel Property Effect on Combustor Performance," ASME Paper 79-GT-178, 1978.
8. Pillsbury, P. W., Cohn, A., Mulik, P. R., and Stein, T. R., "Investigating Combustion Turbine Burner Performance with Coal Derived Liquids Having High Fuel Bound Nitrogen, "ASME Paper 78-GT-126, 1978.
9. Pillsbury, P. W., Cohn, A., Mulik, P. R., and Stein, T. R., "Fuel Effects in Recent Combustion Turbine Burner Tests of Six Coal Liquids," ASME Paper 79-GT-137, 1979.
10. Sarofim, A. F., "Flame Emissivities: Alternative Fuels," Alternative Hydrocarbon Fuels: Combustion and Chemical Kinetics, Vol. 62, Progress in Astronautics and Aeronautics, C. T. Bowman and J. Birkeland, Editors, 1977.
11. Toor, J. S., "Effect of Soot in Flames on Wall Heat Flux," Science Applications, Inc., report, September 1979.
12. Gosman, A. D., Heat and Mass Transfer in Recirculating Flows, Academic Press, New York, 1969.
13. Toor, J. S. and Boni, A. A., "A Model Combustor Heat Transfer Problem-Radiative Transfer Between Surfaces With Nongray Gases and Soot," Heat Transfer 1974, Vol. 1, Proc. of 5th International Heat Transfer Conference, Tokyo, Japan, 1974.
14. Wright, F. J., "The Formation of Carbon Under Well-Stirred Conditions," 12th Symposium (International) on Combustion, The Combustion Institute, Pittsburgh, PA, 1968; pp 867-875.
15. Wright, F. J., "Carbon Formation Under Well Stirred Conditions. Part II." Combustion & Flame 15, 217, 1970.

16. Pershing, D. W., Cicanowicz, J. E., England, G. C., Heap, M.
    P., and Martin, G. B., "The Influence of Fuel Composition and
    Flame Temperature on the Formation of Thermal and Fuel NOx
    in Residual Oil Flames," Seventeenth Symposium (International
    on Combustion, pp 715-726, The Combustion Institute,
    Pittsburgh, PA, 1979.
17. Blazowski, W. S., Sarofim, A. F., and Keck, J. C., "The Inter-
    relationship between Soot & Fuel NO_x Control in Gas Turbine
    Combustors," ASME Paper No. 80-GT-76, presented at the Gas
    Turbine Conference and Products Show, 1980.
18. Beer, J. M., Jacques, M. T., Farmayan, W., and Taylor, B. R.,
    "Fuel-Nitrogen Conversion on Staged Combustion of a High
    Nitrogen Petroleum Fuel", pp 101-10, Eighteenth Symposium
    (International) on Combustion, The Combustion Institute,
    Pittsburgh, PA, 1981.
19. Payne, R., Akiyama, T., and Witkamp, J. G., "Pollutant
    Emission Characteristics of Oil Fired Industrial Process
    Boilers," Paper presented at American Flame Research
    Committee, International Symposium on Industrial Process Com-
    bustion Technology, Newport Beach, California, October, 1980.
20. Hirose, Y., and Tanaka, R., "Low-NO_x Combustion Technology in
    Japan - History and Future Trend," Paper presented at
    American Flame Research Committee, International Symposium on
    Industrial Process Combustion Technology, Newport Beach,
    California, October, 1980.
21. Martin, R. E., and Nickerson, D., "Low NO_x Burner Development
    for High Temperature Refining and Cracking Furnaces," Paper
    presented at American Flame Research Committee, International
    Symposium on Industrial Process Combustion Technology, New-
    port Beach, California, October, 1980.
22. England, G. C., Pershing, D. W., Tomlinson, J., and Heap, M.
    P., "Emission Characteristics of Petroleum and Alternate
    Liquid Fuels," American Flame Research Committee, Inter-
    national Symposium on NO_x Reduction, October, 1979.

Combustion and Emissions of Synthetic Fuel Components

Analysis and Modeling

R. B. EDELMAN, R. C. FARMER, and T.-S. WANG

Science Applications, Inc., Chatsworth, CA 91311

Synthetic fuels derived from non-petroleum sources are expected to play an increasingly important role in meeting the future national energy demand. The properties of these fuels can result in significantly different combustion performance than that obtained with conventional fuels. For example, decreased hydrogen can result in increased flame luminosity and exhaust smoke emission, increased fuel bound nitrogen can result in increased NO_x emissions, and decreased fuel volatility can result in significant modification of the flowfield within a combustion chamber. This investigation relates certain of these phenomena to the basic properties of the fuel by an analytical quasiglobal kinetics model and modular combustor models. Appropriate models have been developed for a typical aromatic and a typical aliphatic component of synthetic fuels, toluene and iso-octane, respectively. Soot and NO_x emissions are given particular attention in these models. Experimental data from several sources have been used to both develop and verify these models.

Synfuels differ from petroleum fuels primarily in the amount of nitrogen and oxygenated species which they contain and in their aromatic content. The nitrogen and oxygen concentrations are in the range of 20-50 times larger in the synfuels; they are present as heterocyclic ring compounds and phenols (1, 2). Coal-derived liquid fuels in the middle boiling distillate range are mainly single-ring aromatics; in the heavy boiling range, they are mainly 2- and 3-ring aromatics (3). These compositional variations have suggested that the tendency for sooting and NO_x emissions of synfuels must be predictable under wide-range conditions and applications. This investigation relates important combustion characteristics, including efficiency and emissions of CO, soot and NO_x to the properties of typical synfuel components. The approach is one

involving the development of a quasiglobal kinetics model to rep-
resent the rate of fuel oxidation including the formation and
decomposition of intermediate hydrocarbons, CO, NO_x and soot.
This kinetics model is designed to characterize fundamental com-
bustion observations in such a manner that it can be used to help
establish effective synfuels utilization criteria. The paper
describes the methodology together with typical examples of its
application.

Quasiglobal Kinetics

The phenomenology of the oxidation process can be conve-
niently described in terms of the major steps identified with the
generic quasiglobal model given in Table I. When a hydrocarbon
fuel is subjected to elevated temperatures the molecules tend to
pyrolyze into smaller fragments. In the presence of even trace
amounts of oxygen, an accelerated pyrolysis, oxidative pyrolysis,
occurs. Many stable and radical hydrocarbon species are made by
these pyrolysis reactions. It is, this large number of species
which makes the description of hydrocarbon combustion difficult.
However, the small stable molecules including acetylene, ethylene,
and methane constitute a large fraction of the pyrolyzed hydrocar-
bon fragments. The parent fuel and these intermediate fragments
partially burn to form species such as CO, H_2 and partially oxi-
dized hydrocarbons including the aldehydes which then react to
completion to form CO_2 and H_2O. Under rich combustion conditions,
soot can both form and subsequently gasify in leaner regions.
Finally, NO_x either from direct fuel nitrogen conversion or ther-
mal fixation will be produced during the combustion process. The
abbreviation of the true reaction mechanism occurs when specific
species and reactions are selected to represent these major steps
that comprise the overall oxidation process. Thus, the current
approach includes pure and oxidative pyrolysis, partial oxidation,
soot formation and gasification, and NO_x formation by thermal fix-
ation and fuel bound nitrogen conversion.
The quasiglobal concept was first introduced in 1969 (4), as
an approach to characterize finite-rate heat release in lean ali-
phatic hydrocarbon combustion. This early work demonstrated that
many observations on the rate of combustion of hydrocarbons could
be predicted by a relatively simple kinetic scheme. One of the
most significant observations made from the available data is the
similarity of ignition delay times for hydrocarbons in homologous
series. There are exceptions to this behavior and methane is an
important example of a hydrocarbon in the paraffin (alkane) series
having significantly longer ignition delay times than the higher
hydrocarbons in the same series. This difference can be traced to
the importance of the methyl radical (CH_3) formed during the
decomposition of methane. For the higher hydrocarbons (propane
and above) the similarity in oxidation behavior suggested to us
that the prediction of significantly more detail of the oxidation

TABLE I. GENERIC QUASIGLOBAL MODEL.

I PURE PYROLYSIS	$\begin{bmatrix} ALIPHATICS \\ AROMATICS \end{bmatrix} \rightarrow \begin{bmatrix} C_2H_2 \\ CH_4 \\ C_2H_4 \\ H_2 \end{bmatrix} \equiv$ INTERMEDIATES
II OXIDATIVE PYROLYSIS	$\begin{bmatrix} ALIPHATICS \\ AROMATICS \end{bmatrix} + \begin{bmatrix} OH \\ O_2 \end{bmatrix} \rightarrow \begin{bmatrix} CH_4 \\ C_2H_2 \\ C_2H_4 \end{bmatrix} + \begin{bmatrix} H_2 \\ C_xH_yO_z \end{bmatrix}$
III PARTIAL OXIDATION	$\begin{bmatrix} ALIPHATICS \\ AROMATICS \\ CH_4 \\ C_2H_2 \\ C_2H_4 \end{bmatrix} + \begin{bmatrix} O_2 \\ OH \end{bmatrix} \rightarrow \begin{bmatrix} H_2 \\ CO \\ C_xH_yO_z \\ CO_2 \\ H_2O \end{bmatrix}$
IV ELEMENTARY STEPS TO COMPLETION	$\begin{bmatrix} CO \\ H_2 \\ C_xH_yO_z \\ H_2O_2 \end{bmatrix} + \begin{bmatrix} O \\ H \\ OH \\ CHO \\ HO_2 \end{bmatrix} \rightleftarrows \begin{bmatrix} H_2O \\ CO_2 \end{bmatrix}$

TABLE I.   GENERIC QUASIGLOBAL MODEL (continued).

V SOOT FORMATION	$\begin{bmatrix} \text{ALIPHATICS} \\ \text{AROMATICS} \\ \text{INTERMEDIATES} \end{bmatrix} \rightarrow \text{SOOT}$
VI SOOT GASIFICATION	$\text{SOOT} + \begin{bmatrix} O_2 \\ CO \\ CO_2 \\ H_2O \\ H_2 \\ OH \end{bmatrix} \rightarrow \begin{bmatrix} CO \\ CO_2 \\ CH_4 \end{bmatrix}$
VII NO$_x$ FORMATION	$\text{FUEL} + \begin{Bmatrix} FBN \\ N_2 \end{Bmatrix} \rightarrow \begin{bmatrix} HCN \\ NH_i \end{bmatrix}$ $\begin{bmatrix} HCN \\ NH_i \end{bmatrix} + \begin{bmatrix} O_2 \\ OH \end{bmatrix} \rightleftharpoons \begin{bmatrix} NO \\ NO_2 \end{bmatrix}$ $\Big\}$ BOUND NITROGEN AND/OR FUEL RICH NITROGEN CONVERSION $\begin{bmatrix} N_2 \\ O_2 \\ N \end{bmatrix} + \begin{bmatrix} O \\ N \\ OH \end{bmatrix} \rightarrow NO + \begin{bmatrix} N \\ O \\ H \end{bmatrix}$ THERMAL FIXATION

process might be obtainable by extending the notion of a single-
step overall reaction to a scheme which characterizes the reac-
tions high up in the chain with one or more "subglobal" steps
coupled to a set of better known detailed reversible reactions to
characterize the kinetics processes at the lower end of the chain.
We introduced the term "quasiglobal" as a definition of this type
of kinetics modeling.

That work led to the demonstration that fuel-lean combustion
and lean NO_x emissions for both long chain and cyclic type hydro-
carbon fuels could be characterized by quasiglobal kinetics (5, 6).
However, the need to address fuel-rich combustion and wide operat-
ing ranges and applications to cover residential, commercial and
industrial utilization became apparent, particularly in view of
the advent of synthetic fuels. Following the suggestions of
Edelman and Harsha (6), the current extended quasiglobal model was
postulated, Table I (7). A significant feature of this model is
the direct coupling of the intermediate radicals to the subglobal
steps high up in the chain.

To address the primary compositional characteristics of coal-
derived type synthetic fuels, a neat aromatic hydrocarbon (tolu-
ene) and a neat aliphatic hydrocarbon (n-octane) were selected for
this study.

Although, in certain instances, rate parameters can be esti-
mated using classical techniques the primary source for this
information is empirical. Typical Arrhenius fits are employed
even for the most detailed kinetics and mechanism treatments that
have been proposed for various chemical systems (8, 9).

The required data for quasiglobal model development includes:
concentrations of major species including soot and nitrogenous
species, reaction temperature, heat loss, and pressure as func-
tions of operating conditions that control the progress of the
oxidation process. Ideally, the source of this information should
be devoid of rate phenomena other than chemical kinetics. Turbu-
lent transport, mixing and multi-dimensionality are such factors
that should be avoided or otherwise properly taken into account in
order to obtain valid data for the development and validation of
the chemical kinetics model. Stirred reactors, plug-flow reac-
tors, shock-tubes, and laminar flat-flames are conceptually
sources of kinetics data. In combination, this array of experi-
mental tools would provide a broad range of operating conditions
useful in developing and validating various aspects of the postu-
lated mechanism. Initiation, propagation, branching, quenching,
and completion of reaction can each be more specifically delin-
eated according to the particular reactor selected. In the cur-
rent research a set of Exxon Jet-Stirred Combustors were selected
as the primary source of data. These reactors are based upon the
Longwell design and have proven to be appropriate for quasiglobal
model development and validation (5). Furthermore, the intense
backmixing characteristic of the Jet-Stirred Combustor represents

the limiting flow behavior of primary zones and flame stabiliza-
tion regions in many practical burners and combustors.

A series of experiments were performed by Exxon Research and
Engineering Co., and the results were utilized in the current
modeling effort. Although the global steps in the quasiglobal
toluene and iso-octane kinetics model were developed to represent
these data, the range of applicability of the model was further
tested by analyzing kinetics data from shock-tube experiments.

The global reactions considered include the conversion by
pure pyrolysis of toluene to acetylene and the conversion of iso-
octane to ethylene, oxidative pyrolysis of the acetylene and eth-
ylene, and partial oxidation of the parent fuels and these hydro-
carbon intermediates to CO, H_2, and H_2O. The specific reactions
and rates for this system are given in Table II. Soot formation
is assumed to be a function of temperature and oxygen and precur-
sor concentrations. In the present study the soot precursors are
taken to be acetylene and toluene, expressed as C_2 hydrocarbons.
Soot oxidation is modeled with the semi-empirical relationship
developed by Nagle and Strickland-Constable (10), which includes
an explicit dependence on soot size, oxygen concentration, and
temperature. The chemical equations and rate expressions for the
overall toluene/iso-octane model are given in Table II. Note that
the precursors that were used preclude iso-octane from forming
soot. This is consistent with the Exxon data but obviously not
valid for all iso-octane combustion conditions. The NO_x emissions
submodel includes thermal fixation reactions, nitrogen/hydrocarbon
interaction reactions, hydrocarbon fragmentation reactions, and a
global fuel-bound nitrogen decomposition reaction. The interac-
tion and fragmentation reactions developed by Levy (11) to repre-
sent methane and C_2 combustion were used in this study. These
interactions include: FBN species decomposition to HCN, HCN con-
version reactions to NO which include reactions involving NH_i spe-
cies as intermediates, and reactions with hydrocarbon radicals
such as CH_3, CH_2, CH, and CHO. The contribution of longer chain
radicals to these interaction routes to NO has not been estab-
lished. The hydrocarbon fragmentation reactions convert the
intermediate hydrocarbons into the small hydrocarbon radicals
which are included in the coupled N_2/HC reaction set.

The global rates were determined by direct comparison of pre-
dictions, using selected sets of rates, with the near adiabatic
data obtained from the Exxon Jet-Stirred Combustor (12). The par-
ticular set of rate parameters resulting from this process are given
in Table II. A detailed comparison between the predictions using
the quasiglobal kinetics model and the Exxon data are shown in
Figures 1 through 5. Figure 1 compares the predicted temperature
to experimental values over a range of equivalence ratios for tol-
uene with near adiabatic operation of the reactor. Species pre-
dictions for CO, CO_2, O_2, soot and unburned hydrocarbons are shown
in Figure 2 for these same experiments. These species were mea-
sured by extracting samples, and the limited chemical analyses

TABLE II. QUASIGLOBAL TOLUENE AND ISO-OCTANE MODEL

GLOBAL STEPS

1	Reaction	$C_7H_8 \rightarrow \frac{7}{2} C_2H_2 + \frac{1}{2} H_2$
	Rate Expression	$[\dot{C_7H_8}] = -A[C_7H_8] \exp \{-E/RT\}$
2	Reaction	$C_7H_8 + OH \rightarrow \frac{7}{2} C_2H_2 + H_2 + \frac{1}{2} O_2$
	Rate Expression	$[\dot{C_7H_8}] = -A[C_7H_8][OH] \exp \{-E/RT\}$
3	Reaction	$C_7H_8 + \frac{7}{2} O_2 \rightarrow 7 CO + 4 H_2$
	Rate Expression	$[\dot{C_7H_8}] = -A[C_7H_8]^{0.5}[O_2] \, T \exp \{-E/RT\}$
4	Reaction	$C_2H_2 + 6 OH \rightarrow 2 CO + 4 H_2O$
	Rate Expression	$[\dot{C_2H_2}] = -A[C_2H_2][OH] \exp \{-E/RT\}$
5	Reaction	$C_2H_2 + 2 OH \rightarrow 2 CO + 2 H_2$
	Rate Expression	$[\dot{C_2H_2}] = -A[C_2H_2][OH] \exp \{-E/RT\}$
6	Reaction	$C_8H_{18} \rightarrow 4 C_2H_4 + H_2$
	Rate Expression	$[\dot{C_8H_{18}}] = -A[C_8H_{18}] \exp \{-E/RT\}$
7	Reaction	$C_8H_{18} + OH \rightarrow 4 C_2H_4 + \frac{3}{2} H_2 + \frac{1}{2} O_2$
	Rate Expression	$[\dot{C_8H_{18}}] = -A[C_8H_{18}][OH] \exp \{-E/RT\}$

TABLE II.   QUASIGLOBAL TOLUENE AND ISO-OCTANE MODEL (continued).

8	Reaction	$C_8H_{18} + 4\ O_2 \rightarrow 8\ CO + 9\ H_2$
	Rate Expression	$[C_8\dot{H}_{18}] = -A[C_8H_{18}]^{0.5}[O_2]\ T\ \exp\{-E/RT\}$
9	Reaction	$C_2H_4 + 8\ OH \rightarrow 6\ H_2O + 2\ CO$
	Rate Expression	$[C_2\dot{H}_4] = -A[C_2H_4][OH]\ \exp\{-E/RT\}$
10	Reaction	$C_2H_4 + 2\ OH \rightarrow 3\ H_2 + 2\ CO$
	Rate Expression	$[C_2\dot{H}_4] = -A[C_2H_4][OH]\ \exp\{-E/RT\}$
11	Reaction	$\frac{7}{2}\ C_7H_8 + C_2H_2 \equiv HC \rightarrow SOOT$
	Rate Expression	$[\dot{SOOT}] = +AT^b[HC]^{1.81}[O_2]^{-0.5}\exp\{-E/RT\}$
12	Reaction	$SOOT + O_2 \rightarrow CO_2$
	Rate Expression	$[\dot{SOOT}] = -12\ P_{O_2}A_t\left[\dfrac{K_A X}{1 + K_Z P_{O_2}} + K_B(1 - X)\right]$

WHERE: $X = \left[1 + K_T/(K_B P_{O_2})\right]^{-1}$

$K_i = A_i \exp\{-E_i/RT\}$, for i = A, B, T, Z

$A_t = 6\ C_S/\rho_S \cdot D_S$ [surface area of soot/vol]

P_{O_2} = partial pressure of O_2 [atm]

C_S = mass soot/vol

ρ_S = soot density

D_S = mean diameter of soot

[SOOT] = concentration of soot [mass/vol]
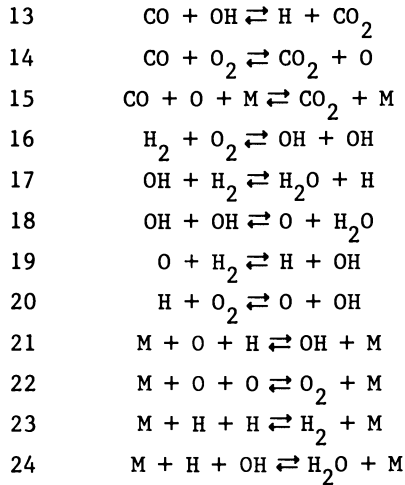
$[\dot{\ }]$ = rate of change of indicated concentration

UNITS: gm mol, CC, K

TABLE II. QUASIGLOBAL TOLUENE AND ISO—OCTANE MODEL (continued).

RATE PARAMETERS FOR GLOBAL REACTIONS

Reaction	A	b	E/R
1	1.259E16	0	4.932E4
2	3.5 E13	0	1.510E3
3	4.60 E11	1.0	3.271E4
4	1.662E15	0	1.208E4
5	1.416E21	−3.0	1.761E3
6	1.259E17	0	4.932E4
7	3.50 E13	0	1.510E3
8	6.055E11	1.0	3.271E4
9	2.202E15	0	1.208E4
10	1.416E21	−3.0	1.761E3
11	4.660E14	−1.94	1.611E4
12A	2.00 E 1	0	1.509E4
12B	4.46 E−3	0	7.649E3
12T	1.51 E 5	0	4.882E4
12Z	2.13 E 1	0	−2.063E3

ELEMENTARY STEPS

Wet CO Mechanism*

13     $CO + OH \rightleftarrows H + CO_2$

14     $CO + O_2 \rightleftarrows CO_2 + O$

15     $CO + O + M \rightleftarrows CO_2 + M$

16     $H_2 + O_2 \rightleftarrows OH + OH$

17     $OH + H_2 \rightleftarrows H_2O + H$

18     $OH + OH \rightleftarrows O + H_2O$

19     $O + H_2 \rightleftarrows H + OH$

20     $H + O_2 \rightleftarrows O + OH$

21     $M + O + H \rightleftarrows OH + M$

22     $M + O + O \rightleftarrows O_2 + M$

23     $M + H + H \rightleftarrows H_2 + M$

24     $M + H + OH \rightleftarrows H_2O + M$

* Rates were taken from Reference 4.

TABLE II.   QUASIGLOBAL TOLUENE AND ISO-OCTANE MODEL (continued).

H_2O_2 Mechanism[+]

25	$M + H_2O_2 \rightleftarrows 2\ OH + M$
26	$H_2O_2 + O_2 \rightleftarrows 2\ HO_2$
27	$H_2O_2 + H \rightleftarrows H_2 + HO_2$
28	$H_2O_2 + OH \rightleftarrows H_2O + HO_2$
29	$HO_2 + OH \rightleftarrows O_2 + H_2O$
30	$HO_2 + O \rightleftarrows O_2 + OH$
31	$HO_2 + H \rightleftarrows 2\ OH$
32	$HO_2 + H \rightleftarrows O_2 + H_2$

HCHO Mechanism*

33	$HCHO + OH \rightleftarrows H_2O + CHO$
34	$HCHO + H \rightleftarrows H_2 + CHO$
35	$HCHO + O \rightleftarrows OH + CHO$
36	$CHO + OH \rightleftarrows H_2O + CO$
37	$CHO + H \rightleftarrows H_2 + CO$
38	$CHO + O \rightleftarrows OH + CO$
39	$HCHO + HO_2 \rightleftarrows H_2O_2 + CHO$
40	$CHO + HO_2 \rightleftarrows O_2 + HCHO$
41	$CHO + O_2 \rightleftarrows HO_2 + CO$
42	$HCHO + M \rightleftarrows H + CHO + M$
43	$CHO + M \rightleftarrows CO + H + M$

+ Rates were taken from Reference 9.
* Rates were taken from Reference 4.
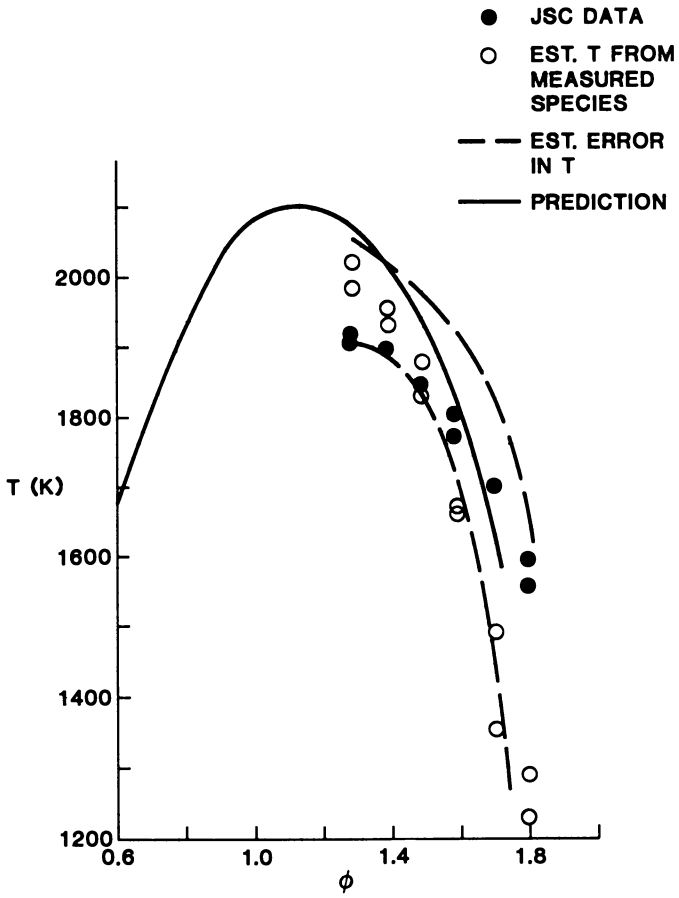
Figure 1. Toluene Combustion as Measured in Exxon JSC and as Predicted.
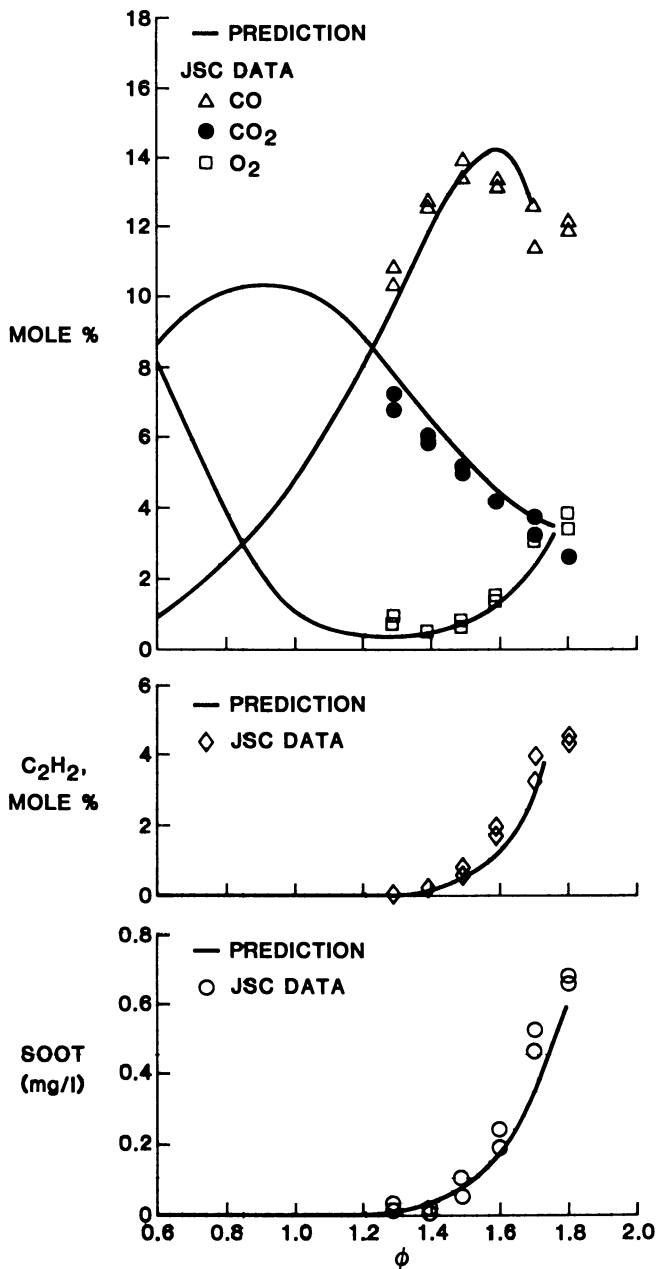
Figure 2.   Toluene Combustion as Measured in Exxon JSC and as Predicted.

indicated the unburned hydrocarbons to be mostly acetylene. The
comparisons are excellent. Neither water nor hydrogen were mea-
sured in this series. However, similar comparisons were also made
for nominal 1900°K and 1700°K isothermal experiments for the same
range of equivalence ratios. Hydrogen was measured in these
experiments. Thus, hydrogen and water (by difference) could also
be compared. For the 1900°K case, the comparisons were very simi-
lar to the adiabatic data shown. For the 1700°K case, the accu-
racy of the measured gas temperature was questionable. Near iso-
thermal operation required adjustment of the nitrogen content in
the "air" stream. This mode of operation did not always yield a
good comparison of temperatures calculated from the energy balance
using the measured species with the measured temperatures. Resi-
dence times for these comparisons were 3 msec and the pressure was
1 atm.

Detailed comparisons for near adiabatic combustion of iso-
octane are shown in Figures 3 and 4. Figure 3 shows temperature
and Figure 4 shows CO, CO_2, O_2 and unburned hydrocarbons as func-
tions of equivalence ratio. The quality of these comparisons is
very good and is similar to that obtained for the toluene experi-
ments. Soot was not observed to form in measurable quantities for
iso-octane mixtures which could be stably burned in the Jet-
Stirred Combustor.

The rate parameters for soot formation in fuel-rich toluene
oxidation were determined in the same manner that was used for the
selection of the other global rates. Figure 2 shows the compari-
son of the predictions with the data for pure toluene and Figure 5
shows comparisons for blends of toluene and iso-octane using the
same rate parameters. The trends for the blends are proper, but
the amount of soot formed is somewhat underpredicted. Since the
soot oxidation model depends on an assumed mean particle size of
25 nm, a study of the effect of soot particle size showed that the
results were relatively insensitive to this assumption and that
under these operating conditions only about 25 percent of the soot
would be consumed by oxygen attack (12). This relative insensi-
tivity suggested that both soot gasification by the other species
given in Table I and synergistic enhancement of soot formation
from aliphatics in mixtures with aromatics should be considered in
our future work.

Although the prediction of NO_x emissions under lean and stoi-
chiometric combustion with the extended Zeldovich mechanism is
adequate for certain applications, predictive methods for fuels
containing bound nitrogen and for rich combustion conditions
require substantial improvement. However, the early studies of
Fenimore (13, 14) demonstrated the potential importance of HCN and
NH_i type species in fuel-nitrogen interactions. To illustrate the
critical importance of the coupling of nitrogenous species reac-
tions in rich combustion, predictions of NO emissions from rich
iso-octane combustion in a jet-stirred combustor are shown in
Table III. C_2 hydrocarbon fragmentation and oxidation creates
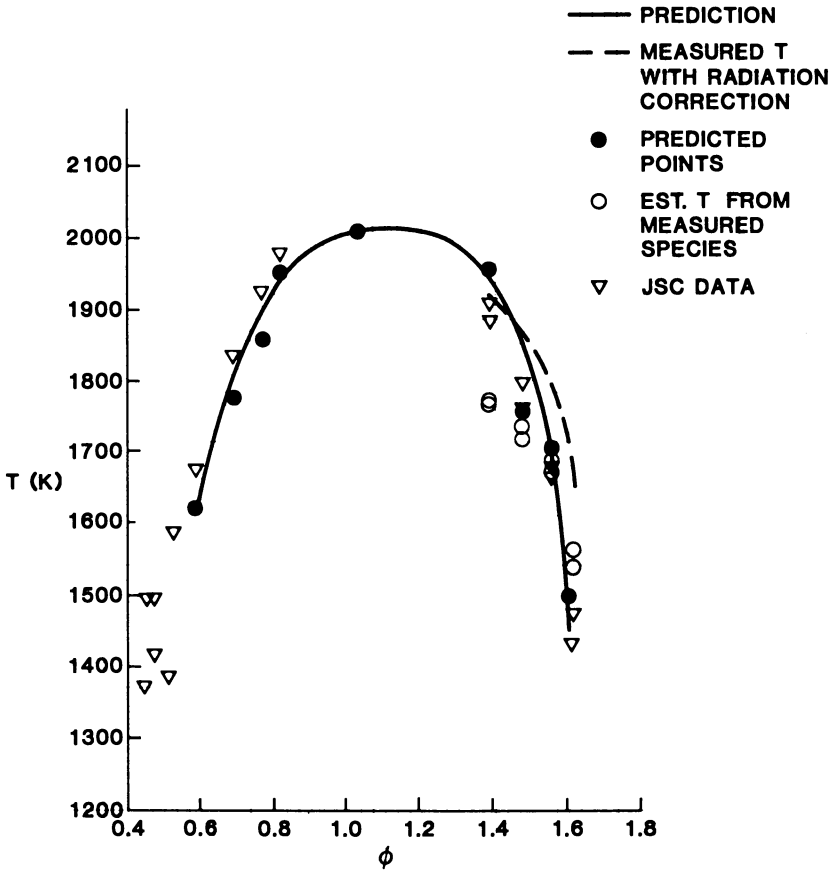
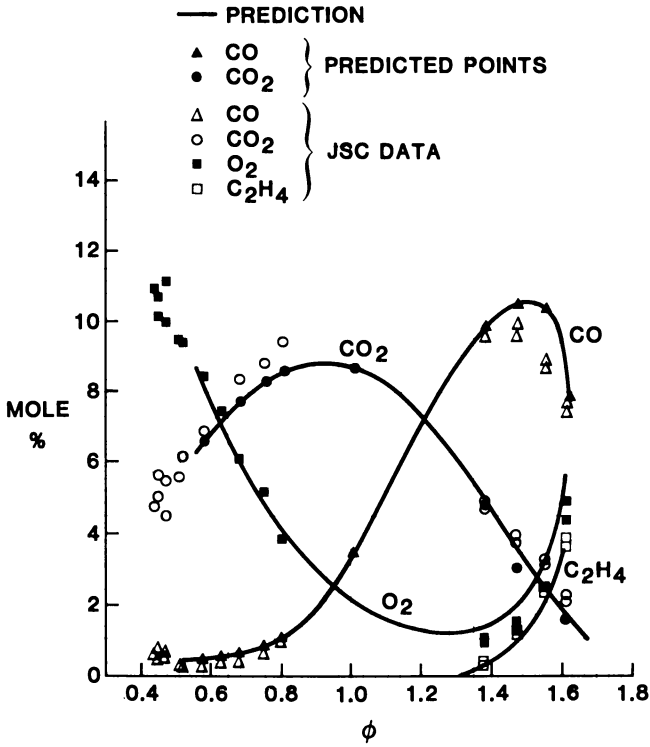Figure 3.   Iso-Octane Combustion as Measured in Exxon JSC and as Predicted.

Figure 4. Iso-Octane Combustion as Measured in Exxon JSC and as Predicted.
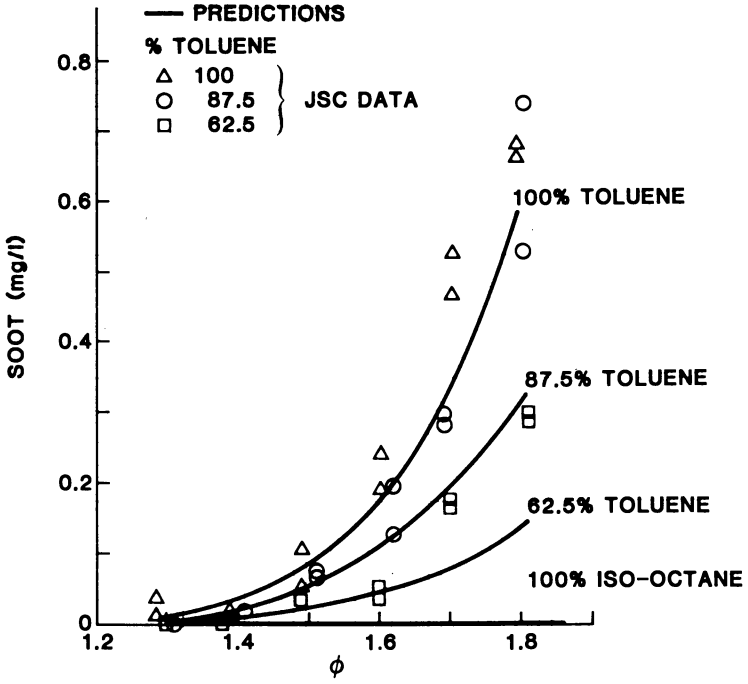
Figure 5.   Soot Emissions From Toluene/Iso-Octane Blends.

TABLE III. NO_x EMISSIONS ANALYSIS

CONDITIONS: Rich iso-octane combustion
in a well-stirred reactor;

Residence time = 3 msec;

Equivalence ratio = 1.8;

Pressure = 1 atm.

	ISO-OCTANE QUASIGLOBAL MODEL WITH HYDROCARBON/ NITROGEN INTERACTION INTERACTIONS	ISO-OCTANE QUASIGLOBAL MODEL WITH HYDROCARBON/ NITROGEN INTERACTION AND C_2 FRAGMENTATION AND OXIDATION REACTIONS
T(K)	2110	2106
NO	4.9E-5	7.5E-3
CO	18.7	16.7
OH	2.3E-2	9.1E-2
O	1.18E-3	3.6E-3
N	2.65E-8	3.17E-4

HCO, CH, CH_2 and CH_3 radicals which modify the H, O and OH radical pool. These radicals interact with nitrogenous compounds to form HCN and NH_i. These species react to form N and ultimately NO and NO_2. Two cases are shown in Table III; the first represents rich combustion with the quasiglobal iso-octane model which yields HCO, H, O and OH radicals that interact with the nitrogenous species. The second case also includes detailed reactions involving the fragmentation and oxidation of C_2 hydrocarbons to HCO and CH_i. Case 2 predicts realistic NO levels for this example. Without these hydrocarbon fragments included, the NO level is two orders of magnitude too low. This example demonstrates the extreme sensitivity of the NO_x emissions prediction to hydrocarbon-NO_x interactions among species which do not affect the thermal state of the combustion or the major, stable products of combustion and suggests that such interactions require further investigation.

The range of applicability of the quasiglobal kinetics model was further investigated by considering other experiments which characterized different aspects of the combustion mechanism. Initiation processes, as measured with shock-tube experiments, were considered as a severe test of the model which was developed with jet-stirred combustor data which are controlled primarily by recombination reactions that occur during the latter stages of combustion. Quasiglobal toluene kinetics model predictions were compared with shock-tube ignition delay data and with McLain and Jachimowski's (15) detailed kinetics prediction for these delays. This comparison is shown in Figure 6; the agreement is excellent. Ignition delay was defined as the time at which the pressure started to rapidly increase from its initial value. The predicted pressure rise was very rapid, so this parameter was easily obtainable. Similar experimental data for richer combustion and over a wider range of pressure and diluent concentrations would be desirable, yet the conditions presented are significantly different from those of the Jet-Stirred Combustor flow for which the global kinetics rates were determined.

Conclusions

Quasiglobal kinetics models, which have previously been shown to represent lean and stoichiometric combustion of a variety of hydrocarbon fuels, have been extended to represent lean and rich combustion of toluene and iso-octane. The model predicts the thermal state of the flow and emissions of CO, soot, and NO_x. The thermal state of the flow and the stable species were shown to be accurately predicted for jet-stirred combustor experiments. For rich combustion, hydrocarbon intermediates and soot are additional combustion products. The global reactions and rates were developed to represent near-adiabatic jet-stirred combustor data and were then verified by comparison to the near iso-thermal jet-stirred combustor data. NO_x emissions behavior was investigated with the quasiglobal kinetics model to represent rich combustion

and an NO_x emissions model. NO_x emissions predictions are quali-
tatively correct, and results indicate that more work needs to be
done to describe the formation and interaction of hydrocarbon
fragments such as HCO and CH_i with nitrogenous species.

    Since the jet-stirred combustor represents only a limited
range of experimental conditions, the extended quasiglobal kinet-
ics model was also used to predict ignition delay times for shock-
tube experiments for toluene. These predictions were in excellent
agreement with the experimental observations. Accurate represen-
tations of both the jet-stirred combustor and shock-tube data are
very encouraging with respect to the apparent generality offered
by quasiglobal modeling. This quasiglobal kinetics model for aro-
matic and aliphatic fuel components represents a major initial
step in describing the combustion behavior of actual synfuels.
However, research is in progress to further examine the range of
applicability of the extended quasiglobal kinetics model and to
develop analogous models for synfuels.

Acknowledgment
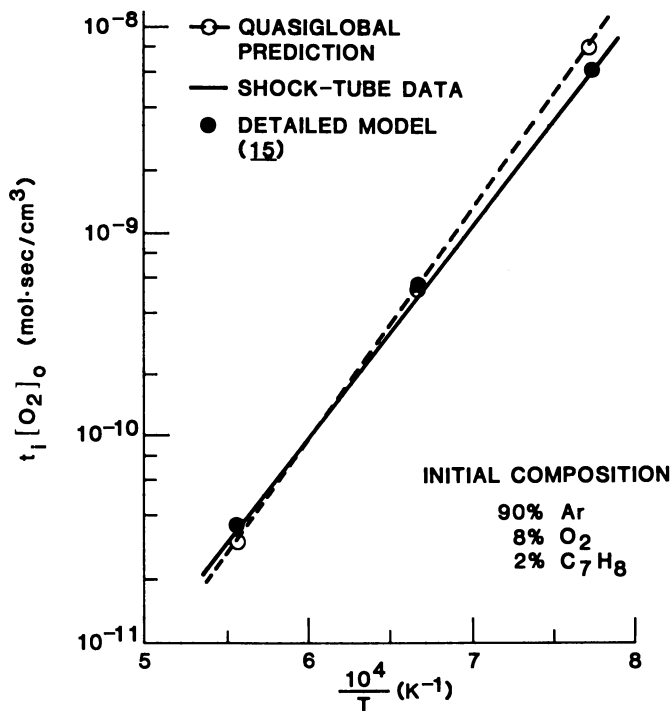
Figure 6. Ignition Delay Comparisons for Toluene.

Literature Cited

1. Muzio, L. J.; Arand, J. K. "Combustion and Emissions Charac-
   teristics of SRC-II Fuels"; WSS 80-12, Western States Section
   of The Combustion Institute, 1980.
2. Burke, F. P.; Winschel, R. A.; Pochapsky, T. C. "Composition
   and Performance of Distillate Recycle Solvents From the SRC-I
   Process"; Fuel, 1981, 60, 562-572.
3. Becker, M.; Bendoraitis, J. G.; Bloch, M. G.; Cabal, A. V.;
   Callen, R. B.; Green, L. A.; Simpson, C. A. "Analytical
   Studies for the H-Coal Process"; DOE FE-2676-1, Mobil
   Research and Development Corp., DOE, 1978.
4. Edelman, R. B.; Fortune, O. F. "A Quasi-Global Chemical
   Kinetic Model for the Finite-Rate Combustion of Hydrocarbon
   Fuels With Application to Turbulent Burning and Mixing in
   Hypersonic Engines and Nozzles"; AIAA Paper 69-86, AIAA,
   1969.
5. Engleman, V. S.; Bartok, W.; Longwell, J. P.; Edelman, R. B.
   "Experimental and Theoretical Studies of NO_x Formation in a
   Jet-Stirred Combustor"; Fourteenth Symposium (International)
   on Combustion, 1973, 755-765.
6. Edelman, R. B.; Harsha, P. T. "Laminar and Turbulent Gas
   Dynamics in Combustors – Current Status"; Prog. Energy
   Combust. Sci., 1978, 4, 1-62.
7. Farmer, R. C.; Edelman, R. B.; Wong, E. "Modeling Soot Emis-
   sions in Combustion Systems"; Particulate Carbon Formation
   During Combustion, 1980, GM Research Symposium.
8. Engleman, V. S. "Survey and Evaluation of Kinetic Data on
   Reactions in Methane/Air Combustion"; Report No. EPA-600/2-
   76-003, 1976.
9. Westbrook, C. K. "An Analytical Study of the Shock Tube Igni-
   tion of Mixtures of Methane and Ethane"; UCRL-81507, Lawrence
   Livermore Laboratory, 1978.
10. Nagle, J.; Strickland-Constable, R. F. Proc. Fifth Carbon
    Conf., 1962, 1, 154-164.
11. Levy, J. M. "Modeling of Fuel-Nitrogen Chemistry in Combus-
    tion: The Influence of Hydrocarbons"; Fifth EPA Fundamental
    Combustion Research Workshop, Newport Beach, CA, 1980.
12. Kowalik, R.; Ruth, L. A.; Edelman, R. B.; Wong, E.; Farmer,
    R. C. "Fundamental Characterization of Alternate Fuel Effects
    in Continuous Combustion Systems"; DOE/ET/11313-1, 1981, DOE.
13. Fenimore, C. P. "Formation of Nitric Oxide From Fuel-Nitrogen
    in Ethylene Flames"; Comb. and Flame, 1972, 19, p. 289.
14. Fenimore, C. P. "Reactions of Fuel-Nitrogen in Rich Flames";
    Comb. and Flame, 1976, 26, p. 249.
15. McLain, A. G.; Jachimowski, C. J. "Chemical Kinetic Modeling
    of Benzene and Toluene Oxidation Behind Shock Waves"; NASA TP
    1472, 1979, NASA.

Synthetic Fuel Atomization Characteristics

R. G. OEDING
Spectron Development Laboratories, Inc., Costa Mesa, CA 92626

W. D. BACHALO
Aerometrics, Inc., Mountain View, CA 94042

A visualization study of fuel atomization
using a pulsed laser holography/photography tech-
nique indicates that basic spray formation
processes are the same for both a coal-derived
synthetic fuel (SRC-II) and comparable petroleum
fuels (No. 2 and No. 6 grade). Measurements were
made on both pressure swirl and air assisted
atomizers in a cold spray facility having well
controlled fuel temperature. Quality of the
sprays formed with SRC-II was between that of the
No. 2 and No. 6 fuel sprays and was consistent
with measured fuel viscosity. Sauter mean
droplet diameter (SMD) was found to correlate
with fuel viscosity, atomization pressure, and
fuel flow rate. For all three fuels, a smaller
SMD could be obtained with the air assisted than
with the pressure swirl atomizer.

The substitution of synthetic liquid fuels, derived from
coal and shale, for dwindling petroleum resources is a major
element of the future energy picture. The utilization of these
synthetic fuels in an energy-efficient and environmentally-
acceptable manner requires an improved understanding of funda-
mental combustion processes. Specifically, the low hydrogen to
carbon ratio and high fuel nitrogen content typical of these
synthetic fuels requires modifications to conventional combus-
tion approaches for control of NO_x and particulate emissions.
Atomization is the initial phase of the spray combustion
process and has a strong influence on subsequent combustion and
pollutant formation mechanisms. Although a number of combus-
tion studies (1-3) have been conducted utilizing coal-derived
liquid fuels, very limited spray characterization data exists
for these alternate fuels.
This paper summarizes the results of an experimental
study to visualize and compare spray formation processes

associated with typical atomizers using both a coal-derived
synthetic fuel (SRC-II middle distillate) and petroleum fuels
(No. 2 and No. 6 grade fuel oils). Emphasis is placed on the
qualitative assessment of fuel and atomizer influences on spray
formation and quality.

Experimental

Spray Facility

The experimental study was conducted in a laboratory-
scale cold spray facility. The experimental configuration,
shown schematically in Figure 1, consisted of a 61 cm (24 in.)
diameter cylindrical spray chamber with a vertically oriented
atomizer and spray, a fuel supply system, and an exhaust system
with liquid/vapor removal. Windows for optical access were
mounted along a horizontal optical axis. Variable speed
blowers placed upstream supplied a 10 m/s primary air flow
through a 15.2 cm (6 in.) diameter tube surrounding the
injector and a 0.5 m/s screen air to maintain a uniform flow
within the test section. Wire mesh filters were used in the
base of the chamber to remove liquid fuel while the remaining
fuel vapor/air mixture was exhausted by a large variable speed
blower through an exterior mounted carbon filter.

A nitrogen pressurized fuel system provided fuel to the
atomizer at well controlled temperatures up to 240°F. Pre-
heating was provided by a combination of reservoir and line
heaters. Atomizer air was obtained from the laboratory air
supply.

Atomizers

Both air assisted and pressure swirl atomizers typical of
oil burning systems were used in this study. The pressure
swirl atomizers utilized fuel pressure and tangential slots to
create a swirl flow within an internal chamber and orifice.
The fuel emerged from the orifice as a conical liquid sheet and
subsequently disintegrated into a conical spray. Delavan atom-
izers in three different sizes (nominal flow rates of 1, 2, and
5 gph), three different spray angles (45, 60, and 90 degrees)
and with hollow cone spray patterns were investigated. Nominal
fuel pressures considered were 50, 100, and 150 psig.

The air assisted atomizer selected was the Sonicore
052H. It utilizes a high velocity air jet to shear and frag-
ment the fuel internally. The resulting two phase jet passed
from the orifice into an externally mounted resonator cap
designed to produce a resonant sonic field and enhance atomiza-
tion. Fuel pressures from 0 to 12 psig and air pressures from
3 to 20 psig were used to study both nominal and off-nominal
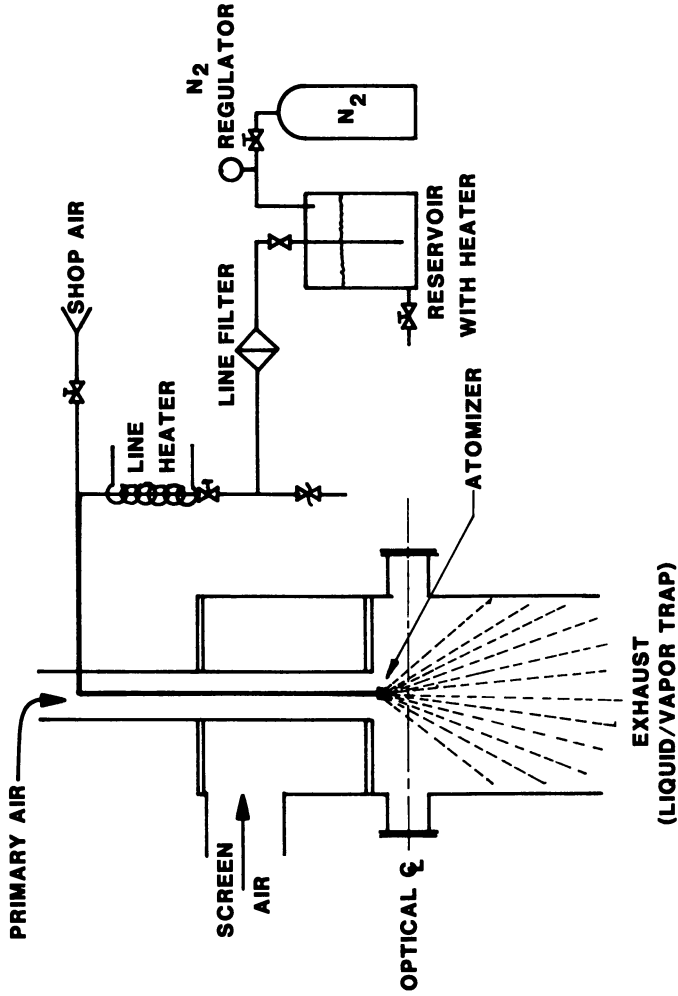operation of the atomizer. This range of operating pressures

Figure 1.
Experimental Configuration

resulted in fuel flow rates (for No. 2 fuel oil) ranging from
0.7 to 4.4 gph.

Fuels

Physical properties of the three test fuels are presented
in Table I. Except for the surface tension of No. 6 fuel oil,
which was a typical value, all properties were measured for the
specific samples tested. The primary differences between the
SRC-II middle distillate and the No. 2 fuel were the higher
specific gravity, surface tension, and viscosity of the
SRC-II. The No. 6 grade fuel, a residual fuel oil, had a much
higher viscosity than either of the distillate fuels. Both the
SRC-II and No. 2 fuel oil were sprayed at a nominal temperature
of 80°F to simulate usage in a non-preheat combustion system.
The No. 6 fuel oil was sprayed at temperatures ranging from
150° to 240°F in order to assess spray formation processes and
spray quality over a broad range of viscosities.

TABLE I

PHYSICAL PROPERTIES OF TEST FUELS

Property	SRC-II Middle Distillate	No. 2 Fuel Oil	No. 6 Fuel Oil
Specific gravity at 15°C (60°F)	0.97	0.86	0.94
Surface tension at 27°C (80°F) (Dyne/cm)	30.9	27.1	(35.0)
Viscosity (cs) at 27°C (80°F)	5.0	4.0	-
60°C (140°F)	2.1	1.8	70.4
99°C (210°F)	-	-	16.3

Diagnostic Technique

The dynamic events associated with spray formation pro-
cesses were observed instantaneously using pulsed laser
holography and photography. Optical holography is a technique
which stores, for later reconstruction, all of the coherent
optical information that has passed through or is reflected
from a volume of interest. Holograms of fuel sprays including
atomizer, spray formation region, and initial spray field were
obtained and reconstructed to provide three-dimensional images

suitable for detailed plane-by-plane study (and measurement).
A pulsed ruby laser was used to provide the necessary coherent
illumination. The laser pulse duration was 20 nanosec which
was adequate to freeze the motion of the sprays to less than
1 μ. Double pulsed holograms were also obtained (pulse separa-
tions 5 and 10 μsec) in order to determine velocity and observe
physical changes. The basic arrangement and performance speci-
fications for the general purpose holocamera used for this
study have been presented previously (4). In addition to
holograms, high resolution back-lighted photographs with the
same field diameter as the holograms were obtained by blocking
the reference beam and imaging the object beam. Imaging optics
provided a 3x pre-magnification for both holograms and photo-
graphs. This resulted in a real sample volume diameter of ap-
proximately 3.8 cm (1.5 in.).
     Particle size data were obtained for selected test condi-
tions directly from holograms and photographs. Spray measure-
ments were made at an axial distance of approximately 2.5 cm (1
in.) from the injector where spray formation processes had been
completed and spherical droplets formed.

Observations and Discussion

Pressure Swirl Atomizer

     Spray formation processes associated with pressure swirl
atomizers are illustrated in Figure 2, a back-lighted laser
photograph of a preheated No. 6 fuel spray. Fuel pressure is
utilized to produce, via a swirl chamber and orifice, a conical
liquid sheet. As the sheet expands, unstable wave forms
develop due to interaction with the atmosphere and surface
tension forces leading to disintegration of the sheet. This
"wavy sheet" mode of disintegration is one of several iden-
tified by Fraser (5) and is the dominant mode observed in this
study. The unstable wave crests eventually blow out forming a
complex network of liquid ligaments or threads.
     Droplet formation occurs primarily through the surface
tension and viscosity dominated breakup of these liquid threads
due to symmetric (or dilational) waves as described by Rayleigh
(6) for inviscid liquids and by Weber (7) for viscous fluids.
Figure 3 shows the double pulsed image of the droplet formation
process for No. 2 and SRC-II fuel sprays under identical
atomizer conditions. These two photographs illustrate typical
differences seen between these two fuels.
     For the No. 2 fuel spray, droplet formation from liquid
threads was rapid with typical wave length-to-diameter ratios
close to a value of 4.5 as predicted by Rayleigh. Droplet
formation was slower and less orderly for the SRC-II with long
ligament extending into the initial spray region. While the
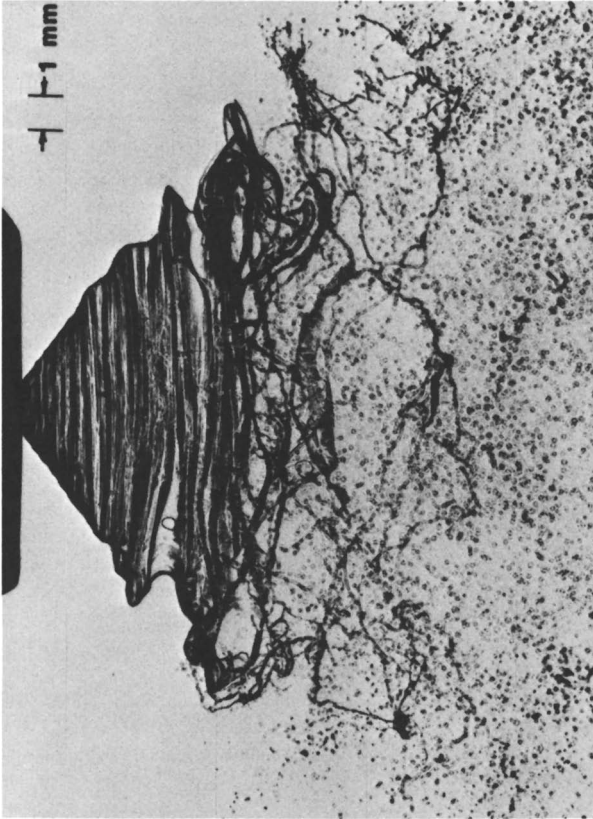slightly higher surface tension of the SRC-II should enhance

Figure 2.
Spray Formation by Pressure Atomizer.
Atomizer is Delavan 90A at 100 psig, 2 gph.
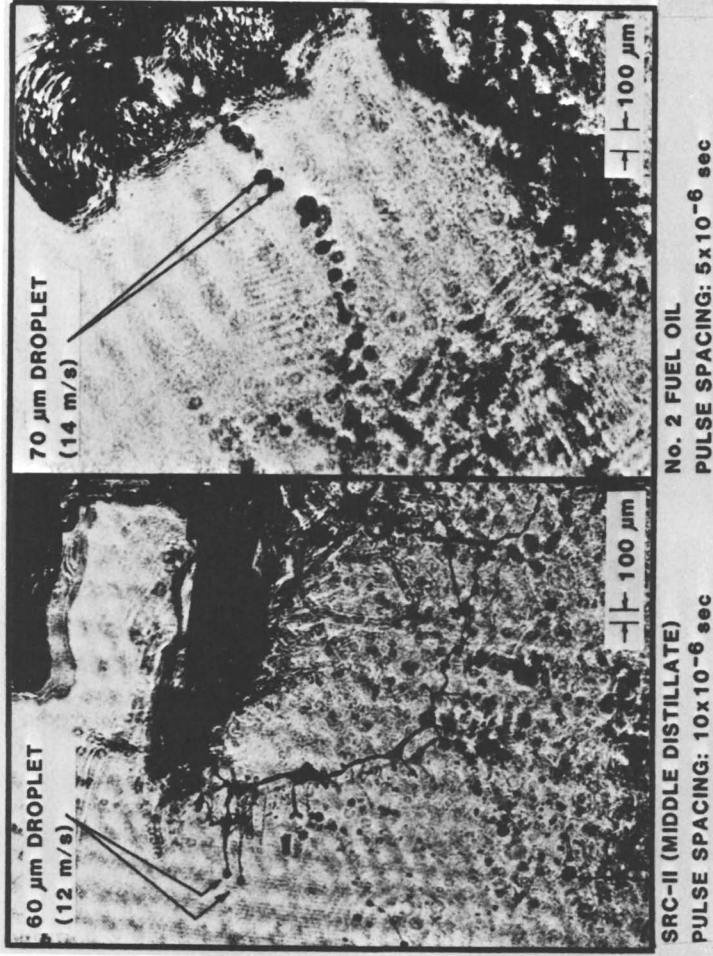Fuel is No. 6 Oil at 210°F.

Figure 3.
Double Pulsed Image of Droplet Formation Process.
Atomizer is Delavan 60A at 100 psig.

droplet formation, the longer and more persistent ligament
development suggests viscosity as the dominant physical pro-
perty difference between the two fuels. Evidence of distortion
and breakup of large droplets was observed in the spray
formation region, while droplet coalescence in the downstream
spray was not obvious in these rapidly expanding hollow cone
sprays.

The influence of design and operating variables on spray
formation for pressure swirl atomizers has been well studied
(e.g., 8,9). Effects of fuel pressure and nominal flow rate
(atomizer scale) are illustrated in Figure 4 for a 60 degree
hollow cone spray. Liquid breakup length decreases and spray
quality increases with both increasing pressure and decreasing
atomizer scale. Also, as flow rate increases, the spray
assumes a more distinct conical shape. The effect of increas-
ing the spray angle, although not shown, is to decrease breakup
length and improve spray quality.

The effects of viscosity on spray formation are shown in
Figure 5 for a No. 6 fuel oil sprayed with three different
levels of preheating. At the low temperature (high viscosity)
and low pressure condition, a conical liquid sheet could not be
established and the fuel emerged from the atomizer as a
swirling jet. Due to the tangential velocity component, the
jet remained intact for only a short distance before spreading
and breakup occurred. With decreasing viscosity and/or
increasing pressure, a large placid sheet was formed which
eventually broke up due to a very distinct low frequency
instability. As viscosity was further reduced, higher
frequency wave forms developed, liquid breakup length
decreased, and spray quality improved. Viscosity affects both
the breakup of the liquid sheet (and resulting ligament
diameter) by retarding higher frequency instabilities and the
formation of droplets by increasing ligament wave length and,
hence, the resulting droplet size. Since the maximum preheat
temperature of 240°F was well below the boiling point of this
residual fuel oil, no significant vaporization effects on spray
formation were believed to be present.

A limited number of droplet size measurements were made
from the holograms and photographs in order to obtain a quanti-
tative assessment of spray quality. These data were obtained
in the initial spray region and expressed in terms of the
Sauter Mean Diameter (SMD). Since the spray is evolving
rapidly and mean droplet sizes are changing in this initial
spray region, measurements were made at the same distance from
the atomizer to provide a relative comparison of spray
quality. Variations in SMD with pressure, liquid mass flow
rate, and viscosity were examined. Figure 6 presents SMD as a
function of fuel viscosity and includes all three test fuels.
SMD correlates well with viscosity to the 0.21 power. This is
in good agreement with a value 0.20 used in standard droplet
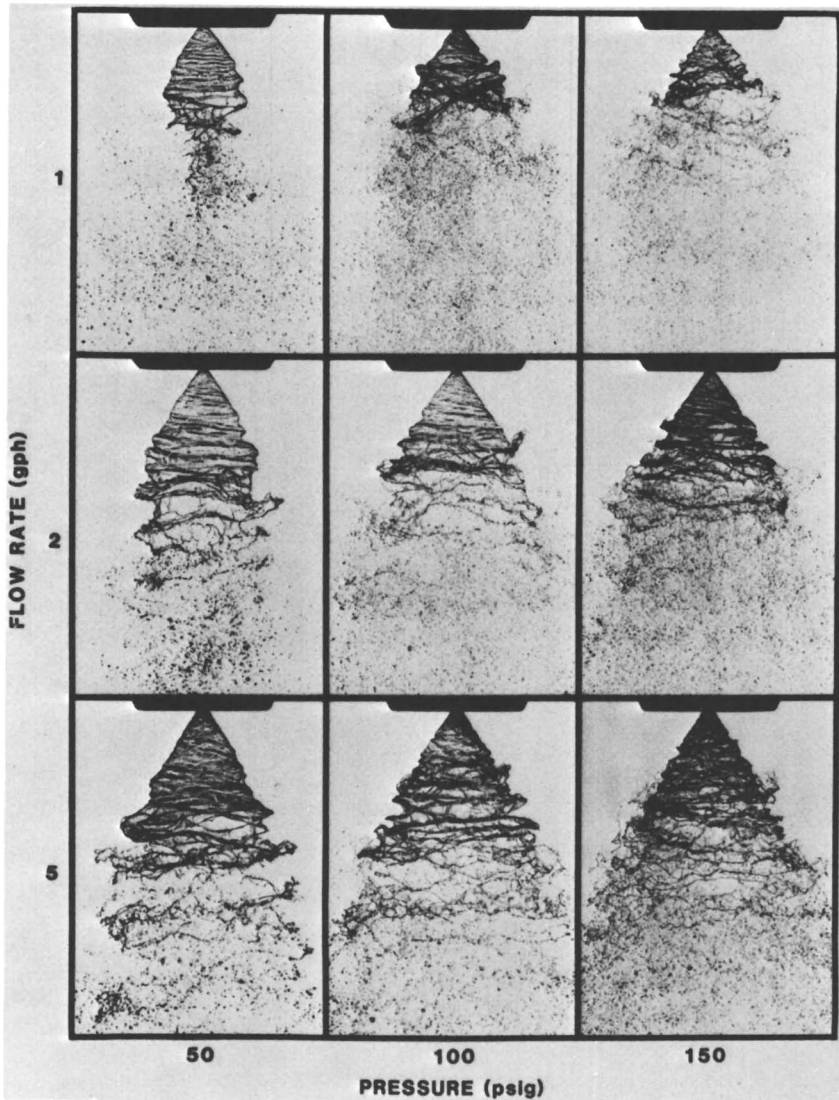
Figure 4.
Effects of Atomizer Size and Fuel Pressure on Spray Formation.
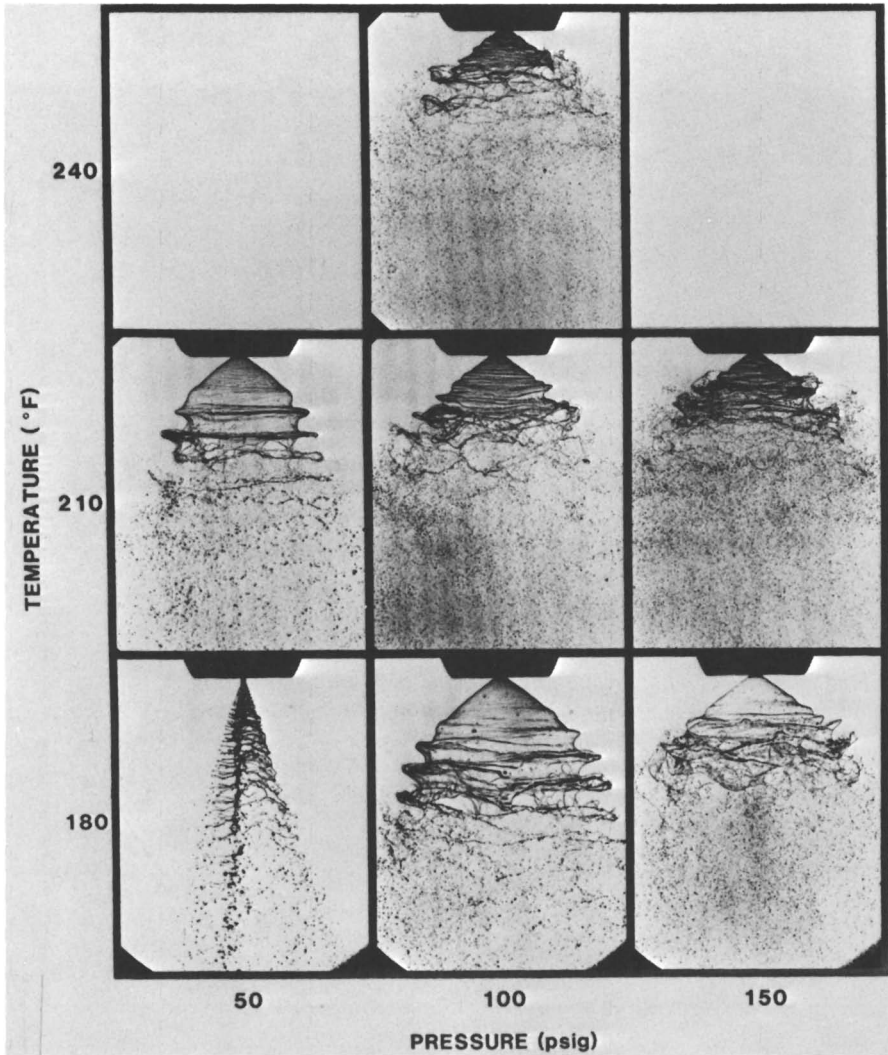Atomizer is Delavan 60A. Fuel is SRC-II Middle Distillate.

Figure 5.
Effects of Fuel Viscosity and Pressure on Spray Formation.
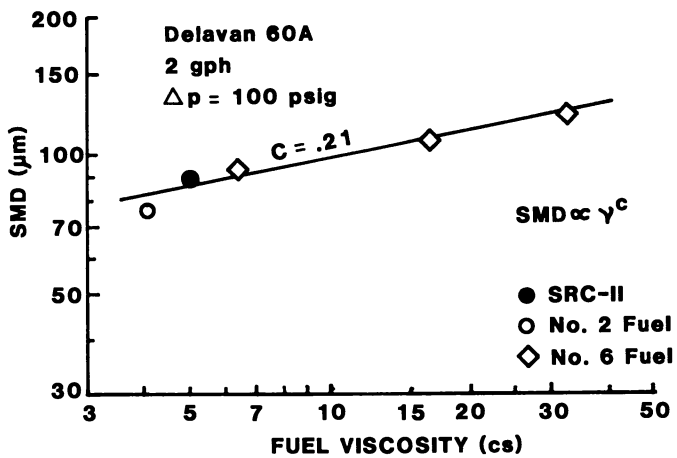Atomizer is Delavan 90A, 2 gph and Fuel is No. 6 Oil.

Figure 6.
Effect of Viscosity on Mean Droplet Size.

size correlations (11). The lower value of SMD shown by the
No. 2 fuel oil in Figure 6 also reflects its slightly lower
density and surface tension relative to SRC-II. The effects of
specific atomizer and fuel properties on SMD are typically cor-
related in the form

$$SMD = \frac{K \, W_f^b \, v^c \, \sigma^d}{\Delta p_f^a}$$

where K is a constant (dependent on specific atomizer
geometry), W_f is fuel mass flow rate, σ is surface tension, v
is kinematic viscosity, and Δp_f is fuel pressure drop.

The specific values of exponents a, b, and c determined for the
two distillate fuels are presented in Table II. The
correlation of SMD with mass flow rate, pressure, and viscosity
are in generally good agreement with typical values for
petroleum fuels (11). Due to the limited properties variation
available with these three fuels, the effects of surface
tension and density could not be determined independently.

TABLE II
MEAN DROPLET SIZE CORRELATION FOR
PRESSURE SWIRL ATOMIZER

Exponent	Typical	SRC-II	No. 2
a	0.4	0.48	0.30
b	0.25	0.28	0.22
c	0.2	0.17*	0.21*
d	0.6	--	--

*Includes No. 6 fuel oil data

Sonicore Atomizer

Spray formation processes associated with the Sonicore
atomizer are illustrated by the photograph shown in Figure 7.
For the fuels studied, spray formation appeared to occur by two
processes. Some of the fuel ligaments were deflected aero-
dynamically by the presence of the resonator cap, were drawn
out into fine threads, and broke up into relatively small
droplets (10-40 μ). The remaining fuel impinged on the reso-
nator cap or supports and was deflected or sheared off to form
relatively large droplets (100 μ and greater). The effects of
the resonant sonic field were not obvious, although the initial
ligament formation and deflection may have been influenced by
the sonic field.
The effects of fuel and air pressure on spray formation
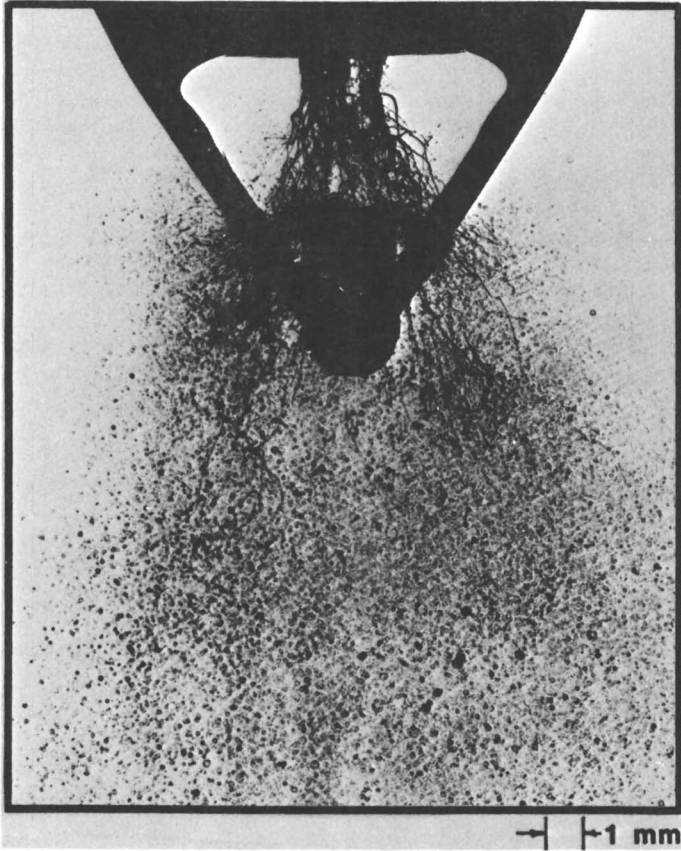are shown in Figure 8 for the SRC-II. The four conditions

Figure 7.
Spray Formation by Sonicore Atomizer. Air Pressure is 1 psig
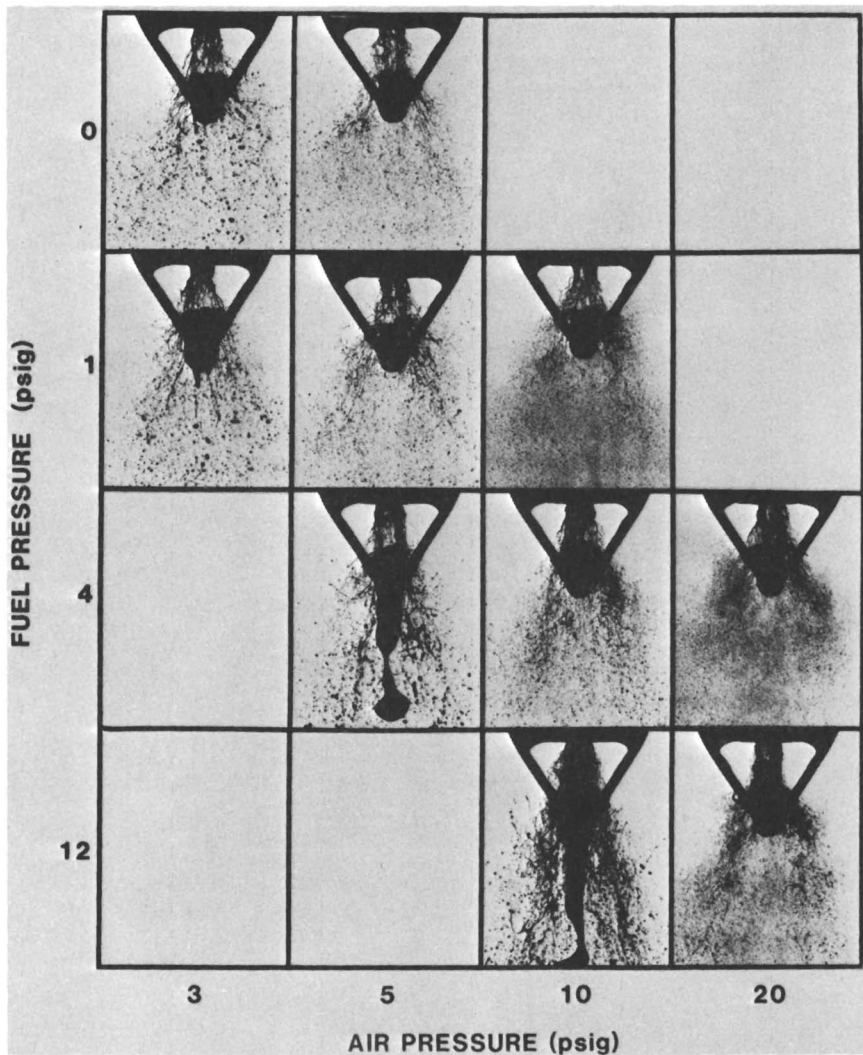and Fuel Pressure is 10 psig. Fuel is SRC-II Middle Distillate.

Figure 8.
Effects of Fuel and Air Pressure on Spray Formation.   Atomizer
is Sonicore 052H.   Fuel is SRC-II Middle Distillate.

shown along the diagonal correspond to nominal operating con-
ditions for a No. 2 fuel oil. Conditions to the right of the
diagonal represent a higher air-to-fuel ratio (AFR) and result
in better atomization and spray quality. Conditions to the
left of the diagonal represent a lower AFR and result in poorer
atomization and a coarser spray. Although not shown, the No. 2
fuel oil (for comparable operating conditions) formed droplets
quite close to the resonator cap and did not develop long
threads as seen with the SRC-II. Thus, spray quality obtained
with the No. 2 fuel oil appeared to be consistently better than
obtained with the SRC-II.

The effect of fuel viscosity on spray formation is illus-
trated in Figure 9 for a No. 6 fuel oil at four different
levels of preheat. Kinematic viscosity varies from approxima-
tely 58 cs at 150°F to 6.3 cs at 240°F. The atomizer operating
conditions correspond to the nominal conditions shown along the
diagonal on the previous figures. As temperature was increased
(viscosity decreased), the liquid breakup processes were
enhanced and spray quality was improved. At the higher vis-
cosity conditions, the liquid resists deformation and is drawn
out into long ligaments which eventually atomize inefficently
in regions of relatively low air velocity. A quantitative
assessment of fuel viscosity effects with the Sonicore atomizer
is presented in Figure 10 which compares SMD as a function of
viscosity for all three fuels at two nominal operating con-
ditions. As shown in the figure, SMD appears to correlate well
with viscosity to the 0.33 power for these specific operating
conditions. The fact that this viscosity exponent is larger
than for the pressure swirl atomizers is consistent with obser-
vations for a variety of air assisted atomizers (12).

A direct comparison of fuel effects on spray formation
for both a pressure swirl and the Sonicore atomizer is shown in
Figure 11. A visual comparison of breakup length, ligament
disintegration, and spray quality (size and uniformity) illus-
trates trends consistent with fuel viscosity, surface tension
and density differences. While viscosity appears to have a
dominant effect on spray formation processes for the range of
fuel properties considered in the present study, the similarity
between the SRC-II and preheated No. 6 fuel oil seen in Figure
11 is consistent with the greater surface tension of these two
fuels. Based on previous studies (e.g. 9, 12), fuel density
per se is not believed to have had a significant influence on
atomization.

Summary/Conclusion

A study to visualize and compare spray formation
processes for both a coal-derived synthetic fuel and comparable
petroleum fuels has been completed. Although the results were
primarily qualitative, a limited amount of particle size data
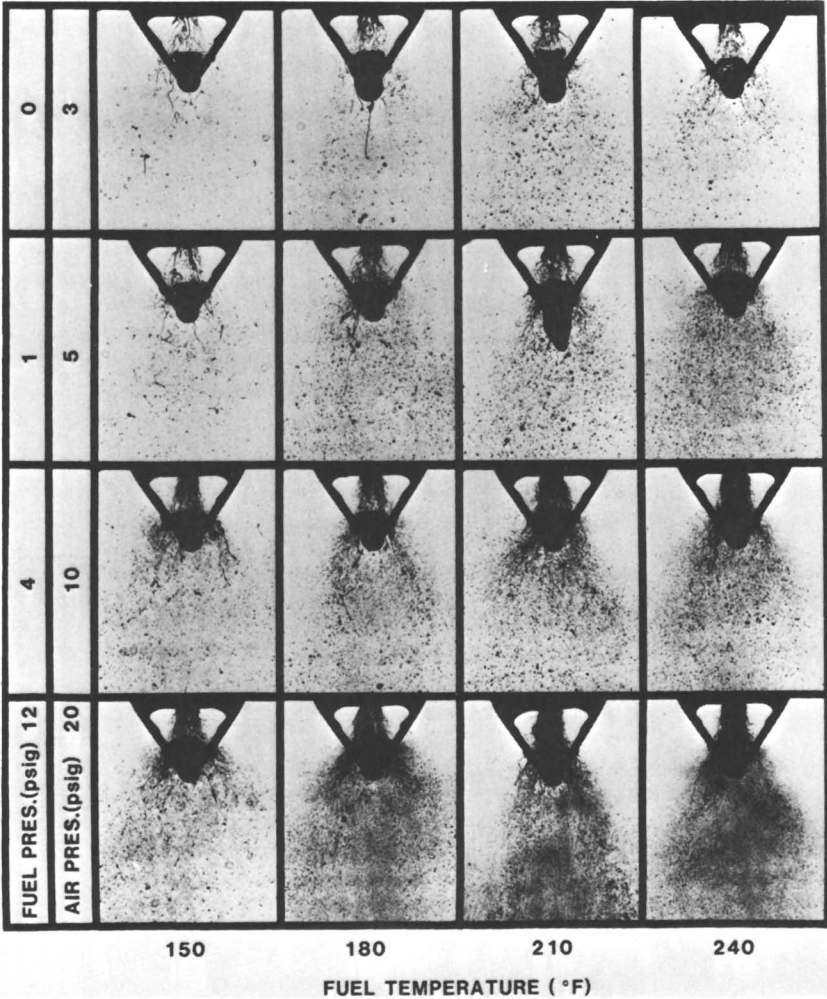
Figure 9.
Effect of Fuel Viscosity on Spray Formation. Atomizer is
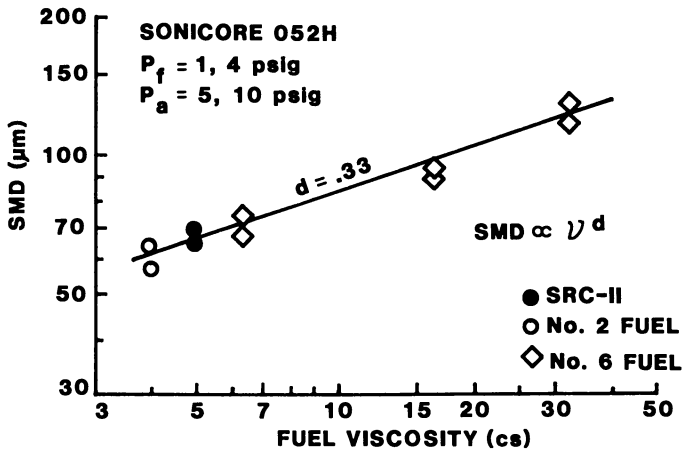Sonicore 052H. Fuel is No. 6 Oil.

Figure 10.
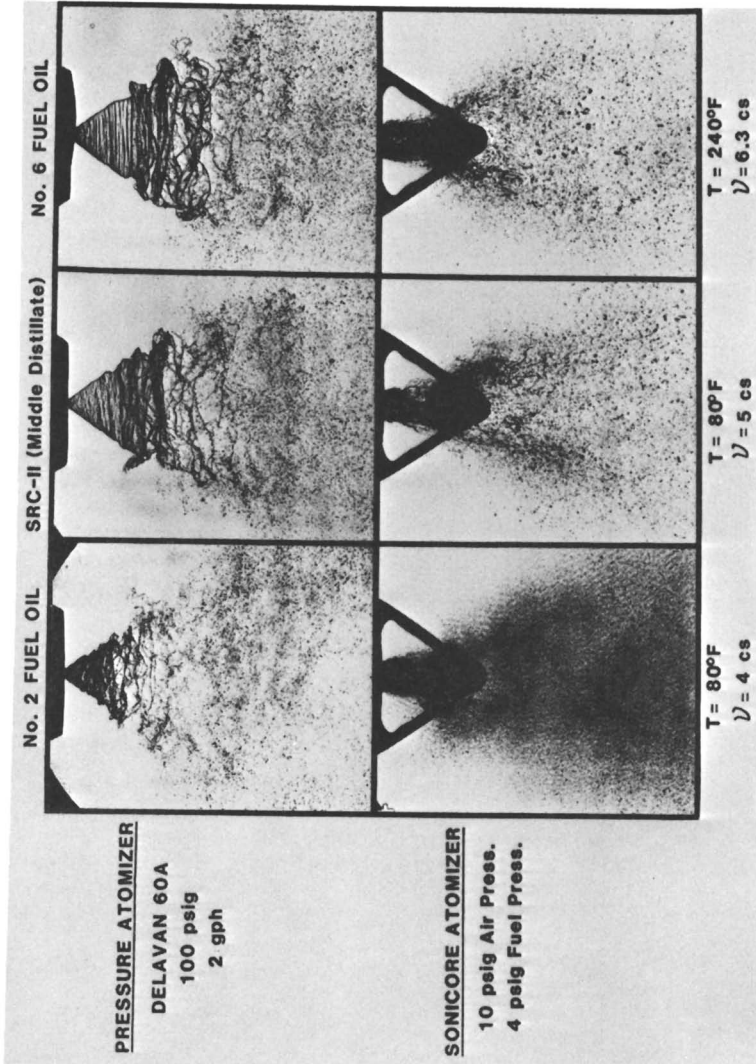Effect of Viscosity on Mean Droplet Size.

Figure 11.
Effect of Fuel on Spray Formation.

were obtained in the initial spray region. The results and conclusions can be summarized as follows:

1. Pulsed laser holography and photography provide a powerful technique for the instantaneous visualization of spray processes.
2. Mean droplet size as measured from the holograms and photographs was consistent with the visual observations of spray formation and spray quality.
3. While atomizer operating conditions had a strong influence on spray characteristics, the expected trends were observed with both types of atomizers.
4. All three fuels exhibited the same basic spray formation processes. No new or exotic modes of droplet formation were observed with the SRC-II, although distinct differences in ligament length and breakup time were seen.
5. For comparable fuel flow rates, the Sonicore atomizer could provide a spray with smaller SMD. Increasing the air-to-fuel ratio improved spray quality and can be used to compensate for increased fuel viscosity.
6. The highest quality spray for comparable atomizer conditions was obtained with the No. 2 fuel oil followed by SRC-II middle distillate and the No. 6 residual fuel (preheated up to 240°F).
7. Both droplet size data and visual spray quality correlated with fuel viscosity for both atomizer types. While fuel viscosity variations were large and had a dominant effect on spray formation, differences between SRC-II and No. 2 fuel oil are also consistent with surface tension and liquid density differences.

Acknowledgments

Literature Cited

1. Muzio, L. J., Arand, J. K., and Rovesti, W. C. Comb. Inst., West. States Sect., Wss 80-12, 1980.
2. Downs, W., Vecci, S. J., Barsin, J. A., and Rovesti, W. C., ASME Paper 79-WA-FU-2, 1979.
3. Piper, B. F., Hersh, S., and Nazimowitz, W., KVB Inc., Report FP-1029, 1979.
4. Trolinger, J.D. Optical Engineering 1975, 14.
5. Fraser, R. P. "Sixth Symp. on Combustion"; Reinhold, New York, 1957; p. 687.
6. Rayleigh, Lord "Theory of Sound"; 2nd Ed., MacMillan, London, 1894.

7. Weber, C. A Angew Math. Mech. 1931, 11, 136.
8. Taylor, G. I. Quart. J. Mech. Appl. Math. 1950, 111, 129.
9. Dombrowski, N. "Biochemical and Biological Engineering
    Science, Vol. 2"; Academic Press, London and New York,
    1968.
10. Dombrowski, N., and Johns, W. R. Chem. Eng. Sci. 1963, 18,
    203.
11. Kablish, T. R., and Schwartz, H. R., ASME Gas Turbine Con-
    ference and Products Show, Brussels, Belguim, 1970.
12. Lefebvre, A. H., Prog. Energy Combust. Sci. 1980, 6, 233.

RECEIVED October 29, 1982

Staged Combustion

Bench-Scale Pyrolysis–Oxidation Studies of Coal-Derived Liquids

JAMES R. LONGANBACH, LISA K. CHAN, and ARTHUR LEVY

Battelle, Columbus Laboratories, Columbus, OH 43201

Emissions of NO_x and soot are two of the problems in the combustion of coal-derived synthetic liquid fuels resulting from their high concentrations of nitrogen and aromatics. The changes in nitrogen concentration and aromatic structure during pyrolysis and oxidation have been studied and related to the use of staged combustion to decrease emissions. Four 50°C distillation cuts taken from SRC II middle and heavy distillates have been subjected to pyrolysis/oxidation in a quartz tube, after vaporization in a preheated stream of helium/oxygen. After trapping, the liquid products have been analyzed for nitrogen content and aromatic structure. Liquid recoveries averaged 95 percent of fuel weight fed at 500°C, 74 percent at 700°C, and 54 percent at 900°C in the presence or absence of oxygen. Only solids were produced at 1100°C. The concentrations of unsubstituted aromatics and nonbasic nitrogen have been shown to increase in the recovered liquids with increasing pyrolysis temperature while the concentration of basic nitrogen decreased. When oxygen (7 to 73 percent of stoichiometric) was added, the concentrations of unsubstituted aromatics decreased. The significance of these results for the staged combustion of synfuels is discussed.

Coal-derived synthetic liquid fuels are potentially attractive substitutes for imported oils. Coal-derived liquids, however, have a tendency to form excessive amounts of soot and to produce high NO_x emission levels during combustion compared to distillate oils (1). Polycyclic organic matter (POM) may also be enhanced along with the soot formation.

The overall objective of the research program is to study
the pyrolysis and oxidation behavior of a synfuel and to inte-
grate this behavior in staged combustion to determine the effects
of staged combustion on the formation of soot and NO_x.

The focus of this study is the chemistry of the partially
pyrolyzed and oxidized liquid fuel which survives as pyrolysis
and oxidative pyrolysis proceed. The experiments have been de-
signed so that these products are not completely destroyed and
can be recovered for analysis. The analyses include measurements
of basic nitrogen, average molecular weight, molecular weight
distribution and unsubstituted aromatics by gas chromatography,
and H^1 NMR studies to determine average molecular structure
parameters.

Experimental

Materials. Samples of SRC II middle and heavy distillates
were obtained from the Pittsburg and Midway Coal Mining Company.
These were distilled into 50°C boiling point range fractions and
labeled as follows: MD-2 (150-200°C), MD-3 (200-250°C), MD-4
(250-300°C), HD-2 (300-350°C), HD-3 (350-400°C), and HD-4 (400-
450°C). HD-3 and HD-4 could not be used in the apparatus because
they contained solids at room temperature.

The remaining four distillate fractions were characterized
in detail as was each liquid product obtained. The results for
the starting materials are listed in Table I.

Analytical Methods. Molecular weights were measured by
summing the areas obtained by simulated distillation using gas
chromatography, calibrated by injecting a series of standard
aromatic compounds.

Each sample was also characterized by elemental analysis.
Accurate total nitrogen analyses were obtained using the semi-
micro Kjeldahl technique.

Basic nitrogen levels were measured by titration with per-
chloric acid in acetic acid (2). The acid titrant was standard-
ized by titrating standard pyridine samples. Nonbasic nitrogen
was calculated as the difference between total and basic nitrogen.

The hydrogen distribution was measured by H^1 NMR. The
Brown-Ladner correlations (3) were used to calculate structural
parameters such as aromaticity (f_a), number of substituents on
aromatic rings (R_s), and substituent length (n).

Tetralin-type structures containing attached aromatic and
aliphatic rings with very short aliphatic side chains seem to
fit the structural data best. Except for MD-2 and MD-3, which
average slightly more than one half oxygen atom per molecule,
the molecules do not contain significant amounts of heteroatoms
(i.e., N, S or O), moisture or inorganics. However, compared
to petroleum-derived fuels, they do contain substantial amounts
of N and O.

TABLE I.   ANALYTICAL DATA FOR SRC II DISTILLATE FRACTIONS

Sample	MD-2	MD-3	MD-4	HD-2
BP Range, °C	150-200	200-250	250-300	300-350
Molecular Weight g/mole	137[1]	156	177	201
Elemental Analyses (Wt. Percent)				
C	82.6	83.4	87.3	90.
H	9.8	9.3	9.2	8.1
Total N	0.55	0.81	1.05	0.64
S	0.22	0.24	0.31	0.07
O	6.5	5.5	1.5	0.8
Basic N	0.49	0.75	0.80	0.42
Nonbasic N	0.06	0.06	0.25	0.22
NMR Parameters				
H-α to Aromatic	0.31	0.42	0.43	0.40
H-aliphatic	0.48	0.32	0.34	0.27
H-aromatic	0.17	0.21	0.22	0.32
H-Phenolic	0.04	0.05	0.01	0.01
Boiling Point Distributions °C				
151	6.76	--	--	--
174	11.45	--	--	--
196	39.85	6.54	--	--
216	34.65	37.64	0.48	--
235	4.01	27.40	10.90	--
253	--	17.94	--	--
287	2.87	7.89	54.55	31.28
317	0.35	0.60	33.49	59.52
344	0.15	0.49	0.05	8.65
369	0.22	0.63	0.03	0.18
Structural Parameters				
f_a [2]	0.44	0.51	0.51	0.64
H_{aro}/C_{aro} [3]	1.	1.	1.	0.88
σ [4]	0.60	0.59	0.52	0.40
R_s [5,6]	2.7	3.6	3.6	3.0
n [7]	2.6	1.8	1.8	1.9
C_a [8]	4.4	6.2	6.9	8.5
R_a [9]	<1.	<1.	1.1	1.5

[1] Measured by GC simulated distillation.

[2] f_a= fraction of total carbon which is aromatic.

[3] H_{aro}/C_{aro} = ratio of substitutable aromatics.

[4] σ = fraction of the available aromatic edge atoms occupied by substituents.

[5] R_s = number of substituted aromatic ring carbons.

[6] R_s was calculated by assuming $H_{aro}/C_{aro} \leq 1$.

[7] n = number of carbon aroms per saturated substituent.

[8] C_a = total number of aromatic carbon atoms.

[9] R_a = number of aromatic rings.

Apparatus. The bench-scale pyrolysis/oxidation apparatus shown in Figure 1 was used. The synthetic fuel distillate fraction was fed to the system at a constant rate via a syringe pump. The liquid fuel was vaporized in the vaporizer shown in Figure 2. Helium, or helium/oxygen in the oxidation experiments, flowed through the vaporizer, which was large enough to allow the fuel to be vaporized and mixed with no fractionation. The fuel vapor/gas mixture was carried into a 5.3 cm I.D. by 61-cm long quartz tube. Thermocouples were spaced down the center of the tube to record the temperature profile as the experiment took place. After passing through the pyrolysis/oxidation zone, the vapors were collected in traps cooled with liquid nitrogen. The volume of uncondensed gas was measured and gas samples were analyzed in an on-line gas chromatograph.

At the conclusion of each experiment the gas and fuel flow were stopped, the collection system was isolated, evacuated and allowed to warm to room temperature and the volume of condensed gas was measured.

The liquids were collected and analyzed as previously described. After some experiments, the solids coating the tube walls and thermocouples were burned off in oxygen and the resulting CO_2 and H_2O were collected and weighed to calculate mass balances. The average complete mass balance was 96.4 percent.

Results and Discussion

Reaction Conditions. Each of the four SRC II distillation cuts was pyrolyzed at 500, 700, 900, and 1100°C at approximately 7 seconds residence time in helium. The fuel vapor concentration averaged 1.4 volume percent. Oxidative pyrolyses were done at the same temperatures and residence times using MD-4 at average stoichiometric oxygen concentrations of 6.6, 20.4, and 73.0 percent. The range of concentrations at each level was large. The reaction conditions are listed in Table II.

Product Recoveries. Average total gas, liquid, and solid recoveries are shown in Table III on a normalized basis. It was assumed that there were no solids left in the tube at 100 percent of stoichiometric oxygen. Solids formation increased with increasing temperature. Solids formation decreased with increasing oxygen concentrations at 700, 900, and 1100°C. At 500°C no solids were formed. Liquid product formation decreased and gaseous product formation increased with increasing oxygen concentration at all temperatures.

Visually, there appeared to be very little reaction at 500°C. No solids were deposited on the pyrolysis tube and virtually no gases were formed. Chemically, the most notable change was a
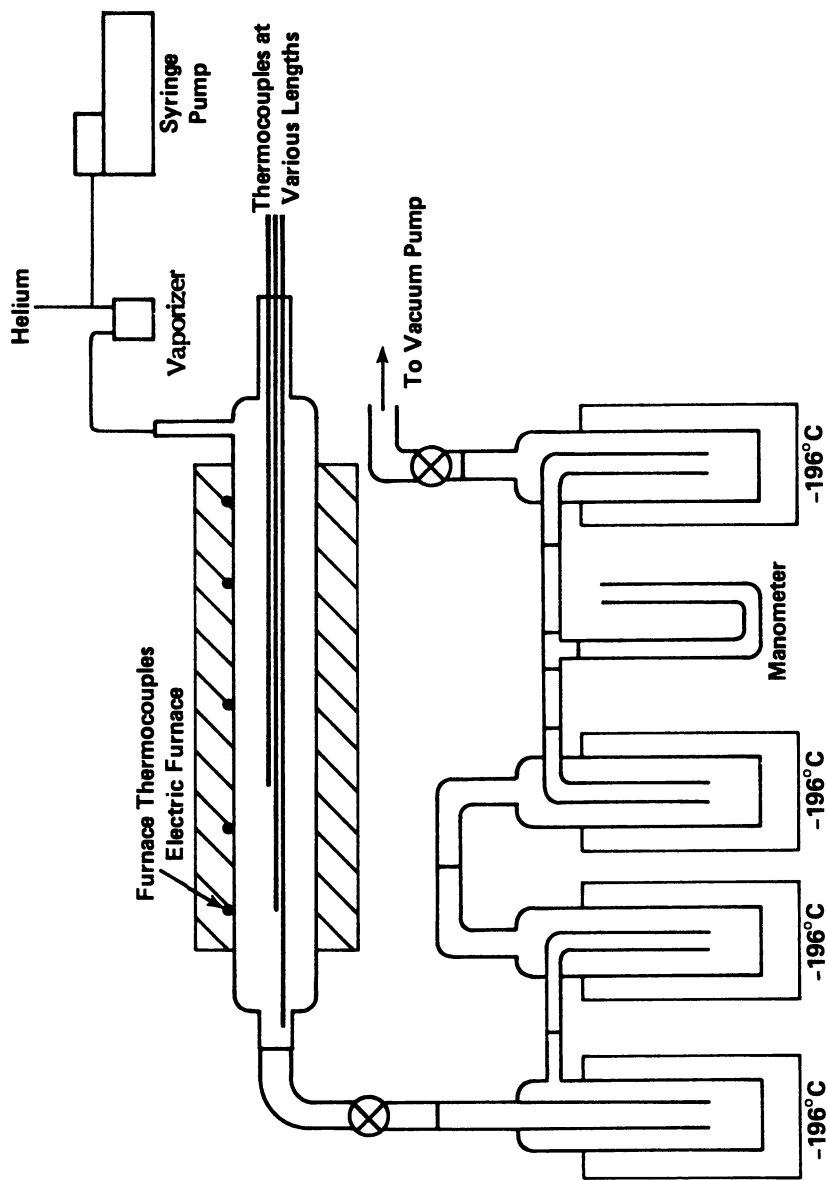
FIGURE 1.
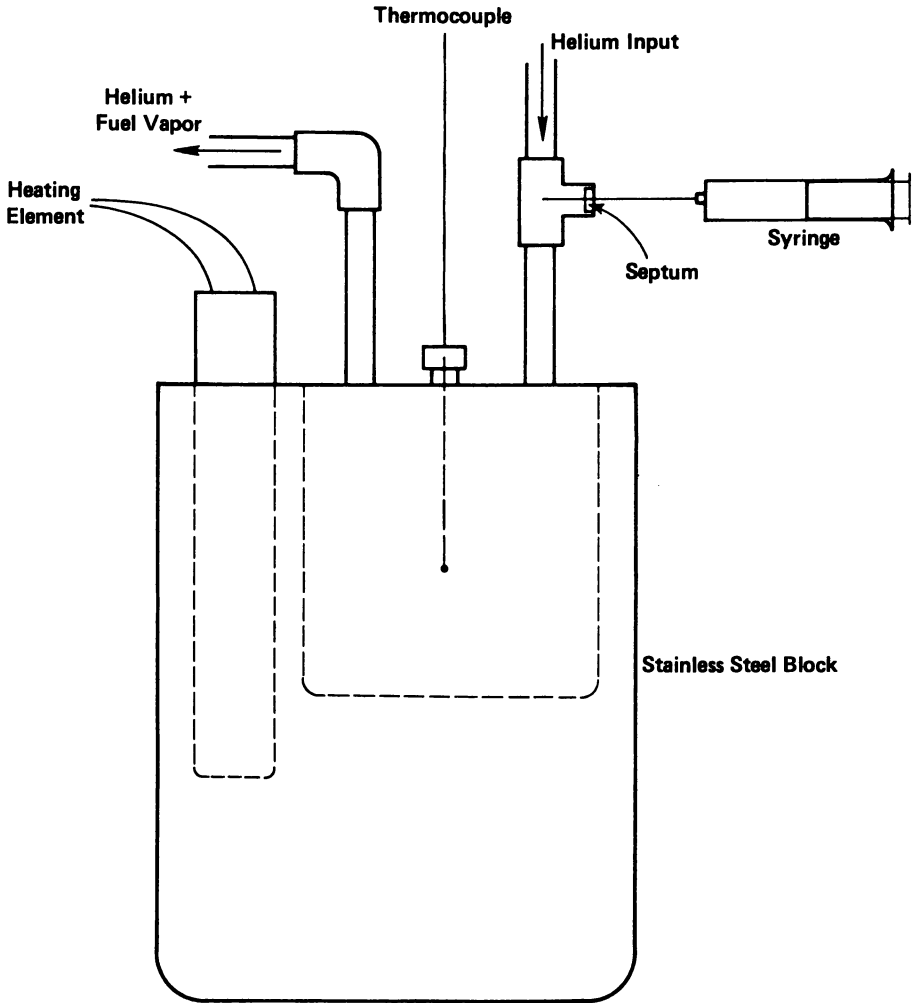PYROLYSIS–OXIDATION APPARATUS

FIGURE 2.
SCHEMATIC OF THE FUEL VAPORIZER

TABLE II. OXIDATIVE-PYROLYSIS REACTION CONDITIONS

Run No.	Fuel	Vaporizer/ Reactor Temp., °C	Total Gas Flow, ℓ/min	Fuel Flow, ml/min	O_2 Conc., % (GC)	Fuel(1) Vapor Conc., %	Residence Time, sec	Stoic. O_2,(2) %	Fuel Equiv. Ratio, (3) φ
21	MD-2	265/502	3.9	0.32	0	1.23	7.2	--	--
18	MD-2	247/699	3.1	0.34	0	1.48	7.2	--	--
22	MD-2	252/896	2.6	0.33	0	1.87	7.1	--	--
25	MD-3	303/505	3.9	0.47	0	1.62	7.2	--	--
24	MD-3	243/698	3.1	0.39	0	1.69	7.2	--	--
23	MD-3	288/896	2.6	0.33	0	1.70	7.1	--	--
60-28	MD-4	344/493	3.9	0.33	0	1.04	7.3	--	--
58-24	MD-4	/(700)	3.4	0.32	0	1.15	6.6	--	--
19	MD-4	343/898	2.6	0.33	0	1.55	7.1	--	--
32	MD-4	332/1104	2.2	0.35	0	1.99	7.1	--	--
17	HD-2	389/500	3.9	0.37	0	1.08	7.2	--	--
16	HD-2	404/699	3.1	0.35	0	1.28	7.2	--	--
14	HD-2	399/905	2.6	0.33	0	1.44	7.1	--	--
26	MD-4	293/513	4.26	(0.33)	1.6	0.98	6.5	9.5	11
27	MD-4	293/704	3.32	0.31	1.4	1.18	6.7	6.9	14
28	MD-4	347/897	2.82	0.34	1.5	1.51	6.6	5.7	18
34	MD-4	371/1066	1.92	0.31	1.5	2.02	8.4	4.3	23
31	MD-4	357/513	3.92	0.41	5.0	1.32	7.1	22.0	4.5
30	MD-4	338/710	3.31	0.30	4.6	1.14	6.7	23.5	4.2
29	MD-4	343/899	3.25	0.32	4.9	1.24	5.7	22.9	4.4
35	MD-4	349/1096	2.19	0.34	4.4	1.94	7.2	13.1	7.6
39	MD-4	(300)/515	3.80	0.32	15.5	1.06	7.3	84.8	1.2
38	MD-4	329/704	3.80	0.25	15.6	0.83	5.9	109.	.91
40	MD-4	352/899	2.80	0.35	15.2	1.57	6.6	56.0	1.8
36	MD-4	343/1096	2.20	0.33	14.1	1.88	7.2	43.3	2.3

(1) MD-4, molecular formula assumed = $C_{13}H_{16}$, MW = 172, density = 0.98 g/ml.

(2) Stoichiometric Oxygen for MD-4 = 17 moles O_2/mole.

(3) Fuel equivalence ratio, $= \dfrac{\text{Fuel/Air, actual}}{\text{Fuel/Air, stoichiometric}} = \dfrac{100}{\text{stoichiometric oxygen}}$

TABLE III. NORMALIZED AVERAGE RECOVERIES OF SOLIDS, LIQUIDS AND GASES FROM
PYROLYSIS AND OXIDATIVE-PYROLYSIS OF SRC II DISTILLATE FRACTIONS

Av. Percent of Stoich. Oxygen Temp, °C	0%			7%			20%			73%		
	Gas	Liquid	Solid	Gas	Liquid	Solid	Gas	Liquid	Solid	Gas	Liquid	Solid
500	3.2	96.8	0.0	4.0	96.0	0.0	4.6	95.4	0.0	6.3	93.7	0.0
700	4.4	87.7	7.9	20.8	76.2	3.0	(24.6)[1]	72.1	(3.4)[1]	28.3	71.7	(0.0)[2]
900	4.8	74.7	20.5	25.4	60.4	14.5	33.2	56.2	10.6	50.1	49.9	(0.0)[2]
1100	5.5	0.0	94.5[3]	23.8	0.0	(76.2)[3,4]	33.9	0.0	66.1[3]	66.3	0.0	(33.7)[2,3]

(1) Based on averages of data at conditions of higher and lower oxygen concentrations.
(2) Based on assumption that no solids remained in tube at high oxygen levels.
(3) Solids caught in condenser traps combined with solids left on reactor wall.
(4) By difference.

decrease in sulfur content from an average of 0.21 weight per-
cent in the distillation cuts to 0.06 weight percent in the
liquid products. Other chemical changes were small. When the
temperature was increased from 500 °C to 1100 °C, several changes
occurred in each of the distillate fractions.

Aromaticity. The ratio of aromatic carbon to total carbon
increased from an average of 0.53 in the starting material and
0.56 at 500 °C to 0.83 at 700 °C, 0.95 at 900 °C, and 0.99 at 1100 °C
(for the solids). The number of aromatic rings increased propor-
tionally. There was almost uniform behavior among the different
boiling point fractions, as shown in Figure 3. Aromatization of
the ring systems is an important reaction during pyrolysis.
        Figure 4 shows the relationship between aromaticity of the
liquid products at each temperature and the stoichiometric amount
of oxygen available during oxidative pyrolysis. Aromaticity does
not appear to increase significantly with increasing concentration
of oxygen at any temperature.
        The number of aromatic ring substituents and the average
substituent length decreased with increasing pyrolysis temperature
as shown in Figures 5 and 6, respectively. These data include
aliphatic rings attached to aromatic rings at two points, as in
tetralin-type molecules. The numbers of substituents decreased
from approximately three per ring in the starting material and at
500 °C to approximately one per ring at 900 °C. The aliphatic
substituents are very short, ranging from an average of less than
two carbon atoms at low temperatures to less than one carbon atom
per substituent (including phenolic functional groups) at 900 °C.
Data could not be obtained on the solids produced at 1100 °C.

Molecular Weight. Aromatization of hydroaromatic structures,
rather than removal of aliphatic substituents, was suggested be-
cause the weight per molecule remained approximately constant with
increasing temperature up to 900 °C. The shift to solid products
at 1100 °C probably represents a significant increase in molecular
weight.
        The relationship between molecular weight and fraction of
stoichiometric oxygen is shown in Figure 7. At 500 and 700 °C,
molecular weight declined but at 900 °C the molecular weight in-
creased with increasing fraction of stoichiometric oxygen. Oxida-
tion (the addition of oxygen) appears to be the cause of the
molecular weight increase. No data could be obtained at 1100 °C.

Elemental Composition. The weight percent of carbon was
roughly constant from 500 °to 900 °C but jumped significantly at
1100 °C, as shown in Figure 8. The 1100 °C sample was collected in
the condensers and was probably obtained in approximately the
same residence time as the samples obtained at the lower tempera-
tures. Hydrogen dropped to less than 1 weight percent and oxygen
(by difference) also dropped to about 1 weight percent at 1100 °C.
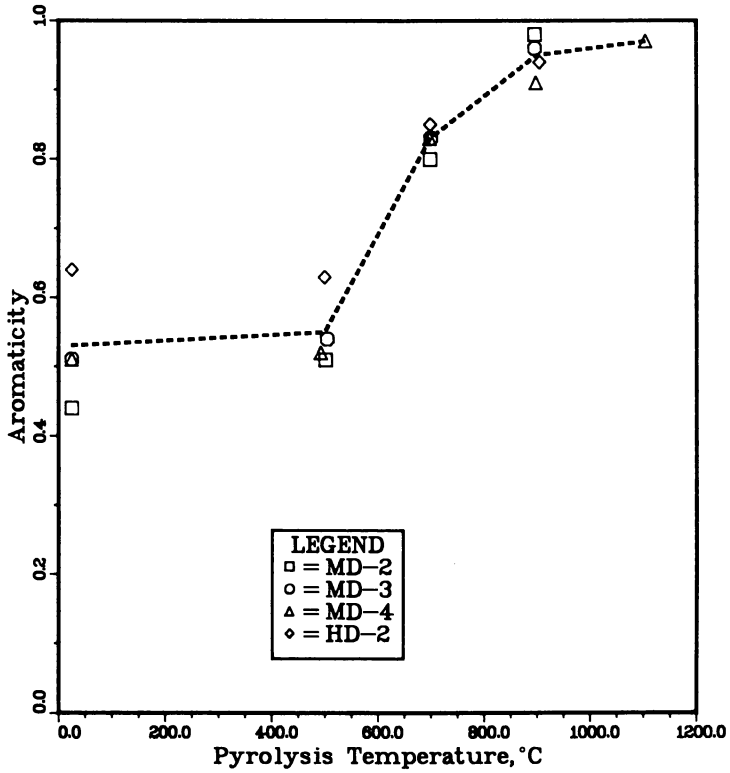
FIGURE 3.
AROMATICITY OF LIQUID PRODUCTS VERSUS PYROLYSIS TEMPERATURE
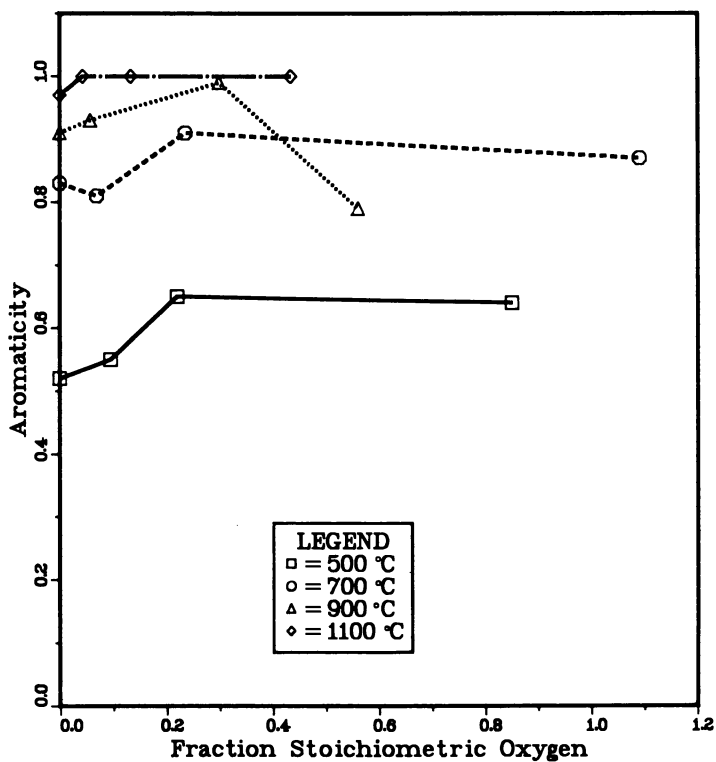
FIGURE 4.
AROMATICITY VERSUS FRACTION OF STOICHIOMETRIC OXYGEN
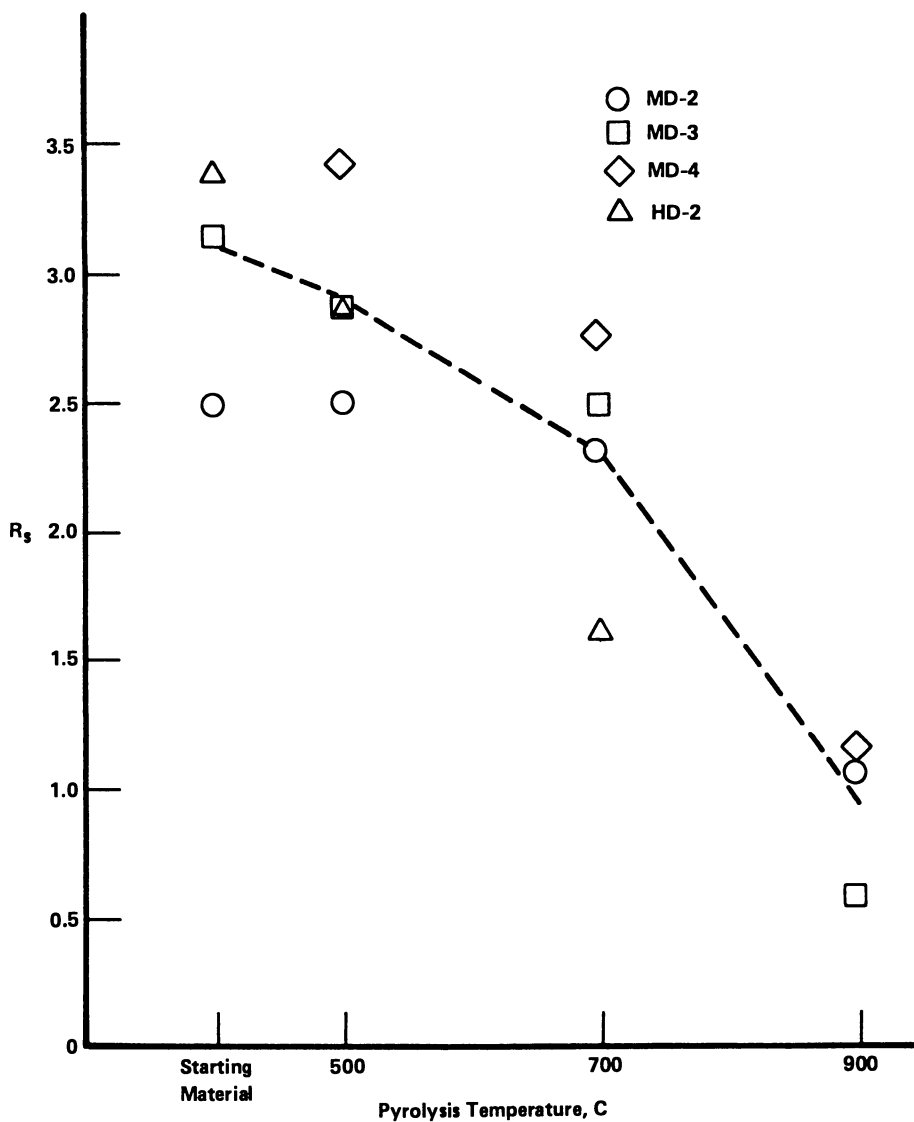
FIGURE 5.
NUMBER OF AROMATIC RING SUBSTITUENTS (R_s) VERSUS PYROLYSIS
TEMPERATURE
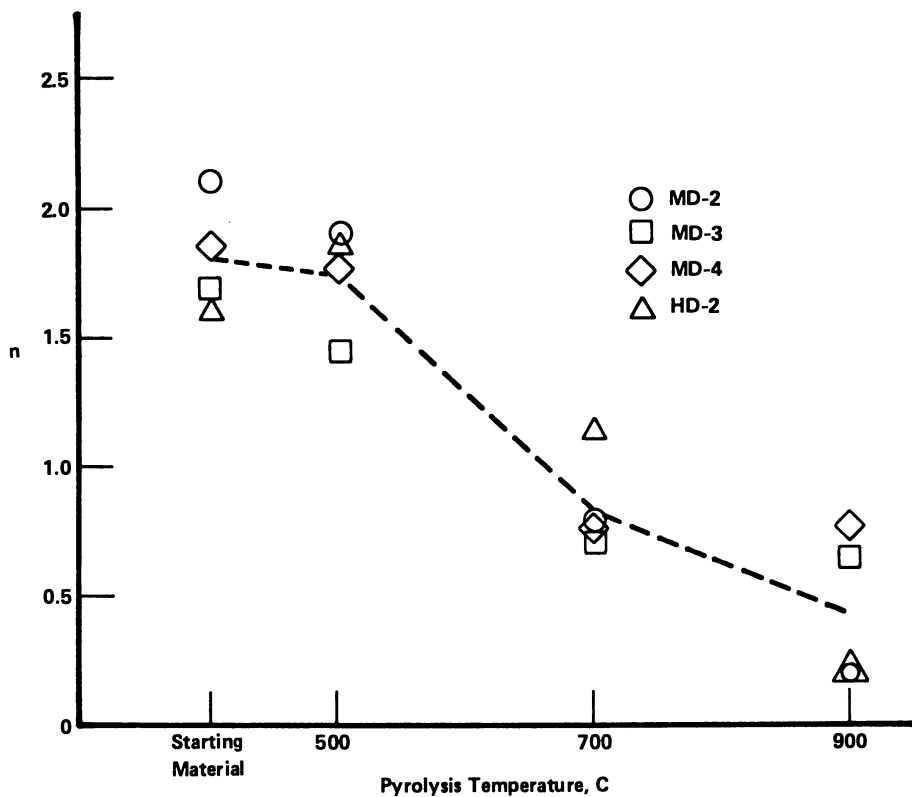
FIGURE 6.
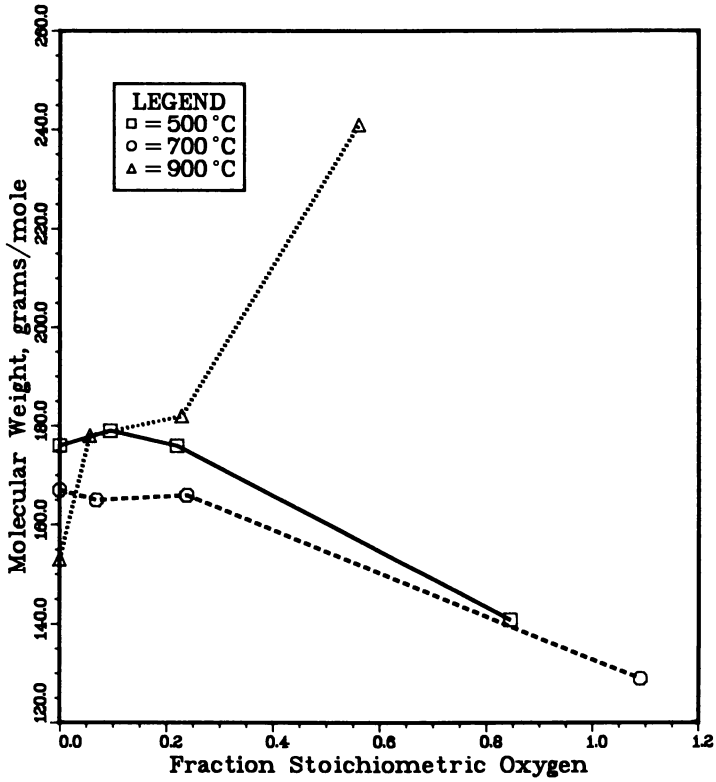SUBSTITUENT LENGTH (n) VERSUS PYROLYSIS TEMPERATURE

FIGURE 7.
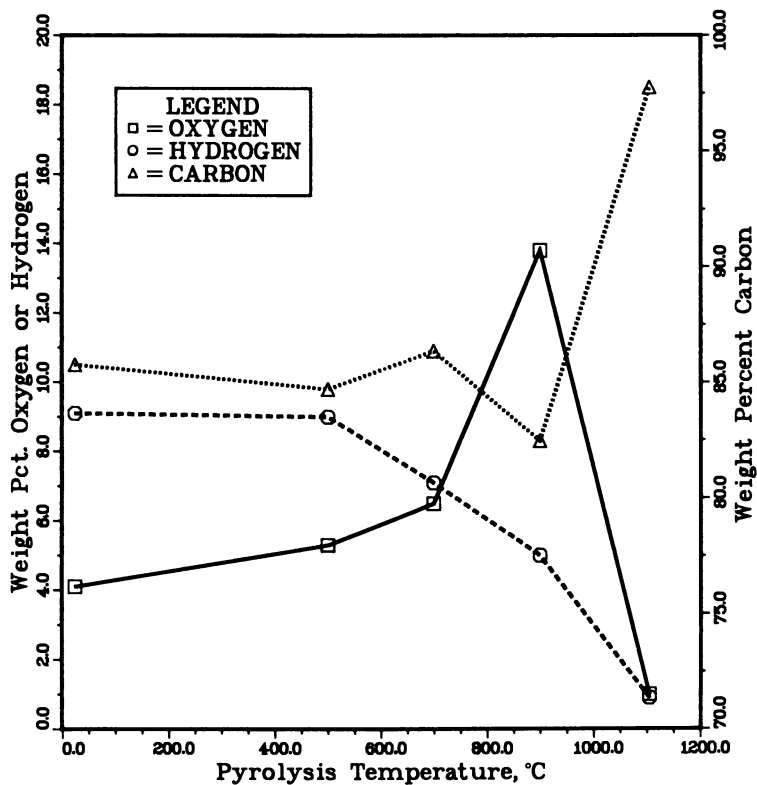MOLECULAR WEIGHT VERSUS FRACTION OF STOICHIOMETRIC OXYGEN

FIGURE 8.
CARBON, HYDROGEN AND OXYGEN CONTENT VERSUS PYROLYSIS TEMPERATURE

Compounds containing oxygen and hydrogen are destroyed between 900° and 1100°C at the residence times used in these experiments (about 7 seconds). A highly carbonaceous material, presumably with a graphitic structure, was obtained at 1100°C. There appeared to be little difference in the carbonaceous products obtained at 1100°C from the different SRC II distillation fractions.

There was a significant increase in the concentration of other elements, presumably oxygen, up to 900°C. The increase in oxygen must result from preferential retention in the liquid products of the oxygen in the SRC II distillation cuts. There is no other source of oxygen in the system. This is not surprising since the nonliquid products consist of soot (carbon) and light gases (primarily methane). Most or all of the oxygen in the SRC II distillation cuts is phenolic. The phenolic substituent apparently inhibits soot formation, possibly by quenching free radicals formed thermally during pyrolysis.

The hydrogen distribution is shown in more detail versus temperature in Figure 9. The average number of hydrogen atoms per molecule decreased and aliphatic hydrogen decreased to no more than one per molecule at 900°C. There was an increase in the number of aromatic hydrogens per molecule.

The changes in elemental composition of the oxidation-pyrolysis liquids with increasing fraction of stoichiometric oxygen are shown in Figures 10-12. Carbon and hydrogen declined slightly while oxygen content increased. This is apparently due to oxygen incorporation in the molecules by oxidation. A mechanism such as the one described by Santoro and Glassman, in which dihydroxy benzenes are intermediates, is in agreement with this observation (4).

Unsubstituted Aromatics. The analyses indicated that the mixture was simplified during pyrolysis until it consisted primarily of unsubstituted aromatics such as benzene, naphthalene, phenanthrene, and pyrene. Of course, aromatization is not the only mechanism occurring since liquid products with both higher and lower molecular weights than the starting liquids, as well as gases and carbon, were formed.

However, substantial amounts of the unsubstituted aromatics were found, as shown in Figure 13. At 900°C more than 60 percent of each liquid product was unsubstituted aromatics. The amounts of one, two, and three ring molecules (i.e., benzene, naphthalene, and phenenthrene) varied with the molecular weight of the starting material. For example, the liquid product of MD-3 at 900°C was more than 50 percent benzene while naphthalene was more than 30 percent of the liquid product from MD-4 at 900°C. These unsubstituted aromatics are more thermally stable than substituted aromatic molecules and can be considered soot precursors in staged combustion processes.
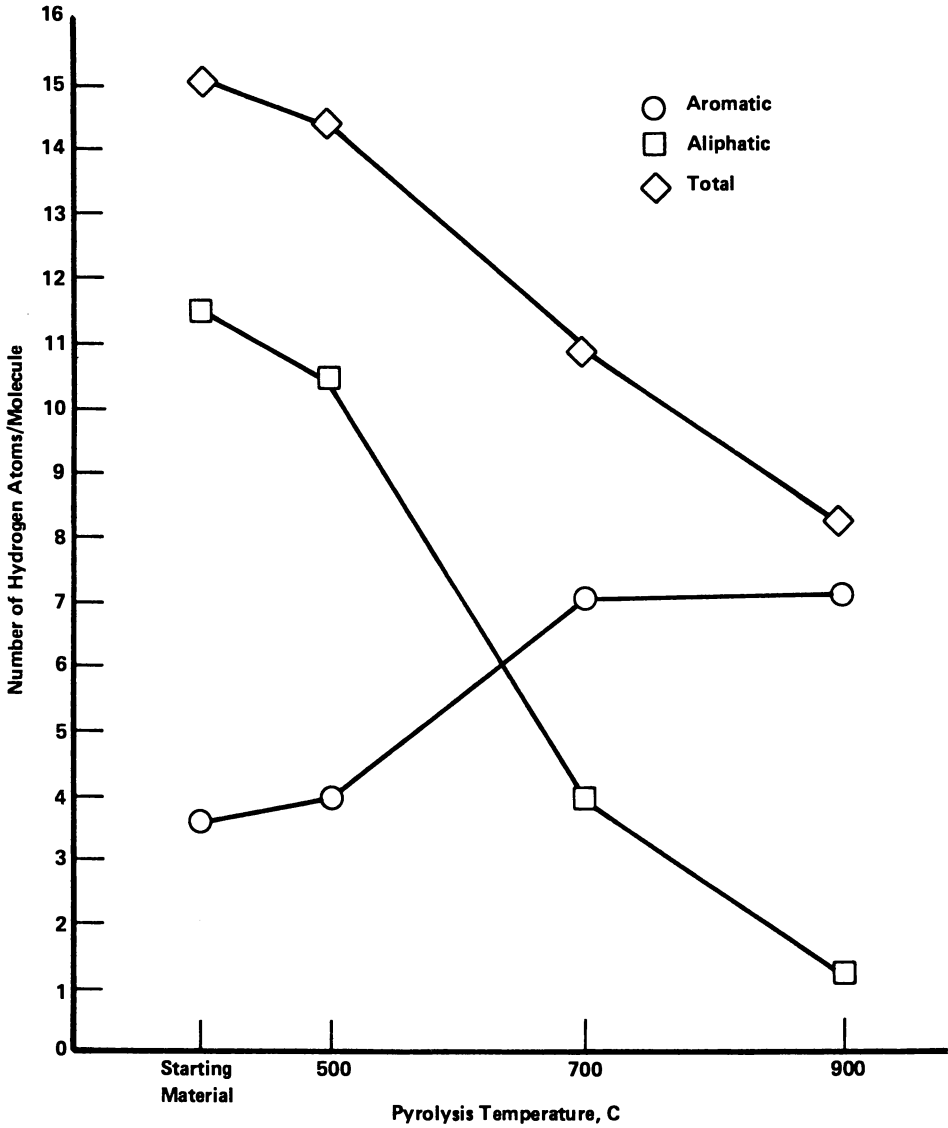
FIGURE 9.
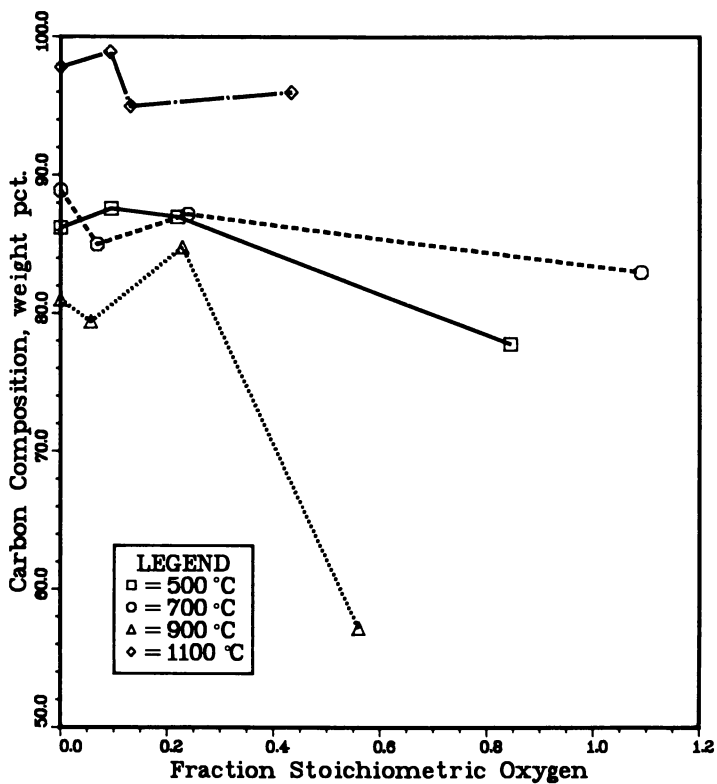HYDROGEN DISTRIBUTION VERSUS PYROLYSIS TEMPERATURE

FIGURE 10.
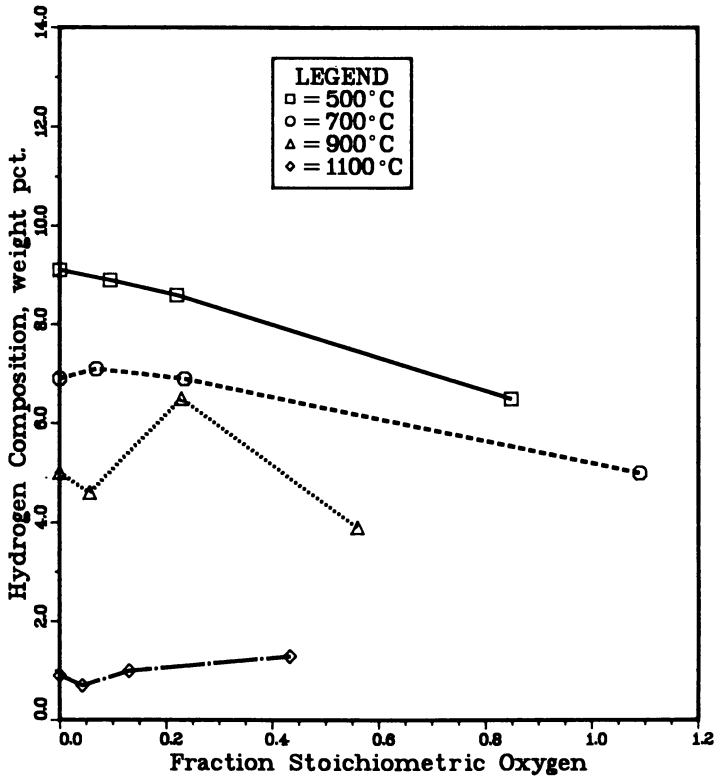CARBON COMPOSITION VERSUS FRACTION OF STOICHIOMETRIC OXYGEN

FIGURE 11.
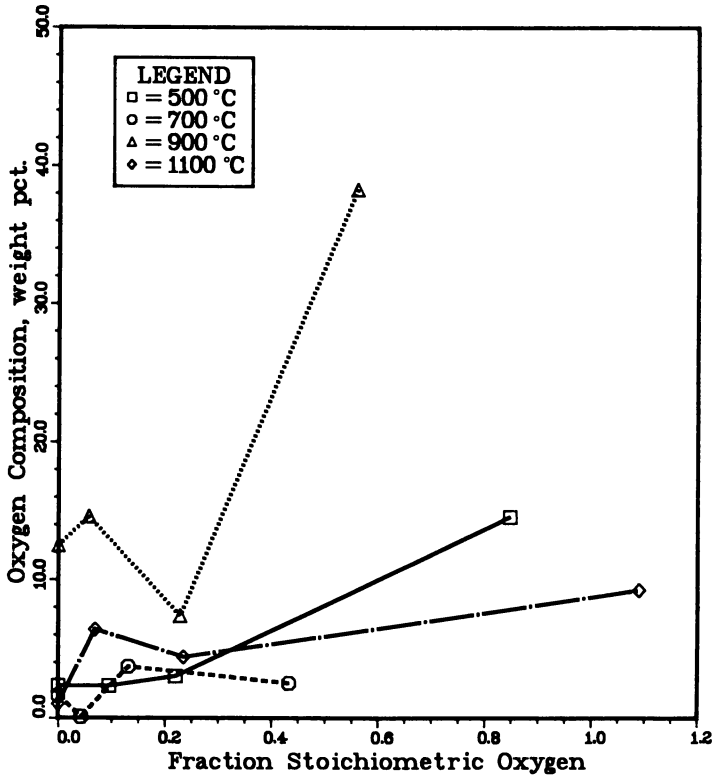HYDROGEN COMPOSITION VERSUS FRACTION OF STOICHIOMETRIC OXYGEN

FIGURE 12.
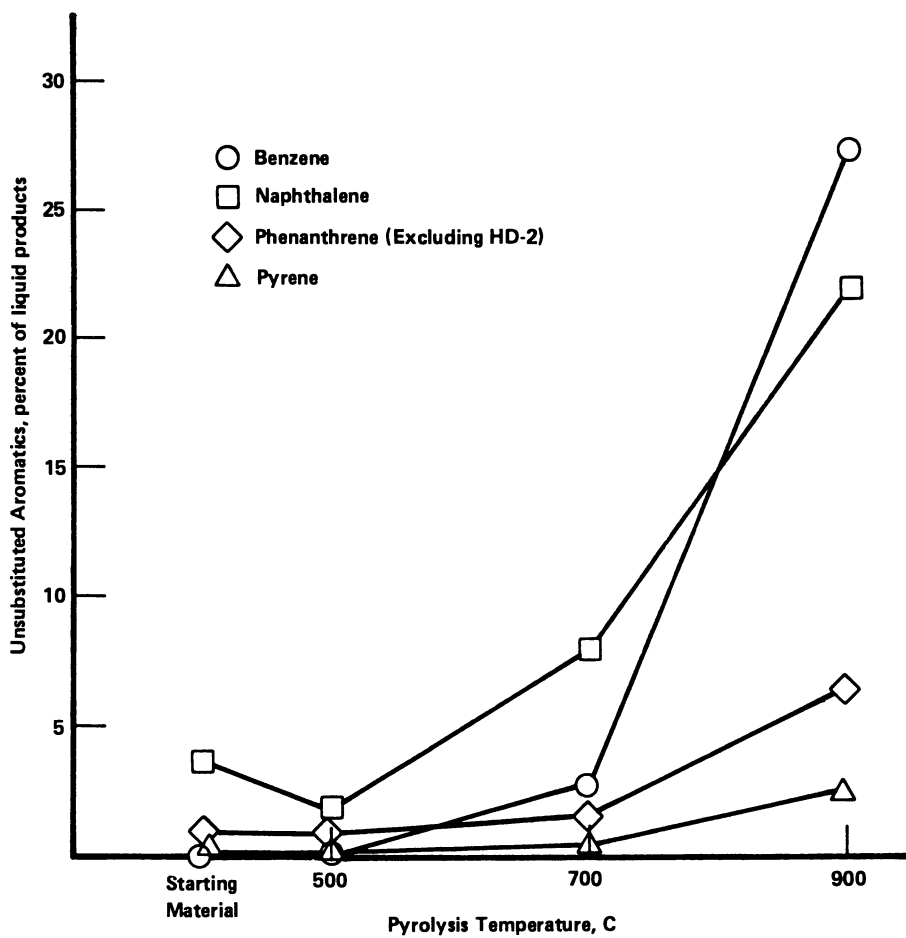OXYGEN COMPOSITION VERSUS FRACTION OF STOICHIOMETRIC OXYGEN

FIGURE 13.
UNSUBSTITUTED AROMATICS IN THE LIQUID PRODUCT VERSUS PYROLYSIS
TEMPERATURE

Figure 14 shows the amounts of unsubstituted aromatics in the liquid products versus fraction of stoichiometric oxygen present. At the highest concentrations of oxygen and 900°C, the amounts of unsubstituted aromatics decreased, apparently due to the formation of molecules with oxygen substituted on the aromatic rings.

Nitrogen Distribution. As shown in Figure 15, total nitrogen was unchanged from room temperature to 500°C, was preferentially retained in the unpyrolyzed liquids between 500 and 700°C and was destroyed at an increasing rate from 700 to 1100°C. There was a conversion of basic to nonbasic nitrogen below 500°C and basic nitrogen appeared to be less stable than nonbasic nitrogen at all temperatures. It is currently thought that basic nitrogen is primarily pyridine and quinoline-type compounds, which are relatively stable, and nonbasic nitrogen is pyrole and similar compounds, which are generally less stable. These results suggest that the assumed nitrogen types are incorrect.

Figure 16 indicates that nitrogen distribution remains approximately constant as the fraction of stoichiometric oxygen is increased.

Summary

The oxidative pyrolysis reactions of SRC II distillation cuts boiling from 150°C to 350°C are similar. Aromatization occurs as temperature is increased, resulting in nearly constant carbon concentration and molecular weight from 500°C to 900°C with a significant loss of total hydrogen (although aromatic hydrogen increases) and a significant increase in oxygen concentration. This indicates that phenolic oxygen is a relatively stable functional group, while short aliphatic side chains are lost to produce large amounts of unsubstituted aromatics. These are presumed to be soot precursors in staged combustion.

Nonbasic nitrogen is more stable than basic nitrogen. Total nitrogen content increases up to 700°C although a significant interconversion of basic to nonbasic nitrogen occurs around 500°C. The stable nonbasic nitrogen compounds may be the major source of NO_x emissions from the second stage of staged combustion.

As the percent stoichiometric oxygen is increased, aromaticity remains constant. Carbon and hydrogen content and the concentration of unsubstituted aromatics decrease as oxygen is added by oxidation.

Thus, the most likely survivors of fuel-rich, first-stage pyrolysis are unsubstituted and oxygen substituted aromatics and nonbasic nitrogen compounds. These are the precursors to soot and NO_x formation during oxygen-rich, second-stage combustion.
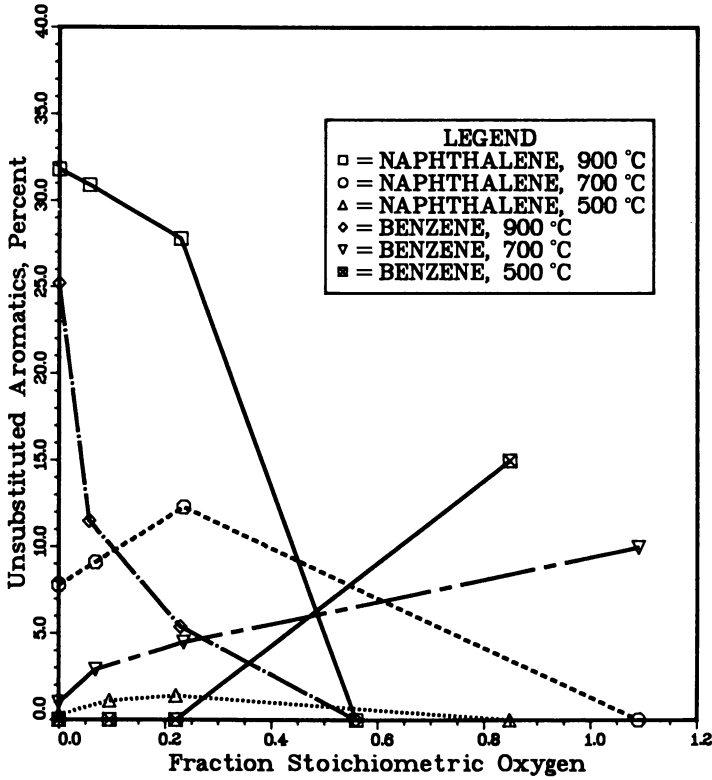
FIGURE 14.
CONCENTRATION OF UNSUBSTITUTED AROMATICS IN THE LIQUID PRODUCT
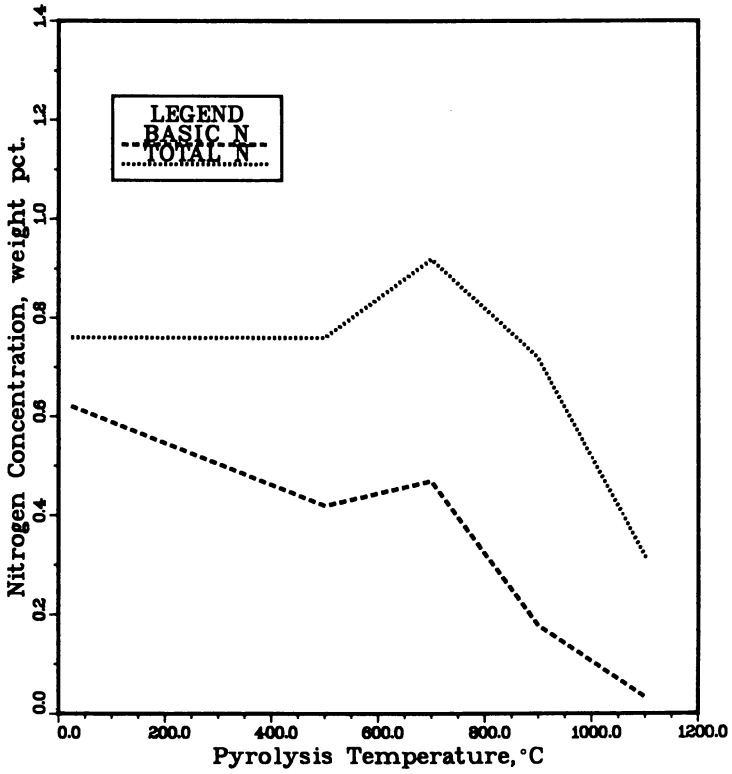VERSUS FRACTION OF STOICHIOMETRIC OXYGEN

FIGURE 15.
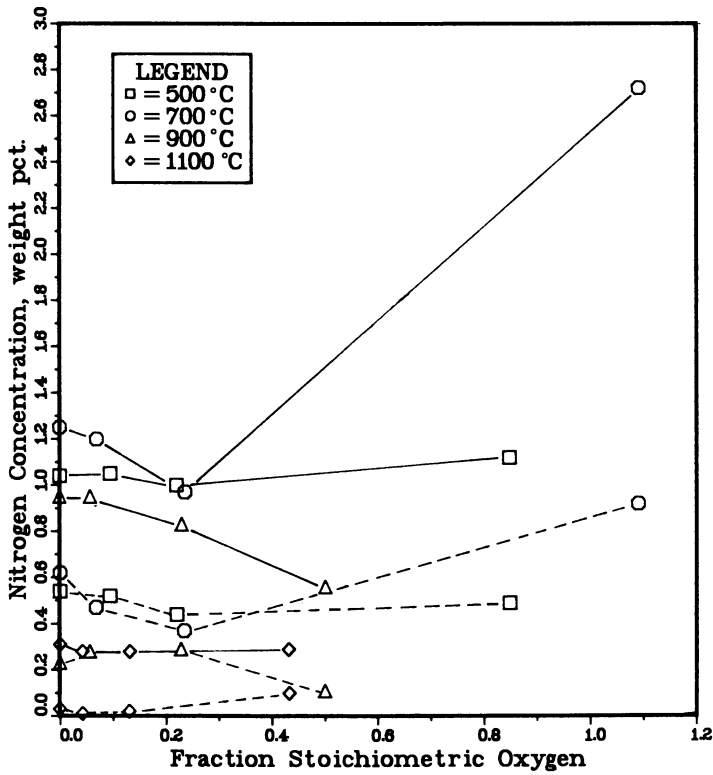NITROGEN DISTRIBUTION VERSUS PYROLYSIS TEMPERATURE

FIGURE 16.
NITROGEN DISTRIBUTION VERSUS FRACTION OF STOICHIOMETRIC OXYGEN
(Total N ———, Basic N ———)

Acknowledgment

Literature Cited

1. Black, C.H.; Chin, H.H.; Fischer, J.; Clinch, J.D. "Review and Analysis of Spray Combustion as Related to Alternative Fuels"; Argonne National Laboratory; Report No. ANL-79-77 prepared for the U.S. Department of Energy; Contract No. W-31-109-Eng-38.
2. Moore R.T.; McCutchan, P.; Young, D.A.; Anal. Chem. 1951; 23 (11), 1639-1641.
3. Schwager, I.; Farmanian, P.A.; Yen, T.F. "Analytical Chemistry of Liquid Fuel Sources", ACS Advances in Chemistry Series 170; American Chemical Society: Washington, D.C. 1978; Chapter 5.
4. Santoro, R.J.; Glassman, I.; Combustion Science and Technology 1979; 19, 161-164.

RECEIVED October 29, 1982

Nonequilibrium Distillation Effects in Vaporizing Droplet Streams

S. HANSON, J. M. BEER, and A. F. SAROFIM

Massachusetts Institute of Technology, Department of Chemical Engineering,
Cambridge, MA 02139

The combustion of fossil fuels in the United States will be complicated by an increased reliance on fuels with high nitrogen and low hydrogen content. The problem will be aggravated by the displacement of petroleum-based fuels by coal-derived synthetic fuels and shale oil.

Previous studies on the contribution of fuel nitrogen to NO_x emissions (1,2) used specific combustion systems and fuels doped with fuel nitrogen. These experiments provided useful information for the systems studied and indicated that the most effective method for limiting the formation of NO_x from fuel nitrogen is staged combustion. Staged combustion takes advantage of the fact that fuel nitrogen in the gas phase is strongly dependent on the oxygen available. This method consists of a fuel-rich first stage, in which the fuel nitrogen is released and converted mostly to N_2, followed by a second stage in which the remaining oxygen is added to complete the combustion. The process requires that the fuel nitrogen be evolved into the gas phase prior to exiting the first stage, and with sufficient residence time to participate in the gas phase reactions that form N_2. Therefore, the objective of this study has been to determine the rate of nitrogen evolution from vaporizing fuel droplets.

In order to obtain detailed information on the evolution of fuel nitrogen, a laminar flow drop tube furnace, able to simulate conditions found in actual combustion systems, was adopted for this study.

The nitrogen in fuels consists of complex, mostly heterocyclic compounds. In petroleum crudes, these include pyrroles, indoles, isoquinolines, acridines, and porphyrins. During refining most of these concentrate in the heavy resin and asphaltene fractions, which might suggest their relatively late release in the

combustion of residual fuel oils. However, the evolution of nitro-
gen from a heavy fuel oil droplet during its vaporization in a
flame differs significantly from the results of equilibrium distil-
lation obtained under slow heating conditions at atmospheric pres-
sure.

The evolution of a particular compound is determined by the
rate of droplet vaporization, the relative volatility and diffusi-
vity in the liquid phase of the compound in question. Because of
the complex composition of fuel oils, it is difficult to separate
the relative importance of these effects since the measured nitro-
gen evolution is a summation of many fractions, each of which is
influenced to a different extent. In order to reveal the role of
diffusion and relative volatility in the evolution of fuel nitro-
gen, a complementary set of experiments were performed using n-
dodecane doped with pyridine, quinoline or acridine.

In the following, experimental results are presented of the
evolution of fuel nitrogen during equilibrium distillation and in-
ert pyrolysis of droplet arrays in the laminar flow furnace for
three fuel oils and a doped model fuel.

EXPERIMENTAL

The experimental furnace is a vertically oriented laminar
flow drop tube furnace having a 30 cm long uniformly hot test sec-
tion with optical access. The fuel droplet array is introduced on
the logitudinal axis concurrently with the ambient gas. The drop-
let stream is interrupted at several points in its trajectory by a
sampling probe inserted axially from the base of the furnace. The
probe quenches and transports the entire flow to a sampling train
which recovers the fuel droplet residue for analysis. The above
process is repeated at several furnace temperatures for each fuel.
A detailed description of the system is to be found in references
(3) and (4).

RESULTS

Table 1 presents the fuel properties and composition of the
fuels studied, namely, an Indo-Malaysian residual petroleum fuel,
a Gulf #6 petroleum fuel, and a raw Paraho shale oil. These fuels
all have a C/H atomic ratio of about 0.6 and have similar boiling
curves. However, when one considers the nitrogen content, differ-
ences in composition and behavior emerge. The Indo-Malaysian re-
sidual petroleum fuel contains the least nitrogen, 0.25% by weight;
the raw Paraho shale oil contains the most, 2.15% by weight. The
Gulf #6 petroleum fuel resembles the Indo-Malaysian petroleum fuel
more closely in source and composition, having 0.44% by weight ni-

TABLE 1: FUEL OIL ANALYSIS

	Raw Paraho Shale Oil	Indo-Malaysian Petroleum	Gulf #6 Petroleum
API Gravity at 15°C	37	21.8	13.2
Viscosity ssu at 40°C	100	300	----
ssu at 70°C	27	50	----
ssu at 100°C	12	18	----
Flash Point °C	49	99	68
Pour Point °C	27	16	4.5
Heat of Combustion			
Gross Btu/lb	19,400	19,070	18,400
Net Btu/lb	18,240	17,980	17,260
Elemental Analysis			
Carbon %	83.55	87.08	88.29
Hydrogen %	11.69	12.05	12.31
Nitrogen %	2.15	0.25	0.44
Sulfur %	0.74	0.23	----
Ash %	0.09	0.036	<0.05
Oxygen %	1.65	0.48	----

trogen. The differences in behavior of these fuels due to their
origin becomes even more apparent when considering the equilibrium
distillation results in Figures 1 and 2. The boiling curves for
these fuels are quite similar, but the fractional variation in C/H
atomic ratio and nitrogen concentration singles out the raw Paraho
shale oil for special consideration. Whereas the Indo-Malaysian
petroleum shows a gradually increasing C/H atomic ratio of the re-
sidual material, and the Gulf #6 petroleum shows a strong increase
in C/H atomic ratio, the raw Paraho shale oil exhibits no tendency
to vary its C/H atomic ratio. The evolution of nitrogen shows a
similar anomalous behavior. The natural fuels tested retain most
of their nitrogen, evolving no more than 1/4 of the original nitro-
gen after vaporizing over 3/4 of the mass. On the other hand, the
shale oil evolves nitrogen and mass proportionately.

    The equilibrium data presented clearly shows the shale oil
to behave differently from the petroleum fuels. However, under
conditions of rapid vaporization in an inert atmosphere a 150 μm
droplet array of these fuels exhibited trends not disclosed by the
equilibrium data. Figures 3, 4 and 5 display the non-equilibrium
evolution of fuel nitrogen with respect to mass vaporized for shale
oil, Indo-Malaysian petroleum, and Gulf petroleum respectively.
The shale oil is seen to yield up its nitrogen proportionately to
the mass evolved after an initial delay which increases with in-
creasing vaporization rate (temperature). During this delay, va-
porization is taking place; however, no nitrogen containing spe-
cies are evolved. The Indo-Malaysian petroleum and Gulf petroleum
fuels show no obvious temperature dependence. The Indo-Malaysian
delays evolution of its nitrogenous species until about 20% mass
vaporization has taken place, after which an initially rapid evo-
lution of nitrogen occurs which declines with increasing extent of
vaporization. The Gulf petroleum does not delay its evolution of
nitrogen but immediately evolves it proportionately to the mass.

    In order to identify the type of material associated with the
evolved nitrogen, the C/H atomic ratios for the residual fuel drop-
lets are presented in Figure 6. The shale oil has a C/H atomic
ratio which increases with mass vaporized, and a rate of increase
which is greater with higher rates of vaporization. Comparision
with its equilibrium behavior shows that the initial delay in the
nitrogen evolution is associated with light nitrogen deficient
species, and that these species are extracted to a greater extent
at higher rates of vaporization in agreement with the increased
delays in nitrogen evolution.

    Table 2 presents the properties and composition of the model
fuels used. The low concentration of acridine is a result of its
poor solubility. The boiling curves are similar to that of n-do-
decane. The equilibrium distillation curves for these mixtures
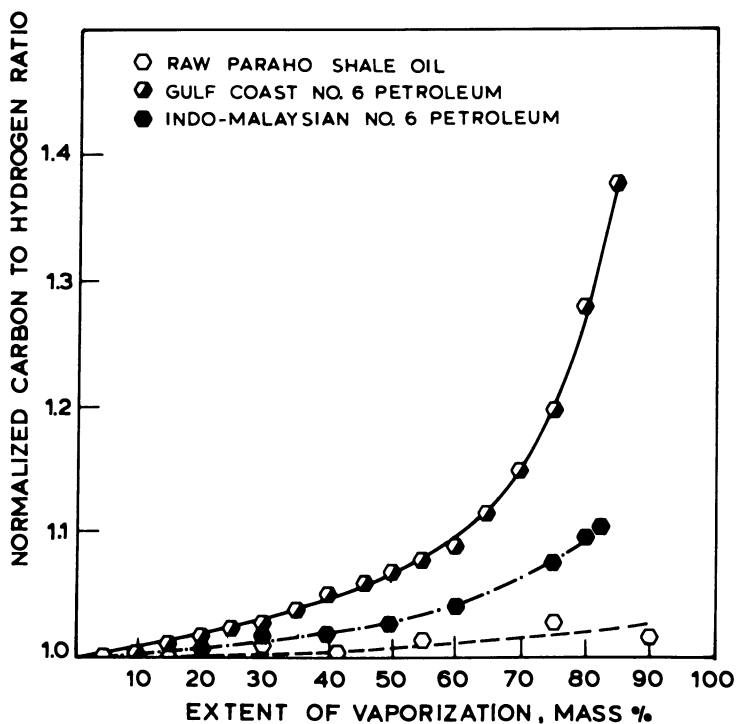are presented in Figure 7. The pyridine, being particularly vola-

Figure 1. Normalized carbon to hydrogen atomic ratios of fuel residues during equilibrium batch distillation of Gulf Coast No. 6 petroleum fuel oil, Indo–Malaysian No. 6 petroleum fuel oil, and Raw Paraho shale oil.
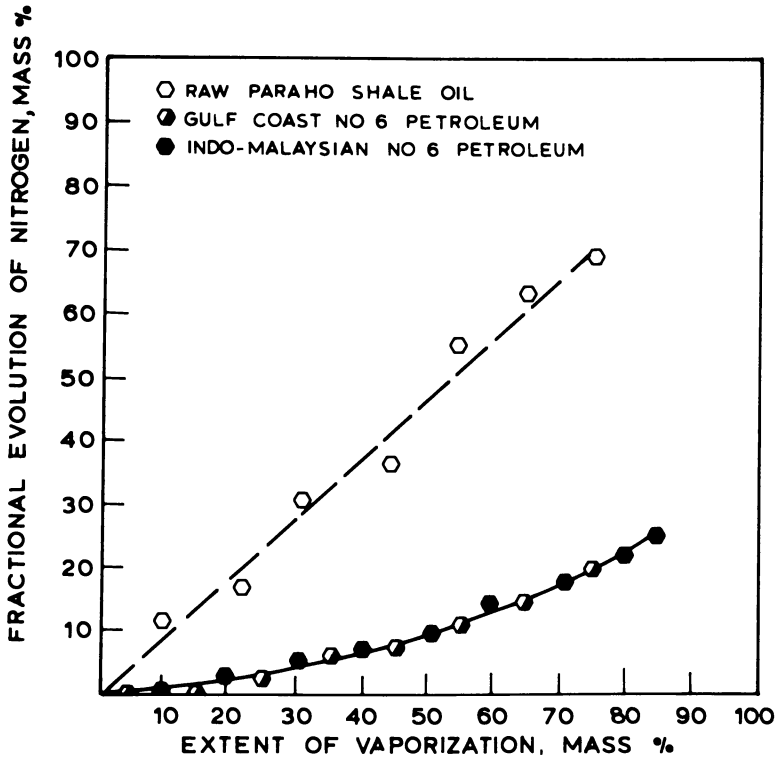
Figure 2.   Nitrogen evolution during equilibirium batch distilla-
tion of Gulf Coast No. 6 petroleum oil, Indo–Malaysian No. 6
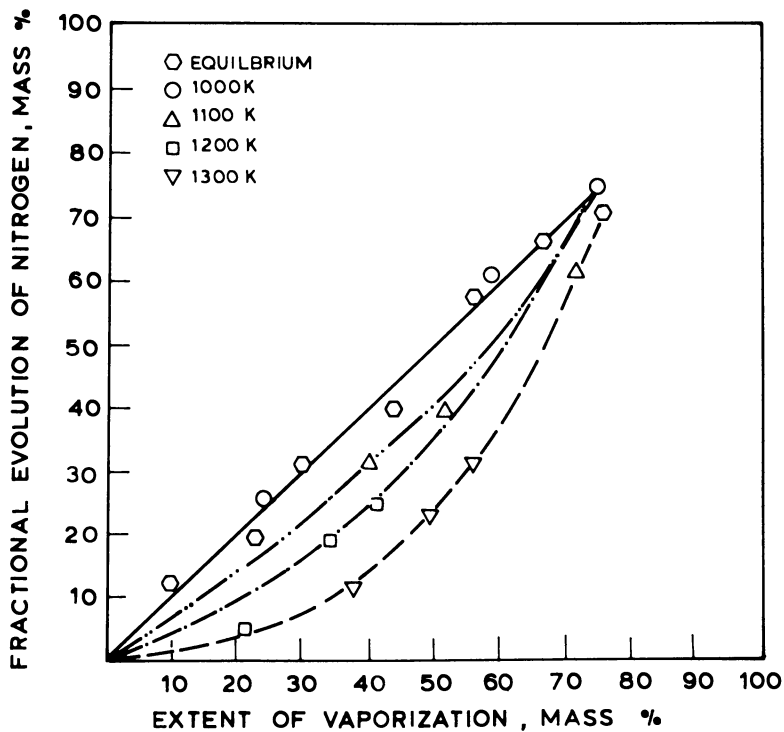petroleum fuel oil, and Raw Paraho shale oil.

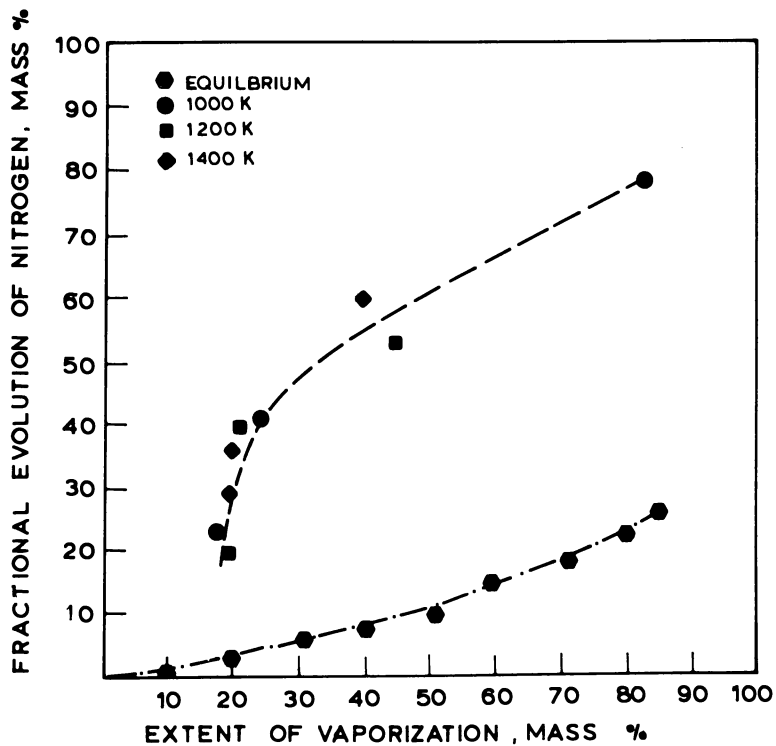Figure 3. Nitrogen evolution from pyrolysing 150 μm droplet arrays of Raw Paraho shale oil.

Figure 4. Nitrogen evolution from pyrolysing 150 μm droplet arrays of Indo–Malaysian No. 6 petroleum fuel oil.
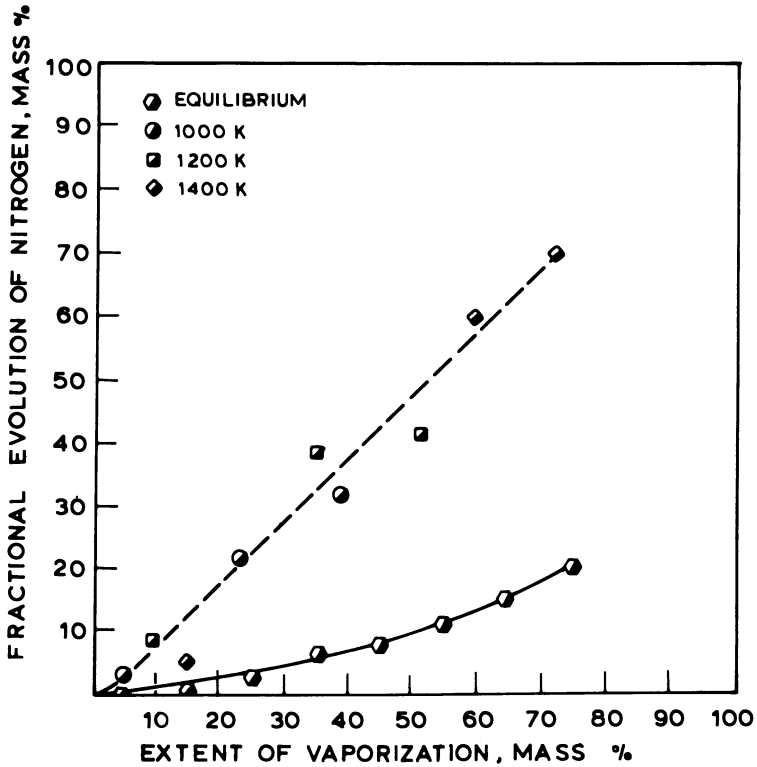
Figure 5. Nitrogen evolution from pyrolysing 150 μm droplet arrays of Gulf Coast No. 6 petroleum fuel oil.
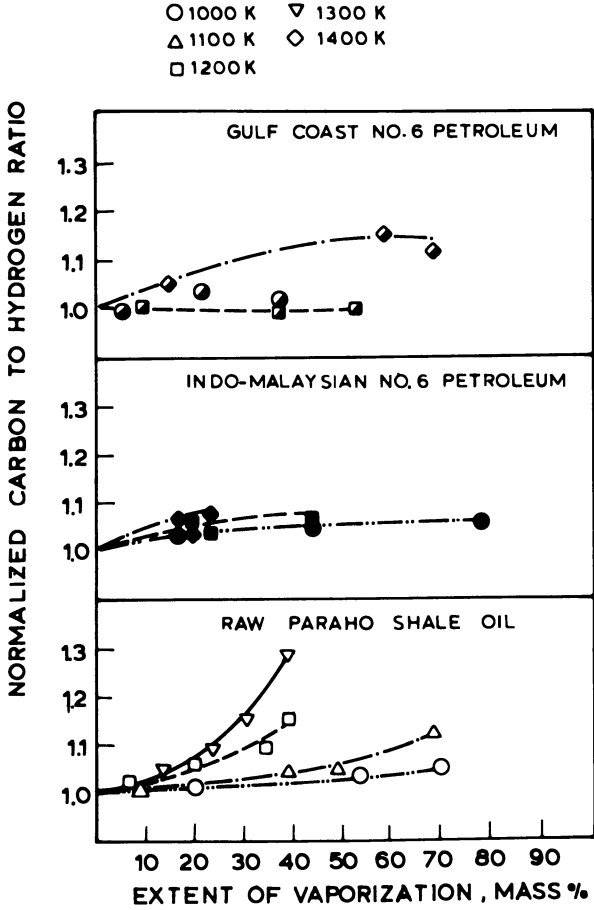
Figure 6. Normalized carbon to hydrogen atomic ratios of fuel residues from pyrolysing 150 μm droplet arrays of Gulf Coast No. 6 petroleum fuel oil, Indo–Malaysian No. 6 petroleum fuel oil and Raw Paraho shale oil.

TABLE 2:   MODEL FUEL PROPERTIES

	n–Dodecane	Pyridine	Quinoline	Acridine
Molecular Weight	170.3	79.1	129.2	179.2
Normal Boiling Point, °C	216.2	115.4	237.7	346.0
Mole Fractions Mixture 1	0.874	0.126	---	---
Mole Fractions Mixture 2	0.867	---	0.133	---
Mole Fractions Mixture 3	0.984	---	---	0.016
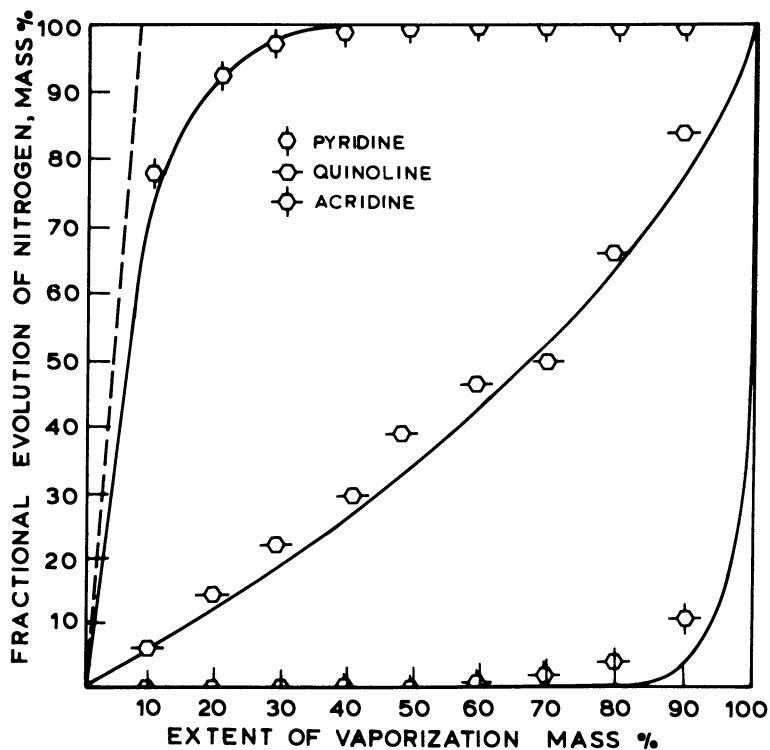
Figure 7. Nitrogen evolution during equilibrium batch distilla-
tion of n–dodecane doped with pyridine, quinoline, or acridine
(Data points are experimental, solid lines are calculations from
theory.)

tile, has been totally evolved when the extent of vaporization is 40%. At the other extreme, acridine is barely beginning to evolve at an extent of vaporization of 80%. The quinoline, having a boiling point not much greater than n-dodecane, is uniformly evolved as expected for a moderately lower relative volatility with respect to n-Dodecane.

The results of the fractional evolution of dopant as a function of extent of vaporization for a 150 μm droplet array in an inert environment is shown in Figure 8. The dopants all exhibited improved rates of vaporization compared to their equilibrium rates. The extreme cases of pyridine and acridine showed no observable effect of vaporization rate. However, the quinoline data displays a temperature dependent behavior.

DISCUSSION

When a droplet of fuel oil is introduced into a hot, oxygen deficient environment, the droplet will heat up until its surface attains the initial boiling point of the fuel. Internally to a lesser or greater extent, depending upon the droplet size, a thermal gradient will be established. At the droplet surface the more volatile compounds are evolved. This causes several effects.

In the gas phase the radial convective flux thickens the boundary laye ⁻ surrounding the droplet causing reduced rates in heat transfer and a reduction in drag experienced by the droplet. As the droplet vaporizes the temperature profile in the boundary layer adjusts to provide the enthalpy flux to the surface needed for vaporization. A transient persists throughout the vaporization of a multicomponent fuel, since the surface temperature is always rising with changing surface composition. The changing surface temperature also influences the liquid phase temperature profiles. However, once vaporization has begun, this is a small contribution relative to the latent heat lost with the volatile species.

In the liquid phase the loss of light (low C/H atomic ratio) species from the surface causes a concentration profile to be established for each compound. The lighter compounds, being deficient at the surface, diffuse to the surface; and the heavier compounds, being concentrated at the surface, diffuse towards the center of the droplet. The combined effects of vaporization and diffusion determine the surface composition and thereby the surface temperature. This combination of temperature and composition determines the relative volatilities of the species present at the surface and hence the vapor phase composition.

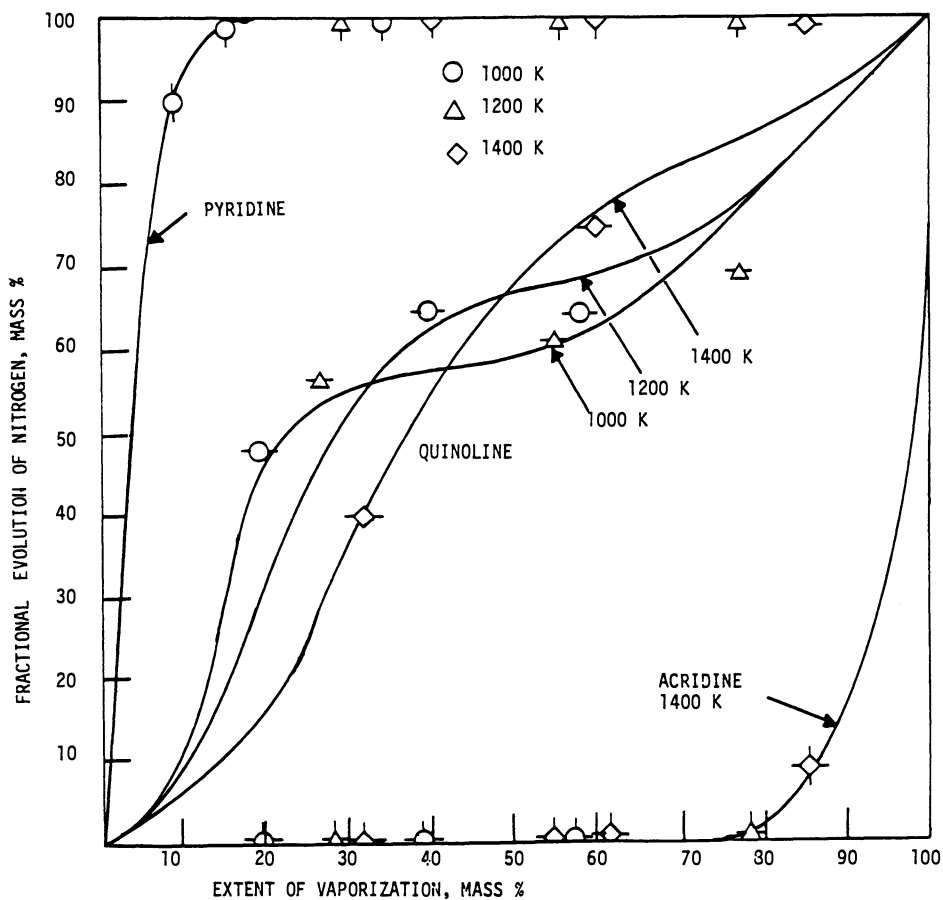In the case of equilibrium distillation under well-mixed con-

Figure 8. Nitrogen evolution form pyrolysing 150 um droplet arrays of n-dodecane dopes with pyridine, quinoline or acridine. (Data points are experimental, solid lines are calculations from theory.)

ditions, the evolution of a particular component from an ideal so-
lution is given by the following thermodynamic expression:

$$y_i = \frac{x_i}{P} \exp\left\{\frac{\Delta H_v}{R}\left(\frac{1}{T} - \frac{1}{T_{bi}}\right)\right\} \qquad 1)$$

where

y_i is the vapor phase mole of fraction i

x_i is the liquid phase mole of fraction i

P   is the ambient pressure

ΔH_v is the enthalpy of vaporization

R   is the ideal gas constant

T   is the liquid temperature

T_{bi} is the normal boiling point for pure i

The vapor phase contribution of the component in question is
influenced by its liquid phase mole fraction and temperature. The
overall composition determines the temperature and competition
with other species of differing relative volatilities can shift
the contribution of any particular component in its attempt to
satisfy the constraints $\Sigma x_i = 1$ and $\Sigma y_i = 1$. Thus, a fuel con-
taining a single nitrogenous compound may, due to the influence
of other species, produce a nitrogen distillation curve similar
to that presented for shale oil or Indo-Malaysian petroleum. For
shale oil it is known that there are many nitrogen containing spe-
cies, and what one observes is the summation of the nitrogen evol-
ved by all of them. The utility of the distillation curve is not
that it identifies which nitrogenous species are present, but that
it represents one extreme of vaporization from droplets where dif-
fusive mixing is rapid relative to weight loss by vaporization.

Following the arguments presented one may interpret the beha-
vior observed for the fuels studied. It should be mentioned that
these fuels have Lewis numbers of approximately 20 and therefore
internal temperature gradients of droplets are not significant.
Under these conditions a droplet which has undergone rapid vapori-
zation will have center temperature in excess of the saturation
temperature for the composition. The low boiling species trapped
in the droplet are superheated and have been observed to increase
the drop size by internal vaporization. The inclusion of effects
such as superheating and liquid phase reactions within the droplet
is not necessary for the interpretation of the experimental data.
Although such a qualitative description of non-equilibrium distil-
lation of multicomponent fuel droplets is simplified, it does ad-
dress the major factors affecting the evolution of fuel nitrogen.

Shale oil droplets, vaporizing at 1000 K, yield nitrogenous
species in a fashion similar to that exhibited during equilibrium
distillation. The C/H atomic ratio indicates a slight difference
in that the vaporizing droplet is evolving a product weighted to-
wards the light species, whereas the equilibrium product is compos-
ed of a uniform distribution that does not affect the residual C/H
atomic ratio. The rate of vaporization is not so great that the
nitrogen evolution appears significantly different from the equili-
brium case since diffusion processes are adequate to maintain a
uniform concentration of nitrogen containing species so as to give
an appearance similar to that of the equilibrium nitrogen evolution.
When increased rates of vaporization are encountered, light frac-
tions are removed from the droplet surface at such a rate that a
steep gradient in these compounds is created enabling more of the
light fractions to reach the surface where, because of the higher
surface temperature caused by bias in composition towards higher
molecular weights, the low molecular weight species are preferen-
tially vaporized. This preferential vaporization continues until
the surface concentration of the heavier nitrogen containing species
is large enough, relative to the light species concentration, to
offset the temperature effect. At this point, the nitrogen con-
taining species are evolved, and in this particular case, they are
vaporized at the same rate as the mass. Increasing the rate of
vaporization still further creates steeper initial surface concen-
tration gradients, greater penetration of the droplet by the con-
centration profile, higher surface temperatures and lower surface
concentrations of light species, resulting in a greater portion of
nitrogen deficient light species being evolved prior to nitrogen
evolution. The rate of vaporization for a given droplet size is
controlled by the ambient temperature and cannot be increased in-
definitely since liquid phase reactions at higher temperatures be-
come significant, terminating the above process by the formation
of a char. The tendency towards this end is evidenced by the
greater rate of increase in the C/H atomic ratio with increasing
temperature. The behavior discussed for shale oil is caused by
having a distribution of nitrogen containing species weighted to-
wards the higher molecular weights dispersed in a fuel having com-
ponents of widely varying molecular weight, and in which no compo-
nent is sufficiently abundant to dominate the fuel's overall be-
havior.

The Indo–Malaysian petroleum retains most of its nitrogen in
the residue from equilibrium distillation. The C/H atomic ratio
of the residue increases gradually throughout the distillation.
Thus one may infer the nitrogen to be held primarily in high mole-
cular weight species. The droplet pyrolysis results show a delay
in the nitrogen evolution similar to the shale oil. However, the
participation of nitrogen containing species is independent of tem-
perature. Apparently, the relative volatility of the light nitro-
gen deficient fraction is sufficiently great that for all tempera-

tures to which this fuel was subjected the rate of vaporization
could not exceed the rate of diffusion of light species until 20%
mass vaporization had occurred. The C/H atomic ratio supports this
description. During the first 20% mass loss the C/H atomic ratio
of the residue increases slightly, indicating a loss of light mat-
erial, after which it levels off due to the surface temperature
and composition being such that the heavy nitrogen containing frac-
tions may participate in the vaporization.

    The Gulf petroleum has an equilibrium profile similar to the
Indo-Malaysian petroleum except that the C/H atomic ratio increases
so much more rapidly. This rapid increase in C/H atomic ratio sug-
gests that no nitrogen free light components exists in large a-
mounts. This is complemented by the pyrolysis data in which no
delays and no significant temperature dependence were observed in
the nitrogen evolution. However, the nitrogen is bound in heavier
molecular weight species, but the adjustment in surface composition
is rapid (rate of vaporization) with respect to the diffusive pro-
cesses, permitting these heavier species to compete in the vapori-
zation. The C/H atomic ratio during droplet pyrolysis does not
deviate from the original fuel composition except at the highest
temperature, 1400 K, when a char is formed.

    The equilibrium distillation behavior of the model fuels is
adequately covered in the fuel oil discussion. However, the case
for the rapid droplet vaporization, which was not clearly seen for
fuel oils, is more amenable to analysis for a binary system. The
surface gradients are given by the following relationship,

$$\left(\frac{\partial m_i}{\partial r}\right)_L = \frac{\dot{m}''}{D_L} (m_{iL} - m_{iV}) \qquad\qquad 2)$$

where

   $\dot{m}''$ is the mass rate of vaporization per unit sur-
       face area

   m_i is the mass fraction, component i

   D   diffusivity

   L   subscript, denoting liquid phase

   V   subscript, denoting vapor phase

For a binary mixture the diffusivity is the same for both compo-
nents. The process is thermally controlled, thus no vapor phase
gradients are involved. As can be seen the steepness of the sur-
face gradient is proportional to the mass rate of vaporization and
the volatility of the component. Also, the gradient is inversely
proporational to the diffusivity. Since the primary component of

the model fuels is dodecane, the boiling curves for the fuels were essentially the same, i.e., that of n-dodecane. The experimental results showed the behavior of the model fuels to follow a d^2-law with no observable effects of composition. Thus, for the model fuels, given a particular furnace temperature, the results of nitrogen evolution differ only as a consequence of volatility and diffusivity differences.

The pyridine, being a highly volatile and mobile compound relative to n-dodecane, is able to escape the surface and be transported to it with great ease, thereby being depleted more rapidly than equilibrium. In contrast, the n-dodecane is retained. For the binary system under consideration there is a limit to this behavior, shown by the dashed line on Figure 7, which is the total evolution of pyridine with no evolution of n-dodecane.

If diffusion is not able to transport enough material to the surface to satisfy the vaporization requirement, the surface composition will shift towards the heavier molecular weight component, which increases its relative volatility. This is seen to happen for the case of acridine, where its high molecular weight results in a smaller diffusivity and its low volatility prevents it from being evolved until its surface concentration has increased sufficiently. However, because of the lower diffusivity the surface concentration will increase more rapidly than equilibrium conditions, permitting the higher rate of vaporization observed.

The behavior of a quinoline doped fuel shows a similar trend to the acridine case but also exhibits a transitional behavior due to differing mass rates of vaporization. The discussion of Figure 7 for pyridine limited the resulting evolution for the volatile component to an area bounded by the equilibrium curve and the maximum rate of evolution line. This is valid when the surface concentration remains low or constant throughout the vaporization process, but if an intermediate buildup of surface concentration takes place, then a new equilibrium curve must be generated and if any loss of the compound has taken place a new maximum limit must be designated.

CONCLUSIONS

The evolution of fuel nitrogen is not a function of total nitrogen content of a fuel only, but is strongly dependent upon the distribution of nitrogenous compounds in the fuel. The rate of fuel nitrogen evolution is not completely determined by the composition of the fuel, but may be influenced by the rate of vaporization, which is determined by droplet size and ambient temperature.

Generally, if the fuel has a preponderance of nitrogen in the

heavier molecular weights, the nitrogen evolution will be better than equilibrium results suggest. If the fuel contains a light nitrogen free fraction to any significant extent, the nitrogen evolution will be retarded by the improved evolution of the light fraction. If the fuel has a broad spectrum of nitrogenous compounds, it is difficult to make any generalizations, other than be certain that one has complete vaporization.

LITERATURE CITED

(1) Martin, G. B., and E. E. Berkau, "An investigation of the conversion of various fuel nitrogen compounds to NO in oil combustion," presented at the 70th AIChE National Meeting, Atlantic City, N.J., American Institute of Chemical Engineers, New York, August 1971.

(2) Turner, D. W., R. L. Andrews, and C. W. Siegmund, "Influence of combustion modification and fuel nitrogen content on nitrogen oxides emissions from fuel oil combustion," presented at 64th Annual AIChE Meeting, San Francisco, Calif., American Institute of Chemical Engineers, New York, November 1971.

(3) Beer, J. M., A. F. Sarofim, L. D. Timothy, S. P. Hanson, A. Gupta, and J. M. Levy, "Two phase processes involved in the control of nitrogen oxide formation in fossil fuel flames," Proceedings of the Joint Symposium on Stationary Combustion NO_x Control, U.S. Environmental Protection Agency and Electric Power Research Institute, IERL-RTP-1086, Vol. 4, pp. 43-83, October 1980.

(4) Hanson, S. P., Sc.D. Thesis, M.I.T., 1982.

Intermediate Btu Gas Global Flame Kinetics

ARTHUR LEVY, HERBERT A. ARBIB, and E. LEWIS MERRYMAN

Battelle, Columbus Laboratories, Columbus, OH 43201

Global rates determined from $CO-H_2-CH_4$ flames were effectively applied to Zeldovich, Frank-Kamenetski, Semenov (ZFKS) burning velocity equations. Four intermediate BTU flame mixtures were probed and analyzed. The fuel mixtures, $CO/H_2/X$ where X = methane or natural gas, in the mole ratio 1/1/0.22, were burned in 13 percent excess air and slightly rich. With the aid of mole fraction profiles, carbon, hydrogen and oxygen mole balances were obtained and global kinetic rates were calculated. Burning velocity calculations were carried out using the ZFKS theory and global rates validated by our present experiments. Correlations of measured and calculated burning velocities are good. The substitution of natural gas, with its inherent impurities (some four percent of other hydrocarbons), for methane has no measurable influence on the burning behavior of the intermediate BTU fuel mixtures.

The ability to develop reliable predictions for synthetic natural gas mixtures and the ability to design burners for these gas mixtures remain a key issue for the uses of low- and inter-mediate-Btu gas. Numerous methods for assessing interchange-ability have been used over the years. For the most part, these are empirical and reasonably useful methods; i.e., indices for lift, flashback, yellow-typing. In an attempt to approach this problem from a more fundamental point of view, we have been studying for the past few years ways of combining some of the more fundamental combustion properties of flames, such as global rates of reaction, flashback, quenching distance and burning velocity. In this paper, we present some of our more recent results where we have developed the global kinetics for some ternary fuel systems $CH_4 - H_2 - CO$ and natural gas $- H_2O - CO$ and have correlated these flame data and other plug flow data with burning velocity data.

Experimental

Four flat, disc-shaped laminar flow flames were probed and
analyzed using standard microprobing techniques. The flames were
composed primarily of CO, H_2, O_2, and Ar with small amounts of
CH_4 or natural gas added to simulate intermediate Btu gas mix-
tures. Gas compositions used in the probings are presented in
Table 1. Flames A and B contained excess air, air/fuel equi-
valence ratio = 1.13; Flames C and D were slightly fuel rich,
air/fuel equivalence ratio = 0.93. Each of the mixtures had a
$CO/H_2/X$ (X = methane or natural gas) mole ratio of 1/1/0.22.

All of the gases were more than 99 percent pure except for
the natural gas which had the following composition (furnished by
Matheson):

Gas	Percent	Gas	Percent
Methane	96.5	N-Pentane	0.028
Ethane	1.86	Hexane	0.030
Propane	0.36	Heptane	0.018
Iso-Butane	0.059	Oxygen	0.0023
N-Butane	0.076	Carbon dioxide	0.676
Iso-Pentane	0.035	Nitrogen	0.312

The flames were stabilized on a sintered-copper-frit flame burner
at pressures of 110 to 115 torr. The copper frit was water-
cooled to prevent or reduce the tendency of H_2 to burn in and/or
below the frit.

An uncooled 1/4-in. O.D. quartz probe with a 70 micron I.D.
tip was used to withdraw samples from the flames. The pressure
differential between the flame and the inside of the probe was
approximately 70:1. The flame samples were analyzed on a
Finnigan Model 1015 quadrupole mass spectrometer. Argon was sub-
stituted for nitrogen as a diluent in the flames to allow better
CO analysis with the mass spectrometer.

Temperature measurements (corrected for radiation) were made
with silica-coated Pt-Pt/10% Rh thermocouples, about 4 mils in
diameter. The temperature and species concentration profile as a
function of distance through the flame provided the basic data
for the kinetic analyses.

Results

Flame Analyses. Smoothed temperature and mole fraction ver-
sus distance plots and the associated net reaction rate versus
distance plots for a fuel-lean and fuel-rich flame are shown in
Figures 1 and 2, respectively. The computer-generated symbols
in the figures identify the species associated with each curve;
they do not denote data points. Approximately 16 data points
from each flame were used to generate the curves.

TABLE 1. TERNARY FUEL MIXTURES

Gas	Mole Fraction				Fuel Percent
	Flame				
	A	B	C	D	
CO	0.0818	0.0818	0.0838	0.0838	39.8
H_2	0.0818	0.0818	0.0838	0.0838	39.8
CH_4	0.0182	--	--	--	8.85
Natural gas	--	0.0183	0.0186	--	8.85
CO_2	0.0236	0.0236	0.0242	0.0242	11.5
O_2	0.1342	0.1341	0.1129	0.1129	--
Ar	0.6604	0.6604	0.6767	0.6767	--
Equivalence Ratio, Q*	1.13	1.13	0.933	0.933	

*
$$\frac{(A/F)}{(A/F) \text{ stoich}}$$
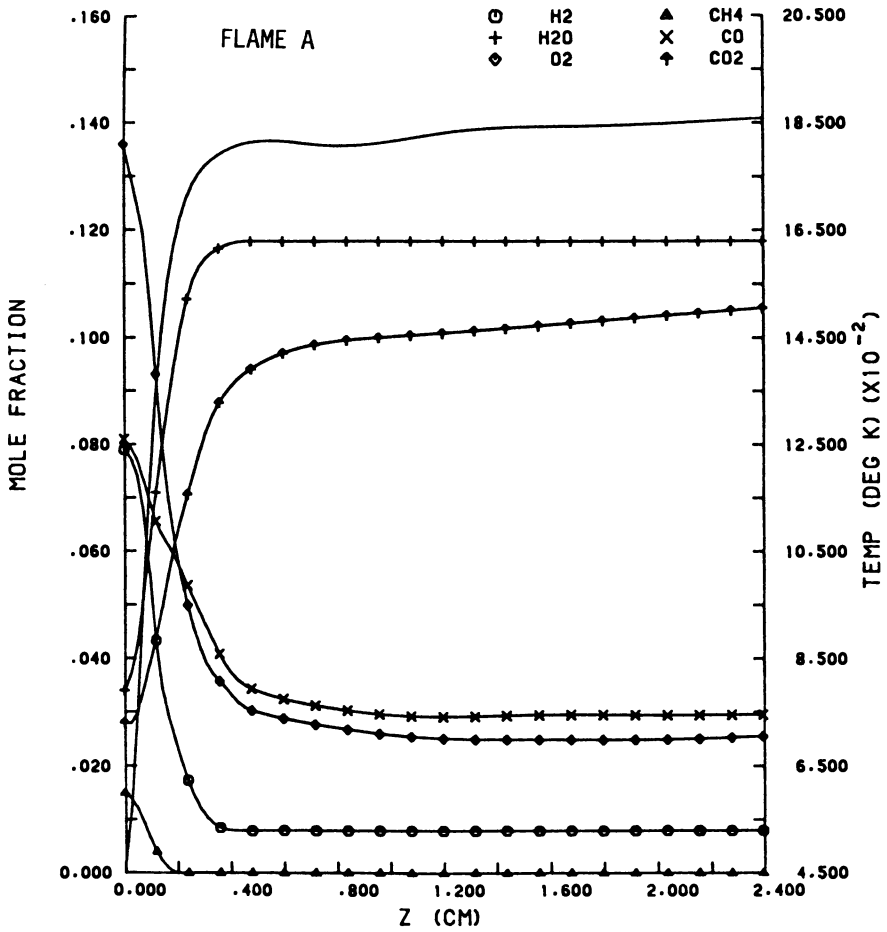
Figure 1a. Mole fractions for Flame A.
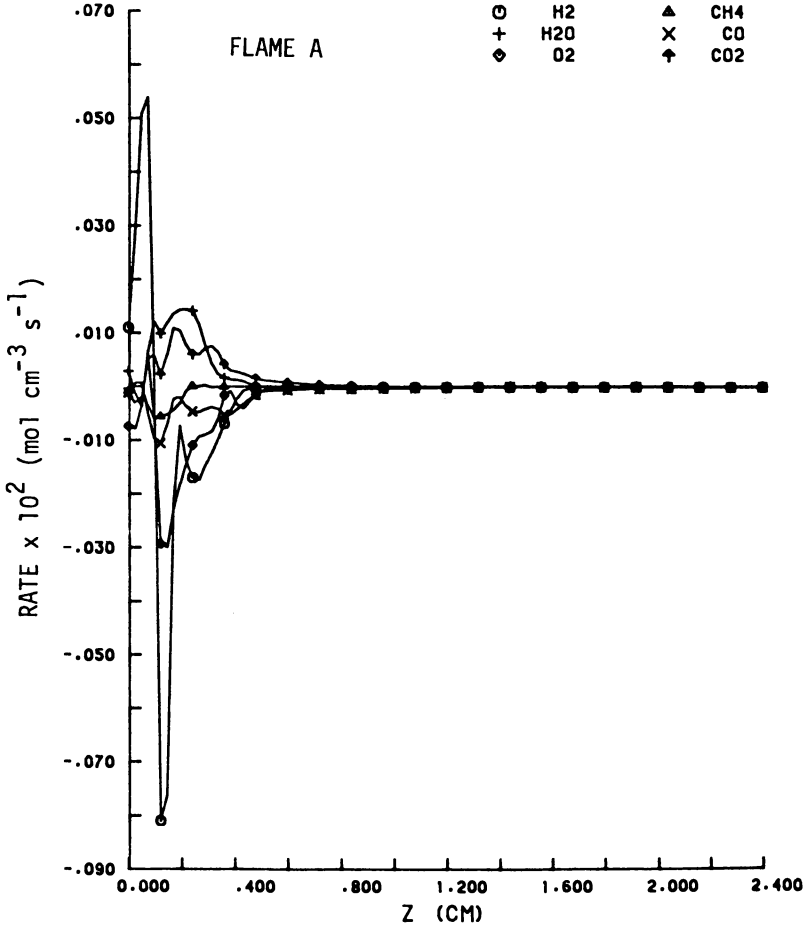
Figure 1b. Rate profiles for Flame A.
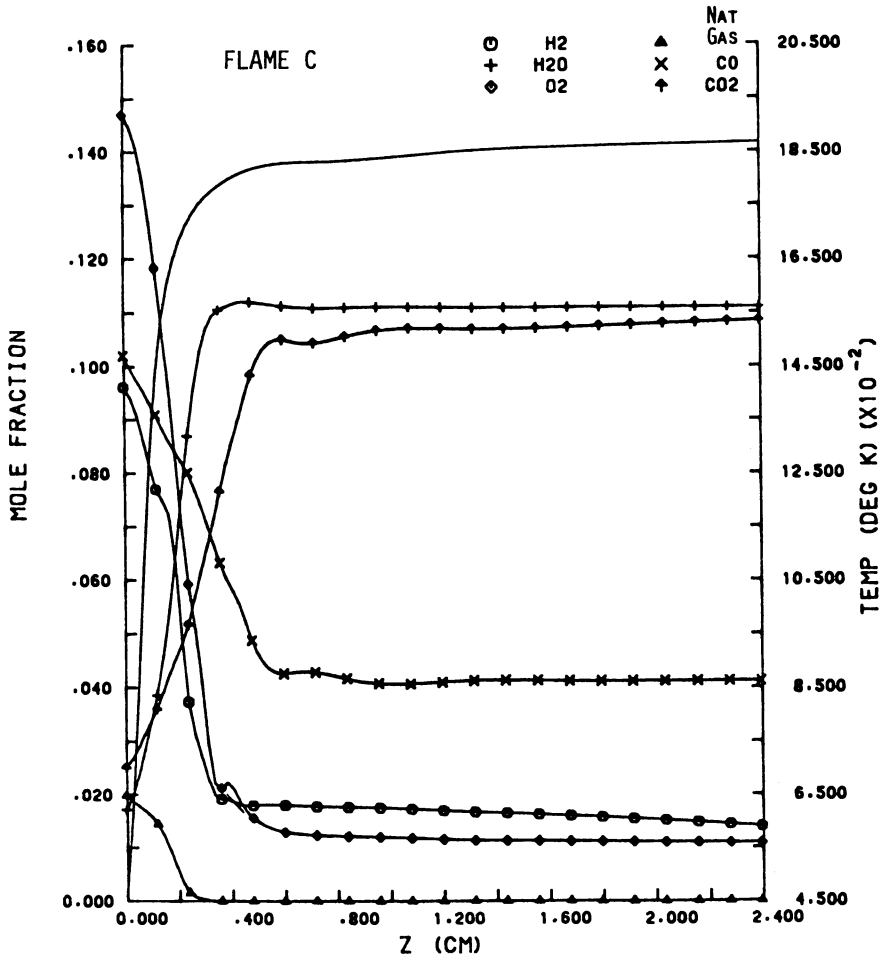
Figure 2a. Mole fractions for Flame C.
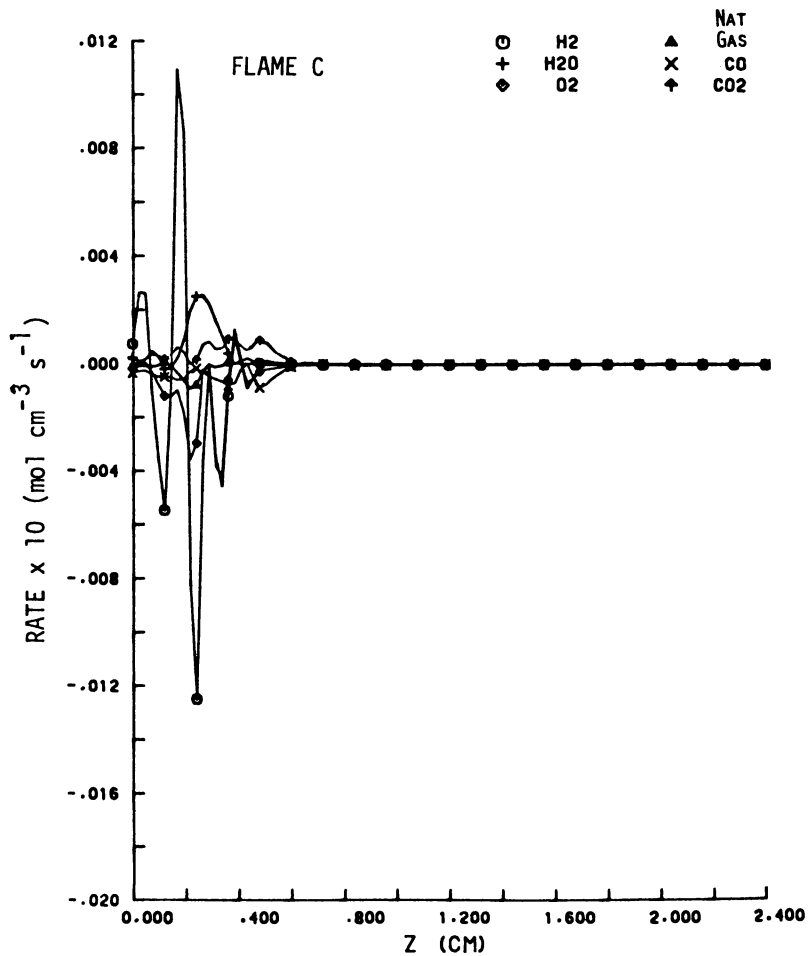
Figure 2b. Rate profiles for Flame C.

Excess Air Flames.   Concentration Profiles. Data from
Flame A, Figure 1-a, show typical mole fraction profiles obtained
from a ternary IBtu mixture burning in excess air. The profiles
show that the hydrocarbon is completely consumed in the flame and
that all but a few percent of the hydrogen is also consumed under
the excess oxygen conditions. Slightly greater consumption of
hydrogen appeared to occur when natural gas was substituted for
methane in the O_2-rich environment. The water profiles show
early and rapid formation of H_2O, in agreement with the early and
near complete consumption of CH_4 and H_2.

Somewhat unexpected is the relatively low consumption of CO
in the excess oxygen flame. The CO profile of Figure 1-a shows
only about 60 percent of the CO was oxidized to CO_2. Other fuel-
lean flames probed also showed incomplete combustion of the CO.
Equilibrium CO levels were not attained in most of the flames.
The CO oxidation appears to be kinetically limited in these tern-
ary fuel mixtures due to the inhibiting effect of methane and the
competition of methane for the OH radicals.

Rate Data. Figure 1-b shows typical rate profiles for the
formation and depletion of the major species present in the excess
air flames as represented by Flame A. The rates are computer
generated and reflect, in some cases, an over-magnification of
small deviations in the original data, mainly associated with the
mole fraction profiles. Additional smoothing of data would im-
prove the continuity of the curves, but overall, the trends and
relative rate values would remain about the same.

The rate curves of Figure 1-b indicate an early formation of
hydrogen in each flame followed by immediate and rapid consump-
tion downstream. Overall, the rate data indicate that the maxi-
mum rates of depletion of reactants are slightly less in the flame
with natural gas (Flame B), while the maximum rates of formation
of CO_2 and H_2O, are about equal in both flames.

Taking into account the error span in the mole fraction
curves and rate data for each species in the two excess air
flames, it is concluded that the kinetic processes are, within
experimental error, essentially the same in both flames, the
presence of natural gas versus pure methane having no overriding
effects.

Table 2 summarizes the maximum rate values for the excess
air and the fuel-rich flames. The numbers in parentheses below
each rate value is the temperature at which the maximum rate was
observed.

Fuel-Rich Flames.   Concentration Profiles. Typical mole
fraction curves for a substoichiometric flame are shown in
Figure 2-a for Flame C. Mole fraction profiles in Flames C and D
were nearly identical for each corresponding species in the sub-
stoichiometric flames in the presence of methane or natural gas.

As in the excess oxygen flames, the hydrocarbons are com-
pletely consumed in the fuel-rich flames. However, as might be

TABLE 2. MAXIMUM RATE RESULTS, IBTU FLAMES

Maximum Rate $\times 10^2$ (mol cm^{-3} s^{-1})

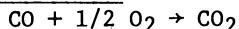| Flame	Formation			Depletion				
	H_2	CO_2	H_2O	H_2	CO	CH_4	Nat Gas	O_2
A	0.053 (970)*	0.011 (1560)	0.014 (1675)	0.081 (1345)	0.011 (1345)	0.00060 (1180)	--	0.030 (1470)
B	0.032 (680)	0.012 (1790)	0.019 (1635)	0.044 (1495)	0.0027 (1240)	--	0.0060 (1385)	0.021 (1680)
C	0.109 (1605)	0.0099 (1795)	0.025 (1735)	0.125 (1715)	0.0088 (1815)	--	0.0092 (1685)	0.036 (1685)
D	0.028 (1595)	0.0084 (1765)	0.029 (1725)	0.065 (1725)	0.0065 (1795)	0.0066 (1725)	--	0.029 (1680)

* Kelvin

expected, less hydrogen and CO (in comparison with Flame A) were
consumed under the fuel-rich conditions. Water also appears
early in these flames reflecting the early burnout of the hydro-
gen-containing species.

Rate Data. The rate profiles for Flame C are shown in
Figure 2-b. As in the excess oxygen flames, the profiles show
multiple peaks some of which, as mentioned earlier, result from
the computer smoothing routine. The rate profiles, while showing
similar trends in each flame, differ in the maximum rate values
(see Table 2). In contrast to the oxygen-rich flames, data from
the fuel-rich flames generally show higher maximum rates of de-
pletion of reactants and formation of products in the flame con-
taining natural gas, Flame C. However, as in the oxygen-rich
flames, the rates in both of the fuel-rich flames agree within a
factor of 2, except for the H_2 formation rates (and the CO de-
pletion rates in the oxygen-rich flames). The factor of 2 vari-
ation is considered within the error range of the kinetic data
in these and the oxygen-rich flames. Maximum rates occur at
comparable temperatures in the fuel-rich flames, a condition not
observed in the excess oxygen flames.

Mole Balances. Mole balances based on the global reactions
$$CO + 1/2 \ O_2 \rightarrow CO_2$$
$$H_2 + 1/2 \ O_2 \rightarrow H_2O$$
$$CH_4 + 2 \ \ O_2 \ \ \rightarrow CO_2 + 2H_2O$$
for each of the four flames are tabulated below.
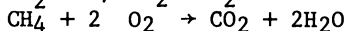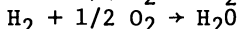
Flame No.	Carbon Balance $-(\Delta CO + \Delta CH_4)$	ΔCO_2	% Dev	Hydrogen Balance $-(\Delta H_2 + 2\Delta CH_4)$	ΔH_2O	% Dev
A	0.068	0.077	13	0.104	0.085	–18
B	0.046	0.081	76	0.113	0.098	–13
C	0.080	0.084	5	0.122	0.095	–22
D	0.077	0.082	6	0.114	0.097	–15

Flame No.	Oxygen Balance $-[1/2(\Delta CO + \Delta H_2) + 2\Delta CH_4]$	ΔO_2	% Dev
A	0.094	0.109	16
B	0.089	0.125	40
C	0.111	0.135	22
D	0.106	0.131	24

The carbon balance is exceptionally good for each of the flames,
except for Flame B. This no doubt is related to the abnormally
low CO values in that flame (which we suspect are probably re-
lated to a calibration factor in the spectrometer). Hydrogen and
oxygen percent deviations are high, particularly so for the oxygen.
Hydrogen deviation can vary up to 20 percent in hydrocarbon

flames, but deviations should be less in these flames since hydrogen was added initially. Oxygen variations usually are below 10 percent. The high intercept values for O_2 at zero distance (see mole fraction profiles) account for most of this deviation. Sensitivities for O_2 could be adjusted so that the intercept values agree more closely with the cold gas values for O_2. This would bring the percent deviation down considerably. However, mole fractions were used as derived from the mass spectrometer data. For comparison purposes, as used in this study, the deviation should not interfere with overall conclusions.

Correlation of the Burning Velocity Data

One of the objectives of this program was to assess the possibility of correlating global rate data with appropriate burning velocity equations. Global rate data have for the most part been derived from plug flow data, e.g., Dryer and Glassman (1), and turbulent reacting systems, e.g., Howard et al (2). Flame-generated rate data have been developed [e.g., Fristrom and Westenberg (3)] from flame microstructure studies, but have not been applied to burning velocity calculations. In this section, we describe some correlation data of global rates with burning velocity.

Application of the Thermal Theory to Multiple Reactions. For a flame driven by a single exothermic reaction (of the type $nA \rightarrow B + C \ldots$), the laminar burning velocity S_L according to the classical thermal theory of Zeldovich, Frank-Kamentskii and Semenov (ZFKS) is given by (4)

$$S_L = [\frac{2\lambda}{\rho_u c_p} \frac{I}{T_f - T_u}]^{1/2}, \text{ with } I \equiv \frac{1}{a_u} \int_{T_u}^{T_f} w \, dT \qquad (1)$$

where a (mol/cm^3) is the reactant concentration in the fuel/oxidizer mixture, T the temperature, ρ the thermal conductivity, c_p the specific heat, w the reaction rate, and the subscripts u and f refer to the unburned and the final state in the flame, respectively (λ/c_p is assumed constant). Expression of w in Arrhenius form allows the integral I to be approximated. For more than one exothermic reaction occurring simultaneously, it can be shown that Equation 1 remains valid as a predictive expression for S_L, except that the reaction rate integral I is now given by

$$I = \frac{1}{\sum_i a_i \Delta H_i} \sum_i \Delta H_i \int_{T_u}^{T_f} w_i \, dT \qquad (2)$$

where ΔH_i (J/mol.) is the heat of the reaction in which i is the reactant, a_i (mol_i/cm^3) are the initial concentrations in the fuel/oxidizer mixture, and w_i $(mol_i/cm^3 s)$ is the molar rate of production of species i. Expressing concentrations in mol frac-

tions x_i ($a_i = x_i p_u / RT_u$), and employing perfect gas assumption ($p = \rho RT/\overline{M}$), Equation 1 can be written

$$S_L = \frac{RT_u}{p_u} \left[\frac{2\lambda}{\overline{M}_u c_p} \frac{I'}{T_f - T_u} \right]^{1/2} \tag{3}$$

and correspondingly, the integral I' is expressed by

$$I' = \frac{1}{X} \left[\sum_i \Delta H_i \int_{T_u}^{T_f} w_i dT \right] \tag{4}$$

with

$$X \equiv \sum_i x_i \Delta H_i \tag{5}$$

In the Semenov theory (4), if the reaction is of the second order, i.e.,

$$w = kab \exp(-E/RT) \tag{6}$$

the reaction rate integral I can be approximated by

$$I \simeq \frac{K}{a_u} a_{eff}^m b_{eff}^n \frac{RT_f^2}{E} \exp(-E/RT_f) \tag{7}$$

where

$$a_{eff} = a_u \frac{T_u}{T_f} \left(\frac{RT_f^2/E}{T_f - T_u} \right)$$

$$b_{eff} = b_u \frac{T_u}{T_f} \left(\frac{RT_f^2/E}{T_f - T_u} \right) \tag{8}$$

In the following, we shall assume that this approximation holds whatever the order of the reaction, i.e., if

$$w = a^m b^n \exp(-E/RT) \tag{9}$$

then

$$I \simeq \frac{K}{a_u} a_{eff}^m b_{eff}^n \frac{RT_f^2}{E} \exp(-E/RT_f) \tag{10}$$

An improvement in Equation 3 can be brought about by substituting

λ/c_p with $\lambda_f c_{pf}^2 / \overline{c_p}^3$, where the bar denotes the mean value (5).

The Present Model

The ternary flames considered here have three driving exo-thermic reactions:

$$CO + 1/2 \ O_2 \rightarrow CO_2 \tag{11}$$

$$H_2 + 1/2 \ O_2 \rightarrow H_2O \qquad (12)$$

$$CH_4 + 2 \ O_2 \rightarrow CO_2 + 2H_2O \qquad (13)$$
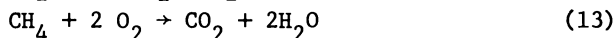
For the computation of the reaction rate integral that appears in the expression for S_L, the following two-step model was devised (confirmed by the measured concentration profiles):

1. In a first step, CH_4 is depleted to form CO and H_2O, and H_2O is formed also by oxidation of the H_2 in the mixture:

$$CH_4 + 2 \ O_2 \rightarrow CO + 1/2 \ O_2 + 2H_2O \qquad (14)$$

$$H_2 + 1/2 \ O_2 \rightarrow H_2O \qquad (15)$$
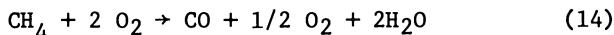
2. In a second step, CO (both from the CH_4 reaction and that initially present in the mixture) reacts to form CO_2:

$$(CO)' + 1/2 \ O_2 \rightarrow (CO_2)' \qquad (16)$$

$$(CO)'' + 1/2 \ O_2 \rightarrow (CO_2)'' \qquad (17)$$
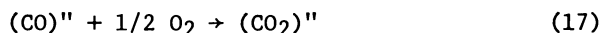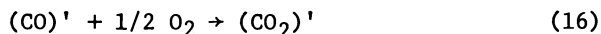
For the reaction rates of Equations 14 to 17 global expressions from the literature were adopted. For reactions 14, 16, and 17, the overall correlations of Dryer and Glassman (1) were used, expressing respectively the methane disappearance rate, the rate of reaction of carbon monoxide with oxygen in the presence of water, and the appearance rate of carbon dioxide in the methane-oxygen reaction:

$$- \frac{d[CH_4]}{dt} = 10^{13.2}[CH_4]^{0.7}[0.2]^{0.8} \exp\left(-\frac{48,000}{RT}\right), \quad (18)$$

$$- \frac{d[CO]}{dt} = 10^{14.6} \ [CO][H_2O]^{0.5}[O_2]^{0.25} \exp\left(-\frac{40,000}{RT}\right) \quad (19)$$

$$\frac{d[CO_2]}{dt} = 10^{14.75}[CO][H_2O]^{0.5}[O_2]^{0.25} \exp\left(-\frac{43,000}{RT}\right) \quad (20)$$

For reaction 15, the only expression found in the literature for the global rate of water formation was the one by Fenimore and Jones (6)

$$\frac{d[H_2O]}{dt} = \frac{8[H_2]}{[CO]} \frac{d[CO_2]}{dt} \qquad (21)$$

and this was used in conjunction with Equation 19 assuming

$$\frac{d[CO_2]}{dt} = - \frac{d[CO]}{dt} \ , \ \text{so that}$$

$$\frac{d[H_2O]}{dt} = 8 \times 10^{14.6}[H_2][H_2O]^{0.5}[O_2]^{0.25} \exp\left(-\frac{40,000}{RT}\right) \quad (22)$$

When using Equation 22, a non-zero concentration of water has to be assumed even if no water is initially present in the reactants. Best results were obtained by taking $[H_2O] = [H_2] + 2[CH_4]$, i.e., the total water eventually to be in the combustion products under oxidizing conditions, although part of it is produced by depletion of hydrogen. This can be justified by noting that Equation 7 was derived for rate expressions in which both reactants were depleted during combustion, and assumed that the reactant concentration in the combustion zone is constant and equal to $a_{eff} < a_u$ and

$b_{eff} < b_u$. When one of the species appearing in the rate expression actually increases during the reaction, it is plausible that introduction of its initial value makes Equation 7 intolerably small.

Alternative expressions for the global rates of Reactions 14 and 16 were tried while developing the model. For the $CO \rightarrow CO_2$ conversion (Reaction 16) the overall correlation derived by Howard et al. (2) was initially used, but with this the calculated values of S_L were considerably lower than the measured ones. For the methane disappearance rate (Reaction 14) the correlations proposed by Westbrook and Dryer (7) were tried, and these gave results negligibly different from those obtained by Equation 18.

Validation of the Global Rates Expressions.   In order to validate the global rate expressions employed in the model, temperature and concentration profiles determined by probing the flames on a flat flame burner were studied. Attention was concentrated on Flames B and C. The experimental profiles were smoothed, and the stable species net reaction rates were determined using the laminar flat-flame equation described in detail by Fristrom and Westenberg (3) and summarized in Reference (8). A plot of the logarithm$_{10}$ of $Aexp(-E/RT)$ for three of the four rate expressions used is shown in Figures 3, 4, and 5 (for Equations 18, 19, and 22, respectively).

Initially, an attempt was made to develop original global rate expressions for Reactions 14 to 16 from these rate data. It soon became clear, however, that the number of experimental points was too few to allow the attainment of this goal. Moreover, since a ternary system was being analyzed, the concentration profiles had an intricate form which made numerical differentiation to retrieve the rates somewhat inaccurate. It was therefore decided to use these rate data to check the overall rate expressions derived by other authors and used in the present model.

It is apparent that the adopted correlations represent in an acceptable way the experimental data at high temperatures. The best agreement is obtained for the CO depletion (Equation 19), while for H_2O formation and CH_4 disappearance, the agreement is less satisfactory. Given however, the relatively small number of
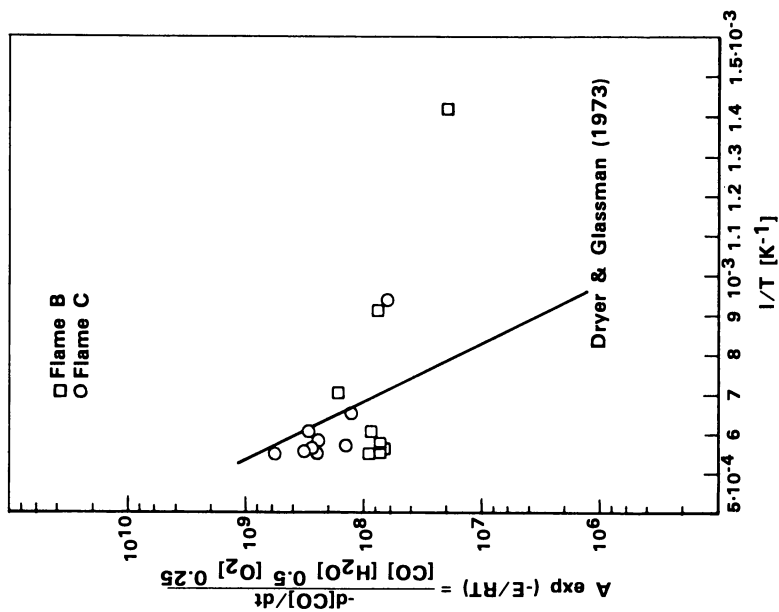
Figure 4. Global rate constant vs. 1/T for water formation reaction (Eq. 22).
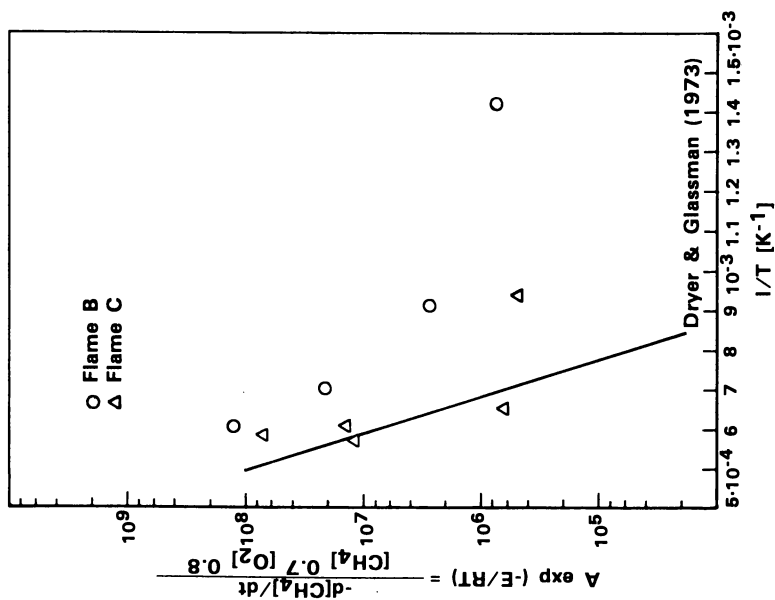
Figure 3. Global rate constant vs. 1/t for carbon monoxide oxidation reaction (Eq. 19).
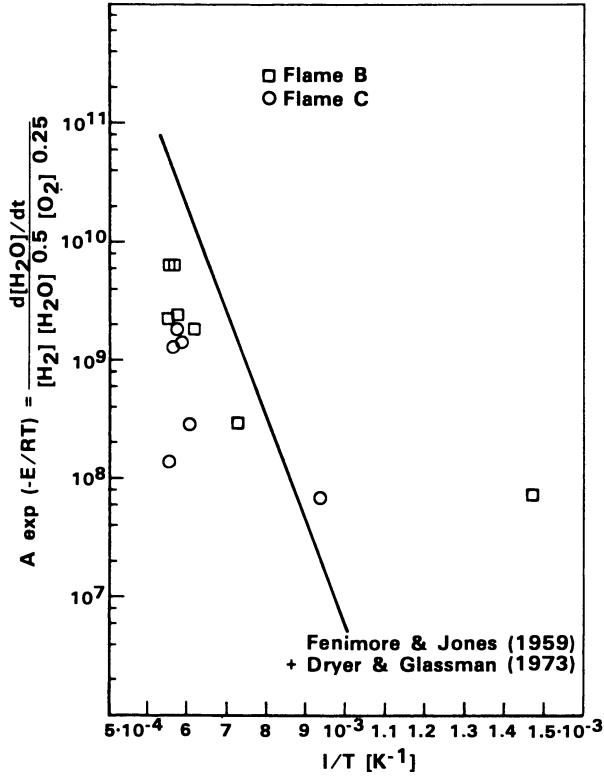
Figure 5.   Global rate constant vs. 1/T for water
formation reaction (Eq. 22).

experimental data points, it should be deemed satisfactory that
they fall around the used correlations (which are plotted within
their claimed range of validity).

   Results and Discussion. The burning velocity was calculated
by the model described above for a number of different gas mix-
tures burning at stoichiometric conditions. Table 3 presents the
compositions of the various gas mixtures studied. Each mixture
is characterized by a mixture number MN and a mixture ratio R.
The mixture ratio R is a volume concentration of index fuel
$(CO + H_2)$ relative to the sum of index and limit fuels, where
the limit fuel is $CO + CH_4$ or $H_2 + CH_4$. Mixtures having the
same value of MN yield the same composition of combustion pro-
ducts and adiabatic flame temperature when burning stoichio-
metrically with air. This choice was made in order to assess
whether adiabatic flame temperature and final composition were
significant factors in explaining differences of behavior for
different fuel compositions. Additional details on the select-
ion of gas mixtures composition can be found in Reference (9).
   The adiabatic flame temperatures T_f were calculated by the
computer code NASA SP 273. λ and c_p were computed by the corre-
lations of Mansouri and Heywood (10).
   The calculated values of S_L were compared with the experi-
mental ones obtained for the same mistures by measurements in a
wedge-shaped flame. A plot of calculated versus measured S_L is
shown in Figure 6. It is clear that the model predicts correctly
the change in S_L that is to be expected from a change in mixture
composition, while the calculated values are satisfactorily
close to the measured ones. The better fit between calculated
and predicted values here as compared with the rate correlation
in Figures 3, 4, and 5 also reflects the better fit near stoich-
iometric conditions and at higher flame temperature (11).

Conclusions

   Measurements of temperature and concentration in $CO-H_2-CH_4$
(or natural gas) flames were carried out. Rate profiles were
developed for two excess air and two slightly fuel-rich flames
as a function of temperature. Substitution of natural gas for
methane does not bring about a marked change in the overall
reactivity of these systems. Application of a modified theory
analysis to these multiple-fuel flame mixtures allows one to
satisfactorily correlate calculated values of the burning
velocity with measured values.

TABLE 3. COMPOSITION OF THE GAS MIXTURES STUDIED
(mol fractions)

Mixture Number MN	Mixture Ratio R	CO	H_2	CH_4	CO_2	O_2	N_2
1	1.0	0.590	0.295	0.0	0.115	0.0	0.0
	0.50	0.566	0.147	0.096	0.151	0.039	0.0
	0.0	0.542	0.0	0.193	0.187	0.078	0.0
2	1.0	0.295	0.590	0.0	0.115	0.0	0.0
	0.50	0.147	0.373	0.205	0.191	0.083	0.0
	0.0	0.0	0.156	0.410	0.268	0.166	0.0
3	1.0	0.442	0.442	0.0	0.115	0.0	0.0
	0.50	0.360	0.221	0.171	0.179	0.069	0.0
	0.0	0.277	0.0	0.342	0.243	0.138	0.0
4	1.0	0.257	0.128	0.0	0.115	0.0	0.500
	0.67	0.249	0.085	0.028	0.131	0.0	0.507
	0.50	0.245	0.064	0.042	0.140	0.0	0.511
	0.33	0.240	0.043	0.055	0.148	0.0	0.514
	0.0	0.232	0.0	0.083	0.164	0.0	0.521
5	1.0	0.128	0.257	0.0	0.115	0.0	0.500
	0.50	0.064	0.162	0.087	0.167	0.0	0.521
	0.0	0.0	0.067	0.173	0.218	0.0	0.541
6	1.0	0.192	0.192	0.0	0.115	0.0	0.500
	0.50	0.155	0.096	0.073	0.158	0.0	0.518
	0.33	0.148	0.064	0.097	0.173	0.0	0.523

$$R = \frac{(CO + H_2)}{(CO + H_2) + ([CO \text{ or } H_2] + CH_4)}$$
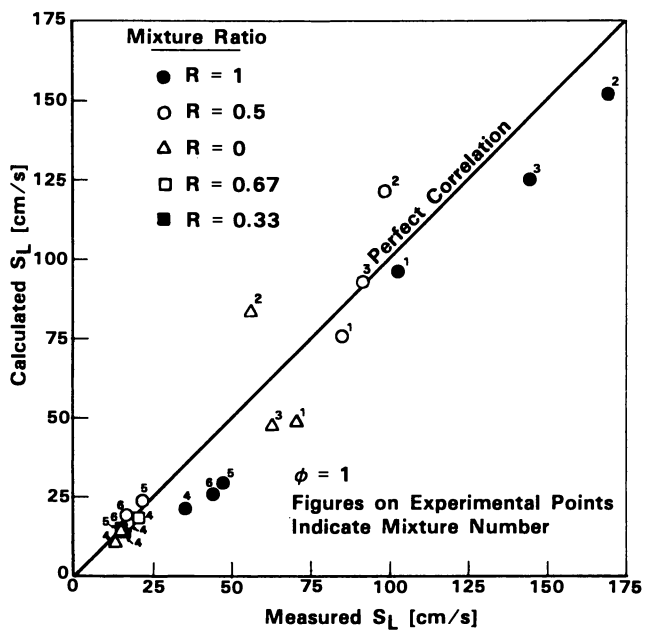
Figure 6. Correlation of calculated vs. measured burning velocities.

Acknowledgment

Literature Cited

1. Dryer, F. L., and Glassman, I., 14th Symp. (Int.) on Combust. 987 (1973).
2. Howard, J. B., Williams, G. C., and Fine, D. H., 14th Symp. (int.) on Combust., 975 (1973).
3. Fristrom, R. M., and Westenberg, A. A., Flame Structure, McGraw–Hill (1965).
4. Semenov, N. N., NACA TM 1026 (1942).
5. Evans, M. W., Chem. Reviews, 51, 363 (1952).
6. Fenimore, C. P., and Jones, G. W., J. Phys. Chem., 63, 1834 (1959).
7. Westbrook, C. K., and Dryer, F. L., The Combust. Inst. CSS 1981 Spring Meeting; UCRL–84943 Preprint.
8. Levy, A., Overley, J. R., and Merryman, E. L., Battelle Topical Report, Contract No. (ERDA) E(49–18)–2406, July 26, 1977.
9. Ball, D. A., Putnam, A. A., Radharkrishman, E., and Levy, A., Battelle Topical Report, Contract No. (ERDA) E(49–18)–2406, July 26, 1977.
10. Mansouri, S. H., and Heywood, J. B., Combust. Sci. Technol., 23, 251 (1980).
11. Westbrook, C. K., and Dryer, F. L., Combust. Sci. Technol., 27, 31 (1981).

Continuous Combustion Systems

A Study of Fuel Nitrogen Conversion in Jet-Stirred Combustors

R. M. KOWALIK and L. A. RUTH

Exxon Research and Engineering Company, Linden, NJ 07036

Results from laboratory jet-stirred combustor experiments suggest that the conversion of fuel-bound nitrogen to total fixed nitrogen (TFN=NO+HCN+NH_3) in fuel-rich mixtures is strongly related to the concentration of unburned hydrocarbons (HC's) within the combustor. Most conversion trends with equivalence ratio, residence time, and combustor type may be explained in terms of the effects of these variables on HC concentrations. Changes in these variables which reduce HC's generally reduce the degree of fuel nitrogen conversion. Fuel type (aliphatic vs aromatic) effects on conversion appear to be most pronounced for very rich, short residence time conditions. At these conditions toluene/pyridine mixtures produce less TFN and more soot than similar isooctane/pyridine mixtures. This trend may be related to an interaction between soot and HCN.

Synthetic liquid fuels derived from coal and shale will differ in some characteristics from conventional fuels derived from petroleum. For example, liquid synfuels are expected to contain significantly higher levels of aromatic hydrocarbons, especially for coal-derived fuels, and higher levels of bound nitrogen. These differences can affect the combustion system accepting such fuels in important ways. In continuous combustors, i.e. gas turbines, the increased aromatics content of coal-derived fuels is expected to promote the formation of soot which, in turn, will increase radiation to the combustor liner, raise liner temperature, and possibly result in shortened service life. Deposit formation and the emission of smoke are other potential effects which are cause for concern. Higher nitrogen levels in synfuels are expected to show up as increased emissions of NO_x (NO+NO_2). An earlier paper presented results of an experimental study on the effect of aromatics and combustor

operating conditions on soot formation (1). This paper focuses on the effect of increased fuel nitrogen and aromatics on the emission of NO_x.

NO_x can be formed either from atmospheric nitrogen ("thermal" NO_x) or from the oxidation of nitrogen compounds present in the fuel ("fuel" NO_x). The rate of formation of thermal NO_x is very sensitive to temperature, and techniques which have been developed to control this type of NO_x are based largely on limiting peak flame temperatures. The formation of fuel NO_x, by contrast, is much less dependent on temperature, and methods to control thermal NO_x are generally ineffective for fuel NO_x. Conventional petroleum-derived distillate fuels are low enough in nitrogen so that thermal NO_x predominates, and existing control techniques are usually adequate to keep NO_x emissions within acceptable levels. However, typical liquid fuels derived from coal and shale may have nitrogen concentrations that are an order of magnitude higher than those in petroleum-derived distillates and, for such fuels, the NO_x due to fuel nitrogen usually predominates. Although extensive treatment to remove fuel nitrogen at the refinery would eliminate any potential emission problem owing to fuel NO_x, it would almost certainly be cheaper and more energy efficient to modify the combustor and/or combustion conditions to minimize fuel NO_x emissions. It is toward this latter end that this research is directed.

Although gas turbine combustion systems operate with overall air/fuel ratios which are quite fuel-lean, perhaps three times stoichiometric, stabilization of the combustion process requires that a portion of the combustor, the primary zone, operate stoichiometric or fuel-rich. Under fuel-lean conditions, fuel-bound nitrogen can be converted directly to NO_x. Under fuel-rich conditions, fuel-bound nitrogen can be converted to HCN and NH_3 in addition to NO_x. Of course, in either case, the most desirable product of converted fuel nitrogen would be molecular nitrogen, N_2. The sum of the gaseous fixed nitrogen species (excluding N_2) is called total fixed nitrogen, or TFN. Under fuel-rich conditions, TFN consists primarily of NO_x, HCN, and NH_3. It should be appreciated that in any two-stage combustion process, it is vital to minimize the formation of TFN in the fuel-rich primary stage because HCN and NH_3, if formed, can be oxidized to NO_x in the fuel-lean secondary stage. Thus, any strategy for minimizing the emission of NO_x from the combustion of high nitrogen fuels in gas turbines must, in the fuel-rich primary zone, minimize the conversion of fuel nitrogen to TFN.

A further point is that the equilibrium levels of TFN under fuel-rich combustion conditions are very low. The stable form of nitrogen is N_2. In practical combustors, however, equilibrium is not attained because of the slow rates of both chemical and physical (mixing) processes. The chemical processes consist of reactions convering fuel-nitrogen species to N_2, the reaction of NO with hydrocarbon species to form HCN, and the subsequent slow conversion of HCN to N_2.

In this paper we report on factors which affect the conversion of fuel nitrogen to TFN in laboratory jet-stirred combustors which serve to simulate the primary zone in a gas turbine. The independent variables in the experiments were fuel type (aliphatic isooctane vs. aromatic toluene), equivalence ratio (fuel-to-oxygen ratio of combustor feed divided by stoichiometric fuel-to-oxygen ratio), average gas residence time in the combustor, and method of fuel injection into the combustor (prevaporized and premixed with air vs. direct liquid spray). Combustion temperature was kept constant at about 1900K in all experiments. Pyridine, C_5,H_5N, was added to the fuels to provide a fuel-nitrogen concentration of one percent by weight.

Experimental

Combustors. The fuel nitrogen conversion experiments were conducted in two Exxon jet-stirred combustors: the Jet-Stirred Combustor (JSC) and the Liquid Fuel Jet-Stirred Combustor (LFJSC). Both combustors operate at atmospheric pressure and temperatures of 1600-2000K. Figure 1 contains a schematic diagram of the JSC. Homogeneous air/fuel mixtures enter this combustor through forty 0.5 mm diameter jets positioned near the radial center of a refractory-lined hemispherical reaction zone. Fuels are prevaporized and preheated to 575K prior to mixing with air, which is also preheated to 575K. Total air plus fuel flow rates are chosen such that near sonic injection jet velocities are obtained to vigorously stir the contents of the reaction zone and produce mixtures of essentially uniform temperature and composition. Combustor temperatures are inferred from a thermocouple mounted in one of the radial exhaust ports; samples for composition analyses are withdrawn with a hot water-cooled stainless steel probe inserted through another exhaust port. Additional thermocouples are located in the refractory lining and on the steel shell to obtain temperatures for estimates of combustor heat losses. Two different size reaction zones were used in the fuel nitrogen conversion experiments; one had a 5.08cm inside diameter; the other had a 7.62cm inside diameter. Outside diameters of the two combustor modules were equal. Details of the construction of the JSC and its air and fuel supply systems may be found in Reference (2).

The LFJSC has a spherical jet-stirred zone (diameter = 5.08 cm) followed by a cylindrical plug flow zone (diameter = 2.2 cm; length = 7.6 cm); both zones are refractory lined. Primary combustion air enters the jet-stirred zone through two nozzles positioned 180° apart. A set of four 1.1 mm diameter air jets from each nozzle is aimed towards the corners of a cube imagined to sit within the spherical zone. One set of air jets is rotated 45° with respect to the other to allow the opposing jets to mesh rather than to collide. Flow rates are chosen to produce near
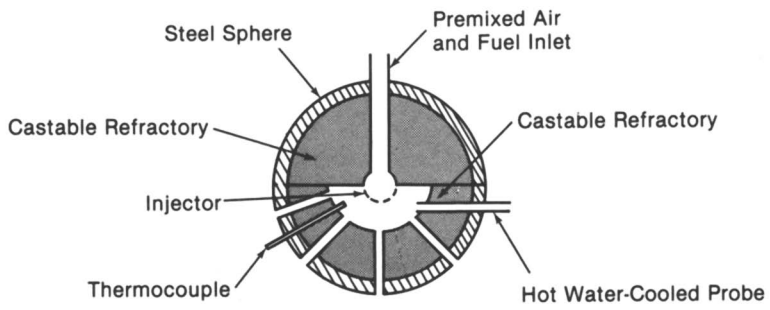
Figure 1. Jet-Stirred Combustor

sonic injection velocities. Fuel sprays enter the combustor at
two positions 90° from the air nozzles. Air atomizing nozzles
obtained from Spraying Systems Company produce the fuel sprays.
All air and fuel inlet streams enter the LEJSC at room tempera-
ture. Exhaust gas samples are withdrawn from the combustor with
a hot water-cooled stainless steel probe at the end of the plug
flow zone. A thermocouple is also inserted near the center of
the spherical reaction zone for temperature measurements. In the
fuel nitrogen conversion experiments approximately 30% of the
total combustion air was directed through the fuel nozzles.
Sauter mean diameters of the corresponding fuel sprays were esti-
mated to be of the order of 5 μm. Additional details of the
LEJSC construction and instrumentation may be found in References
(1) and (3).

     Gas Analysis. Gas samples from both combustors are analyzed
with a common instrument train. Sample gases collected in the
probes are transferred through electrically heated Teflon lines
to a 400K oven. Within the oven samples are sequentially direc-
ted to four separate conditioning/analysis streams. The first
stream exits the oven and passes through a cold water trap ($\approx$
10°C) to remove most of the combustor water. It then proceeds to
four conventional gas analyzers for measurements of CO and CO_2
(nondispersive infrared), O_2 (amperometric), and H_2 (gas chroma-
tograph) concentrations. The second stream is diluted inside
the oven with 400K nitrogen (dilution ratio $\approx$ 20:1) and trans-
ferred via electrically heated stainless steel lines to a flame
ionization hydrocarbon analyzer for measurements of total un-
burned hydrocarbon (HC) concentrations (vol. % as methane). The
nitrogen dilution is employed to keep HC concentrations within
the linear range of our instrument. The third analysis stream
is drawn through a pair of soot collection filters in the oven
and subsequently sent to a cold water trap and a positive dis-
placement wet test meter. Soot concentrations are then computed
as the weight of soot collected per measured volume of sample
gas flow. The final analysis stream is diluted in the oven with
400K air (dilution ratio $\approx$ 10:1) and transferred in unheated
Teflon lines to a catalytic converter/chemiluminescent analyzer
for measurements of NO and total fixed nitrogen (TFN) concentra-
tions. NO concentrations are obtained directly from the chemi-
luminescent analyzer; TFN concentrations are obtained by passing
the sample, after dilution with air, through a catalytic reactor
which converts all TFN species to NO and then measuring the NO
with the chemiluminescent analyzer. The reactor utilizes a
platinum catalyst and carefully controlled temperatures and
pressures to achieve near 100% conversion of TFN species to NO
(4). Addition of air to the sample assures an oxidizing atmos-
phere in the catalytic reactor and prevents water condensation
within the unheated sample lines.

Results

Principal results from the fuel nitrogen conversion experiments with pyridine doped isooctane and toluene are summarized in Tables I and II. In these tables JSC-S and JSC-L refer to the 5.08 and 7.62 cm diameter versions of the JSC, respectively; ϕ is the overall equivalence ratio of the mixtures; τ is the average residence time of the gases in the combustor computed as the combustor volume divided by the reactants' volumetric flow rate at 1900K; TFN is the weight % of fuel nitrogen emitted as TFN; NO is the volume % of TFN emitted as NO; HC is the volume % of unburned hydrocarbons in the combustion gases (as CH_4), and SOOT is weight % of fuel carbon collected as soot. The TFN values may also be interpreted as the approximate weight % of fuel nitrogen converted to TFN since additional experiments with undoped toluene and isooctane suggested that "thermal" TFN contributions were generally of the order of 20% of the "thermal" plus "fuel" TFN values. With this qualification, the term "fuel nitrogen conversion" is applied to "thermal" plus "fuel" TFN values throughout the balance of the paper.

The data in the tables are averages from two consecutive sequences of measurements. Typical repeatability between measurements was ±10%. Soot concentration measurements were made during all of the LFJSC runs and during the fuel rich (ϕ=1.6, 1.8), short residence time (3,6 ms) toluene runs in the JSC. Previous experiments suggested that measurable quantities of soot would probably not be produced at leaner conditions or longer residence times in the JSC. Flames for the richest (ϕ=1.8) toluene mixtures in the JSC at 8 and 10 ms residence times, however, appeared slightly yellow indicating the possibility of appreciable soot concentrations. Soot yields from the isooctane mixtures in the LFJSC were less than 0.01%.

During the JSC experiments oxygen concentrations in the "air" were varied to maintain indicated thermocouple temperatures of approximately 1900K. Variations from 1900K were generally less than 25K, except for the two richest (ϕ=1.8) isooctane mixtures at 10 and 20 ms residence times. For these runs oxygen concentrations were limited by the gas supply system, and indicated temperatures were approximately 1800K. For the LFJSC experiments, oxygen concentrations were selected to provide specific adiabatic flame temperatures since indicated thermocouple temperatures appeared to be affected by the impingement of the fuel sprays on the thermocouple bead. The adiabatic flame temperatures were 2400K for the toluene mixtures and 2300K for the isooctane mixtures. These temperatures were approximately equal to corresponding adiabatic flame temperatures of toluene and isooctane mixtures run in the JSC at an equivalence ratio of 1.2 and a residence time of 6 ms. Heat losses estimated from the JSC shell and refractory temperatures did not vary significantly as fuels and flow rates (residence times) were changed within each com-

Table I. Results from fuel nitrogen conversion
experiments - isooctane fuel.

Combustor	ϕ	τ (ms)	TFN $\left(\genfrac{}{}{0pt}{}{\% \text{ of}}{\text{fuel N}}\right)$	NO $\left(\genfrac{}{}{0pt}{}{\% \text{ of}}{\text{TFN}}\right)$	HC $\left(\genfrac{}{}{0pt}{}{\text{vol. \%}}{\text{as } CH_4}\right)$
JSC-S	1.2	3	65	74	0.03
"	1.4	3	88	28	0.59
"	1.6	3	83	12	1.97
"	1.8	3	96	5	4.34
"	1.2	6	93	65	< 0.01
"	1.4	6	66	74	< 0.01
"	1.6	6	41	52	0.13
"	1.8	6	62	9	2.11
"	1.2	8	87	77	< 0.01
"	1.4	8	72	72	0.01
"	1.6	8	51	60	0.09
JSC-L	1.2	8	88	53	< 0.01
"	1.4	8	69	43	0.10
"	1.6	8	62	21	0.34
"	1.8	8	74	11	1.80
"	1.2	10	73	55	< 0.01
"	1.4	10	53	53	< 0.01
"	1.6	10	50	37	0.22
"	1.8	10	77	5	2.49
"	1.2	20	73	69	< 0.01
"	1.4	20	46	62	< 0.01
"	1.6	20	40	66	< 0.01
"	1.8	20	38	24	0.07
LFJSC	1.2	6	67	55	0.23
"	1.4	6	56	46	1.04
"	1.6	6	61	27	1.73

Table II. Results from fuel nitrogen conversion
experiments - toluene fuel.

Combustor	ϕ	τ (ms)	TFN (% of fuel N)	NO (% of TFN)	HC (vol. % as CH_4)	SOOT (% of fuel C)
JSC-S	1.2	3	72	56	0.19	--
"	1.4	3	72	32	0.31	--
"	1.6	3	86	11	1.68	0.07
"	1.8	3	69	9	3.57	0.24
"	1.2	6	94	77	< 0.01	--
"	1.4	6	65	77	0.02	--
"	1.6	6	53	39	0.32	< 0.01
"	1.8	6	58	12	1.46	0.04
"	1.2	8	82	82	< 0.01	--
"	1.4	8	61	80	0.01	--
"	1.6	8	54	64	0.02	--
JSC-L	1.2	8	74	62	< 0.01	--
"	1.4	8	54	43	0.13	--
"	1.6	8	67	22	0.95	--
"	1.2	10	75	63	0.01	--
"	1.4	10	59	52	0.20	--
"	1.6	10	54	31	1.01	--
"	1.8	10	49	25	2.15	--
"	1.2	20	56	92	< 0.01	--
"	1.4	20	47	69	< 0.01	--
"	1.6	20	28	61	0.01	--
"	1.8	20	31	34	0.39	--
LFJSC	1.2	6	70	55	0.49	0.77
"	1.4	6	62	52	0.71	1.52

bustor module. Average values for JSC-S and the JSC-L were approximately 180 and 305 cal/s, respectively. For an equivalence ratio of 1.4 and an average residence time of 8 ms, these heat losses correspond to about 20% and 10% of the total heat inputs to the JSC-S and JSC-L, respectively. Heat losses for the LFJSC were not measured.

Discussion

Data from the present set of experiments suggest that the conversion of fuel nitrogen to TFN in jet-stirred combustors depends upon the equivalence ratio and average residence time of gases within the combustor, the fuel type and certain physical characteristics of the combustors. However, the effects of these primary variables on fuel nitrogen conversion appear to be related to their effects on the concentrations of unburned hydrocarbons and soot in the exhaust gases. These effects and their relationships to unburned hydrocarbon and soot concentrations are discussed below.

Blazowski, et al. (5) have previously suggested that fuel nitrogen conversion to TFN is strongly related to concentrations of unburned hydrocarbons (HC's) in combustors. They argue that the level of fuel nitrogen conversion should decrease with increasing equivalence ratio until appreciable HC's appear in the system, i.e. the hydrocarbon breakthrough point. For richer mixtures HC's and fuel nitrogen conversion to TFN should increase with increasing equivalence ratio. They further suggest that the equivalence ratio at which HC's breakthrough should be determined by other characteristics of the combustor system such as residence time, temperature and mixing and that this equivalence ratio should be somewhat leaner than the equivalence ratio for minimum equilibrium conversion of fuel nitrogen to TFN, which is typically around 2.0. Our results are in general agreement with these predictions. Figure 2 provides an example of the general trends of fuel nitrogen conversion and HC concentrations with equivalence ratio. In this example, minimum fuel nitrogen conversion was obtained at an equivalence ratio of 1.6, just before hydrocarbon concentrations became appreciable (>0.5% as CH_4). Similar qualitative trends were obtained for most of the other conditions tested.

The pattern of increasing conversion for equivalence ratios richer than the hydrocarbon breakthrough equivalence ratio appeared to depend on the fuel, however. Figure 3 provides a comparison of fuel nitrogen conversion from isooctane and toluene at the richest equivalence ratios tested in the JSC. For both fuels, HC's increased as the equivalence ratio was increased from 1.6 to 1.8. Corresponding increases in fuel nitrogen conversion were found for isooctane mixtures at 3, 6 and 10 ms residence times, but toluene mixtures at these conditions produced either smaller increases or decreases in conversion with increasing
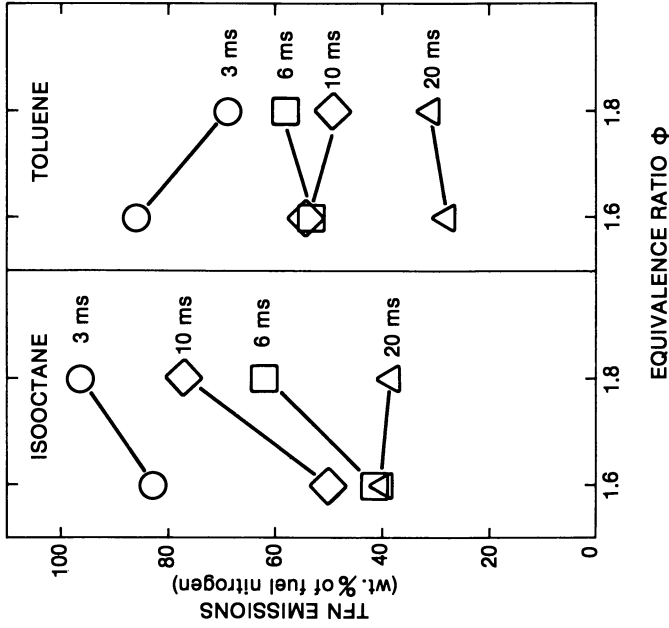
Figure 3.

TFN Emissions vs. Equivalence Ratio for
Prevaporized Isooctane and Toluene Fuels at
Various Combustor Residence Times
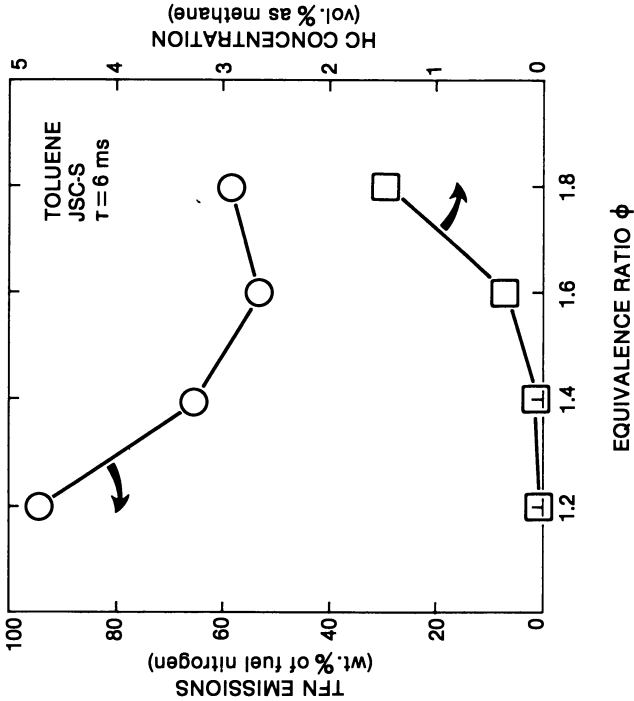
Figure 2.

TFN Emissions and HC Concentration vs.
Equivalence Ratio for Prevaporized Toluene Fuel

equivalence ratio. The different conversion trends may be related to another significant difference between isooctane and toluene mixtures at these conditions, specifically the concentrations of soot within the combustor. Isooctane mixtures produced negligible quantities of soot at these conditions; toluene mixtures had soot yields of the order of 0.1%.

Any interaction between fuel nitrogen conversion and soot concentrations, however, may be peculiar to the mixture equivalence ratios. Data from the limited LFJSC experiments, which were obtained at relatively leaner equivalence ratios (ϕ=1.2, 1.4), indicated that fuel nitrogen conversion trends for isooctane and toluene were similar even though differences in soot yields from the two fuels were more pronounced than those observed in the JSC experiments. Since the equivalence ratio of the mixtures does affect the distribution of TFN species in the stirred combustor exhaust gases, the interaction of soot with a particular TFN species might explain the apparently different effects of soot on fuel nitrogen conversion in the two combustors. Since HCN is the predominant non-NO, TFN species in the very rich (ϕ=1.8) JSC cases, an interaction between HCN and soot appears to be a possible explanation of the observed fuel-type effects on fuel nitrogen conversion in the JSC.

Data from other researchers have hinted at interactions between HCN and soot. Seeker, et al. (6) studied a pair of coal flames which had two different diameter coal particles. With the larger particles (80μm), soot clouds formed near the particle during devolatilization, and relatively low levels of HCN were detected in the combustion gases. With the smaller particles (40μm), soot clouds were not observed, and relatively high levels of HCN were detected. Lanier (7) proposed that a heterogeneous reaction between soot and HCN, in which HCN is converted to molecular N_2, might be responsible for these observations. With an extrapolated global reaction rate obtained from packed bed studies (8) and conservative estimates of expected conditions in the soot cloud, he estimated that a significant portion of the HCN produced from the coal particles could be removed by heterogeneous reaction with soot. Comparisons of these conditions with those in the JSC indicate that soot loadings in the JSC are several orders of magnitude too small for this particular mechanism to be important; however, Wendt (9) has observed similar HCN/soot effects in premixed flat flames, which may have had soot loadings of the same order of magnitude as those obtained in the JSC. Wendt's flames were produced with fuel-rich mixtures of natural gas, cyanogen, helium, and oxygen. When SO_2 was added to these flames relative soot levels decreased, HCN concentrations increased, and N_2 concentrations decreased. Whether or not a heterogeneous reaction is responsible for these soot and HCN trends is not clear at this time; nevertheless, the results do appear to suggest that soot and HCN reaction mechanisms may be related.

The effects of residence time on fuel nitrogen conversion may

be explained in terms of the corresponding behavior of HC concentrations. Levels of fuel nitrogen conversion and HC concentrations generally decreased with increasing residence time (Figure 4). Minimum levels of conversion (Figure 5) and hydrocarbon breakthrough also tended to occur at richer equivalence ratios for longer residence times. These trends are consistent with equilibrium considerations, since longer residence times would allow nonequilibrium TFN and HC concentrations to relax toward their much lower equilibrium levels. The observed residence time effects, however, may have been slightly affected by the actual gas temperatures in the experiments. Although the experiments were conducted at constant indicated thermocouple temperatures, actual gas temperatures were of the order of 150K hotter than the indicated temperatures due to radiative and conductive heat losses from the thermocouple bead to cooler combustor walls. The differences between indicated and actual gas temperatures were also slightly larger at the longer residence times. Since higher temperatures at fixed residence times do reduce hydrocarbon concentrations (3), the observed reductions in hydrocarbon concentrations and fuel nitrogen conversion for longer residence times may be partially attributable to increased actual gas temperatures at the longer residence times. Maximum variations among actual gas temperatures for the different residence times were estimated to be of the order of 50K.

Combustor type also appeared to be significant. Comparisons among the JSC and LFJSC data at a residence time of 6 ms (Figure 6) suggested that fuel nitrogen conversion was lower in the LFJSC for relatively leaner equivalence ratios (ϕ=1.2, 1.4) but higher for the one richer isooctane mixture (ϕ=1.6) tested. HC concentrations were larger in the LFJSC for all equivalence ratios, and these additional HC's were probably responsible for the larger fuel nitrogen conversion in the ϕ=1.6 isooctane mixture. The other differences among the LFJSC and JSC results may have been related to the methods of fuel injection and mixing within the combustors or to variations in actual gas temperatures and heat losses between the two combustors.

Comparisons of the results from the two different diameter JSC's at a residence time of 8 ms suggested that fuel nitrogen conversion was similar at the leaner equivalence ratios (ϕ=1.2, 1.4), but at richer equivalence ratios fuel nitrogen conversion and HC concentrations were larger in the larger JSC (Figure 7). The latter results may be due to relatively higher actual gas temperatures and/or relatively leaner equivalence ratios in the smaller JSC. Higher actual temperatures may have been present in the smaller JSC due to smaller average gas velocities and corresponding larger thermocouple measurement errors. Equivalence ratios inferred from measured exhaust gas concentrations were also relatively leaner in the smaller JSC than in the larger JSC. Either condition, i.e. higher temperatures or leaner equivalence ratios, is consistent with smaller HC concentrations in the
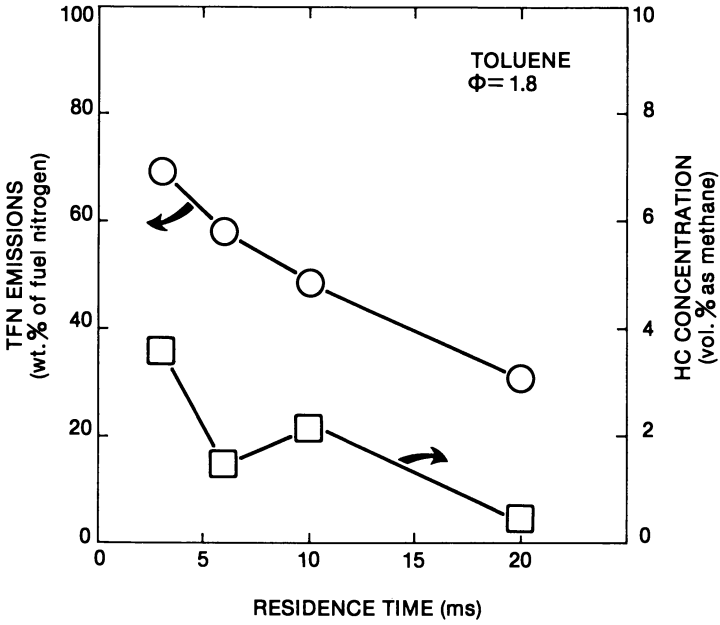
Figure 4. TFN Emissions and HC Concentration vs. Residence Time for Prevaporized Toluene Fuel
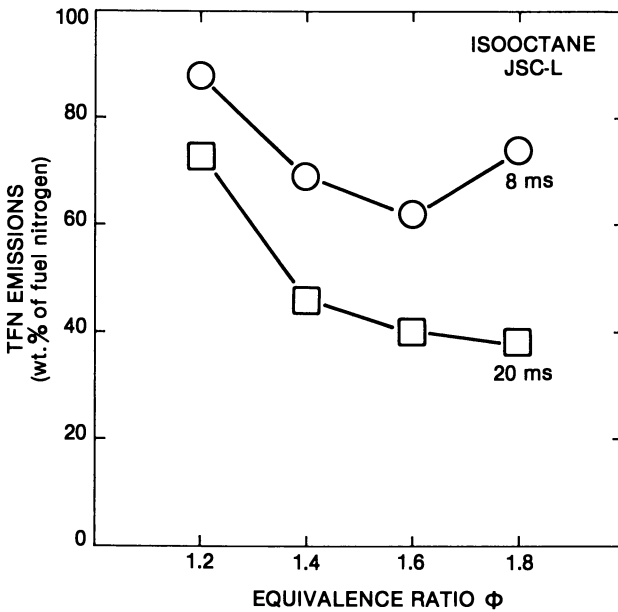
Figure 5. TFN Emissions vs. Equivalence Ratio for Prevaporized Isooctane Fuel at Two Residence Times
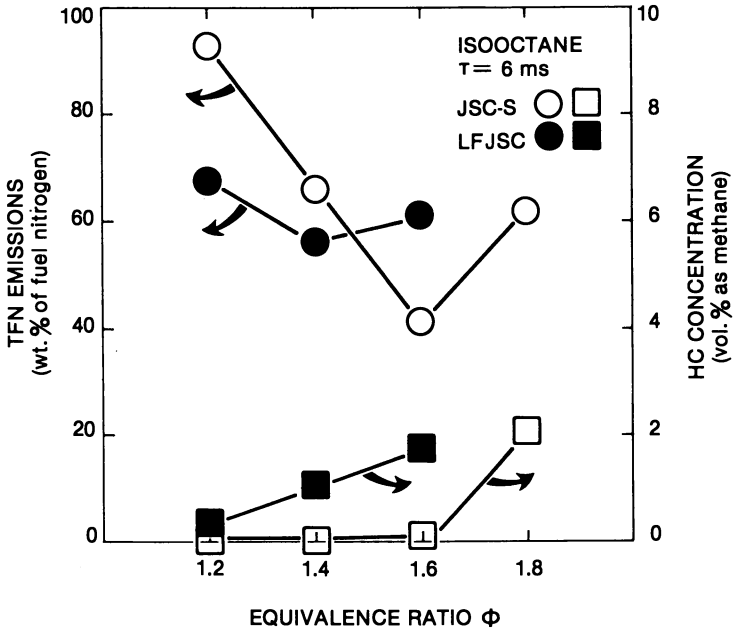
Figure 6. TFN Emissions and HC Concentration vs. Equivalence Ratio for Liquid Spray and Prevaporized Isooctane Fuel
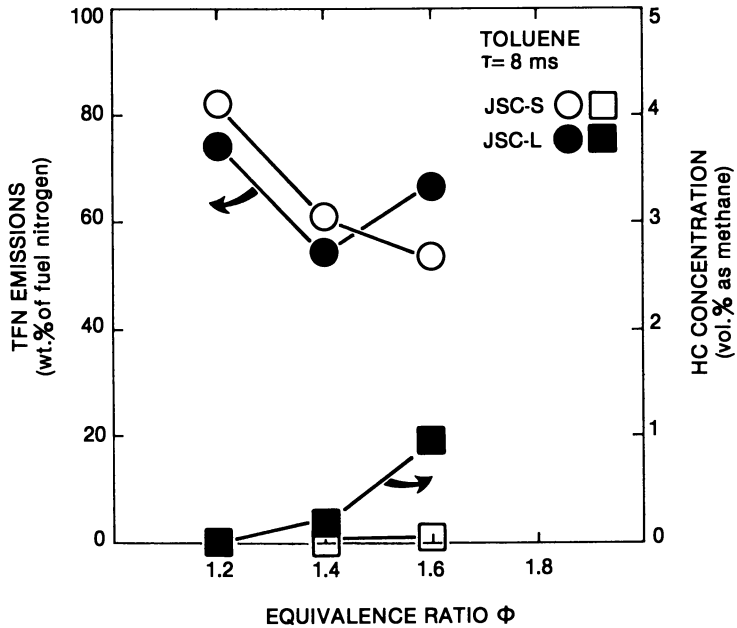
Figure 7. TFN Emissions and HC Concentration vs. Equivalence Ratio in Two Combustors of Different Size for Prevaporized Toluene Fuel

smaller J SC; however, uncertainties in the data preclude any further distinction between the two likely causes of the differences in results. Mixing arguments following Evangelista, et al. (10) do not appear to explain observed differences since relative mixing intensities at fixed residence time should have been larger in the larger J SC and since one would normally expect larger HC concentrations with smaller mixing intensities.

The observed differences among the data obtained at similar JSC and LEJSC operating conditions suggest that comparisons of data from the various combustors must allow for possible effects of combustor type in the results. Extensions of the results to larger, commercial size gas turbine combustors or to similar laboratory combustors should also be made with extreme caution. Qualitative trends such as the dependence of fuel nitrogen conversion on HC concentrations should be valid within a given combustor; however, quantitative numerical results may depend strongly on specific combustor characteristics. For example, HC concentrations for $\tau=10ms$ toluene runs in the larger J SC, were larger than HC concentrations for $\tau=6ms$ toluene runs in the smaller J SC, even though the general trend within each combustor was smaller HC concentrations for longer residence times.

Summary and Conclusions

Results from experiments in three laboratory jet-stirred combustors suggest that the conversion of fuel-bound nitrogen to total fixed nitrogen (TFN) in fuel-rich mixtures is strongly related to the concentration of unburned hydrocarbons (HC's) within the combustor. As mixture equivalence ratios increased from 1.2 to 1.8, the fraction of fuel nitrogen converted to TFN usually decreased to a minimum and then increased. The minimum level of conversion generally occurred at an equivalence ratio near that at which appreciable HC's first appeared in the exhaust gases. Variations of residence time and combustor type which reduced HC's also reduced the degree of fuel nitrogen conversion. Fuel type (aliphatic vs. aromatic) differences were most pronounced at very rich ($\phi=1.8$), short residence time ($\tau \leq 10ms$) conditions. At these conditions toluene/pyridine mixtures produced less TFN and more soot than similar isooctane/pyridine mixtures. These trends suggested a relationship between soot production and fuel nitrogen conversion, possibly a heterogeneous interaction between soot and HCN.

Acknowledgment

Literature Cited

1. Kowalik, R. M.; Ruth, L. A. "Particulate Carbon: Formation During Combustion"; Siegla, D. C.; Smith, G. W.; Ed.; Plenum Press: New York, 1981, p. 285.
2. Blazowski, W. S.; Edelman, R. B.; Harsha, P. T. "Fundamental Characterization of Alternate Fuel Effects in Continuous Combustion Systems", Summary Technical Progress Report for the period 15 August 1977 – 14 August 1978 under Department of Energy Contract EC-77-C-03-1543, September, 1978.
3. Blazowski, W. S.; Edelman, R. B.; Wong, E. "Fundamental Characterization of Alternate Fuel Effects in Continuous Combustion Systems", Summary Technical Progress Report for the period 15 August 1978 – 31 January 1980 under Department of Energy Contract DE-AC03-77ET 11313, February, 1980.
4. Hardy, J. E.; Knarr, J. J. *J. Air Pollut. Control Assoc.* 1982, 32, 376.
5. Blazowski, W. S.; Sarofim, A. F.; Keck, J. C. *J. Eng. Power* 1981, 103, 43.
6. Seeker, W. R.; Samuelson, G. S.; Heap, M. P.; Trolinger, J. P. "18th Symp. (Int.) on Combustion"; The Combustion Institute: Pittsburgh, 1981; p. 1213.
7. Lanier, W. S. unpublished work.
8. DeSoete, G. G., *Riv. Combust.* 1981, 35, 1.
9. Wendt, J. O. L., personal communication.
10. Evangelista, J. J.; Shinnar, R.; Katz, J.; "12th Symp. (Int.) on Combustion"; The Combustion Institute: Pittsburgh, 1969; p. 901.

Synthetic Fuel Character Effects on a Rich–Lean Gas Turbine Combustor

LEONARD C. ANGELLO and WILLIAM C. ROVESTI

Electric Power Research Institute, Palo Alto, CA 94303

THOMAS J. ROSFJORD

United Technologies Research Center, East Hartford, CT 06108

RICHARD A. SEDERQUIST

United Technologies Corp., South Windsor, CT 06074

Five fuels including No. 2 fuel oil, SRC II, H-Coal, and EDS middle distillates, and hydro-treated Paraho shale oil residual were tested in a subscale 5-inch diameter, staged rich-lean combustor at conditions representative of baseload and part power settings of 30-MW utility combustion turbine. A minimum NO_x emission level corrected to 15% oxygen of approximately 35 ppmv was attained for all the fuels despite fuel bound nitrogen levels of up to 0.8 percent by weight. Smoke emissions did depend on fuel properties and ranged between a SAE Smoke Number of 20 to 45 at baseload operation. Indication of increased smoke and liner heating with reduced fuel hydrogen content was observed, although the indicated trends were not as consistent as those for lean combustors.

Rich-lean combustion systems are a recent generic class of stationary gas turbine combustors capable of low NO_x emission performance with fuels containing high concentrations of nitrogen. Several rich-lean combustor designs are currently under development by utility gas turbine manufacturers as part of the ongoing DOE/NASA Low NO_x Heavy Fuel Combustor Concepts Program (1). As illustrated in Figure 1 the rich-lean combustor concept is similar to the fuel staging technique used in boiler combustion systems for controlling NO_x emissions from fuels containing high fuel-nitrogen. In brief, a small amount of primary air is mixed with the fuel in the head-end of a rich-lean combustor. This creates a fuel rich combustion zone to release nitrogen from fuels containing nitrogen compounds and maximizes the early formation of molecular nitrogen. This rich burn step is followed by the rapid introduction of secondary air

to achieve complete combustion of unburned hydrocarbons and
carbon monoxide under fuel lean conditions to minimize the
formation of thermal NO_x. The combustion process is optimized
in the rich stage to minimize the formation of NO_x and molecules
such as NH_3 and HCN which would convert readily to NO_x in the
lean stage. Sufficient residence time in the lean stage assures
complete combustion of even poor quality fuels.

The purpose of this paper is to present the results of an
experimental program sponsored by the Electric Power Research
Institute (EPRI). The purpose of the effort was to determine,
by subscale combustor rig test and data analysis, the effects of
synthetic fuel property variations on the emissions,
performance, and durability characteristics of rich-lean
combustion systems. Fuel property variations were investigated
by testing five fuels including No. 2 petroleum distillate fuel,
coal-derived middle distillate fuels produced by the SCR-II, H-
Coal and EDS processes, and a shale oil residual fuel. Tests
with these fuels provided data for realistic ranges of fuel
viscosity, and hydrogen and nitrogen content. Tests were
performed at conditions representative of full- and partial-
power settings of a 30-MW utility combustion turbine.

Test Program

Test Facility. The experimental program to document the
consequences of burning fuels that possess chemical and/or
physical properties which differ from fuels in common use was
conducted in the test facility shown schematically in
Figure 2. The total airflow was supplied to the test cell by a
positive displacement compressor, metered by a calibrated
venturi and heated in an electrical resistance-type heater. The
airflow which exited the heater was divided into a primary
airflow, which fed the rich-stage combustor, and a secondary
airflow which was injected through the combustor quench
section. Variations in the primary-secondary airflow split were
achieved by actuating a pneumatic control valve located in the
primary air line; a high temperature gate valve located in the
secondary air line provided the supply system pressure drop
necessary for control. A calibrated venturi was located in the
primary line to meter the primary airflow and hence permit
calculation of the rich combustor equivalence ratio. The
secondary airflow rate was calculated as the difference of the
total and the primary airflow rates.

The model combustor used in the present study was a copy of
one configuration (Configuration 2C) evaluated under the
DOE/NASA Low NO_x Heavy Fuel Combustor Concepts Program, and
consisted of four component sections: fuel preparation, fuel-
rich combustion, air quench, and fuel-lean combustion sections
(2). All of the test fuel was injected into a rich combustion

Secondary airflow

Fuel →

Primary → airflow

$\phi \sim 1.4\text{-}1.6$

$\phi \sim 0.3$

| Fuel preparation | Fuel-rich combustor | Rapid quench | Fuel-lean combustor |
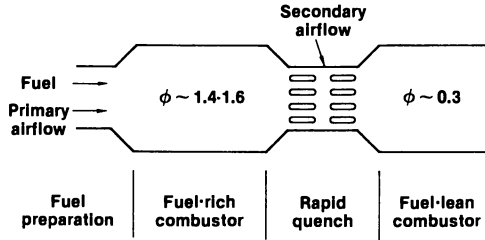
Figure 1. Elements of Rich–Lean Staged Combustor

AIR SUPPLY

TOTAL FLOW VENTURI

SECONDARY AIR

ELECTRICAL AIR HEATER

PRIMARY AIR

VALVE TO CONTROL AIRFLOW SPLIT

PRIMARY AIRFLOW VENTURI

FUEL

RICH

LEAN

EXHAUST

COOLED COMBUSTOR SECTIONS

EXIT INSTRUMENTATION
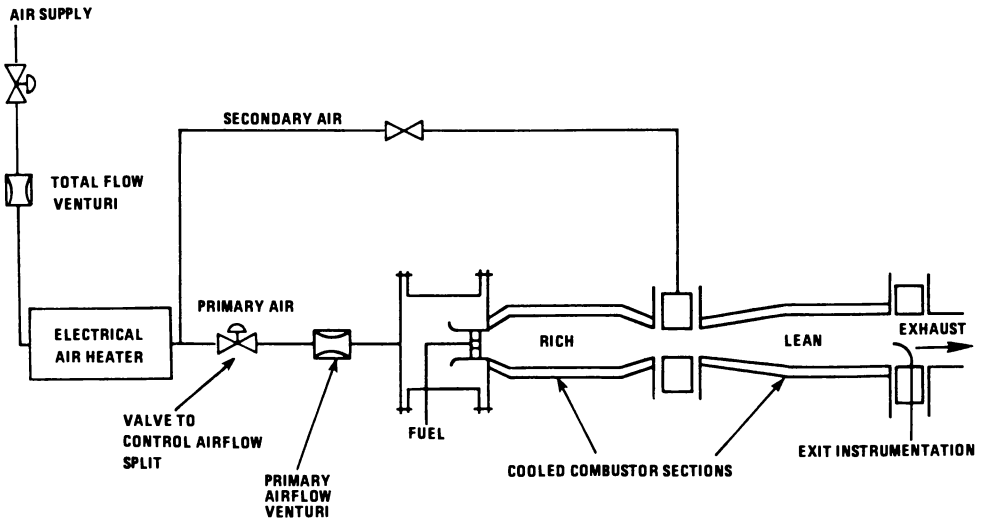
Figure 2. Synthetic Fuel Combustor Rig

chamber through the fuel preparation section. This section consisted of a single, air-assist fuel injector which was centrally mounted in an annular, vane-type swirler; the swirler-nozzle assembly was recessed approximately 1.2 inches from the rich combustor inlet. Several injector models were evaluated during the combustor shakedown tests; excessive smoke levels or nozzle failure (e.g., loss of nozzle resonator cap) were experienced with most. Acceptable operation was attained with use of a Delavan® swirl air injector; all reported data were acquired using this injector. The nozzle assist airflow was metered with a calibrated venturi and was included in calculation of the primary and total airflow rates. Most of the data were acquired with an air-assist pressure of 300 psi at the fuel injector; limited tests were performed to investigate the influence of higher or lower assist-air pressure levels.

The fuel-rich combustion chamber was a 5-inch diameter cylindrical section, 11.0 inches long, with 1.9-inch long conical sections at both the inlet and exit (Figure 3). The entire chamber was double-jacketed to allow a nominal 40 GPM water coolant flow rate. An H_2/O_2 torch was incorporated in the design to ignite the burner. The quench section was a 3-inch diameter cylindrical section, 3 inches long, containing 16 slots to permit the addition of the secondary airflow to the rich combustor effluent. The fuel-lean combustor consisted of a 10.6-inch long conical diffuser followed by a 5-inch diameter cylindrical section to give an overall length of 18 inches from the quench section exit to the exhaust measurement plane (Figure 3). This combustor was also double-jacket; the water coolant used for the rich burner was also used for the fuel-lean device.

The combustor exit conditions were documented by a five-port ganged sampling probe, a three-point thermocouple rake and a smoke probe. The water-cooled sampling probe spanned the combustor diameter, and contained five 0.034-inch diameter inlet orfices. The probe was designed to achieve an aerodynamic quick-quench of the captured streams in order to minimize chemical reaction within the probe. The captured sample was transferred in an electrically-heated sample line to an emission analysis system capable of continuously monitoring the emissions of carbon monoxide, oxygen, carbon dioxide, unburned hydrocarbons and oxides of nitrogen. A water-cooled smoke probe was designed in accordance with SAE ARP1179. The probe, which had a sample inlet diameter of 0.07 inches, was sized to isokinetically sample the gas stream at the baseload condition. Three PT6RH/PT30RH thermocouples were mounted on a water-cooled strut with a vented radiation shield around each sensor.

Test Fuels

Five fuels were investigated including: No. 2 petroleum
distillate fuel, coal-derived middle distillate fuels produced
by the SRC-II, H-Coal and EDS processes and shale oil residual
fuel. Detailed analyses of each test fuel are presented in
Table 1. The No. 2 petroleum distillate fuel and the coal-
derived liquids had similar distillation and viscosity ranges
but displayed significantly different levels of hydrogen and
fuel-bound nitrogen content. The hydrocarbon-type also showed
considerable variation, with excess of 75% of the SRC-II fuel
having an aromatic character. In addition the intial boiling
point of the H-Coal distillate fuel was somewhat lower than the
other distillate fuels.
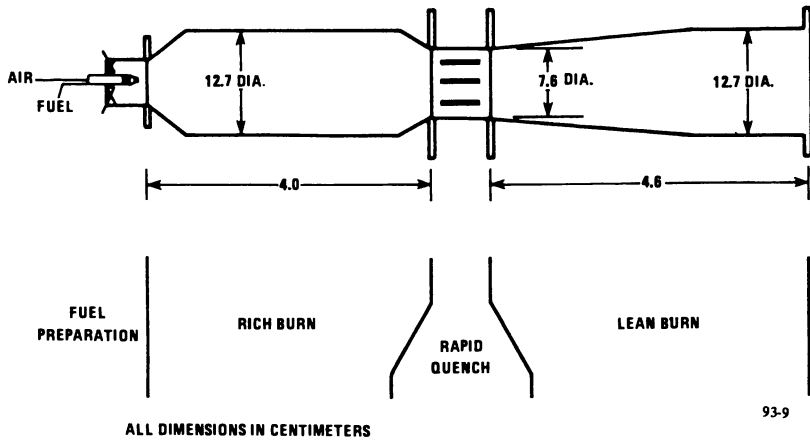
Figure 3.   Subscale Rich-Lean Combustor Configuration

TABLE 1   TEST FUEL ANALYSES

Property	Unit	No. 2	SRC-II	H-Coal	EDS	Shale
Physical Properties						
Specific Gravity 40°C	—	0.841	0.9610	0.872	0.894	0.863*
Pour Point	F	-5	-40	-45	-55	95
Flash Point	F	152	164	90	167	235
Gross Ht. of Combustion	Btu/lb	18280**	17161	17725	19266	19350
Kinetmatic Viscosity 40C	cs	2.53	3.49	1.58	2.40	12.9
100C	cs	1.04	1.114	0.69	0.95	3.77
Chemical Properties						
Carbon	wt%	87	86.04	88.21	88.12	86.7
Hydrogen	wt%	12.95	8.97	11.28	11.31	12.69
Surfur	wt%	0.25	0.2495	0.08	0.01	0.02
Nitrogen	wt%	0.02	0.75	0.32	0.02	0.46
Saturates	vol%	64.8	19.3	39	40	--
Olefins	vol%	0.7	2.9	0.04	0.1	--
Aromatics	vol%	34.5	77	60.09	60	--
Distillation						
Initial boiling point	F	360	312	240	390	480
10%	424	400	326	425	616	
50%	510	466	408	468	747	
90%	605	536	500	568	848	
End point recovery		660	560	590	596	855
Recovery		98.5	98.0	98.0	98.5	94.0
Residue		1.5	2.0	2.0	1.5	6.0

*At 49°C
**Net Heat of Combustion

The shale oil residual had been hydrotreated to a substantial degree, providing it with a hydrogen content very similar to the No. 2 petroleum distillate fuel. The shale oil residual fuel had viscosity characteristics similar to a viscous No. 4 petroleum distillate fuel. The nitrogen content of the hydrotreated shale oil residual was 0.49 weight percent.

Test Conditions

Tests were performed over a matrix of conditions to establish emissions and heat load characteristics for each test fuel. The tests were structured to allow determination of both combustion tradeoffs (e.g., low NO_x emissions vs. low smoke emissions) and the influence of varying selected fuel properties (e.g., nitrogen or hydrogen content) on the emission levels.

Three categories of tests were performed. The first category included tests to determine the change in combustor emissions as the primary combustor equivalence ratio (ϕ_ρ) was varied between 1.0 and 1.8. These tests were referred to as signature tests, and were performed at both baseload and 50% power operating conditions. For these tests the total airflow and airflow split between the primary and secondary streams were held constant while the fuel flow rate was varied. With this technique, the primary combustor equivalence ratio was changed while holding the residence time in this chamber nearly constant. The second category of test conditions included design point operation at peak, baseload and 70% load conditions of an utility gas turbine. These points were selected to match the test points from the DOE/NASA Low NO_x Program allowing comparison with data from that program. The third category of test conditions focused on off-design operation to investigate the influence of rich combustor residence time and pressure on combustor emissions; off-design tests departed from baseload and 70% power design points.

Test Results

Tests with No. 2 Petroleum Distillate Fuel. Tests were performed with No. 2 petroleum distillate fuel to establish a baseline for comparison with the other test fuels.

The NO_x emissions signature is shown in Figure 4 for operation at both the baseload and 70% power conditions. The NO_x emissions started at very high levels for equivalence ratios near unity and decreased rapidly to values less than 50 ppmv for $\phi_\rho > 1.3$. The minimum NO_x level of approximately 37 ppmv was equivalent for either operating condition and was achieved for both at $\phi_\rho = 1.55$. Equilibrium chemistry considerations would lead to the conclusion that the rapid decline in NO_x emissions was a result of both the decreased flame temperature and reduced

oxygen concentration at the fuel-rich operation conditions.
These effects would stongly reduce thermal fixation of molecular
nitrogen to NO_x. While these considerations offer an
explanation for the final level of NO_x achieved, it must be
realized that the fuel was injected as a spray and not as a
fully-vaporized air mixture. Hence for any equivalence ratio
there were regions of near stoichiometric combustion with the
attendant production of high levels of NO_x. Therefore, an
annihilation mechanism must have been present to reduce these
initial levels to the very low NO_x emissions attained. The
combustor smoke emissions varied with the primary zone
equivalence ratio, as shown in Figure 5. There was no apparent
distinction between the smoke levels achieved at either the
baseload or the 70% operation condition; the data fell into a
band with increasing smoke production for higher primary
combustor equivalence ratio. The tradeoff of choosing either to
minimize NO_x emissions or smoke emissions is shown in Figure 6,
which is a cross-plot of the previous two figures. Operation at
the threshold of visible smoke (SAE Smoke Number=20) could be
achieved with NO_x emissions less than 50 ppmv; attempts to
further reduce the smoke emissions to lower values would result
in excessive NO_x emissions.

   One operating concern for a rich combustor is the occurrence
of high combustor wall temperatures. In a fuel-rich combustor,
air cannot be used to film-cool the walls and other techniques
(e.g., fin cooling) must be employed. The temperature rise of
the primary combustor coolant was measured and normalized to
form a heat flux coefficient which included both convective and
radiative heat loads. Figure 7 displays the dependence of this
heat flux coefficient on primary combustor equivalence ratio.
These data were acquired in tests in which the combustor airflow
was kept constant. If convective heat transfer were the
dominant mechanism a constant heat flux coefficient of
approximately 25 Btu/ft^2-hr-deg F would be expected. The higher
values of heat flux and its convex character indicate that
radiative heat transfer was an important mechanism.
Furthermore, there is an apparent tradeoff between the
temperature of the radiating-medium and the effective emissivity
of the medium. That is, at equivalence ratios near unity the
gas temperatures would be maximum, but few carbon particles have
formed. As the equivalence ratio was increased, the temperature
decreased, but the number of radiating particles began to
increase resulting in a net increase in the radiative
mechanism. At high equivalence ratios, the temperature of the
radiating particles decreased sufficiently to override the
abundance of radiating particles and consequently the heat flux
coefficient diminished. Comparison with the previous figures
reveals that the region of primary zone equivalence ratio
desired for low NO_x operation and acceptable smoke emissions
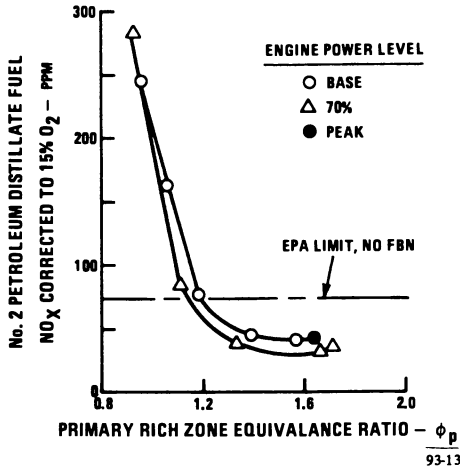
Figure 4.
NO_x Dependence on Primary Combustor
Equivalence Ratio for No. 2 Petroleum
Distillate Fuel
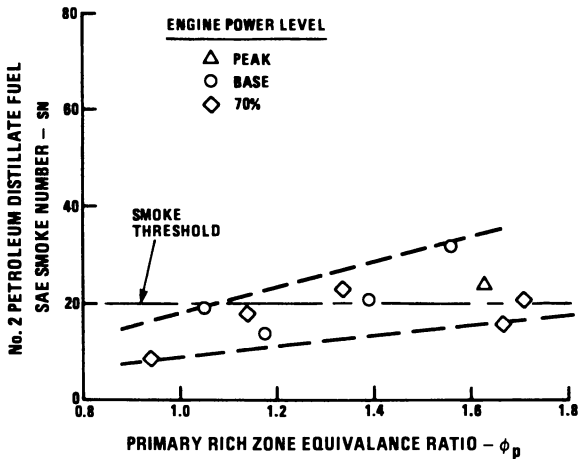
Figure 5.
Smoke Dependence on Primary Conbustor
Equivalence Ratio for No. 2 Petroleum
Distillate Fuel
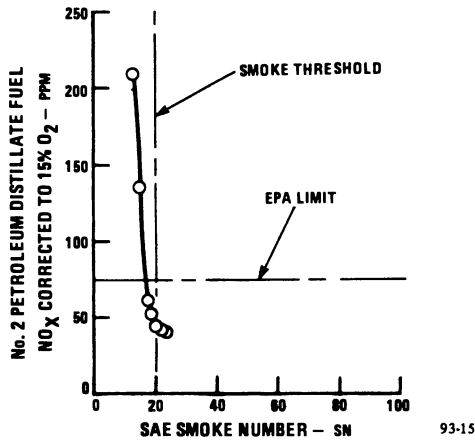
Figure 6.
Tradeoff on NO_x and Smoke Emissions for
No. 2 Petroleum Distillate Fuel
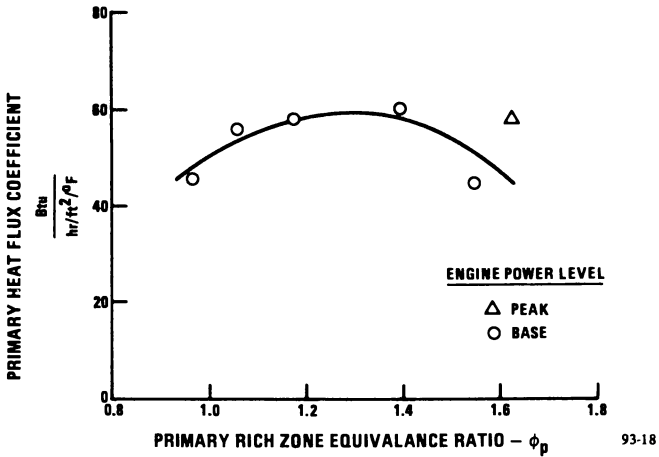
Figure 7.
Average Heat Transfer to Primary Combustor
Wall for No. 2 Petroleum Distillate Fuel

also produced the maximum heat transfer to the primary combustor walls.

Test Results with Middle Distillate Coal-Derived Fuels. Tests were performed with middle distillate fuels produced by the SCR-II, H-Coal, and EDS processes. The composition of these fuels represented significant variations in the fuel–hydrogen content, the fuel–nitrogen content, and the mix of characteristic hydrocarbon compounds.

NO_x emissions signatures were obtained for the SCR-II, H-Coal and EDS fuels at baseload and part-power test conditions. For each fuel the NO_x started at a very high level (greater than 200 ppmv) for equivalence ratios near unity and decreased rapidly with increasing equivalence ratio. For all three fuels the minimum NO_x level was independent of the simulated power condition, with a level of 35 to 40 ppmv achieved for $\phi p = 1.55$. This minimum value is most significant for the SCR-II fuel which contained 0.75 percent nitrogen in the fuel. If this fuel nitrogen content were fully oxidized, the NO_x level would approach 350 ppmv at baseload operation. Again it is believed that high concentrations of NO_x are formed in the rich combustor but that annihilation reactions are sufficient vigorous to reduce the emissions to the observed values. The combustor smoke emission increased with primary combustor equivalence ratio. The data indicated a significant difference between operation at baseload and 50% power conditions for the SCR-II and H-Coal fuel. For these two fuels, smoke emissions were significant at high power operation but nearly non-existent for operation at pressures below 100 psi. There was no systematic distinction between these operating conditions for the data acquired using EDS fuel; the smoke levels were more characteristic of high power pressure operation. The three fuels are compared in Figure 8 to show the tradeoff in choosing either to minimize NO_x emissions or smoke emissions. It would be desirable to operate in the lower left-hand region of this plot and hence attain low emissions of both species. The data acquired for H-Coal and EDS indicate the ability to attain NO_x emissions less than 50 ppmv for SAE SN=10. Higher emissions of either species would have to be expected if operating on SCR-II fuel.

The average heat flux coefficient to the primary combustor wall is plotted for the fuels in Figure 9. The results in general displayed a convex character as was observed with NO. 2 fuel. The level of the heat transfer coefficient and its convex trend indicates the importance of radiative heat transfer for these fuels. The maximum value of the coefficient for SCR-II fuel exceeded the maximum for other fuels by 30%. The hydrogen content of SCR-II was less than that for the other fuels tested which apparently resulted in a more intense radiating medium.
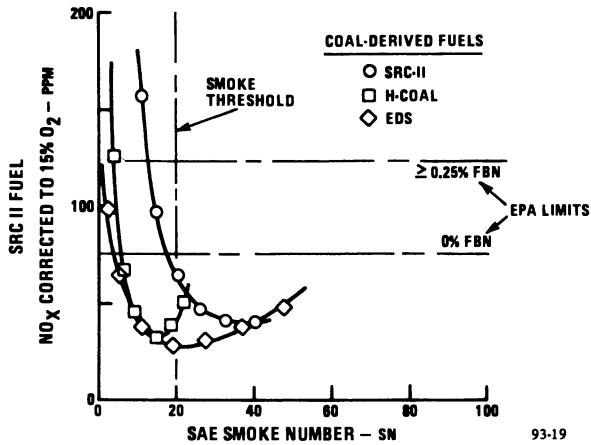
Figure 8.
Comparison of Trade-off of NO$_x$ and Smoke
Emissions at Baseload Conditions for Coal-Derived Fuel
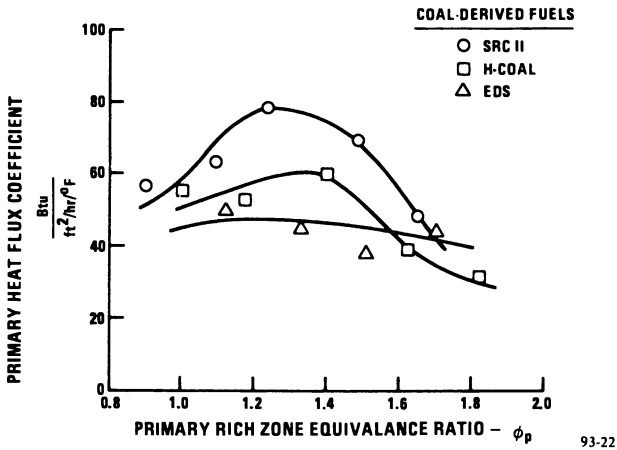
Figure 9.
Comparison of Primary Combustor Wall Heat
Loading for Coal-Derived Fuels at Baseload

Again the maximum is observed at primary combustor equivalence ratios close to that desired for minimum NO_x emission operation.

Test Results with Shale Oil Residual Fuel. Tests were performed with a shale oil residual fuel which had the viscosity characteristics of a heavy No. 4 petroleum distillate fuel. The tests were performed after heating the fuel to 160°F to reduce its viscosity to 7 cs in an attempt to enhance the fuel atomization and vaporization process. Even with this degree of heating, this fuel has a viscosity twice the level of other fuels tested.

The NO_x signature at both baseload and 50% power conditions was similar to the other fuels tested, reached a minimum of 40 ppmv at $\phi p=1.5$. The corresponding smoke emissions were higher than for other fuels tested (Figure 10). These levels are attributed to relatively poor atomization because of the higher fuel viscosity. A single data point is shown for which the air-assist pressure was increased from 300 psi to 500 psi to improve the fuel atomization. A substantial reduction in smoke emissions was observed with the smoke number decreasing from SAE SN=40 to 3. The NO_x emissions increased from 32 to 50 ppmv with the enhanced air assist indicating that the fuel preparation process offers an emissions tradeoff. In a limited number of tests, it was determined that heating the assist air did not improve the smoke emissions. The NO_x levels obtained were independent of the operation of the primary combustor. Neither reducing the residence time nor changing the pressure level significantly affected the NO_x levels. The heat flux to the combustor wall was comparable to that for NO. 2 petroleum distillate fuel.

Discussion of Test Results

The test data acquired were analyzed to determine the fuel property effects on the staged combustor performance. Influences on the emissions and the heat flux to the primary combustor wall are presented in this section. Comparisons with data acquired by Westinghouse Electric Corporation in another EPRI-sponsored contractual program (RP989-1) in which similar test fuels were combusted in a conventional, lean combustor are also presented (3).

NO_x Emissions. The nitrogen content in the distillate fuels ranged from 0.0 to 0.75 wt%. The influence of this range on NO_x emissions is displayed in Figure 11. The values plotted correspond to the minimal NO_x level for each fuel. Since the minima occurred over a small range of primary combustor equivalence ratio (1.5 $<\phi p$ <1.57) these data also represent operation at constant combustor conditions. As can be observed, the NO_x emissions were independent of fuel nitrogen. An
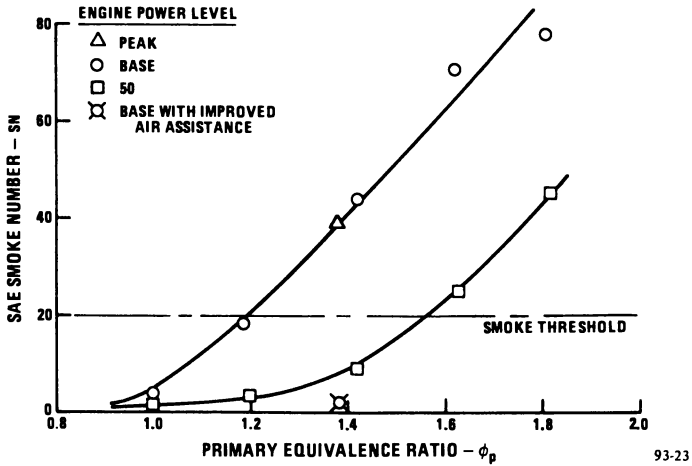
Figure 10.
Smoke Dependence on Primary Combustor
Equivalence Ratio for Shale Oil Residual
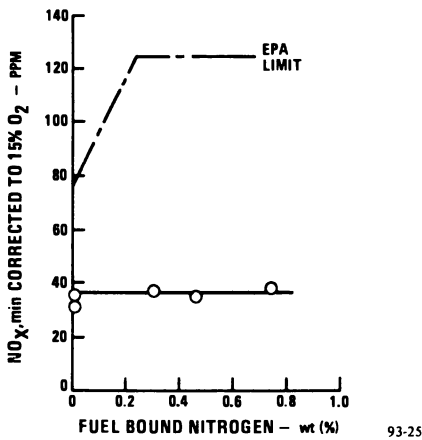
Figure 11.
Dependence on NO_x Emissions on Fuel-Bound
Nitrogen

emissions level of approximately 37 ppmv was attained for all
fuel nitrogen concentrations, and for all combustor power levels
investigated. This level is substantially below the maximum
emissions permitted by EPA regulations for fuel with or without
fuel-bound nitrogen. Apparently a vigorous annihilation
mechanism is present in the rich burner which results in low NO_x
despite significant fuel-bound nitrogen concentrations.

The NO_x levels obtained from the staged combustion
investigation were substanially less than obtained from a lean
combustor (Figure 12). At exit temperatures representative of
baseload operation, the rich-lean combustor produced NO_x levels
approximately one-third the levels associated with the lean
combustor. Unlike the staged combustor emissions increased with
increased fuel-bound nitrogen.

Smoke Emissions. The smoke emissions did depend on the fuel
chemical properties. Figure 13 displays the smoke numbers
attained at baseload operation for the range of fuel hydrogen
content in the test fuel. While a general trend of increased
smoke with decreased hydrogen can be observed, the correlation
is not satisfactory. H-Coal and EDS fuels had equivalent
hydrogen content but H-Coal produced significantly less smoke.
These two test fuels had similar physical properties (the
viscosity of H-Coal was slightly less than the viscosity of EDS)
and disltillation end points. The initial boiling point (IBP)
of H-Coal was considerably lower than the EDS value; the EDS IBP
corresponded to the 40% point on the H-Coal distillation
curve. This difference does not mean theat H-Coal injected into
the combustor vaporized 40% faster than the EDS fuel; a detailed
droplet vaporation study at the conditions of the head end of
the rich combustor would be required to quantify this
difference. It is likely that somewhat higher vaporization
levels were achieved for H-Coal which would favor lower smoke
production levels.

The viscosity of the fuel did affect the smoke level. While
No. 2 petroleum distillate fuel and shale oil residuals had
similar chemical compositions, they differed significantly in
their viscosities. The more viscous fuel produced greater smoke
levels (Figure 14), presumably because of degraded fuel
atomization. Correlations developed for air-atomizing injectors
to predict the Sauter Mean Diameter (SMD) of the fuel spray
generally consisted of two terms--one term responsive to the
atomizing airflow and one term dependent on the fuel
viscosity. The higher viscosity would contribute to a larger
spray SMD through the second term. A single test was performed
using a higher assist airflow to reduce the contribution of the
first term. A substantial reduction in the smoke level was
achieved, indicating that the fuel properties were responsible
for the relatively high initial smoke level and that proper fuel
preparation could reduce smoke to a more acceptable level.
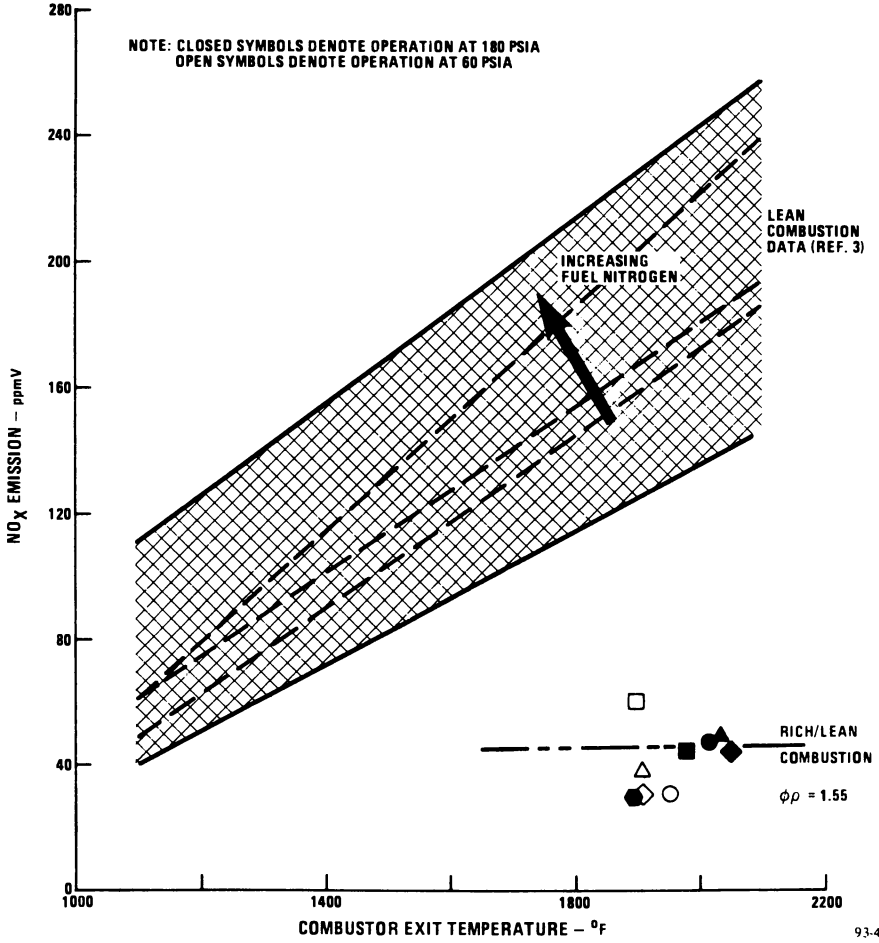
Figure 12.
Rich-Lean vs. Lean Combustor NO$_x$ Emissions
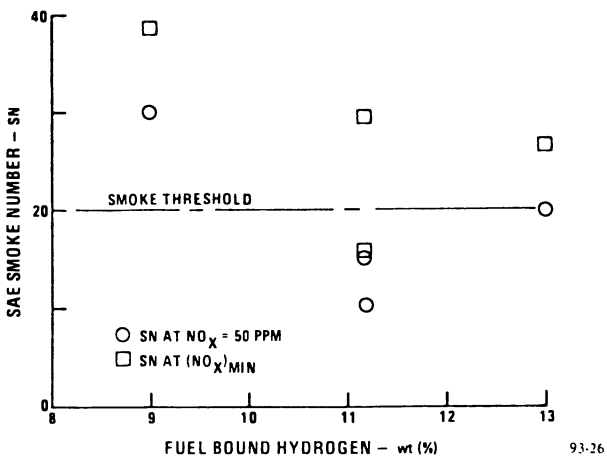
Figure 13.
Dependence of Smoke on Hydrogen Content
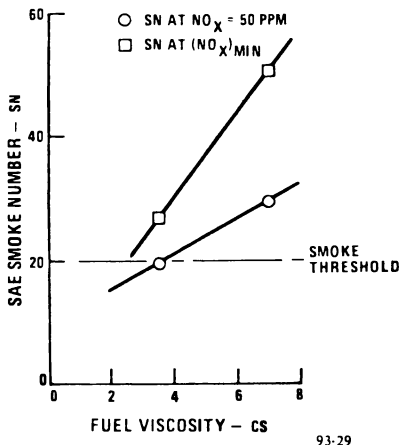
Figure 14.
Observed Dependence of Smoke Emission on
Viscosity of Chemically Similar Fuels

   Combustor Heat Load. The heat flux to the primary combustor
increased with decreased in hydrogen content (Figure 15). This
result is consistent with the trend of increased smoke emissions
with decreased hydrogen. That is, an increase in primary
combustor carbon particle loading would be expected to accompany
increased smoke emissions. Hence, the radiative heat transfer
would also increase. Again, there was a different level for the
two fuels which contained equal hydrogen content. However,
whereas the EDS fuel resulted in greater smoke levels, it
generated less radiant heat transfer to the wall than H-coal
fuel. No explanation is offered for this apparent dis-
crepancy. It is noted that the heat flux determination is
subject to error as the average temperature rise to the primary
combustor coolant was only 10°F; thus these results should be
regarded as qualitiative and not quantitative.
   It can be shown that the staged combustor heat flux data can
be used to evaluate liner heat load in a manner equivalent to
the temperature parameter often used for lean combustors ($\underline{4}$).
This is:

$$(Q-Q_{No.2})/Q_{No.2}=(T_W-T_{W,No.2})/(T_{W,No.2}-T_i)$$

where:

Q	= Heat Flux attained with Test Fuel
$Q_{No.2}$	= Heat flux attained with No. 2 Petroleum Distillate Fuel
$T_{W, No. 2}$	= Liner Temperature obtained with No. 2 Petroleum Distillate Fuel
T_i	= Combustor Inlet Temperature

   This equality allows both the correlation of water-cooled
combustor data with air-cooled combustor data, and the predicted
of the fractional increase in wall temperature for air-cooled
rich combustors using water-cooled combustor heat flux data.
The staged combustor data have been normalized at a primary
equivalence ratio of 1.55 for alltest fuels (Figure 16). The
fractional increase in heat flux is generally consistent with
the lean combustor temperature parameter data presented by
Westinghouse ($\underline{3}$). As with the correlation of the rich-lean
smoke data, the heat flux parameter does not display a unique
correlation to fuel hydrogen content.
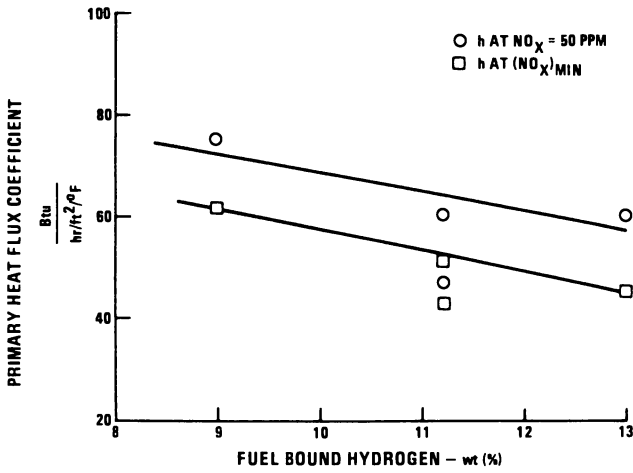
Figure 15.
Dependence of Primary Combustor Heat Load
on Fuel Hydrogen
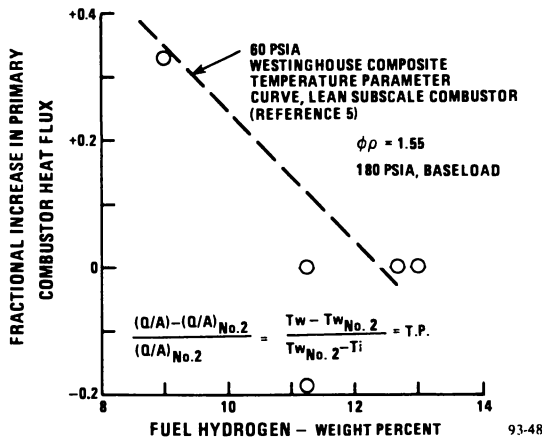
Figure 16.
Rich–Lean vs. Lean Combustor Liner Heating

Summary of Results

The data acquired in the evaluation of a subscale, rich-lean staged combustor indicated a substantial tolerance for fuel property variations while retaining a low emissions operation characteristic. In particular, it was observed that :

1. NO$_x$ emissions were independent of the fuel-bound nitrogen content. A minimum NO$_x$ level of approximately 37 ppmv (corrected to 15% oxygen) was attained even for fuels containing 0.75 wt% nitrogen.

2. Smoke emissions increased with hydrogen deficient fuels. Results indicated that the smoke level was primarily sensitive to fuel hydrogen content and fuel preparation technique. Smoke levels also showed sensitivity to fuel viscosity and initial boiling point. A better understanding of these interrelated effects is necessary to more confidently translate these subscale results into definitive design data.

3. Primary combustor heat load increased with hydrogen deficient fuels, and maximized near values of $\phi\rho$ desired for low emission operation. The correlation of the combustor heat flux with fuel hydrogen content for the water-cooled, staged combustor was consistent with air-cooled, lean combustor data.

Acknowledgment

Literature Cited

1. Lister, E.; Niedzwiecki, R.W.; Nichols, L. "Low NO$_x$ Heavy Fuel Combustor Concepts Program", ASME Paper 80GT-69, March 1980.

2. Russell, P.L.; Beal, G.W.; Sederquist, R.A.; Schultz, D. "Evaluation of Concepts for Controlling Exchaust Emissions from Minimally Processed Petroleum and Synthetic Fuels", ASME Paper 81-GT-157, March, 1981.

3. DeCorso, S.M.; Pillsbury, P.W.; Bauserman, G.; Mulik, P.R.;
    Ambrose, M.J.; Stein, T.R. Gas Turbine Combustion
    Performance on Synthetic Fuels. EPRI Publication AP-1623,
    Volume II, EPRI Contract RP989-1, Final Report, June 1981.

4. Blazowski, W.S. "Combustion Considerations for Future Jet
    Fuels", Sixteenth Symposium (International) on Combustion,
    Combustion Institute, 1977, pp. 1631-1639.

Combustion of Coal-Derived Fuel Oils

M. W. PEPPER, J. PANZER, and H. MAASER

Exxon Research and Engineering Company, Linden, NJ 07036

D. F. RYAN

Exxon Research and Engineering Company, Baytown, TX 77520

Combustion tests of fuel oil blends derived from the
Exxon Donor Solvent (EDS) process were carried out in
a laboratory 50 hp test boiler and a commercial 1425 hp
boiler. All tests showed that coal derived fuel oils
burn cleanly compared to petroleum fuels with low levels
of smoke and particulates. Emissions of NO_x were re-
lated to fuel nitrogen content for both the petroleum
and coal-derived fuels.

Polynuclear aromatic hydrocarbon (PNA) emissions were
higher for EDS fuels in lab scale tests. These emis-
sions appeared to be due to the pyrolysis of high
molecular weight PNA into smaller ring structures.

Tests in the commercial boiler showed no significant
differences in PNA emissions from EDS fuel oil and
petroleum regular sulfur fuel oil. It is speculated
that increasing the boiler size decreases the surface-
to-volume ratio which provides a smaller quench zone
for partially pyrolyzed combustion products. Emissions
of PNA from the commercial scale combustion of coal-
derived fuels may not be a problem.

One phase of the Exxon Donor Solvent (EDS) coal liquefaction
research and development program addresses the quality of liquid
products. The broad objectives of EDS product quality studies
are to identify potential end-uses for coal-derived liquids and
to evaluate the properties of these liquids to allow meaningful
assessment in these end-uses.

This paper covers the combustion performance of EDS fuel oil
blends, with primary emphasis on the emissions of polynuclear
aromatics (PNA). Previous testing of EDS fuel oil blends (1,2)
and other coal derived fuel oil blends (2) has shown that emis-
sions of particulate and smoke are lower with coal-derived fuel
oils than from the combustion of petroleum-derived fuel oils.

NO_x emissions tend to be higher due to the higher fuel nitrogen
levels of coal-derived fuel oils. However, it appears, based on
small scale lab tests (2) and limited commercial tests (3), that
staged combustion should allow NO_x emissions standards for coal-
derived fuel oils to be met. One environmental concern that had
not been addressed in these tests is the emissions of PNA. This
is a potential concern due to the highly aromatic nature of coal-
derived fuel oils.

The EDS coal liquefaction process exhibits broad feed coal
and product slate flexibility. A wide range of coals can be pro-
cessed, yielding a product slate which can be varied from pre-
dominantly heavy fuel oil, through a naphtha plus distillate
slate, to a high naphtha yield slate. A generalized flow diagram
of the EDS process is depicted schematically in Figure 1. In
this configuration, coal is slurried with a hydrogen donor sol-
vent and fed in admixture with molecular hydrogen to the preheat
furnace and the liquefaction reactor system. The primary lique-
faction products are separated by atmospheric fractionation into
light hydrocarbon gases, naphtha and a hydrogen deficient sol-
vent. The latter stream, having a nominal boiling range of 350
to 750°F, is recycled to liquefaction following catalytic hydro-
genation to restore its donor hydrogen level. Excess solvent is
withdrawn following hydrogenation as distillate product. Vacuum
fractionation is used to separate vacuum gas oil (VGO) from lique-
faction bottoms.

VGO disposition and the bottoms processing step influence the
product slate. One option is to produce only distillate and
lighter products. This is achieved by extinction recycle of the
VGO along with a portion of the bottoms, as shown in Figure 1.
Bottoms purged from the system are then used to generate hydro-
gen, fuel or process heat. A second option is to produce a pre-
dominantly heavy fuel oil slate. This is achieved by withdraw-
ing VGO as product and processing the bottoms with a FLEXICOKING*
(Service Mark of Exxon Research and Engineering Co.) process unit
to recover additional liquids. One option for the FLEXICOKING
process is to produce a coker liquid containing 1000°F+ material.

In this program, two types of fuel oil blends were combusted.
One type of blend was derived only from primary liquefaction prod-
ucts, VGO and solvent, having a nominal boiling range of 350 to
1000°F and are referred to as 350-1000°F blends. Fuel oils were
also blended by adding coker liquids, containing 1000°F+ material,
to the 350-1000°F blends and are referred to as 350°F+ blends.

The work reported here was carried out in two phases. The
first phase was conducted in a laboratory test boiler to deter-
mine the relative PNA emissions from a variety of EDS and petro-
leum fuels. The second phase of testing was conducted in a com-
mercial boiler to determine the effect of unit size on PNA emis-
sions. This testing was made possible by the start-up and opera-
tion of the Exxon Coal Liquefaction Pilot Plant (ECLP) which has
a throughput of 250 tons per day and can produce approximately
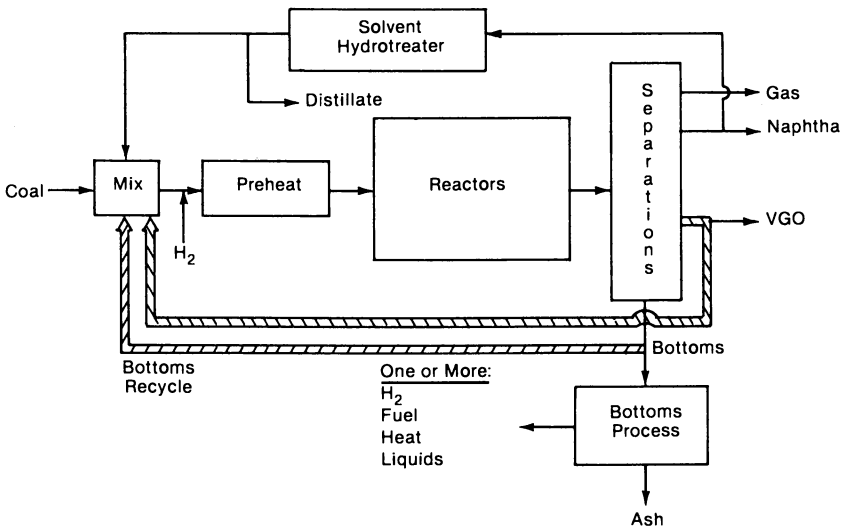
Figure 1. Exxon donor solvent (EDS) direct coal liquefaction process.

500 barrels per day of liquid product. Prior to start-up of ECLP, the quantity of fuel oil available would not allow such large scale testing.

Phase 1 - Laboratory Combustion Testing

In establishing the relative levels of PNA emissions from EDS fuel oils and petroleum fuels, all experiments were run in a 50 hp fire tube boiler under nominally identical combustion conditions. These were an excess O_2 level of 2 percent, fuel feed rate of 0.45 kg/min., and a nozzle temperature such that the fuel viscosity was about 30 cSt to maintain equivalent atomization.

The emission measurements during this testing included NO_x, smoke, particulate and PNA. NO_x was determined by a non-dispersive infrared analyzer, and smoke by the Bacharach test. Both the particulates and PNA were sampled by a source assessment sampling system (SASS). The SASS system isokinetically samples a fraction of the stack gas and traps particulates in a series of cyclones, which classify the particulate by size. Final filtration is through a fiberglass filter mounted in an oven heated to 200°C to prevent condensation of acids. In this program, the cyclones were not used, since previous work (3) had shown the particulate from coal-derived fuel oils to be small, with an average diameter on the order of 0.4 μm. The PNA which is not deposited on the particulate is collected on XAD-2 resin after the gas has been cooled to 15-20°C. PNA analyses were carried out on a combined extract from the particulate, XAD-2 resin, other condensates in the system, and the solvent rinses used to clean the SASS system.

Two types of analytical tests were run to determine PNA in the fuel and emissions. For both tests, the SASS extracts or fuels were extracted with solvents, followed by silica gel chromatography to isolate a PNA-rich fraction for further analyses. The first analytical test, a GC/UV procedure, determined the concentration of 23 specific PNA representative of frequently encountered 3 to 6 ring PNA. The second analytical test, a GC/flame ionization detector (FID) procedure, was also conducted to provide a measure of the total PNA content by ring size in the same range.

Seven fuels were burned in these initial tests: two petroleum fuels, one regular sulfur fuel oil (RSFO) and a low sulfur fuel oil (LSFO), and five EDS fuel oils. The EDS fuel oils were blended from components produced in the one ton per day pilot unit at the Exxon Research and Engineering site in Baytown, Texas. Products from the liquefaction of two coals, a bituminous Illinois coal from the Monterey No. 6 mine, and a sub-bituminous Wyoming coal from the Wyodak mine, were tested. Fuel oil blends were made with products from each of the coals, with and without coker liquids, to produce four of the EDS fuels. The fuel oil derived from Illinois coal containing coker liquids was blended

from a solvent with a nominal initial boiling point of 400°F and is, therefore, referred to as a 400°F+ blend. The fifth EDS fuel consisted of an Illinois 350-1000°F fuel oil blend to which 40 wt. % Wyodak coker liquids had been added. Characteristics of these fuels are shown in Table 1.

The emission results from the combustion tests, along with the PNA analyses of the fuels, are shown in Table II. In agreement with previous work (2,3), particulates and smoke from EDS fuel oil combustion were generally low relative to petroleum fuel oils. NO_x emissions tended to be higher due to the higher fuel nitrogen content of EDS fuel oils.

PNA levels in both the EDS fuel oils and their combustion emissions are higher than comparable levels for petroleum fuels. PNA emissions from EDS fuel oils were up to three orders of magnitude greater than from LSFO combustion. One interesting trend in the data, shown in Table II, is that blends containing coker liquids have less fuel PNA, but higher PNA emissions than fuels produced from the same coals, but without coker liquids. The lower PNA content of EDS fuel oils containing coker liquids appears to be due to the fact that only 3 to 6 ring PNA compounds are measured by the available analytical techniques. Blends containing coker liquids with 1000°F+ material contain PNA's greater than six rings, which dilutes the fraction of PNA found in the 3- to 6-ring range. The higher PNA emissions from the coker liquid blends appear due to the mechanism of PNA emissions discussed below.

This initial data indicated that PNA emissions may have resulted from pyrolysis of higher molecular weight PNA to smaller ring structures, with subsequent quenching of the pyrolysis products before oxidation could occur. The importance of pyrolysis is supported by two sets of data. The first is the higher PNA emissions with the coker liquid blends compared to the blends without coker liquids, even though coker liquid blends contain less PNA in the three to six ring range. Pyrolysis of the larger PNA to smaller ones would explain this data, since fuel oils containing coker liquids contain higher quantities of heavier PNA than blends without coker liquids. Correlations of PNA in the emissions to fuel PNA show that the PNA emissions of any one compound do not correlate well with the same compound in the fuel. However, the emission data of specific PNA compounds do show statistically significant correlations with compounds that during breakdown might be expected to yield the specific PNA. For example, phenanthrene in the emissions does not correlate with the fuel phenanthrene, but does show a very significant correlation, R^2 = 0.99, with chrysene and benzo(a) pyrene in the fuel. Similar correlations are obtained for other specific PNA. While neither of these arguments provide conclusive proof concerning the mechanism of PNA emissions, they appear to indicate that pyrolysis is an important mechanism in the emission of PNA's from fuel oil combustion.

TABLE I

LABORATORY COMBUSTION TEST FUELS

Fuel	RSFO	LSFO	Illinois (Monterey No. 6) 350/1000°F	Illinois (Monterey No. 6) 400°F+	Illinois 350/1000°F With Wyodak Coker Liquids	Wyoming (Wyodak) 350/1000°F	Wyoming (Wyodak) 350°F+
API Gravity	15.5	20.2	9.3	0.1	-0.4	5.7	-5.1
Sp. Gravity	0.9626	0.9328	1.0050	1.0752	1.079	1.0313	1.1195
H/C Mol Ratio	1.58	1.68	1.23	1.13	1.08	1.10	0.99
N, wt. %	0.44	0.24	0.43	0.81	0.83	0.48	0.86
S, wt. %	2.39	0.12	0.38	0.87	0.41	0.10	0.18
Ash, wt. %	0.09	<0.01	0.01	0.03	0.03	<0.01	0.07
Viscosity, cst @ 210°F	41	13	1.9	10	7.2	2.3	26
Composition							
IBP-650°F			69	50	46	36	27
650-1000°F			31	37	37	64	49
1000°F+			0	13	17	0	22
Coker Liquids			No	Yes	Yes	No	Yes

TABLE II

INITIAL LABORATORY TEST DATA

	Fuel PNA μg/g	Emissions, PNA, μg/m³ GC/UV	Emissions, PNA, μg/m³ GC/FID	Bacharach Smoke Number	Particulate, Wt. % of Fuel	Fuel Nitrogen Wt. %	NOx Emissions PPM @ 10% Excess Air
RSFO	270	10.3	--	6.5	0.16	0.44	333
LSFO	1140	1.3	--	2	0.04	0.24	255
Illinois 350/1000°F	25000	15.2	44.2	2	--	0.43	--
Illinois 400°F+	18000	17.0*	--	<1	--	0.81	585
Wyodak 350/1000°F	67900	154	--	<1	0.01	0.48	402
Wyodak 350°F+	33400	1120	--	1	0.03	0.86	423
Illinois 350/1000°F Plus Wyodak Coker Liquids	14700	13.1	99.5	2	--	0.83	--

*Does not include 3-ring data

Phase 2 - Commercial Tests

The objective of this phase was to determine whether the de-
creased surface-to-volume ratio in an industrial unit would re-
duce the partial pyrolysis of the fuel and result in lower PNA
emissions than observed from the smaller laboratory boiler.   A
test of PNA emissions was, therefore, conducted at the Exxon
U.S.A. terminal in Charleston, South Carolina. The boiler avail-
able at this site was a Cleaver Brooks Model DL-68 water tube
unit rated at a maximum capacity of 50,000 lb/hr. of steam at 185
psig. This is roughly equivalent to 1425 hp, or a scaleup of ap-
proximately 30 from the laboratory boilers. The conventional
fuel used in this unit was RSFO with a maximum feed rate of 24.6
ℓ/min. or 22.7 kg/min. The boiler was installed in August, 1978,
and is used to raise steam for the terminal operations with heavy
fuel oil products.

A series of four fuels were burned in the Charleston boiler
including the RSFO that was being used as the boiler fuel, and
three fuels from the ECLP pilot plant. These EDS fuels were de-
rived from the operation on Monterey No. 6 mine coal and included
the solvent, a blend of 22 wt. % VGO/78 wt. % solvent, and a
blend of 35 wt. % VGO/65 wt. % solvent. The three EDS fuels were
chosen to span a range of PNA concentrations.

The characteristics of the test fuels are shown in Table III.
Comparing the 35 wt. % VGO/65 wt. % solvent blend to the Illinois
350-1000°F fuel oil derived from the one ton per day pilot plant
(Table I) indicates these fuels were similar. The PNA level in
the ECLP fuel oil does appear to be lower than that of the blend
tested in the laboratory boiler. The concentration of PNA in the
EDS fuel oils is still, however, 15 to 30 times greater than the
RSFO.

The only apparent anomaly in the EDS test fuels is their re-
lative PNA content, with the solvent containing more total PNA
than the two blends with the vacuum gas oil. Based on the nomi-
nal boiling ranges of these components, it would be expected that
the majority of the PNA would be in the vacuum gas oil. However,
a significant quantity of three ring PNA is present in the sol-
vent used in these tests, as indicated in Table IV. This may be
due to a higher end-point solvent being produced in the ECLP
pilot plant. The four plus ring PNA do show the expected trend
and increase with the concentration of VGO in the blend, indicat-
ing that the heavier PNA is contributed mainly by the VGO.

The testing used similar procedures to those described for
the laboratory test program. The fuels were blended in tank
trucks at the ECLP pilot plant at Baytown, Texas and driven to
Charleston, South Carolina. The fuels were loaded hot and re-
mained at an elevated temperature in insulated tank trucks. Fuel
temperature for the combustion of the EDS fuels was approximately
43°C. The preheating system was bypassed with the EDS fuels to
prevent sediment formation due to incompatibility in the fuel

TABLE III

COMMERCIAL TEST FUELS

	RSFO	Solvent	22% VGO/ 78% Solvent	35% VGO/ 65% Solvent
API Gravity	13.7	17.1	12.3	6.5
H/C Mole Ratio	1.55	1.38	1.33	1.34
N, wt. %	0.49	0.14	0.29	0.60
S, wt. %	2.11	0.07	0.22	0.45
Ash, wt. %	0.09	<0.01	<0.01	<0.01
Viscosity, cSt @ 100°C	41.5	1.28	1.98	4.19
PNA by GC/UV, µg/g				
3 ring	215	9020	4100	4200
4+ ring	185	2180	2940	4830
Total	400	11200	7040	9030

TABLE IV

EMISSIONS FROM COMMERCIAL TESTS

Fuel	Emissions PNA $\mu g/m^3$	Bacharach Smoke Number	Particulate wt. %	NO_x, ppm
RSFO	0.40	4-5	0.33	235
Solvent	0.30	4-6	0.02	140
22% VGO/ 78% Solvent	0.40	3-4	0.02	205
35% VGO/ 65% Solvent	0.30	2-3	0.01	282

system. Viscosities of the EDS fuels varied from 3.8 cSt for the solvent to 38.5 cSt for the 35 percent VGO/65 percent solvent blend. The RSFO was preheated to 104°C to give a 38 cSt viscosity for atomization.

With the exception of fuel viscosity, the test conditions for the fuels were similar. Each fuel was combusted at 3 percent excess O_2 at a feed rate of 15.4 kg/min. for six hours. An atomizing air pressure of 110 kPa was used for all fuels. The stack gas temperature was constant for all the tests at approximately 196°C. Duplicate tests were run on the EDS fuels with only a single test of the RSFO.

Results of these tests are shown in Table IV. The average emissions values are shown for the coal-derived fuels. As previous testing has shown, the EDS fuel oils produced little particulate relative to the petroleum fuel, while the smoke values for the coal-derived materials were equal to or less than that of the RSFO. As with the laboratory testing, the NO_x level was a function of the fuel nitrogen level, although NO_x emissions from the commercial unit were lower than from the laboratory boiler.

The major difference from the laboratory testing is the PNA emissions. First, there is no difference in PNA emissions among the four fuels tested. Secondly, the PNA emissions from the commercial unit are lower than those shown in Table II for the laboratory boiler. This appears true for both the petroleum and coal-derived fuels.

These results suggest that PNA emissions may not be a problem from large scale industrial and utility combustion of EDS fuel oils. However, additional large scale testing will be required for confirmation, particularly since the effects of staged combustion which may be required for NO_x control have also not been considered here. Tests are currently being planned by the Electric Power Research Institute to address these questions. It is expected that these tests will help to resolve the question of PNA emissions from coal-derived fuel oil combustion.

Conclusions

Emissions other than PNA showed similar trends in the laboratory and commercial boilers. Relative to petroleum fuel oils, EDS fuel oils produced low levels of particulate and smoke. NO_x emissions were related to fuel N levels, although NO_x emissions tended to be higher in the laboratory boiler than the commercial boiler.

In lab scale combustion tests, PNA emissions can be significantly higher from EDS fuel oils than petroleum fuels. PNA emissions appear to be caused by the pyrolysis of higher molecular weight PNA into smaller rings and a subsequent quenching of the reactions which would lead to PNA destruction.

Tests in a small industrial boiler, approximately 30 times larger than the laboratory boilers, showed that PNA emissions

from EDS fuel oil combustion were no different from petroleum
fuels. PNA emissions appeared to be lower in the commercial unit
than from similar fuels combusted in the laboratory boilers.
Both results suggest that PNA emissions from commercial combus-
tion of coal derived fuel oils may present no problem. This is
presumably due to the lower surface to volume ratio in the com-
mercial units relative to the laboratory combustors. However,
due to the relatively limited knowledge of the mechanism of PNA
emissions and the effects of combustion variables, additional
large scale testing will be required to demonstrate that PNA emis-
sions from commercial use of EDS fuel oil would not present an
emissions problem.

Acknowledgment

Literature Cited

1. Quinlan, C. W. and Siegmund, C. W., "Combustion Properties of
    Coal Liquids From the Exxon Donor Solvent Process", ACS Meet-
    ing Anaheim, California, March, 1978.
2. "Combustion and Emission Characteristics of Coal-Derived
    Liquid Fuels", EPRI Report AP-1878 RP 1412-5, Palo Alto,
    California, June, 1981.
3. "Combustion Demonstration of SRC II Fuel Oil in a Tangentially
    Fired Boiler", EPRI Report FP-1020, Palo Alto, California,
    May, 1979.

Soot Formation from Synthetic Fuel Droplets

JOHN C. KRAMLICH, GLENN C. ENGLAND, and ROY PAYNE

Energy and Environmental Research Corp., Irvine, CA 92714

Measurements from synthetic fuel spray flames and
laboratory droplet reactors indicated the extent to
which fuel properties and combustion conditions influ-
enced particulate yields. A series of seven fuels
were tested in a 21 kW spray combustor for total par-
ticulate by gravimetric sampling and soot by Bacharach
smoke number. Variations in total particulate were
dominated by the tendency of the fuel to form ceno-
spheres while smoke number correlated with the C:H
ratio of the fuel. The laboratory droplet studies
were performed in a gas flame supported reaction
environment. These results confirmed the correlation
between soot yield and C:H ratio. In addition, two
distinct forms of disruptive droplet combustion were
observed.

The future use of synthetically produced fuel oils, such as
coal and shale derived liquids, poses certain environmental ques-
tions with regard to burning these fuels with a minimum of pollu-
tant emission. Of principal concern is the potential for exces-
sive emissions of NO_x and carbonaceous particulate matter, which
result from the high levels of fuel nitrogen and high carbon to
hydrogen ratios typically associated with synthetic fuels. Staged
combustion has been found to be an effective NO_x emission control
technique for fuels containing significant quantities of bound
nitrogen; however, the hot fuel rich first stage can exacerbate
the carbonaceous particulate formation and emission problem. Par-
ticulate emission is, therefore, not only a problem in its own
right, but can influence the ability to control emissions of NO_x.
In order to provide information which may be useful in the
specification of emission control techniques, it is important to
understand those parameters which influence particulate formation
in practical fuel oil combustion systems. Carbonaceous emissions
from liquid fuel spray flames burning synthetic and petroleum

derived fuel oils arise from several sources and may be character-
ized as soot, coke or cenospheres.

Cenospheres and oil coke are formed as a result of liquid
phase cracking reactions, and, with the exception of ash, account
for the major portion of the weight of particulate matter emitted
when burning heavy fuel oils. Fuel composition and atomization
quality appear to be the dominant parameters controlling ceno-
sphere formation.

Emissions of soot on the other hand represent a smaller
fraction of the overall emission, but are probably of greater con-
cern from the standpoint of visibility and health effects. It has
been suggested that soot emissions from fuel oil flames result
from processes occurring in the vicinity of individual droplets
(droplet soot) before macroscale mixing of vaporized material, and
from reactions in the bulk gas stream (bulk soot) remote from
individual droplets. Droplet soot appears to dominate under local
fuel lean conditions (1, 2), while bulk soot formation occurs in
fuel rich zones. Factors which are known to affect soot formation
from liquid fuel flames include local stoichiometry, droplet size,
gas-droplet relative velocity and fuel properties (primarily C:H
ratio).

In this paper, results are presented from a research program
established to investigate soot formation from synthetic fuel
droplets. Specific goals of the research have included the deter-
mination of the propensity of various liquid fuels to form partic-
ulate matter and to link this with fuel properties, and the
obtaining of a phenomenological understanding of carbonaceous par-
ticulate formation and droplet combustion processes involving syn-
thetic fuel droplets. The approach adopted in this program has
involved two separate elements: a fuels screening task in which
gross effects of fuel type, staged combustion and fuel atomization
have been investigated in a small tunnel furnace; and a droplet
studies task where the fate of individual droplets has been traced
at a more fundamental level.

Test Fuels

In the studies carried out to date, eight fuels have been
tested which include six synfuels and two petroleum derived fuels.
The synfuels tested included SRC-II middle and heavy distillate
fuels, a blend of these fuels, and one SRC fuel blended with the
process donor solvent. Composition data for the various fuels are
presented in Table I, where it can be seen that the coal derived
liquids have a higher C:H ratio than either the diesel or residual
petroleum oils, indicative of a higher aromatic hydrocarbon con-
tent. The shale-derived DFM on the other hand is a highly proces-
sed fuel and has a C:H ratio similar to the petroleum diesel oil.
Complete analyses of all the actual fuels tested were unfortunate-
ly not available at the time of writing, and, where necessary,
typical analyses have been taken from previous studies.

Table I.   Fuel Analyses

Fuel	Alaskan Diesel	Indo/Malaysian No. 6	Shale Derived DFM	SRC-II Blend	SRC-II 5.75/1M:H	SRC-II Middle Distillate	SRC-II Heavy Distillate	Synthoil
Symbol	○	□	△	◁	◇	⬠	◖	⬡
C/H	7.21	7.25	6.61	9.70	9.83	9.57	11.65	11.60
Ultimate Analysis								
Carbon (wt %)	86.99	86.53	86.18	89.91	85.91	84.59	88.98	86.30
Hydrogen	12.07	11.93	13.00	9.27	8.74	8.84	7.64	7.44
Nitrogen	0.002	0.24	0.24	0.45	0.96	0.85	1.03	1.36
Sulfur	0.31	0.22	0.51	0.065	0.30	0.20	0.039	0.80
Ash	<0.001	0.036	0.003	0.004	0.04	0.002	0.058	1.56
Oxygen	0.62	1.04	1.07	0.30	4.08	5.43	1.9	2.54
Conradson Carbon Residue (%)	--	3.98	4.1	6.18	0.51	--	--	23.9
Aphaltene %	--	0.74	0.036	4.10	1.73	--	--	16.55
Flash Point (°F)	--	210	182	70	--	147	256	210
Pour Point (°F)	--	61	40	6-72	-55	--	--	80
API Gravity @ 60°F	33.1	21.8	33.1	10	--	13.4	1.3	1.14
Viscosity @ 140°F	33.1	276	38.3	44.5	34.5	36.4	67.2	10,880
SSW @ 210°F	29.9	83	32.4	34.7	30.3	31.8	41.3	575
Heat of Combustion								
Gross Btu/lb	19,270	19,070	19,430	17,980	17,000	17,000	17,120	16,480
Net Btu/lb	--	17,980	18,240	17,130	--	16,190	16,420	15,800

Fuel Screening Studies

Experimental. A series of fuel screening experiments have
been carried out in a bench scale tunnel furnace to determine
gross effects of fuel composition on the emission of particulates
and NO_x under both normal and staged combustion conditions. The
tunnel furnace has been described in detail elsewhere (3) and is
a vertically downfired arrangement, 21 cm in diameter, 2 meters
long, and operates at a nominal 21 kW thermal input. Combustion
air injectors and cooling elements can be located at various
positions within the furnace to provide for optimum two stage com-
bustion and heat extraction. Fuel injection is achieved by means
of a commercial air-assist atomizer, specially adapted to allow
variation of both droplet size distribution and fuel spray momen-
tum (4). Exhaust gas composition is monitored by continuous anal-
yzers for O_2, CO, CO_2 and NO/NO_x; particulate concentration is
determined gravimetrically using an isokinetic sample probe, col-
lecting the particulate on glass fiber filter paper. Soot emis-
sions were measured using a manual Bacharach smoke spot tester.
Further details on sampling methods may be found in the references
(4,5).

Results. Selected experimental results from the fuel screen-
ing studies are presented in Figures 1 and 2 which show the
effects of staged combustion on the emissions of NO_x and particu-
lates. Staged combustion is of interest primarily as a means of
controlling NO_x emissions from the high nitrogen containing syn-
fuels. Particulate emissions generally increase under staged con-
ditions, and the concern is that the higher aromaticity of syn-
fuels might result in excessive soot formation and thus further
aggravate an existing limitation. Staged combustion is achieved
in the tunnel furnace by dividing the airstream to form an initial
fuel-rich combustion zone with sufficient residence time and tem-
perature for decay of fixed nitrogen species to N_2, followed by
a secondary air injection and burnout zone to complete combustion.

Figure 1 shows NO_x and particulate emissions as affected by
the primary zone air/fuel stoichiometric ratio (SR_1) for the eight
fuels tested. In these studies overall excess oxygen was held
constant at 3 percent and the combustion air preheated to 575 K.
Fuel viscosity was also maintained constant at 8.1 $\pm$ 2 cp by
adjusting fuel temperature as necessary. In the case of synthoil,
however, the viscosity could not be reduced below 110 cp without
vapor formation in the fuel heater. The results of Figure 1 show
that staged combustion is effective in controlling NO_x emissions
for all the fuel tests. NO_x emissions decreased rapidly as SR_1
is decreased and reach a minimum at an SR_1 of approximately 0.75.
Minimum NO_x emissions ranged from 50 ppm to 160 ppm for all the
fuels except synthoil, which produced significantly higher minimum
levels. NO_x emissions correlate well with fuel nitrogen under
staged conditions, rising by 84 ppm per 0.1 percent fuel nitrogen
for this particular experimental arrangement. NO_x emissions under
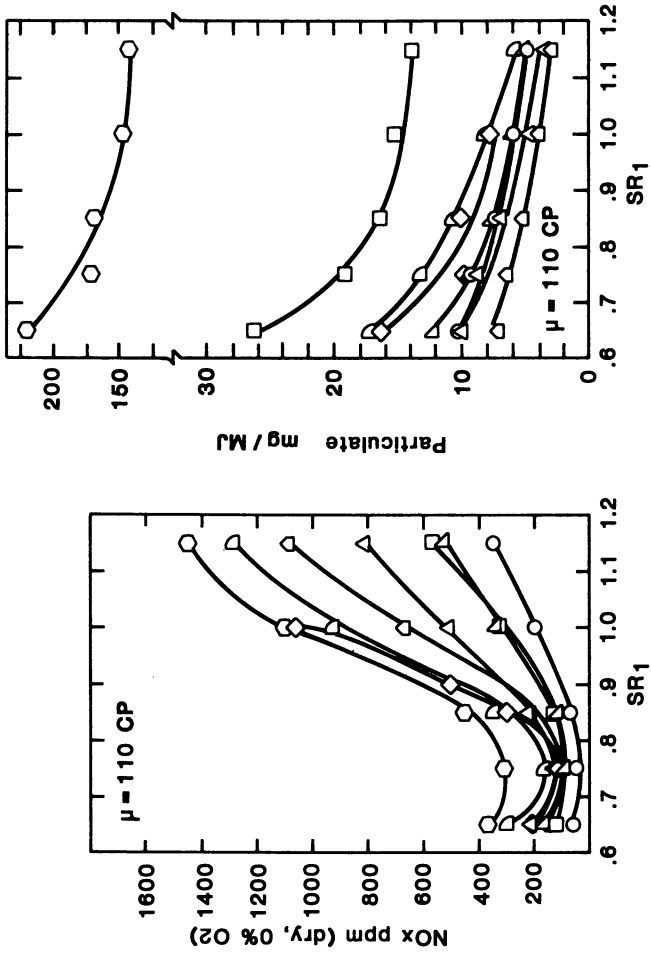
Figure 1. NO$_x$ and particulate emissions under staged combustion conditions.

staged conditions were much less sensitive to fuel nitrogen con-
tent, and above 0.4 percent were almost independent of nitrogen
content. Under these conditions, with heat extraction resulting
in wall heat flux of approximately 38.8 kJ/M^2-sec (12,300 Btu/hr
/ft^2) in the flame zone, most of the synthetic fuels produced
particulate emissions which were comparable to those produced by
the conventional petroleum fuels. The synthoil, however, produced
much higher emissions than the other fuels, which likely results
from both the high ash content of the fuel (1.56 percent) and poor
atomization due to the high viscosity. Particulate emissions were
also not sensitive to overall excess oxygen levels above 2 percent.
Figure 1 also shows that particulate emissions from all fuels
increase steadily as primary zone stoichiometry is reduced. The
increase in emissions, compared to normal single staged combustion,
is not substantially different for synfuels and petroleum derived
fuels. This indicates that all fuels respond in a similar fashion
to the application of staged combustion.

   While detailed SEM analyses of the sampled particulate have
not been carried out, microscopic examination of the samples
reveals some differences between the particulate matter from dif-
ferent fuels. Particulate produced by combustion of the petroleum
residual No. 6 oil is comprised largely of cenospheres with
agglomerated clusters of particles of a smaller size. The large
cenospheres appear to be related to the atomization and vapori-
zation characteristics of the No. 6 oil, while the smaller par-
ticles are characteristic of soot (5,6). The particulate matter
from the diesel oil, the shale DFM and the SRC-II fuels, on the
other hand, consists primarily of clusters of small soot particles.
For the SRC-II heavy distillate fuel, some cenospheres were also
observed, though much fewer than for the No. 6 oil. These trends
can be seen to some extent in the comparison of Bacharach smoke
number measurements and total particulate emissions in Figure 2.
Smoke number may be considered to be related (albeit qualitatively)
to the emission of finer particulate matter. For the experimental
conditions investigated, smoke numbers were generally low for all
fuels except the SRC-II heavy distillate and synthoil. The
results show, however, that smoke number increases more strongly
for the coal derived liquid fuels as the total particulate emis-
sion increases as a result of staged combustion. This increase
is most strongly marked for the SRC-II heavy distillate fuel.

   The screening studies tend to show that there are no substan-
tial differences between synfuels and petroleum derived liquid
fuels in terms of NO$_x$ and total particulate emissions. Both types
of fuel appear to respond in a similar way to the application of
staged combustion and to changes in atomization parameters (not
discussed in the present paper).

Droplet Studies

Experimental. To further understand the process of droplet
combustion and particulate formation, a more fundamental study of
the effects of droplet size, local stoichiometry and gas-droplet
relative velocity has been carried out. This work made use of a
controlled flow variable slip reactor in which the combustion of
droplet streams can be examined under well defined conditions.
The reactor (7) consists of 5 by 28 cm flat flame burner downfired
into a chimney of similar dimensions, fitted with Vycor windows
for optical access. Access ports for droplet injection and sample
probing are provided. As illustrated in Figure 3, fuel droplets
are normally injected ballistically across the face of the burner.
The droplets could be injected as a tightly collimated stream
which behaved as an almost cylindrical source of fuel vapors for
an attached diffusion flame. This resulted in a well defined,
laminar vapor sheet which is separated from the droplets by the
gas flow; the general appearance is shown in the figure. Droplets
were generated by the vibrating orifice technique (8) in an
arrangement by which the droplets could be dispersed sufficiently
to control droplet-droplet spacing. Droplet diameter and spacing
were verified by high resolution spark shadowgraphs. Operating
conditions were selected to minimize the appearance of satellite
droplets.
Soot samples were obtained by use of a nitrogen-quench,
porous-walled probe and Nucleopore filters (7). Gas phase hydro-
carbons were collected by the porous probe as batch samples and
analyzed by standard FID gas chromatography. Thermal measurements
included gas temperature by radiation-corrected bare wire thermo-
couple, and soot temperature by Kurlbaum reversal (9,10) and two
color pyrometry (11).
Results. The fuels studied in this program have been
described previously, and the ranges of the combustion variables
investigated were as follows: droplet diameter 66-190 μm, slip
velocity 300-1200 cm/sec; gas temperature < 1500 K; and stoichiom-
etry 0.5 < Φ < 1.5. Initial drop size was determined by the ori-
fice employed in the droplet generator and was verified through
the use of LDA/visibility measurements and photography. Slip
velocity was calculated as the vector sum of the LDA measured
droplet velocity and the hot gas velocity.
Two extremes of droplet dispersion mode were investigated:
non-dispersed where the droplet stream remained tightly collimated
as it traversed the reactor; and dispersed, where the droplets
were spread across the reactor but there was no side wall impinge-
ment. This approach allowed some control of droplet-droplet
spacing and interaction from a highly collimated stream to a con-
dition where individual droplet behavior was clearly evident.
For all fuels tested, the overall appearance of the flame
produced by the collimated droplet stream was of a narrow, lumi-
nous sheet of soot forming below the droplet stream as shown
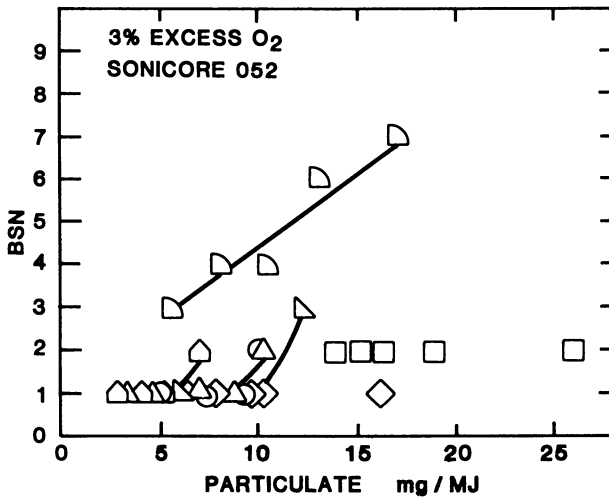
Figure 2.   Bacharach smoke number and total particulate emissions.
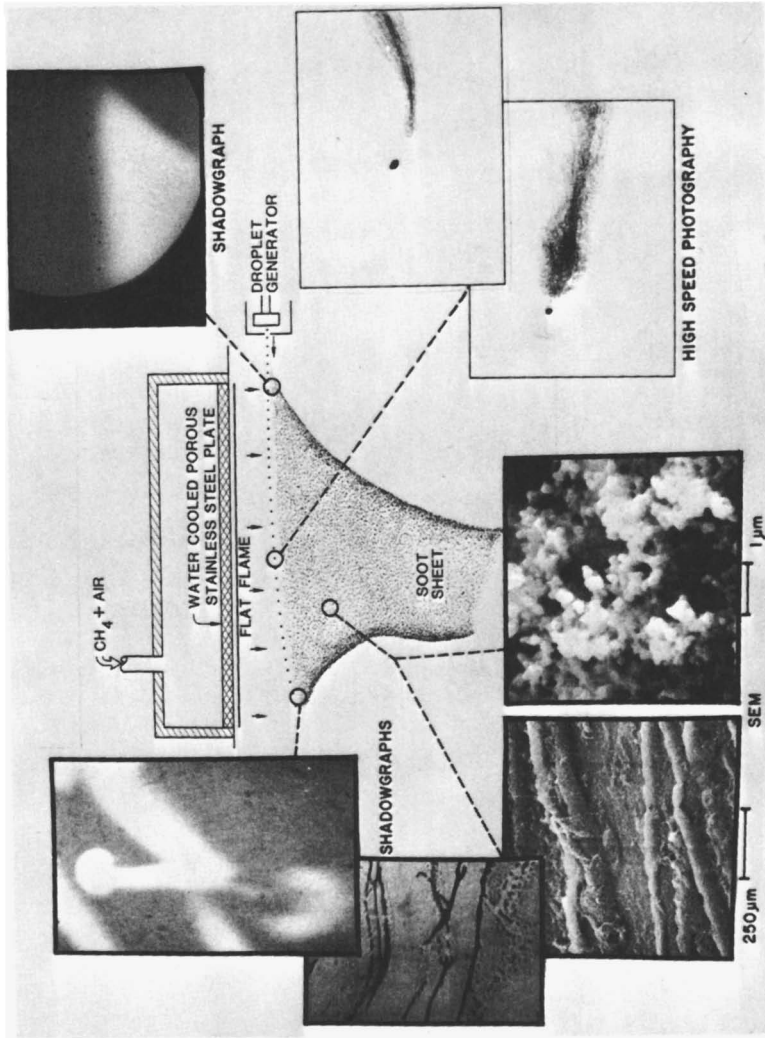
Figure 3. Composite of droplet physical behavior.

schematically in Figure 3. The emission intensity was greatest
directly under the droplets and was increased by excess oxygen in
the free stream. Under fuel-lean conditions, the sheet had sharp,
well-defined edges and tended to collapse into a ribbon near the
bottom of the burner. Under fuel-rich conditions, the boundaries
were diffuse and no collapsing was noticed.

    Figure 3 is a composite of photographs and scanning electron
micrographs of impacted samples at various positions within the
soot sheet for SRC-II middle distillate fuel oil droplets. Soot
first becomes visible in the wake behind droplets as diffuse
trails composed of finely divided material. This soot band
rapidly collapses into long, small-diameter filaments. The visi-
ble sheet is primarily made up of these horizontal filaments that
can grow to lengths greater than one millimeter. High magnifica-
tion photographs of the filaments reveal that they are composed
of very fine (500 A) spherical particles. Such filament formation
is strikingly similar to that observed previously in droplet wakes
(12) and both in laminar (13,14) and turbulent (15) pulverized
coal flames. The far edge of the soot sheet is visually charac-
terized as bright flashes of radiation shown in the streak photo-
graph (top left corner of Figure 3) which terminates the droplet
trajectories.

    The termination of droplet trajectories by a "micro-explos-
ion" of this nature was observed for all of the synthetic fuels
and fuel blends tested, but did not occur for the petroleum
derived No. 6 oil. With this latter fuel, droplets were seen to
burn to extinction and to result in the formation of a carbonace-
ous residue, usually in the form of cenospheres. The termination
of individual droplets was observed, therefore, to be strongly
dependent upon fuel type and could be characterized by three
distinct types of behavior: 1) large (1 mm) micro-explosions with
a distinctly directional behavior (SRC process donor solvent
blend), 2) smaller micro-explosions (SRC-II middle, heavy, middle/
heavy blend, DFM), and 3) carbonaceous residue formation (Indones-
ian-Malaysian No. 6) without micro-explosions. High speed photo-
graphs show the micro-explosions to occur in a time span much
faster than the camera framing rate (1/5000 sec).

    In an attempt to modify the observed droplet behavior, a
brief qualitative investigation was carried out with blends of
SRC-II heavy distillate and pure heptane. The objective was to
enhance droplet disruptive combustion as a means of reducing
effective droplet size and hence soot formation. With these fuels
visible droplet fragmentation was found to occur throughout the
droplet stream. The fragmentation produced new droplets on dif-
ferent trajectories; these in turn were terminated by small dis-
ruptions, as described above. Three blends were used: 60/40,
80/20, and 90/10. Secondary atomization was observed for all
three, although the violence of the activity was noticeably
reduced as the heptane content of the blend became smaller. This
secondary atomization was a completely different process than the

terminal micro-explosion. Secondary atomization has been previously noted in the literature (16) and involves internal droplet boiling. In contrast, terminal micro-explosions occur after a significant amount of material has been removed, are extremely rapid, have a distinct directional character, and leave no observable fragments. A possible mechanism involves the formation of a solid coke surface on the droplet followed by rupture.

In addition to visual observations of a qualitative nature, a number of detailed sampling traverses were made to determine particulate and gaseous species concentrations within the soot sheet. The nature of the sampling system employed results in the sampled solid material being composed largely of soot since cenospheres and heavy solid material follow the droplet trajectories and are not captured by the probe.

The soot concentration, hydrocarbon species and soot temperature in the immediate vicinity of the droplet displayed closely coupled behavior. Hydrocarbon species, listed in approximate order of concentration were C_2H_2, CH_4, C_2H_4, C_2H_6 and C_3's. Resolution of the propane and propylene peaks was not possible under current GC procedure, and these concentrations are reported merely as C_3 compounds. The hydrocarbons were found to decay in the same time frame as the growth of the soot concentration. The zone of chemical activity, defined as where the vaporized hydrocarbon products react to form soot, is approximately 2 cm, which corresponds to 13 msec, after which the soot concentration decays due apparently to oxidation.

The soot temperature was found to exceed the gas temperature as measured by thermocouples in the absence of droplet injection but decayed at a similar rate. This is attributed to bulk heating effects associated with the localized burning of vaporized material. A detailed diffusion flame calculation for a cylindrical source of reactants and relative velocity on the same order as these experimental data, indicate that this bulk heating effect is reasonable.

Both diffusional flame calculations and detailed spatial mapping indicate that the nondispersed injection mode produces a vapor cloud that is characterized by diffusionally controlled combustion and bulk heating while subjecting the droplets to near isothermal conditions. The soot produced in this cloud is strongly influenced by bulk diffusion limitations and as such represents a bulk soot formation extreme. It was found that fuel changes had little effect on the overall soot yield due to this diffusion control. Lower gas temperatures and richer conditions were found to favor soot formation under bulk sooting conditions, probably due to a decrease in the oxidation rate of the soot.

In the dispersed mode, the droplet stream was aerodynamically dispersed to permit the sooting behavior of individual droplets to be investigated. The visual appearance of the flame produced was strikingly different from the nondispersed flame. Instead of a sheet of luminous radiation down the center of the burner, the

flame now was only streaks of light apparently associated with individual droplets. These streaks were broader than expected for droplets alone because of the associated soot formation. Under lean conditions, the droplet/soot streaks became sharp, well-defined thinner streaks while under rich conditions, the streaks were diffuse bands. Again, as in the case for nondispersed injection with the SRC-II middle distillate, the streaks were observed to terminate with a bright flash of radiation. Because the phenomenon was not masked by the highly radiant soot sheet, the micro-explosions were clearly visible and were observed to result in a luminous cloud several times bigger than the droplet streak. Also, it could be seen that every streak ended with such a micro-explosion.

Soot concentrations were much smaller for the dispersed mode than for the non-dispersed mode under similar conditions. For example, the soot concentration was found to be approximately 700 mg/m^3 for 190 μm SRC-II middle distillate droplets under fuel rich (ϕ = 1.33), dispersed conditions. Under similar non-dispersed conditions, the soot concentration was of the order 10^4 mg/m^3.

The yield of soot for the dispersed injection mode was found to be affected by gas stoichiometry in the opposite direction to the effect on non-dispersed injection. As seen in Figure 4 for the SRC-II heavy distillate, the soot concentration was increased by leaner overall gas conditions. Such measurements are consistent with observations of attached flames and higher temperatures within the droplet flame under leaner conditions ([1,2]) both of which can promote droplet soot. These are also consistent with physical observation made in this study.

Soot concentrations were found also to be sensitive to fuel type for dispersed conditions despite the insensitivity observed under the bulk diffusion controlled nondispersed injection mode. For 190 μm fuel oil droplets under rich conditions (ϕ = 1.33), the soot yield could be directly related to the carbon to hydrogen ratio of the fuel (Figure 5). The soot concentration was found to increase by an order of magnitude with a factor of approximately two in the C:H ratio. It is difficult to relate these results directly to the particulate measurements made in the screening studies since the sampling system used in these latter experiments cannot distinguish between soot and other carbonaceous particulate. There is, however, good qualitative agreement in that sooting tendencies (smoke number) are higher in the tunnel furnace for the coal derived liquids (SRC-II heavy distillate in particular) although in terms of total emission, this is masked by the high cenosphere formation with the No. 6 oil.
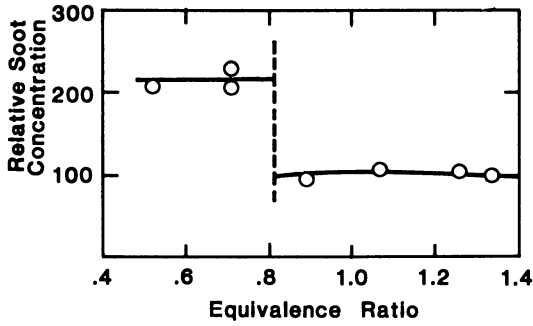
Figure 4. Effect of stoichiometry on soot concentration for dispersed 190 µm SRC-II heavy distillate droplets.
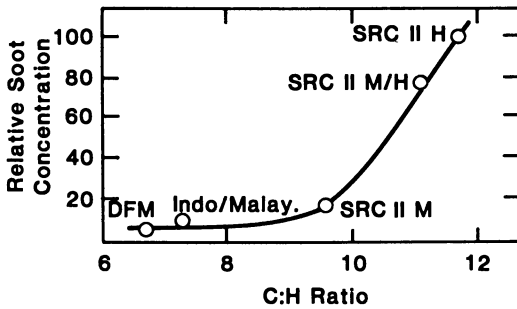
Figure 5. Effect of C:H ratio on fuel type on soot concentration for 190 µm dispersed droplets (ϕ = 1.33).

Conclusions

In spite of the large differences seen in the behavior of different fuels at the droplet level, the fuel screening studies, carried out in a more realistic spray flame environment, suggest that there are no substantial differences between synfuels and conventional petroleum derived liquid fuels. Both studies indicate, however, that soot production is higher for the coal derived liquids, particularly under staged combustion conditions. In an actual combustor, longer residence time at high temperature and excess oxygen will be available compared to the droplet studies reactor, such that some of the trends observed will be masked by soot oxidation in later stages of combustion.

Acknowledgments

Literature Cited

1. Sjogren, A. 14th Symp. (Int.) on Comb. 1973, p. 919.
2. Nakanishi, K.; Kadota, T.; and Hiroyasu, H. Comb. and Flame 1981, 40, 247.
3. England, G. C.; Heap, M. P.; Pershing, D. W.; Nihart, R. K.; and Martin, G. B. 18th Symp. (Int.) on Comb. 1981, p. 163.
4. England, G. C.; Kramlich, J.; Kwan, Y.; and Payne, R. "Third Quarterly Technical Progress Report," DOE/PC/30298-T3, NTIS DE81028391, July 1981.
5. England, G. C.; Kramlich, J.; Kwan, Y.; and Payne, R. "Fifth Quarterly Technical Progress Report," DOE/PC/30298-T5 (available NTIS).
6. Belli, R.; Paoli, L.; and Tarli, R. Paper presented at the 2nd Joint Meeting of the Chemistry and Pulverized Fuel Panel, IFRF Doc. No. F25/ha/6, September 1975.
7. Kramlich, J. C.; Samuelsen, G. S.; and Seeker, W. R. WSS/CI-81-52, presented at the Fall Meeting of the Western States Section of the Combustion Institute, Tempe, Arizona, 1981.
8. Berglund, R. N.; and Liu, B. Y. H. Env. Sci. and Tech. 1973, 147.
9. Gaydon, A. G.; and Wolfhard, H. G. "Flames." 3rd Edition, Chapman and Hall, 1970.
10. Sangiovanni, J. J.; and Dodge, L. G. 17th Symp. (Int.) on Comb. 1979, p. 455.

11. Seeker, W. R.; Samuelsen, G. S.; Kramlich, J. C.; and Heap, M. P. Volume III, Section 4, EPA Final Report 68-02-2631, 1981.
12. Natarajan, R.; and Brzustowski, T. A. Comb. Sci. and Tech. 1970, 2, 259.
13. McLean, W. J.; Hardesty, D. R.; and Pohl, J. H. 18th Symp. (Int.) on Comb. 1981, p. 1239.
14. Seeker, W. R.; Samuelsen, G. S.; Heap, M. P.; and Trolinger, J. D. 18th Symp. (Int.) on Comb. 1981, p. 1213.
15. Szpindler, G. D. CSIRO Investigation Report 381R, Sydney Laboratory, 1970.
16. Lasheras, J. C.; Fernandez-Pello, A. C.; and Dryer, F. L. 18th Symp. (Int.) on Comb. 1981, p. 293.

Effect of Liquefaction Processing Conditions on Combustion Characteristics of Solvent-Refined Coal

R. W. BORIO, G. J. GOETZ, T. C. LAO, A. K. MEHTA, and
N. Y. NSAKALA

Combustion Engineering, Inc., Kreisinger Development Laboratory,
Windsor, CT 06095

W. C. ROVESTI

Electric Power Research Institute, Palo Alto, CA 94303

SRC-I processing has been performed using three
variations in the manner in which mineral matter and
unconverted coal are separated from the hot coal liquid.
These processes are the Pressure Filtration Deashing
(PFD), Anti-Solvent Deashing (ASD), and Critical Solvent
Deashing (CSD). Since these processing conditions may
influence the combustion of SRC-I solids produced, an
experimental program was carried out at both the bench
and pilot plant scale to determine the influence of
processing (i.e., solids separation method) and com-
bustion conditions on carbon burnout of these three
SRC's. Included in this study was an examination of
NO_x emissions (particularly for the CSD and PFD SRC'S)
with the objective of attaining low NO_x emissions
without adversely affecting combustion efficiency.
Reactivity and NO_x emissions results from the SRC testing
were compared with those obtained from two coals that
were previously tested and used as reference coals.
One of these coals was a high reactivity Wyoming sub-
bituminous coal and the other was a low reactivity
Kentucky high volatile bituminous coal.

The Solvent Refined Coal-I (SRC-I) process (1) provides a way
in which coal, by way of direct hydrogenative liquefaction, can be
transformed into an environmentally clean fuel for the electric
utilities. Earlier tests (2, 3, 4, 5) with pulverized SRC-I solid
fuel (SRC), while considered successful, indicated the need for
concern in two areas: carbon in the fly ash and nitrogen oxides
(NO_x) emissions. Although good combustion efficiencies (generally
greater than 98%) were attained there was a substantial amount of
carbon in the particulates (generally greater than 60%). This will
pose a collection problem if an electrostatic precipitator (ESP)
is envisioned for particulate collection because of the very low
resistivity imparted by carbon. In addition, the high nitrogen
contents (1.8-1.9%) of SRC indicate that there is a potential for
high NO_x emissions.

SRC has been produced using three different schemes for sep-
arating the mineral matter and unconverted coal from the hot coal
liquid. These schemes are designated as Pressure Filtration De-
ashing (PFD, 2) Anti-Solvent Deashing (ASD, 6) and Critical Solvent
Deashing (CSD, 7). As these processing conditions may influence
the combustion of SRC solids produced, Combustion Engineering,
under a contract with EPRI, conducted an experimental program to
determine the influence of processing (i.e., solids separation
method) and combustion operating conditions on carbon burnout of
PFD, ASD, and CSD SRC. Included in this study was an examination
of NO_x emissions (particularly for the CSD and PFD SRC) with the
objective of attaining low NO_x emissions without adversely affecting
combustion efficiency. Reactivity and NO_x emissions results from
the SRC testing were compared with those obtained from two pre-
viously tested reference coals, a low reactivity Kentucky high
volatile bituminous coal (KHB) and a high reactivity Wyoming sub-
bituminous coal (WSB).
      The primary objective of this study was to determine the in-
fluence of SRC-I processing (i.e., solids separation) and combus-
tion operating conditions on carbon burnout under combustion
conditions simulating those achievable in boilers originally de-
signed for coal firing. The secondary objective was to examine
combustion operating conditions that resulted in low NO_X emissions
while simultaneously achieving high carbon burnout.
      The primary research tools used in this program were C-E's
Drop Tube Furnace System (DTFS), a bench scale entrained laminar
flow furnace and the Controlled Mixing History Furnace (CMHF), a
pilot scale entrained plug flow furnace. Both the DTFS and CMHF
by virtue of their ability to resolve combustion time into distance
along their respective furnace lengths were used to examine carbon
burnout phenomena associated with the SRC and reference coals. In
addition, the CMHF by virtue of its staged combustion capabilities
was used extensively to evaluate NO_X emissions and to establish
conditions conducive to low NO_X.

RESEARCH FACILITIES AND PROCEDURES

      A number of standard and special bench scale tests along with
the Drop Tube Furnace System (DTFS) and pilot scale Controlled
Mixing History Furnace (CMHF) were employed in this program.
Standard tests consisted of proximate, ultimate, higher heating
value, ash composition, ash fusibility temperatures, Hardgrove
grindability, and screen analyses. Special bench scale character-
ization tests consisted of micro-proximate analysis and micro-
ultimate analysis (C, H, N); micro-proximate and micro-ultimate
analyses were performed on particulate samples collected from
varying stages of combustion in the DTFS and CMHF. In addition,
selected samples of SRC and chars from partial combustion or pyro-
lysis of the SRC were submitted for Thermo-Gravimetric analyses.
      Thermo-Gravimetric Analyses were performed on ASTM volatile
matter char residues ground to -200 mesh. These residues (4-5 mg)
were heated in nitrogen and then burned isothermally (700°C) in air.

The Drop Tube Furnace System (DTFS) consists essentially of an electrically heated 2 inch I.D. x 18 inch long furnace where fuel (1 gm/min) and preheated secondary gas (air or inerts) are introduced. The history of combustion is monitored by solids/gas sampling at various points along the length of the furnace.

The pilot scale Controlled Mixing History Furnace (0.5 x 10^6 Btu/hr) is based on the principle of plug flow which resolves time into distance along the length of the furnace. By sampling at different ports along the length of the furnace, it is possible to examine the burnout and NO_x formation history of a fuel. The CMHF also has flexibility for controlling the primary and secondary air/fuel ratios and for delaying and/or staging secondary air introduction (at any of seven levels along the length of the furnace).

EXPERIMENTAL PROGRAM

The test program was set up in three phases: bench scale, DTFS, and CMHF. Bench scale and DTFS tests were performed on all three fuels, while the CMHF tests were performed only on the CSD and PFD SRC fuels. The low melting temperatures of the SRC resulted in pluggage of both DTFS and CMHF fuel injection systems. Special water cooled fuel injectors were fabricated to alleviate this problem.

Testing in the DTFS involved examining the effects of furnace wall temperature, particle size, and combustion medium on burnout. More extensive testing was conducted on the CSD SRC sample in both the DTFS and CMHF as recommended by EPRI. In the CMHF the effect of two stage combustion was examined. Specifically, first stage stoichiometry, first stage residence time, and overall excess air upon burnout and NO_x formation of the CSD SRC sample were examined. Based on the CSD SRC results, a limited test matrix was established for the PFD SRC sample to examine the effects of first stage stoichiometry and overall excess air on burnout and NO_x.

A plug flow char combustion model was used to predict the combustion efficiencies of SRC under simulated commercial boiler operating conditions. Inputs were based on the volatile yields and char characteristics measured in the CMHF.

RESULTS

Fuel Analyses

Analytical results (Table 1) show that SRC have very high volatile matter and nitrogen contents (52-60% and 1.8-1.9%, respectively, on a dry-ash-free basis) and very low moisture and ash contents (0.1-0.3%, as-received basis in each case). The Higher Heating Values for the SRC (15,920-16,115 Btu/lb, dry-ash-free basis) are much higher than those of reference coals (13,290 and 14,110 Btu/lb for the WSB and KHB coals, respectively).

Table I
ANALYSES OF SRC AND REFERENCE COALS

Analysis	Pressure Filtered Deashed SRC as-rec.	daf	Critical Solvent Deashed SRC as-rec.	daf	Anti Solvent Deashed SRC as-rec.	daf	Wyoming Subbituminous Coal as-rec.	daf	Kentucky High Vol. Bit. Coal as-rec.	daf
Proximate, Wt. Percent										
Moisture (Total)	0.1	-	0.3	-	0.1	-	3.1	-	1.2	-
Volatile Matter	51.6	51.8	59.6	59.8	60.2	60.4	33.0	40.2	33.6	37.3
Fixed Carbon	48.0	48.2	40.0	40.2	39.4	39.6	49.0	59.8	56.6	62.7
Ash	0.3	-	0.1	-	0.3	-	14.9	-	8.6	-
Total	100.0	100.0	100.0	100.0	100.0	100.0	100.0	100.0	100.0	100.0
Ultimate, Wt. Percent										
Moisture (Total)	0.1	-	0.3	-	0.1	-	3.1	-	1.2	-
Hydrogen	5.8	5.8	6.1	6.1	5.9	5.9	3.9	4.8	4.4	4.9
Carbon	88.0	88.4	87.3	87.7	88.1	88.5	59.4	72.4	72.5	80.4
Sulfur	1.0	1.0	1.0	1.0	0.7	0.7	0.3	0.4	0.7	0.8
Nitrogen	1.9	1.9	1.8	1.8	1.9	1.9	1.1	1.3	1.3	1.4
Oxygen (Diff.)	2.9	2.9	3.4	3.4	3.1	3.0	17.3	21.1	11.3	12.5
Ash	0.3	-	0.1	-	0.3	-	14.9	-	8.6	-
Total	100.0	100.0	100.0	100.0	100.0	100.0	100.0	100.0	100.0	100.0
Higher Heating Value, (HHV), Btu/lb	15860	15920	16050	16115	15880	15940	10900	13290	12730	14110
Flammability Index °F	1210		1270		1270		1040		1170	

Hardgrove Grindability Index	148	136	156	13.7	6.8
Ash Loading, lbs/mm Btu	0.2	0.1	0.2		
Ash Fusibility (in Red. Atm)					
I.T., °F	2210	2080	2060	2210	2700+
S.T., °F	2300	2150	2140	2330	2700+
H.T., °F	2380	2220	2210	2480	2700+
F.T., °F	2550	2530	2460	2620	2700+
ΔT (FT-IT), °F	340	450	400	410	-
Ash Composition, Wt. Percent					
SiO₂	28.4	25.6	23.7	62.9	57:5
Al₂O₃	9.5	9.7	14.7	17.4	31.4
Fe₂O₃	17.4	24.1	26.2	3.4	3.5
CaO	1.2	2.7	2.3	3.8	1.6
MgO	0.5	0.9	0.9	1.3	0.7
Na₂O	0.2	0.6	0.8	3.4	0.8
K₂O	0.3	0.8	1.0	0.6	2.0
TiO₂	37.3	27.7	19.3	1.0	1.7
P₂O₅	0.2	0.3	0.4	-	-
SO₂	0.1	0.8	0.6	6.0	0.8
Subtotal	95.1	93.2	89.9	99.8	100.0
ZnO	1.3	1.4	1.0		
ZrO₂	<0.1	<0.1	0.1		
MnO	0.77	0.27	0.50		
CuO	0.05	0.05	0.04		
NiO₂	0.11	0.06	0.13		
SnO₂	<0.1	0.50	0.1		
Total	97.33	95.48	91.37		

Table II depicts the major compositional differences between the CSD, PFD, and ASD SRC are in the soluble fractions. The CSD SRC has significantly less benzene insolubles (i.e., pre-asphaltenes) than do the other two SRC. This compositional difference may be responsible for the CSD SRC greater volatility as discussed later in this report. Both the CSD and ASD SRC have melting temperatures ca. 100°F lower than the PFD SRC, which could significantly affect the design of fuel handling and injection systems.

TABLE II

ADDITIONAL ANALYSES* OF SRC

Analysis		Pressure Filtered Deashed SRC	Cricital Solvent Deashed SRC	Anti-Solvent Deashed SRC
Solvent Extractions				
Oils	WT%	18.9	24.2	26.5
Asphaltenes	WT%	56.8	66.2	52.1
Benzene Insol.	WT%	24.3	11.6	21.4
Calc. Total	WT%	100.0	102.0	100.0
Vacuum Distillation				
-1000°F Fraction	WT%	2.7	5.8	11.0
Softening Point	$^\circ$F	356	248	257
Fusion Point	$^\circ$F	383	284	289

*Provided by EPRI

Physical Characteristics

Pasting occurred on the race, bowl, and balls of the Hardgrove machine during the grindability index determination on all three SRC.In each case an addition of as little as 1% moisture (by weight) eliminated the pasting problem. The effect of moisture addition is clearly shown in Figure 1. The HGI of the SRC are in the 136-156 range, indicating that these materials are more easily ground than coals (coals' HGI are typically less than 100).

Thermo-Gravimetric Char Reactivities

Thermo-gravimetric analysis results are presented in Figure 2. They indicate that: (1) the PFD SRC char is relatively more reactive than the CSD and ASD chars; (2) PFD char reactivity is between those of WSB and KHB coal chars; (3) CSD and ASD char reactivities are both comparable to that of the KHB coal char, but
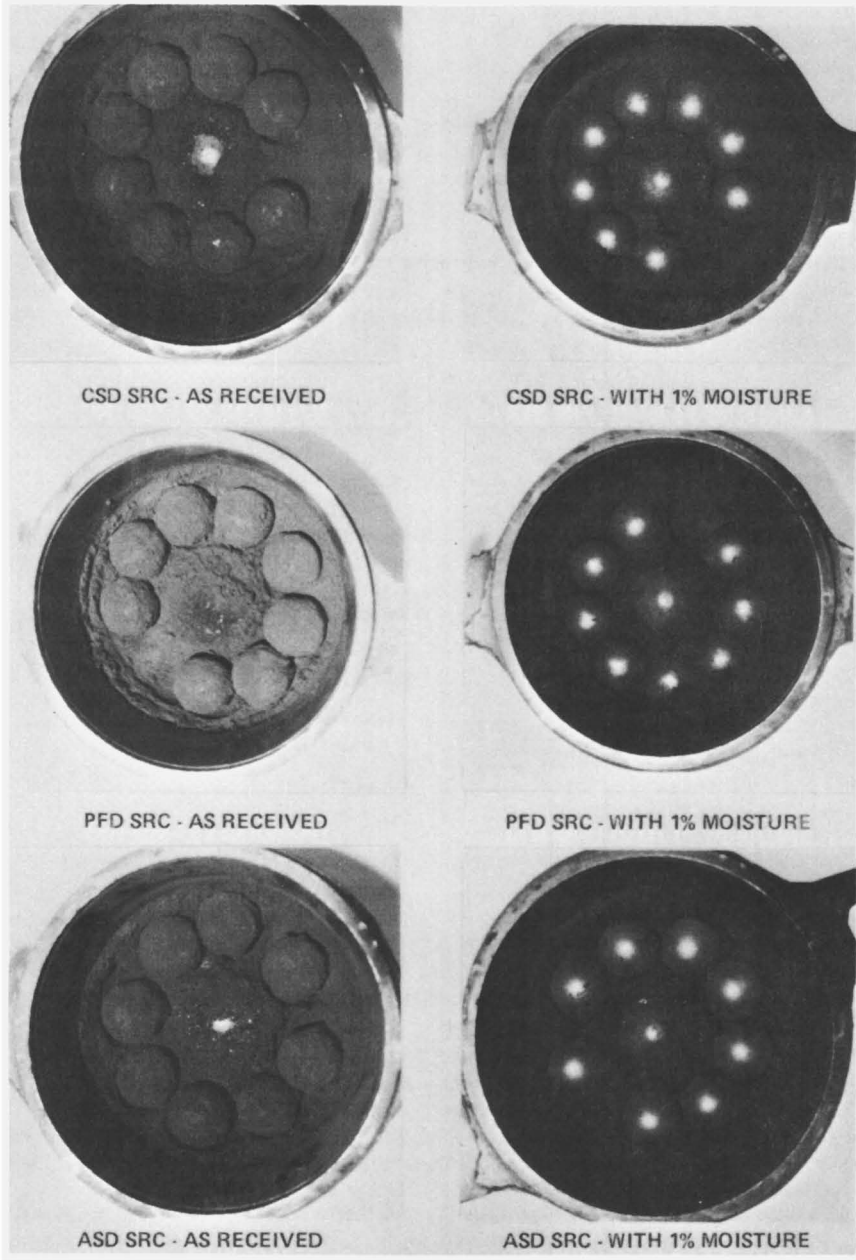
Figure 1. Photographs of SRC-1 after grinding in the Hardgrove machine.
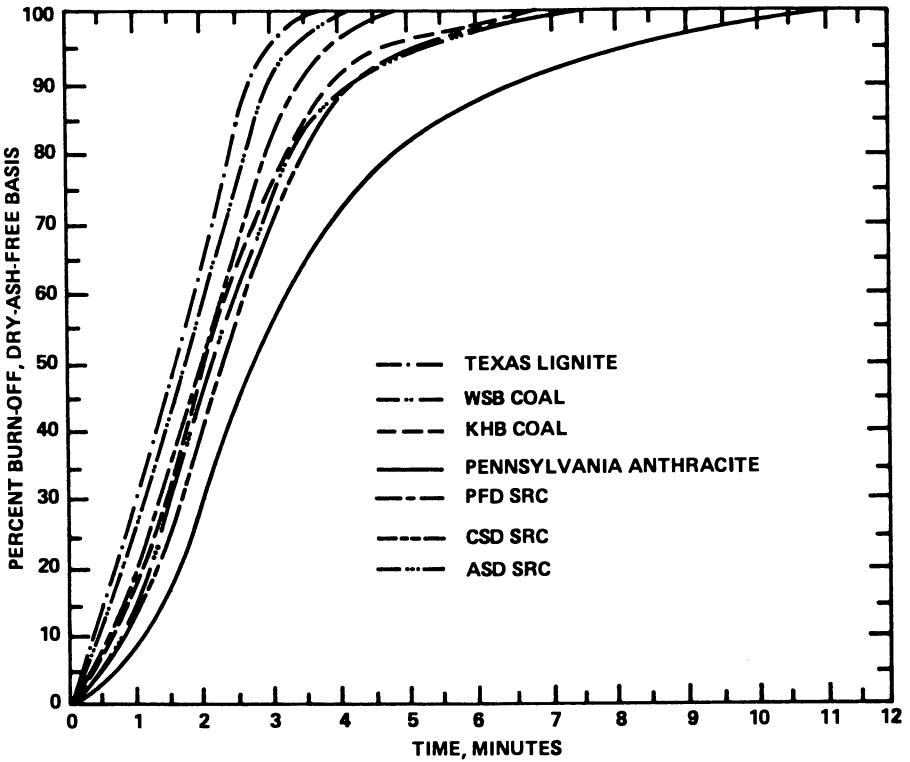
Figure 2.   Thermogravimetric burn-off curves in air at
700°C for SRC and reference coal volatile matter chars.

substantially higher than that of the anthracite char; and (4) the
lignite char is the most reactive of all the chars under this
study.

The TGA char reactivity data indicate that the CSD SRC has a
relatively low reactivity (similar to KHB coal). However, the
extremely high volatile yields of the CSD SRC (illustrated in DTFS
and CMHF results below) leaves very little char for subsequent
burnout and results in a high overall combustion efficiency.

Pyrolysis, Combustion and NO_x Characteristics

Two reference coals and the CSD SRC were pyrolyzed in an argon
atmosphere in the DTFS at 2800°F furnace wall temperature (Figure 3)
In a residence time of about 330 milliseconds, Wyoming subbitumin-
ous (WSB) coal evolved about 50% of its mass as volatile matter the
Kentucky high volatile bituminous (KHB) coal evolved about 53%
volatile matter and the CSD SRC evolved about 99% volatile matter.
These are much higher than the ASTM volatile matter values of 40.2,
37.3, and 59.8% for the WSB, KHB, and CSD fuels, respectively.
The difference between these values is far more pronounced for the
SRC than for the coals.

Figures 4, 5, and 6 show the solid conversion efficiencies of
the three SRC and the reference coals in air in the DTFS at three
temperatures (furnace wall temperatures of 2500, 2700, and 2800°F).
The CSD and PFD SRC and WSB reference coal achieved a high solid
conversion efficiency (>75%) in less than 50 milliseconds, while
the ASD SRC and the KHB reference coal resulted in lower initial
conversion efficiencies, less than 60%. The initial high degree of
conversion of the CSD and PFD SRC results in relatively low amounts
of residual char to be burned in the latter stages of combustion.
The CSD SRC showed the highest initial and overall solid conver-
sion efficiency of all the fuels studied.

The results further show that the solid conversion efficiencies
increase more dramatically with temperature than with residence
time increases. For the CSD SRC solid conversion efficiencies
increased from 91 to 95% at a furnace temperature of 2500°F, as
the residence time increased from 0.05 second to 0.3 second. The
corresponding efficiencies at 2800°F were 97% and 99% respectively
indicating the pronounced effect of higher temperatures.

A relative comparison of the five fuels (three SRC and two
reference coals) indicates that the CSD SRC has a high solid con-
version efficiency similar to the Wyoming subbituminous coal (WSB).
This WSB coal has been found to yield high combustion efficiencies
in utility boilers. The PFD SRC is seen to be less reactive com-
pared to the CSD SRC and the WSB coal in the early stages of com-
bustion, however, overall solid conversion efficiency differences
are reduced with increasing residence time, especially at the
higher temperatures studied. The ASD SRC, however, is seen to
give lower solid conversion efficiencies than the marginal KHB
reference coal at all three temperatures studied. At a furnace
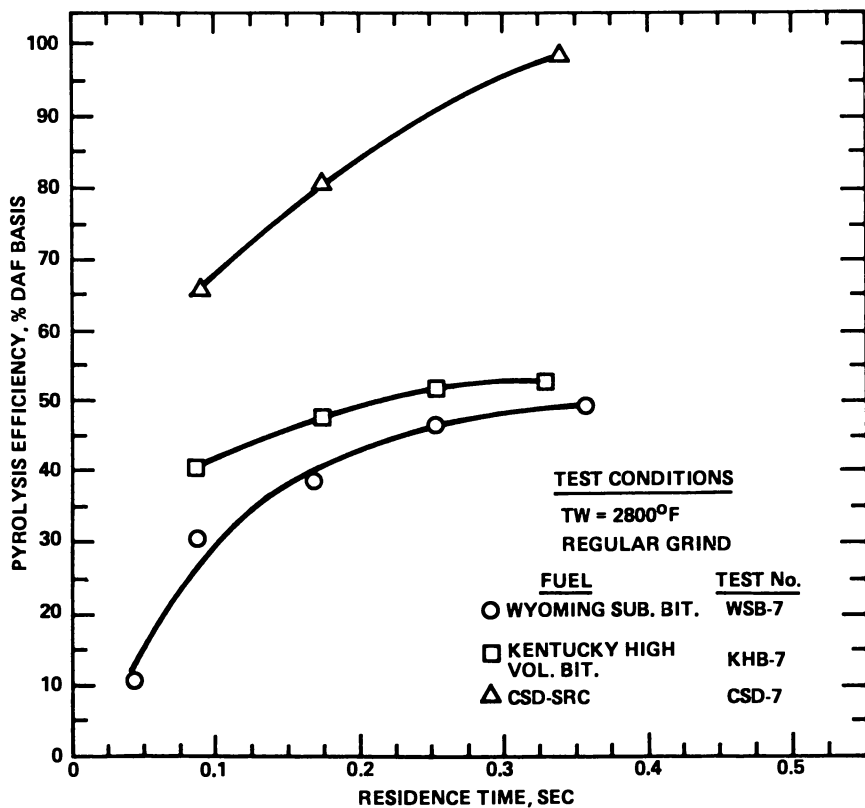
Figure 3. DTFS pyrolysis efficiencies of fuels in argon
at TW = 2800oF.
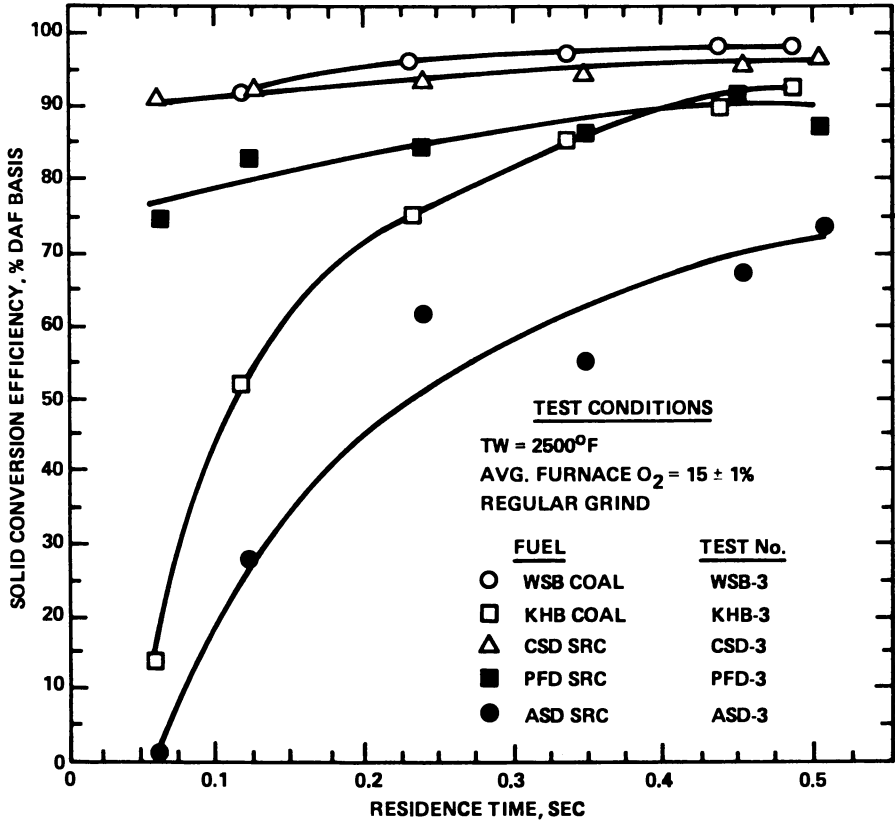
Figure 4. DTFS solid conversion efficiencies of fuels in air at TW = 2500°F.
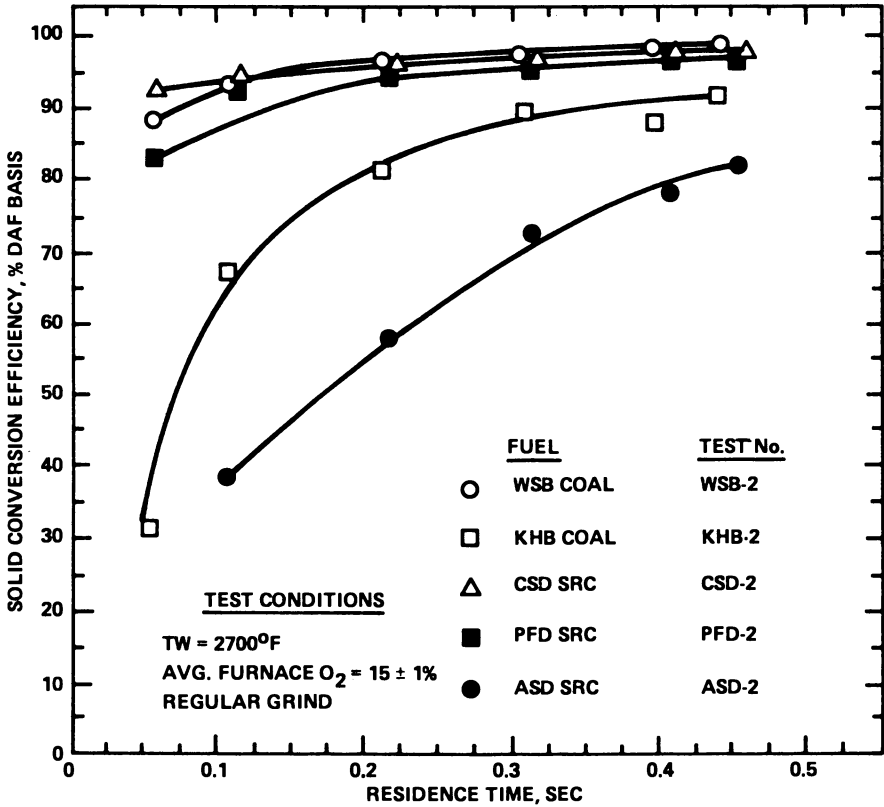
Figure 5. DTFS solid conversion efficiencies of fuels in air at TW = 2700°F.
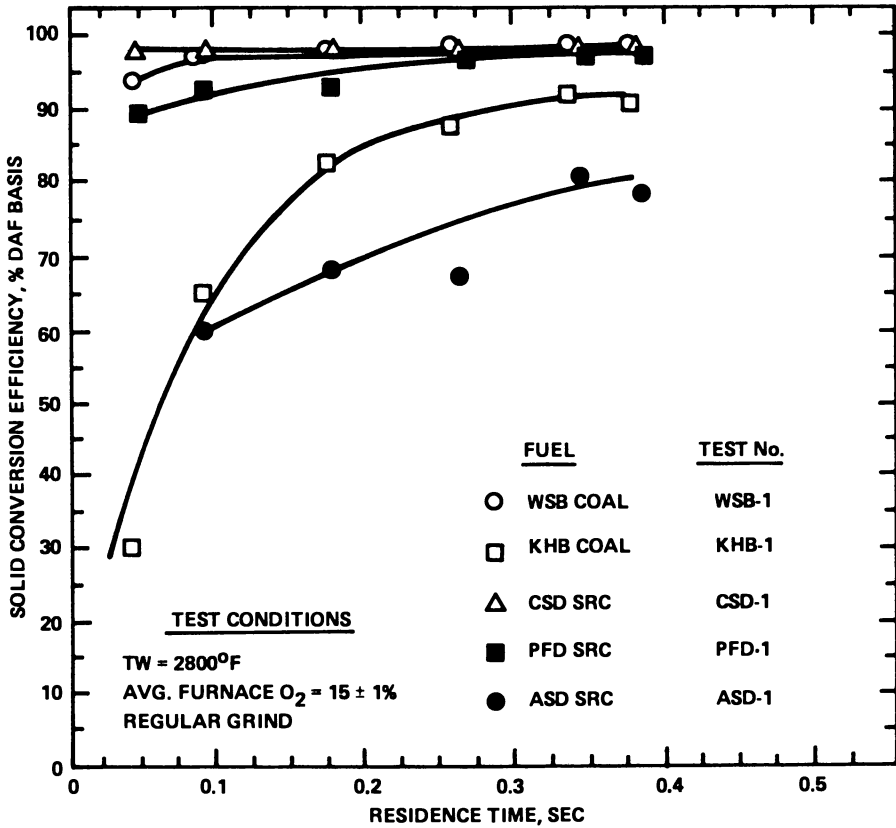
Figure 6. DTFS solid conversion efficiencies of fuels in air at TW = 2800°F.

temperature of 2800°F solid conversion efficiencies at 0.3 second
residence time are 99% for the CSD and WSB fuels, 97% for the PFD
SRC, 90% for KHB, and 77% for the ASD SRC.

Both the CSD and PFD SRC were studied in the CMHF as well as
two reference coals. The effect of primary stage stoichiometry
on NO_x emissions is shown in Figure 7.

For CSD SRC the maximum NO_x reduction was obtained at an opt-
imum primary stage stoichiometry of about 40%. At an overall
excess air value of 20%, baseline, unstaged emissions were 570 ppm
compared to the optimum, staged NO_x emissions of 240 ppm (all
values corrected to 3% O_2). For PFD SRC the minimum NO_x (230 ppm)
was attained at a primary stage stoichiometry of about 55% at the
same overall excess air. The SRC, due to their relatively high
fuel nitrogen contents, have a high NO_x formation potential under
conventional firing conditions. However, staging the combustion
air can result in acceptably low NO_x emissions without jeopardizing
their combustion efficiencies.

Varying the primary stage residence time (Figure 8) showed
the importance of providing a sufficient time in the substoichio-
metric primary stage for achieving low NO_x. The overall solid
conversion efficiencies were unaffected by changes in this para-
meter.

NO_x was found to increase slightly with increasing excess air
for all fuels tested in the CMHF (Figure 9). The rate of increase
in NO_x was small and decreased with increasing excess air. NO_x
increased from 245 ppm to only 288 ppm as excess air increased
from 0% to 35% for CSD SRC. This was not unexpected since all
tests were run under optimum low NO_x primary stage stoichiometries.
Variation in excess air from 0 to 35% under optimized conditions
was found to have little influence on the overall solid conversion
efficiency in the CMHF. This is probably because SRC exhibits
high pyrolysis efficiencies with low amounts of residual chars
being produced for subsequent burnout and because primary stage
conditions had been optimized.

Mathematical Modelling

In order to extrapolate the laboratory results to the field
and to make semiquantitative predictions, an in-house computer
model was used. Chemical reaction rate constants were derived by
matching the data from the Controlled Mixing History Furnace to
the model predictions. The devolatilization phase was not modeled
since volatile matter release and subsequent combustion occurs
very rapidly and would not significantly impact the accuracy of
the mathematical model predictions. The "overall" solid conver-
sion efficiency at a given residence time was obtained by adding
both the simulated char combustion efficiency and the average
pyrolysis efficiency (found in the primary stage of the CMHF).
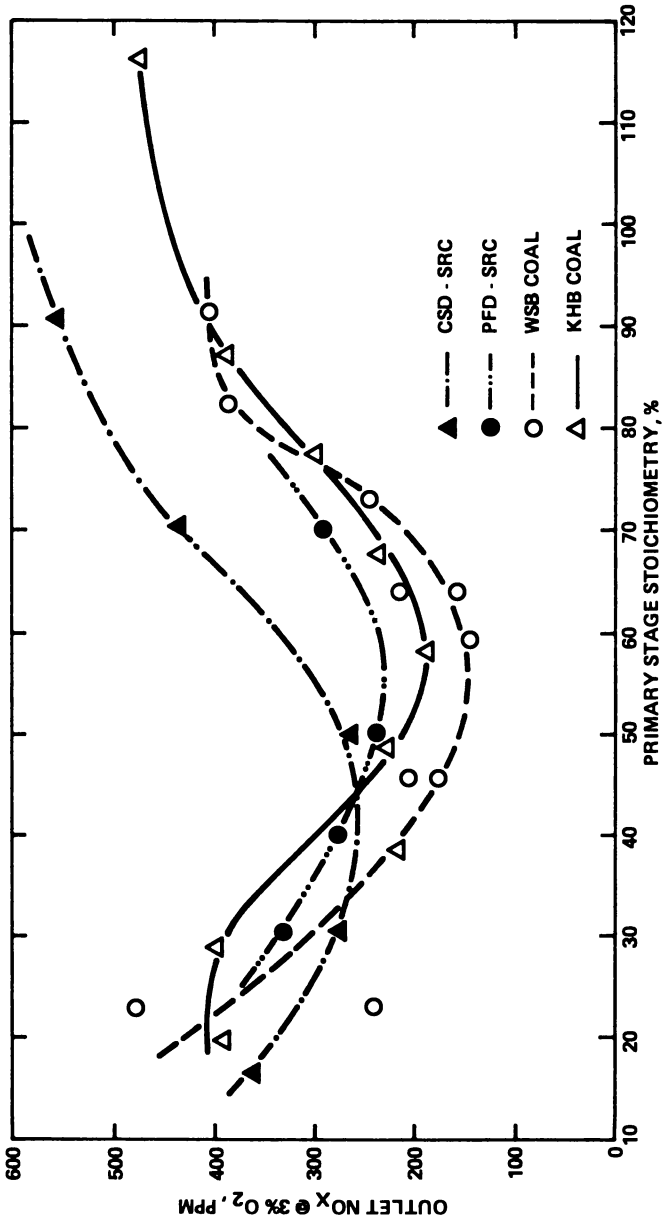
Figure 7. Effect of primary stage stoichiometry on NO_x emissions.
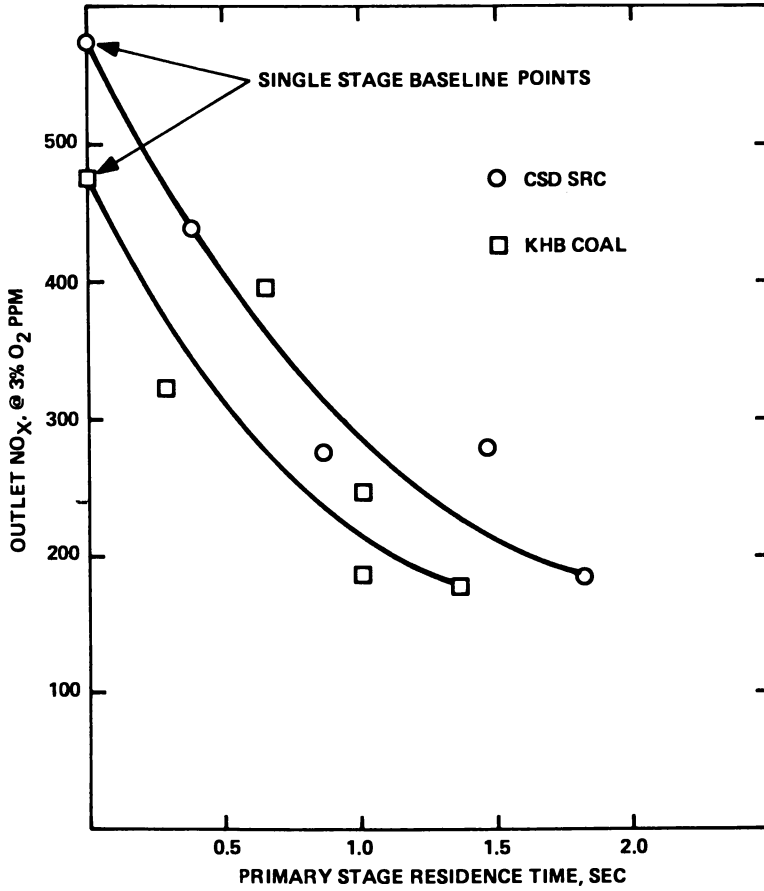
Figure 8.   Effect of primary stage residence time on NO_X emissions.
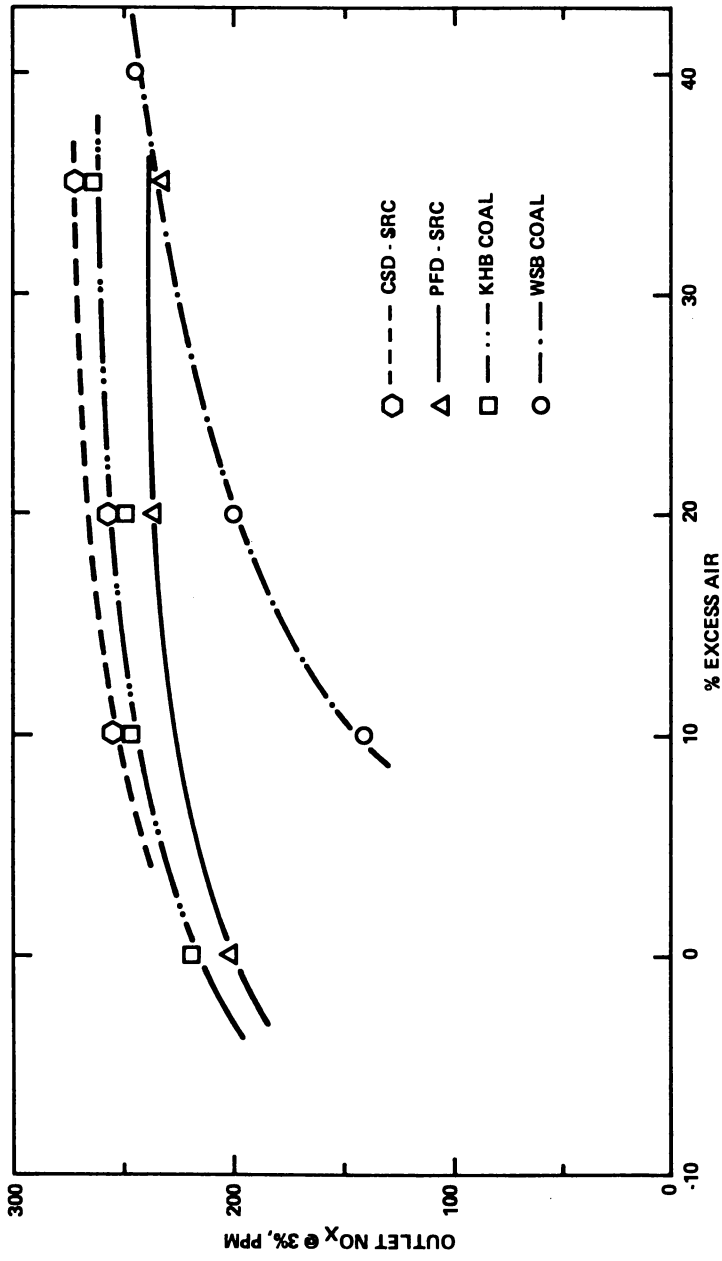
Figure 9. Effect of excess air on NO_x emissions.

The calibrated model was then used to make predictions for a case simulating field conditions for temperature, excess air level, and residence time. The results from the model study showed the following ranking of char reactivities: WSB > PFD > KHB > CSD. This is in agreement with TGS-2 (thermo-gravimetric analysis) results.

Figure 10 shows the predictions of the computer model for the two reference coals and the CSD and PFD SRC. A temperature of 2500°F and 20% excess air were used for this case. The intercepts of the curves on the Y-axis indicate the pyrolysis (devolatilization) efficiencies of the fuels. The plots show the combustion efficiencies of the CSD and PFD SRC, and the WSB coal approach 100% in 2 seconds residence time, whereas, the marginal KHB coal attains about 97% combustion efficiency.

Table III shows the predicted values of carbon in fly ash for these fuels at three different temperatures used in the computer modeling, for a residence time of 2 seconds. This table clearly shows the differences between the reactivities of the different fuels and the significance of the combustion temperatures.

TABLE III

CARBON IN ASH AS A FUNCTION OF TEMPERATURE
AT A 2-SECOND RESIDENCE TIME AND 20% EXCESS AIR*

Fuel	2500°F	2800°F	3140°F
WSB Coal	1.3	0.7	0.4
CSD SRC	12.2	1.9	0.4
KHB Coal	19.4	6.9	3.2
PFD SRC	46.4	26.9	18.5

*Using kinetics determined from CMHF data incorporated into the computer model.

The model predictions indicate that at typical commercial coal firing conditions, the carbon in the fly ash for the CSD SRC would lie between 1.9 and 12.2%, whereas that for the PFD SRC would lie between 26.9 and 46.4%. These results show that the high overall solid conversion efficiency of the CSD SRC is due to its higher pyrolysis/initial solid conversion efficiency.

CONCLUSIONS

The major conclusions that can be drawn from the results obtained during the course of this study are the following:

From an overall combustion efficiency standpoint, both the CSD and PFD SRC are relatively reactive solid fuels comparable in reactivity to subbituminous coal. The ASD SRC is relatively unreactive in comparison.
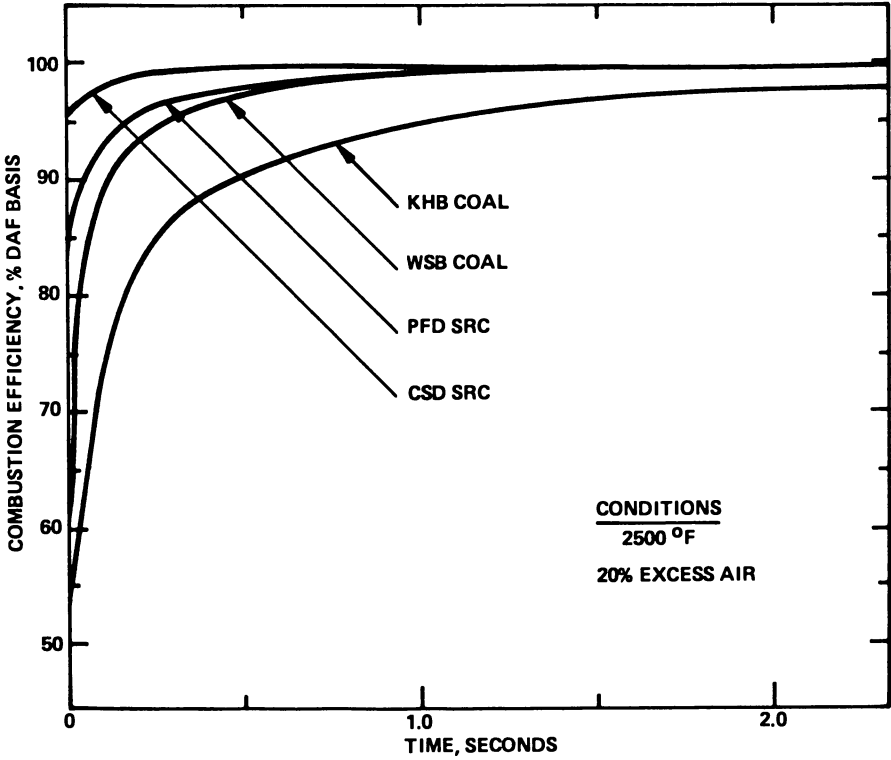
Figure 10. Combustion efficiencies of fuels simulated by computer model.

During the early stages of the burning process, SRC undergoes extensive pyrolysis reaction resulting in the rapid homogeneous gas phase combustion of the released volatiles. Both the pyrolysis reaction and the heterogeneous char combustion are enhanced by increased temperature during this early stage of the burning process.

Rapid pyrolysis is most pronounced in the CSD SRC and is predominantly responsible for achieving high overall solid conversion efficiencies despite the lower char reactivity of the CSD SRC relative to the PFD SRC. The ASD SRC exhibits a markedly lower pyrolysis rate than the other two SRC solids which renders it overall less reactive.

Compared to PFD and ASD, CSD SRC has the potential for producing a low carbon (<10%) fly ash under low NO_x, staged combustion conditions if flame temperature can be maintained sufficiently high during both fuel rich and fuel lean stages, thereby making the CSD SRC fly ash amenable to collection in electrostatic precipitators.

The SRC, due to their relatively high fuel nitrogen contents, have a high NO_x formation potential under conventional firing conditions. However, staging the combustion air can result in acceptably low NO_x emissions without jeopardizing their combustion efficiencies.

CSD and PFD SRC both required the addition of about 1-5 percent moisture to prevent coating of the grinding surfaces during pulverization in the C-E bowl mill. Under the same conditions of pulverization, the CSD SRC resulted in a smaller mean weight size than the PFD SRC.

Of the SRC evaluated, the CSD SRC has the highest potential for success in a utility boiler application from the standpoint of achieving low carbon content fly ash under low NO_x (staged) combustion operating conditions.

RECOMMENDATIONS

Based on the conclusions from this study, it is recommended that a logical follow-up test would consist of a commercial demonstration where CSD SRC is fired in a coal fired boiler. The following specific areas should be addressed:

Proper burner cooling to prevent plugging: This will be necessary because of the low melting temperature of SRC.

Confirm combustion efficiency/NO_x emissions: This will provide the information necessary to scale-up laboratory combustion/ NO_x results to commercial scale.

Measure radiant furnace heat profile: This will enable the comparison of the heat absorption profiles of SRC and coal flame and will also provide the necessary information to make judgements on the adequacy of furnace cooling surfaces.

Determine collectibility of particulates in an ESP: This will provide verification of prediction of carbon burnout based on laboratory results and computer modeling.

It is recommended that the following conditions be employed during combustion testing in the commercial boiler in order to minimize carbon in fly ash and NO_x emissions:

Mill fineness of 90%-200 mesh or finer: To minimize carbon loss, SRC should be pulverized finer than coals. Conventional coal pulverizers, however, should be more than adequate for the job.

Combustion temperatures of 2800°F or greater: These temperatures are typical of conventional coal fired utility operation.

Combustion zone residence time of 2 seconds or greater: This is typical of the range for coal fired utility operation.

Primary stage stoichiometries of 40-50%. Conventional coal utility operation does not involve sufficient staging of air to achieve substantial NO_x reduction. Advanced low NO_x firing systems, however, are now available to allow a high degree of staging.

Primary stage residence time of 0.5 second: Advanced low NO_x firing systems which permit a high degree of air staging are capable of achieving this residence time.

ACKNOWLEDGMENTS

LITERATURE CITED

1. Tao, J.C., et al., "Solvent Refined Coal (SRC-I): Technology Product Markets and Economics," Presented at the Third International Coal Utilization Exhibition and Conference. Houston Texas, November 18-20, 1980.
2. Borio, R. W., Laboratory Analysis of Solvent Refined Coal, EPRI Report 1235-2a, June 1976.
3. Borio, R. W. and G. J. Goetz, et al., Solvent Refined Coal Evaluation: Pulverization, Storage and Combustion, EPRI Report 1235-2a, June 1976.
4. McRanie, R. D., Full-Scale Utility Boiler Test with Solvent Refined Coal (SRC) - Final Report, FE-2222-9, July, 1979.

5. Kokkinos, A., C-E Internal Memo on DOE-PETC SRC Tests, April 1981.
6. Peluso, M. and D. F. Ogren, Coal Processing Technology: Antisolvent Deashing , Chemical Eng. Progress, June, 1979, pp. 41-43.
7. Adams, R. M, et al, Coal Processing Technology: Critical Solvent Deashing of Liquefied Coal, Chemical Eng. Process, June 1979, pp. 44-48.

RECEIVED October 29, 1982

Small-Scale Combustion Testing

G. A. GIBBON, J. M. EKMANN, C. M. WHITE, R. J. NAVADAUSKAS,
H. L. RETCOFSKY, and J. I. JOUBERT

U.S. Department of Energy, Pittsburgh Energy Technology Center,
Pittsburgh, PA 15236

In order to assess the possible environ-
mental impact of substituting synfuels for
petroleum in utility and industrial boilers, two
experimental programs have been undertaken at
the Pittsburgh Energy Technology Center. First,
a fully instrumented 20-hp firetube boiler
capable of burning liquid fuels ranging in com-
bustion characteristics from No. 2 to No. 6
petroleum has been installed in the Combustion
Division. Second, a sampling and analytical
methodology for the organic compounds present in
the exhaust duct of the 20-hp boiler is being
developed by the Analytical Chemistry Division.
This report outlines the progress on this
project to date: twenty-four successful com-
bustion runs have been completed on the 20-hp
boiler, using a variety of petroleum-based fuels
and synfuels; a sampling protocol for organic
vapors in hot exhaust gases has been developed;
significant differences in the composition of
the trace organics in the exhaust gases have
been observed as a function of the fuel being
burned, but total polynuclear aromatic hydro-
carbon levels are comparable for all fuels.

In order to assess any changes in the environmental
impact of industrial or utility boiler exhaust gases upon
changing from petroleum-based fuels to synthetic fuels,
detailed characterizations of the exhaust emissions from both
types of fuels burned under identical combustion conditions
are required.

A 20-hp (approximately 5 gallons of liquid fuel feed per
hour) firetube boiler has been installed in the Combustion
Technology Division of the Pittsburgh Energy Technology Center

(PETC) so such experiments can be performed. The boiler is fully instrumented for heat and material balance measurements, including analysis of the major and minor components of the combustion gases and the total hydrocarbons and particulates present in the gases. In addition, the exhaust duct of the boiler has a sampling port adjacent to the one used for major and minor components; this port is used to sample exhaust gases for the analysis of the trace organic compounds present in the gases.

The Analytical Chemistry Division of PETC is developing the sampling and analytical methodologies for the trace organics. The effort to date has been focused on the problems involved in sampling the hot (ca. 350°F) exhaust gases and on the analysis of the gases for polynuclear aromatic hydrocarbons.

To date, 24 successful tests of 4 to 6 hours each have been completed on the boiler. Eight tests with No. 6 fuel oil and two with No. 2 fuel oil were performed to establish acceptable operating parameters for the boiler and to determine the types and levels of emissions from these petroleum-derived fuels. The petroleum data will be the baseline against which any synfuels test will be compared. The fourteen synfuel tests were single runs on a middle and a heavy distillate product from the SRC-II process, and a total of twelve runs using 3:1, 2:1, and 1:2 blends of the middle and heavy distillates. The details of all the test runs are given in the next section of this report. In general, combustion performance was good in all tests. Total particulate loadings in the stack were small, and CO and total hydrocarbon levels were below 100 ppm and 1 ppm, respectively. The levels of NO_x and SO_2 produced were proportional to the amount of nitrogen and sulfur in the fuel. The heat balances were within the uncertainty of the measurements on which they are based.

Development of the sampling and analytical methodologies for trace organics in the hot exhaust gases has proceeded well, and several of the most recent boiler tests have been sampled successfully. The sampling is accomplished by drawing the hot gases through a heated particulate knockout trap and then through a sorbent bed packed with a carefully cleaned resin (XAD-2). The resin bed is heated above the dew point of the exhaust gases to prevent condensation of water on the resin. The gases are drawn through the sampler with an oilless seal vacuum pump.

The XAD-2 resin is removed from the sampler and extracted with methylene chloride. The extract is concentrated and then analyzed by combined gas chromatography/mass spectrometry (GC/MS). To date, the compounds primarily sought have been the polynuclear aromatic hydrocarbons. The n-alkanes present in the fuels are easily

identified by GC/MS, and these compounds, along with the poly-nuclear aromatic hydrocarbons, are those on which the comparisons are based. There appear to be two sources of trace organics in the exhaust gases: small amounts of the fuel itself not burned during combustion, and the products of combustion (note that #2 and #6 fuel oils are essentially aliphatic). For the petroleum fuels, n-alkanes and poly-nuclear aromatic hydrocarbons are seen in the exhaust gas; for the SRC-II fuels, the alkanes either are absent or present at very low levels, and polynuclear aromatic hydrocarbons not seen in the petroleum exhaust gases are present. No definite conclusion can be drawn from these preliminary results about the relative environmental impact of the two fuels for the following reasons: first, the data are qualitative; second, boiler operating conditions have not been optimized for minimum organic emission for the individual fuels; and last, the data are based on hot exhaust gas sampling and not on stack emissions. Future work on the project will be addressed to these current limitations.

Synfuel Combustion Test Facility

The combustion test program of synthetic liquid fuels is being conducted in a 20-horsepower (hp) firetube boiler and associated equipment. The system consists of a 20-hp, Johnston, three-pass, firetube boiler designed to transfer roughly 670,000 Btu/hr to the water side; a water treatment and feed system; a fuel holding tank and transfer pump; and a stack exhaust duct equipped with numerous sample ports for gaseous and particulate emissions testing.

The boiler is equipped with a package burner that includes the following: an adjustable fuel preheater to permit combustion of No. 6 oil, a fuel/air proportioning con-troller, an atomizing air supply, and a combustion air blower.

All major streams (fuel, combustion air, makeup water, steam and flue gas) and gaseous constituents are measured. Separate measurements are made of the steam production, steam pressure and temperature, makeup water flow, makeup water temperature and pressure, flue gas volumetric flow rate, com-bustion air volumetric flow rate, fuel volumetric flow rate, flue gas and air temperatures, and gaseous constituents. The gaseous effluents are analyzed both at the exit of the boiler and at the sample point for detailed particulate and trace organic measurements. At the exit of the boiler, the following species are measured using a process mass spectro-meter: O_2, CO, N_2, CO_2, H_2O, CH_4, H_2, SO_2, and H_2S. The same device is used to monitor the incoming air stream, closing the loop on major gaseous components (O_2, N_2, and H_2O). Separate analyzers are available at the sample port for O_2, CO_2, CO,

SO_2, NO_x, and total hydrocarbons. The mass spectrometric gas analysis is on a wet basis, as water vapor is not condensed out of the gas, while the analyzers at the sample port measure a gas stream dried using a permeation tube and refrigeration-type dryers in series. In addition to the measurements described above, surface temperature measurements of the boiler skin are made to estimate radiation losses, using the skin temperature, the room temperature and tabulated heat loss factors based on the temperature difference. Particulate mass emission rate and carbon content are measured for heat and mass balance purposes. At present, material deposited within the boiler during a test is collected but not factored into the heat or mass balances, because this deposition is con-sidered to be negligible. Data taken are used to examine the heat balance for the 20-hp system.

To date, the test program has consisted of two periods of No. 6 fuel oil firing, two periods of SRC-II firing, and two combustion runs on No. 2 oil. Each test period was preceded by a few brief tests to shake down the boiler and determine settings for the atomizing air flow, fuel preheat temperature, and fuel/air proportioning controller. To date, eight runs have been made with No. 6 oil: five at about 23% excess air and three at about 11% excess air. Two runs have been completed on No. 2 oil: one at 11% excess air and one at 20% excess air. Five SRC-II fuels have been tested: a heavy distillate, a middle distillate, and three blends. The initial blend of SRC-II was approximately three parts middle distillate to one part heavy distillate. Six runs, three at each of two conditions, were made with this blend. Subsequently, separate supplies of middle and heavy distillate were obtained, and two blends were prepared: one of two parts middle to one part heavy distillate and the second of one part middle to two parts heavy distillate. Three tests were run on each blend. Single tests were run on the middle distillate and heavy distillate alone. Fuel rates were selected to provide equal thermal inputs based on the heating value of the fuel. Analyses of the fuels used are given in Table I.

A complete list of tests, including the fuel used in each test, the actual percent excess oxygen (on a wet basis), and the actual fuel firing rate, is given in Table II. A partial list of the pounds of steam produced per gallon of fuel fired is also given. In general, the stack oxygen levels were held near one of two target ranges (2.0-2.5% or 4.0-4.5%), and the fuel rates were held close to the stipulated value of 5.4 gph (5.2 gph for the No. 2 oil tests). For all tests except the No. 2 oils tests, the average firing rate was 5.4 gph $\pm$ 0.18. The steam production number indicates reasonably similar performance from all the

TABLE I. Fuel Analysis

Fuel %	#2 Fuel+ Oil	#6 Fuel Oil	SRC II "BLENDS"*				
			Mid. Dist. (M)	Blend #1 (3M:1H)	Blend #2 (2M:1H)	Blend #3 (1M:2H)	Heavy Dist. (H)
Carbon	87.3	87.0	85.9	86.2	87.5	89.1	88.9
Hydrogen	12.5	11.0	9.0	8.9	8.5	7.9	7.3
Nitrogen	--	0.30	0.9	0.9	0.9	1.0	1.1
Sulfur	0.21	0.70	0.3	0.2	0.4	0.4	0.5
Ash	--	0.10	0.10	--	0.60	0.3	0.6
Oxygen (diff)	--	1.9	3.8	3.8	2.1	1.3	1.6
Heating Value (Btu/lb)	19840	18610	17260	17590	17140	17130	17050

+Typical analysis of #2 fuel oil
*Mixtures of middle and heavy distillate; Blend #1 received already mixed

TABLE II. Test Conditions for the Synfuels Test Program

Run #	Fuel	%O₂*	Fuel Rate⁺ (gal/hr)	Steam Production/* Gal Fuel (lb steam/gal)
LSF-20	#6 Fuel Oil	3.9	5.6	--
LSF-21	#6 Fuel Oil	2.1	5.4	--
LSF-22	#6 Fuel Oil	4.1	5.4	--
LSF-23	#6 Fuel Oil	4.4	5.4	--
LSF-24	SRC II, Blend 1	3.9	5.4	--
LSF-25	SRC II, Blend 1	2.2	5.4	--
LSF-26	SRC II, Blend 1	3.9	5.4	--
LSF-27	SRC II, Blend 1	2.3	5.6	107.5
LSF-28	SRC II, Blend 1	4.5	5.2	117.6
LSF-29	SRC II, Blend 1	1.9	5.6	--
LSF-30	#6 Fuel Oil	2.3	5.4	111.2
LSF-31	#6 Fuel Oil	4.0	5.4	103.7
LSF-32	#6 Fuel Oil	2.1	5.4	108.3
LSF-34	#6 Fuel Oil	4.1	5.4	110.5
LSF-35	#2 Fuel Oil	4.6	5.2	106.1
LSF-36	#2 Fuel Oil	2.2	5.1	106.7
LSF-37	SRC II, Mid. Dist.	4.4	5.3	111.7
LSF-38	SRC II, Blend 3	2.5	5.6	115.7
LSF-39	SRC II, Blend 3	4.2	5.7	114.0
LSF-40	SRC II, Blend 3	2.2	5.3	115.7
LSF-41	SRC II, Blend 2	2.5	5.6	109.8
LSF-42	SRC II, Blend 2	3.9	5.3	108.7
LSF-43	SRC II, Blend 2	2.6	5.6	109.4
LSF-44	SRC II, Heavy Dist.	2.9	5.5	114.7

*Percent oxygen was set as an experimental condition; two levels were selected: 2.0–2.5% O_2 and 4.0–4.5% O_2.

⁺Fuel rates were set at approximately 5.4 gal/hr and adjusted slightly to maintain the same Btu/hr input for the fuel.

*Pounds of steam produced per gallon of fuel fired.

fuels tested. Direct comparison of performance between fuels
would require complete thermal balances.

In general, combustion performance was good in all
tests. Total particulate loadings in the stack were small for
all tests; CO and total hydrocarbon levels were low--below 100
ppm for CO and one ppm or less for hydrocarbons. Emissions of
pollutants such as NO_x and SO_2 were proportional to the amount
of either nitrogen or sulfur in the fuel. Table III presents
NO_x concentrations (in parts per million, adjusted to dry, 0%
excess air basis) compared to the fuel nitrogen content. In
general, the trend is clear, with the lowest NO_x values occur-
ring for No. 2 oil, which has little or no nitrogen in the
oil; so the measured value for No 2 oil represents NO_x
resulting primarily from atmospheric fixation whereas the
various SRC-blends that have approximately 1% nitrogen
represent a combination of thermal and fuel related NO_x.
Emissions of SO_2 were proportional to the amount of sulfur in
the fuel (Table IV). The reported values for SO_2 are also
adjusted to a dry, 0% excess air basis.

Detailed analyses of the major flows and temperatures
have been utilized to make heat balances for a number of
tests. The heat balance can, in turn, be used to calculate a
heat transfer efficiency for the production of steam, by
either an input-output method or a heat loss method. The
input-output efficiency is the ratio of the enthalpy exiting
the boiler in the steam to the enthalpy entering in the heat-
ing value and sensible heat of the fuel. The heat loss method
sums the flue gas sensible heat, the heat loss due to water
formation in combustion, the heat loss due to radiation from
the hot surfaces of the boiler, and the heat loss due to
incomplete combustion. These losses are divided by the enter-
ing enthalpy, as defined by the input-output method. This
fraction is used to compute the efficiency (ε):

$$\varepsilon \text{ Heat Loss} = (1 - (\text{Heat Loss/Entering Enthalpy})) \times 100$$

A typical heat balance for Run LSF 34 on No. 6 oil is
given in Table V. The calculated efficiencies are also given
in the table. Heat input terms consist of the input heat from
the fuel, the fuel sensible heat, and the makeup water
sensible heat. The heat available from combustion of the fuel
is calculated from the measured volumetric flow rate, the
measured fuel heating value, and the measured fuel density at
the nozzle temperature. The fuel sensible heat contains the
fuel mass flow rate, the measured temperature at the nozzle, a
reference temperature, and an estimated specific heat for the
oil of 0.480 Btu/lb°F. The specific heat was taken from
graphical information in the ASME Power Test Code. Similarly,
the water sensible heat calculation contains a tabular value

TABLE III. <u>NO$_x$ Emissions as a Function of Fuel Nitrogen Content</u>

Fuel	Run #	% Excess Air	% N (fuel)	NO$_x$ (ppm)*
#2 Fuel Oil	LSF 35	26.0	ND	193
#2 Fuel Oil	LSF 36	11.0	ND	178
#6 Fuel Oil	LSF 20	21.0	0.3	329
#6 Fuel Oil	LSF 21	10.5	0.3	261
#6 Fuel Oil	LSF 22	23.0	0.3	364
#6 Fuel Oil	LSF 23	25.0	0.3	353
#6 Fuel Oil	LSF 30	11.5	0.3	292
#6 Fuel Oil	LSF 31	22.0	0.3	350
#6 Fuel Oil	LSF 32	10.5	0.3	312
#6 Fuel Oil	LSF 34	23.0	0.3	331
SRC II, Blend #1	LSF 24	21.5	0.9	599
SRC II, Blend #1	LSF 25	11.0	0.9	456
SRC II, Blend #1	LSF 26	21.5	0.9	493
SRC II, Blend #1	LSF 27	11.5	0.9	517
SRC II, Blend #1	LSF 28	26.0	0.9	548
SRC II, Blend #1	LSF 29	9.5	0.9	434
SRC II, Blend #2	LSF 41	13.0	0.9	480
SRC II, Blend #2	LSF 42	21.5	0.9	604
SRC II, Blend #2	LSF 43	13.5	0.9	528
SRC II, Mid. Dist.	LSF 37	25.0	0.9	590
SRC II, Blend #3	LSF 38	13.0	1.0	557
SRC II, Blend #3	LSF 39	24.0	1.0	576
SRC II, Blend #3	LSF 40	11.0	1.0	549
SRC II, Blend #5	LSF 44	15.0	1.1	622

*Adjusted to a dry, 0% Excess Air Basis

TABLE IV. SO_2 Emissions as a Function of Fuel Sulfur Content

Fuel	Run #	% Excess Air	% S (fuel)	SO_2 (ppm)*
#2 Fuel Oil	LSF 35	26.0	0.20	272
#2 Fuel Oil	LSF 36	11.0	0.20	194
SRC II, Blend #1	LSF 24	21.5	0.20	233
SRC II, Blend #1	LSF 25	11.0	0.20	204
SRC II, Blend #1	LSF 26	21.5	0.20	221
SRC II, Blend #1	LSF 27	11.5	0.20	203
SRC II, Blend #1	LSF 28	26.0	0.20	200
SRC II, Blend #1	LSF 29	9.5	0.20	--
SRC II, Mid. Dist.	LSF 37	25.0	0.30	213
SRC II, Blend #2	LSF 41	13.0	0.40	301
SRC II, Blend #2	LSF 42	21.5	0.40	312
SRC II, Blend #2	LSF 43	13.5	0.40	310
SRC II, Blend #3	LSF 38	13.0	0.40	372
SRC II, Blend #3	LSF 39	24.0	0.40	381
SRC II, Blend #3	LSF 40	11.0	0.40	376
SRC II, Heavy Dist.	LSF 44	15.0	0.50	463
#6 Fuel Oil	LSF 20	21.0	0.70	--
#6 Fuel Oil	LSF 21	10.5	0.70	--
#6 Fuel Oil	LSF 22	23.0	0.70	369
#6 Fuel Oil	LSF 23	25.0	0.70	446
#6 Fuel Oil	LSF 30	11.5	0.70	434
#6 Fuel Oil	LSF 31	22.0	0.70	421
#6 Fuel Oil	LSF 32	10.5	0.70	448
#6 Fuel Oil	LSF 34	23.0	0.70	364

*Adjusted to a dry, 0% Excess Air Basis

TABLE V.   Heat Balance for Run LSF-34

Fuel: No. 6 Fuel Oil
Heating Value of Fuel (Btu/lb) = 18,610

Heat Balance

Input Enthalpy (Btu/hr)		Output Enthalpy (Btu/hr)	
Fuel Heating Value	807380	Steam Production	711550
Fuel Sensible Heat	1040	Heat Losses by	
Make-up Water Sensible Heat	87770	Flue Gas Sensible Heat	93160
		Water in Fuel, etc.*	67470
		Radiation	11655
		Other (unburnt carbon, etc.)+	160
		Total Losses	172445

Total Input Enthalpy 896190   Total Output Enthalpy 883995

Heat Balance: $\dfrac{\text{Input-Output}}{\text{Fuel Heating Value} + \text{Fuel Sensible Heat}} = \dfrac{896190 - 883995}{808420} = 0.015$

Efficiencies: ϵ (Input-Output) = $\dfrac{711500 - 87770}{808420}$ x 100 = 77.2%

ϵ (Heat Loss) = 1- $\dfrac{172445}{808420}$ x 100 = 78.7%

* This term combines the heat loss due to water in the fuel, water in the combustion air, and water from the combustion of hydrogen.

+ This quantity combines a number of terms dealing with the heat loss due to the incomplete combustion of carbon.

for the specific heat of water appropriate to the measured temperature and pressure at the boiler inlet.

Heat output terms consist of the heat contained in the steam and a series of heat loss terms. The heat losses are

o sensible heat leaving the system in the flue gas

o latent and sensible heat lost in water produced by combustion and water carried through the combustion chamber

o radiative heat transfer loss from the surface of the boiler

o losses due to the incomplete conversion of input carbon to CO_2 (unburned CO and unburned C terms)

o sensible heat contained in particulate emissions.

Heat loss terms contain a large number of individual measurements and estimated properties of the boiler surface and flue gas. The radiative loss is estimated using eight measured temperatures -- four of the boiler surface and four of the surrounding air -- plus the actual surface area of the boiler.

Results of the <u>enthalpy</u> balance for this test show that the method of calculation cannot account for 1.5% of the total enthalpy input. This difference is small and may arise from the accuracy of the individual measurements and by the approximation used to calculate some of the quantities, as described above. A preliminary error analysis indicates an uncertainty of $\pm$ 3.3% for the heat balance calculation. The two methods for calculating the efficiency will agree only if the heat balance closes exactly. In general, when the calculated efficiencies do not agree, the heat loss method is selected, as it tends to be the more accurate.

Similar results, heat balances plus calculated efficiencies, are given in Table VI for seven additional tests. Results from LSF-34 are included for comparison. The results for all eight tests are considered satisfactory based on the error analysis mentioned above. For those tests where the enthalpy balance closes within $\pm$ 2.5%, either method for calculating efficiency may be used; for the other four tests, the heat loss method value should be selected. Thermal performance of the unit -- the steam generating capacity compared to the Btu input -- appears to be similar for all eight tests.

Although complete analyses of all tests are not available, the results are encouraging. All fuels tested appear to perform in a similar manner, that is, like No. 2 and No. 6

TABLE VI. Calculated Efficiencies for Selected Tests

Run #	Fuel	(Δ Enthalpy Balance) %	Efficiency (Heat Loss) %	(Input-Output) %
LSF-32	No. 6	+1.2	83.1	81.2
LSF-34	No. 6	+1.5	78.7	77.4
LSF-35	No. 2	-0.32	74.8	75.1
LSF-36	No. 2	+5.0	80.0	74.0
LSF-37	SRC II, Middle Distillate	+5.35	83.8	78.5
LSF-41	SRC II, Blend of 2 Parts Middle Distillate to 1 Part Heavy Distillate	+2.4	78.4	75.6
LSF-42		+5.6	80.7	74.6
LSF-43		+5.8	82.5	76.4

fuel oil.   No difference in rated capacity occurs between
fuels. Particulate, CO, and hydrocarbon emissions are low, as
one would expect from low ash fuels, which atomize and burn
regularly.   No significant difference in soot formation or
tendency to smoke was noticed between fuels.

Analysis of Combustion Products

        The 20-hp synfuels exhaust combustor duct was sampled
during burns of No. 2 and No. 6 fuel oils as well as during
burns of various blends of SRC-II distillates, using a
modified Jones adsorbent sampler (1, 2). The sampling system
used initially caused several problems, which have now been
corrected.   The silicone oil from the sampling train vacuum
pump back-diffused into the sorbent bed.   This problem was
solved by replacing the original pump with an oilless pump. A
second problem has been partially solved.   Initially,
particulates in the duct were sampled using a glass fiber
filter. The filter would begin to plug shortly after sampling
was   initiated,   making   it   difficult   to   draw   sufficient
combustor duct vapors through the sampling system.   The filter
assembly has been replaced by a baffle-type particulate knock-
out trap.
        The Jones adsorbent sampler is filled with the macro-
reticular resin XAD-2, which is used for the collection of
organic vapors in hot gas streams (3).   The XAD-2 is cleaned
immediately prior to use by continuous Soxhlet extraction,
employing the solvent regime in Table VII (4).   After
methylene chloride extraction, the XAD-2 is thermally desorbed
of solvent for 30 minutes at 150°C while a flow of 30 cc/min
of He is passed over it.   After thermal desorption, the XAD-2
is packed into the adsorbent sampler and used immediately.
The sampling conditions have varied slightly from burn to
burn, depending on the fuel used, the oxygen to fuel ratio,
and the fuel feed rate, but in general the conditions are
similar to those given in Table VIII.
        When sampling is completed, the sampler is disassembled,
and the XAD-2 is removed and Soxhlet-extracted for 24 hours,
using approximately 100 mL of methylene chloride.   The result-
ing extract is concentrated to approximately 1 mL using a
Kuderna-Danish evaporative concentrator.   This concentrate is
placed in a Teflon sealed vial and analyzed by combined GC/MS.
The gas chromatographic and mass spectrometric conditions used
for analysis are given in Table IX.
        A total of 24 burns were sampled and analyzed, using the
methods described above.   Typical qualitative analytical
results for two successful burns appear in Table X.   The
compounds were identified on the basis of both mass spectral
and gas chromatographic data (5, 6).   The notations L, M, and

TABLE VII. XAD-2 Cleanup Solvent Scheme

Solvent	Soxhlet Extraction Time
Water	2 hours
Methanol	24 hours
Diethyl Ether	24 hours
Pentane	24 hours
Methylene Chloride	24 hours

TABLE VIII. Exhaust Duct Sampling Conditions

1.	Sorbent bed temperature	70°C
2.	Vacuum at start	15 in. Hg
3.	Duct Temperature	210°C–249°C
4.	Flow rate	25 Lpm
5.	Sampling Time	4–7 hours
6.	Volume of sample taken	5600–8500 liters
7.	Knockout trap temperature	140°C–150°C

TABLE IX. Analytical Conditions

Column	15–20m x 0.30 mm SE–52, 0.25 μm film
Injector temperature	275°C
He flow rate	1 – 2 mL/min
Injection conditions	2.0μL splitless, 45 s splitless period
Temperature program	3-min hold at 30°C, 30° – 300°C @ 4°C/min.
PT/IR transfer line temperature	275°C
Quadrapole scan rate	2 scans/s
Masses scanned	40 – 500 amu
Source temperature	200°C

TABLE X. Summary of GC/MS Data Obtained from a Synfuel
as well as a Petroleum Burn

Compound	Detected in Combustion Emission	
	SRC-II	No. 2 Fuel Oil
Naphthalene	L	M
2-Methylnaphthalene	L	H
1-Methylnaphthalene	L	L
Biphenyl	L	L
2-Ethylnaphthalene	L	L
2,6- & 2,7-Dimethylnaphthalene	L	L
1,3- & 1,7-Dimethylnaphthalene	L	L
1,5-Dimethylnaphthalene	L	L
1,2-Dimethylnaphthalene	L	L
Acenaphthene	L	L
Dibenzofuran	L	L
Fluorene	M	L
9-Methylfluorene	M	ND
2-Methylfluorene	M	ND
1-Methylfluorene	M	ND
Dibenzothiophene	M	L
Phenanthrene	H	H
Anthracene	L	L
Carbazole	L	ND
1-Phenylnaphthalene	L	ND
3-Methylphenanthrene	M	ND
2-Methylphenanthrene	M	ND
9- & 4-Methylphenanthrene	M	ND
1-Methylphenanthrene	M	ND
2-Phenylnaphthalene	L	ND
Fluoranthene	M	L
Benzo(def)dibenzothiophene	L	ND
Pyrene	H	L
Retene	L	ND
Benzo(b)fluorene	M	ND
4-Methylpyrene	L	ND
2-Methylpyrene	L	ND
Benzo(a)anthracene	L	ND
Chrysene/Triphenylene	L	ND
n-Alkanes	L	H

ND = Not Detected;   H = High;   M = Medium;   L = Low
Total Hydrocarbon ≃ 1ppm

H in Table X represent estimated relative amounts for a single chromatogram and have significance only in comparison to other compounds in the same chromatogram. The notation "Total Hydrocarbon ≃ 1 ppm" refers to the hydrocarbon concentration in the combustion exhaust duct as measured by a total hydrocarbon monitor.

These analytical results were obtained on samples collected during the combustion of SRC-II and No. 2 fuel oil. The fuels were combusted under very similar conditions and were collected under identical conditions. The burns were made without any complications, such as flameouts. Therefore, a comparison of the data derived from these combustion experiments appears to be valid and begins to answer the questions of what differences and similarities there are in the organic vapors present in the exhaust duct when a synfuel and petroleum product are combusted.

The collected samples have been initially characterized for polynuclear aromatic hydrocarbons. The results indicate that there is a wider spectrum of polynuclear aromatic hydro-carbons present when SRC-II is combusted than is present when No. 2 fuel oil is combusted. In addition, the petroleum com-bustion gases contained significant amounts of saturated hydrocarbons, which were present at low levels or absent when SRC-II was combusted. The petroleum combustion gases also contained other compounds, as yet unidentified, that were not present when SRC-II was combusted. In both combustion experiments, the organics in the duct appear to be similar to those in the fuel being combusted. The vapors collected appear to represent a mix of uncombusted fuel plus combustion products. It is interesting to note that no flameouts occurred during these combustion experiments. Apparently even during good combustion conditions, some liquid fuel survives the combustion process and appears in the duct.

Literature Cited

1.   Jones, P. W., Giammar, R. D., Strup, P. E., and Stanford, T. B. Efficient Collection of Polycyclic Aromatic Hydrocarbons From Combustion Effluents. Environmental Sci. Technol., 10, 806 (1976).
2.   Strup, P. E., Giammar, R. D., Stanford, T. B., and Jones, P. W. Improved Measurement Techniques for Polycyclic Aromatic Hydrocarbons from Combustion Effluents. Carcinogenesis, Vol. I, ed. by P. W. Jones and R. I. Freudenthal, Raven Press, 1976.
3.   Sonnichsen, T. W., McElroy, M. W., and Bjoiseth, A. Use of PAH Tracers During Sampling of Coal Fired Boilers in Polycyclic Aromatic Hydrocarbons. Ed. by A. Bjorseth and A. J. Dennis, pp. 617-632, Battelle Press, 1980.

4. Strup, P. E., Wilkinson, J. E., and Jones, P. W. Trace Analysis of Polycyclic Aromatic Hydrocarbons in Aqueous Systems Using XAD-2 Resin and Capillary Column Gas Chromatography-Mass Spectrometry Analysis in Carcinogenesis. Vol. III, ed. by P. W. Jones and R. I. Freudenthal, Raven Press, New York 1978.

5. White, C. M., Sharkey, A. G., Lee, M. L., and Vassilaros, D. L. Some Analytical Aspects of the Quantitative Determination of Polynuclear Aromatic Hydrocarbons in Fugitive Emissions From Coal Liquefaction Processes: in Polynuclear Aromatic Hydrocarbons, pp. 261-275, Ann Arbor Science Publisher (1979).

6. Lee, M. L., Vassilaros, D. L., White, C. M., and Novotny, M. Retention Indices for Programmed-Temperature Capillary-Column Gas Chromatography of Polycyclic Aromatic Hydrocarbons. Anal. Chem., 51, 768 (1979).

INDEX